NASA CR-120816
AiResearch 71-7450

FINAL DESIGN REPORT

BRAYTON HEAT EXCHANGER UNIT DEVELOPMENT PROGRAM

by

C. J. Morse, C. E. Richard, and J. D. Duncan

AIRESEARCH MANUFACTURING COMPANY
Los Angeles, California

prepared for

NATIONAL AERONAUTICS AND SPACE ADMINISTRATION

May 29, 1971

CONTRACT NAS 3-10607

NASA Lewis Research Center
Cleveland, Ohio
Gabriel Kaykaty, Project Manager

NOTICE

This report was prepared as an account of Government-sponsored work. Neither the United States, nor the National Aeronautics and Space Administration (NASA), nor any person acting on behalf of NASA:

A.) Makes any warranty or representation, expressed or implied, with respect to the accuracy, completeness, or usefulness of the information contained in this report, or that the use of any information, apparatus, method, or process disclosed in this report may not infringe privately-owned rights; or

B.) Assumes any liabilities with respect to the use of, or for damages resulting from the use of, any information, apparatus, method or process disclosed in this report.

As used above, "person acting on behalf of NASA" includes any employee or contractor of NASA, or employee of such contractor, to the extent that such employee or contractor of NASA or employee of such contractor prepares, disseminates, or provides access to any information pursuant to his employment or contract with NASA, or his employment with such contractor.

Requests for copies of this report should be referred to

National Aeronautics and Space Administration
Scientific and Technical Information Facility
P.O. Box 33
College Park, Md. 20740

NASA CR-120816
AiResearch 71-7450

FINAL DESIGN REPORT

BRAYTON HEAT EXCHANGER UNIT DEVELOPMENT PROGRAM

by

C. J. Morse, C. E. Richard, and J. D. Duncan

AIRESEARCH MANUFACTURING COMPANY
Los Angeles, California

prepared for

NATIONAL AERONAUTICS AND SPACE ADMINISTRATION

May 29, 1971

CONTRACT NAS 3-10607

NASA Lewis Research Center
Cleveland, Ohio
Gabriel Kaykaty, Project Manager

FOREWORD

The program described in this report was conducted by AiResearch Manufacturing Company, a Division of The Garrett Corporation, under NASA contract NAS3-10607. This program was performed under the management of Gabriel Kaykaty, Project Manager, Space Power Systems Division, NASA-Lewis Research Center.

CONTENTS

ILLUSTRATIONS

ILLUSTRATIONS (Continued)

ILLUSTRATIONS (Continued)

ILLUSTRATIONS (Continued)

TABLES

TABLES (Continued)

ABSTRACT

A Brayton Heat Exchanger Unit (BHXU), consisting of a recuperator, a heat sink heat exchanger and a gas ducting system, was designed, fabricated, and tested. The design was formulated to provide a high performance unit suitable for use in a long-life Brayton-cycle powerplant.

A parametric analysis and design study was performed to establish the optimum component configurations to achieve low weight and size and high reliability, while meeting the requirements of high effectiveness and low pressure drop. Layout studies and detailed mechanical and structural design were performed to obtain a flight-type packaging arrangement, including the close-coupled integration of the BHXU with the Brayton Rotating Unit (BRU).

Fabrication development was undertaken and units were manufactured with satisfactory structural integrity and leaktight containment. Evaluation testing was conducted from which it is estimated that near-design performance can be expected with the use of He-Xe as the working fluid.

SECTION I

SUMMARY

AiResearch has designed a Brayton Heat Exchanger Unit (BHXU) consisting of a gas-to-gas recuperator, a gas-to-liquid heat sink heat exchanger, and a gas ducting system that interconnects with other Brayton components to form the Brayton power conversion loop.

This BHXU is selected to operate in a power system with a rated output of 10 KW_e. The design objective for the BHXU is an effectiveness of 0.95 for both the recuperator and heat sink exchanger, a total gas fractional pressure drop through the unit of 0.045, and an operating lifetime capability of 5 years in a space environment. The unit is designed to employ a gaseous helium-xenon mixture with a molecular weight of 83.8 as the primary working fluid. The liquid coolant in the heat sink exchanger is Dow Corning 200 fluid with a viscosity grade of 2.0 centistokes at 25°C.

A parameteric analysis and design study was conducted to establish the most favorable heat exchanger configurations with respect to weight, size, and reliability. Layout studies were performed involving component matching and design tradeoffs to obtain an optimum integral unit. Utilizing these studies, in combination with detailed mechanical and structural analyses, a compact, flight-type arrangement was evolved for integration with the Brayton Rotating Unit, the gas management system, and the Brayton heat source.

Fabrication development was undertaken with emphasis on leaktight containment. Three units were manufactured and they demonstrated satisfactory structural integrity and containment.

Evaluation tests were conducted at reduced temperatures, using air as the heat transfer medium, simulating the design operating conditions. The data were analyzed to verify the design method and extended to estimate the operating performance of the unit with HeXe 83.8 as the working fluid. On this basis, the unit is predicted to have the capability to operate at design conditions with a recuperator effectiveness of 0.941, a heat sink exchanger effectiveness of 0.946, and a total gas fractional pressure drop of 0.039.

SECTION 2

INTRODUCTION

NASA is currently engaged in the development of closed Brayton cycle system technology for generation of electric power in space. The system presently under consideration was chosen to investigate the means of producing power in the range of 2 to 10 KW_e for long durations of time. Such a system is potentially applicable to supplying the power for a manned orbiting space station or base. For extended missions, radioisotope energy sources have been considered and were found to be suitable candidates to deliver the required thermal powers.*

The concept selected for the Brayton power conversion equipment incorporates a single-shaft Brayton Rotating Unit (BRU), consisting of a turbine, a compressor, and an alternator, coupled to a Brayton Heat Exchanger Unit (BHXU). The BHXU consists of two heat exchangers, a gas-to-gas recuperator and a gas-to-liquid heat sink exchanger, plus the gas system ducting that connects the heat exchangers with the BRU. The recuperator transfers heat from the low-pressure turbine exhaust gas to the high-pressure gas leaving the compressor. The heat sink exchanger transfers heat from the low-pressure gas leaving the recuperator to the liquid coolant in the radiator loop for ultimate rejection as waste heat from the cycle.

The program described here includes the design, fabrication, and testing of the BHXU prior to delivery of the unit to NASA for system integration and testing. Cycle conditions on which the design of the BHXU is based are summarized in Table I. These design goals were established by NASA in conjunction with a systems analysis performed to identify operating conditions that result in high overall conversion efficiency.

The final design of the BHXU is described in Section 3. Also included in Section 3 is a summary of the design and off-design performance of the unit under conditions specified by NASA. The thermal and structural design of the BHXU, including parametric tradeoff studies that identify the optimum heat exchanger configurations, are described in Section 4. Fabrication is discussed in Section 5. Testing and test results are presented in Section 6. Detailed technical discussions of several aspects of the design are included as appendixes.

---

*McKhann, G. G., "Preliminary Design of a Pu-238 Isotope Brayton Cycle Power System for MORL," Vol I - Technical Summary, Report No. SM-48832 (NASA CR-68809), Douglas Aircraft Co., Inc., September 1965.

TABLE I

BHXU DESIGN CONDITIONS

Working fluid (gas)	Xe-He mixture Molecular weight = 83.8
Liquid coolant	Dow Corning 200 fluid (2 centistokes at 25°C)
Recuperator hot side	
Gas flow rate, lb/sec	1.28
Inlet temperature, °R	1701
Inlet pressure, psia	24.1**
Recuperator cold side	
Gas flow rate, lb/sec	1.267
Inlet temperature, °R	738
Inlet pressure, psia	43.1**
Recuperator effectiveness	0.95
Heat sink heat exchanger	
Gas exit temperature, °R	540
Effectiveness	0.95
Capacity-rate ratio $\left(\frac{\text{hot side}}{\text{cold side}}\right)$	0.87
Maximum liquid pressure drop, psi	25
Overall BHXU gas pressure drop, percent	4.5

**Structurally, the recuperator hot side is designed to withstand 30.5 psia and the cold side 56.0 psia.

SECTION 3

DESCRIPTION OF DESIGN AND PERFORMANCE OF THE BRAYTON HEAT EXCHANGER UNIT (BHXU)

PACKAGED CONFIGURATION

The layout of the BHXU, selected from several layouts recommended at the conclusion of the preliminary design study, is shown in Drawing SK 51365 which appears at the end of this section. The BHXU final arrangement following detail design is shown in Drawing 187370 at the end of this section. This drawing also illustrates the overall packaging of the BHXU with the Brayton Rotating Unit (BRU), which consists of the turbine, alternator, and compressor. A complete assembly of the BHXU is shown in Figure 1.

The overall dimensions of the BHXU/BRU package are 22.5 by 49.5 by 56.0 in. Estimated weight of the BHXU is 440 lb.

COMPONENT DESCRIPTION

The main part of the BHXU consists of a gas-to-gas recuperator and a gas-to-liquid heat sink exchanger joined by a transition section that manifolds and forms a rigid structure between the two components.

The recuperator design is summarized in Table 2. The recuperator is a pure counterflow plate-fin unit (as shown in Figure 2), with crossflow triangular end sections providing fluid access to the core. The counterflow section uses rectangular offset fins, 0.153 in. high on the low-pressure side and 0.125 in. high on the high-pressure side, in a single-sandwich arrangement on each side. Each sandwich contains three flow-divider strips that run the length of the core and prevent fluid crossflow. The sides of the flow passages are closed by 0.1-in. thick side strips. The construction material is 347 stainless steel throughout the heat exchanger. Nominal tube plate thickness is 0.008 in., but this thickness is increased near the exchanger side plates to provide a more nearly uniform distribution of thermal stresses during transient conditions. Thus, the first, second, and third plates in from the side plates are 0.020, 0.016, and 0.012 in. thick, respectively.

The heat sink heat exchanger design is summarized in Table 3. This exchanger is an eight-pass, cross-counterflow, plate-fin unit, as shown in Figure 3. The fin sandwiches are rectangular offset, 0.125 in. high on the gas side and 0.05 in. high on the liquid side, in a single-sandwich arrangement on each side. During operation of the heat exchanger, alternate liquid sandwiches are redundant (i.e., of the 32 liquid sandwiches, 16 are inactive at any given time) so that, from a thermodynamic standpoint, the gas-side passages are double-sandwich passages. To maintain separation of the two liquid loops, turning between successive liquid passes is accomplished with mitered fin turning sections rather than manifolds. These turning sections are triangular sections of fin sandwich, of the same fin geometry as the rest of the core (rectangular offset, 20 fins per in.), sized to give the same fluid flow area in the turn as in the pass; i.e., the height of the turn triangle is

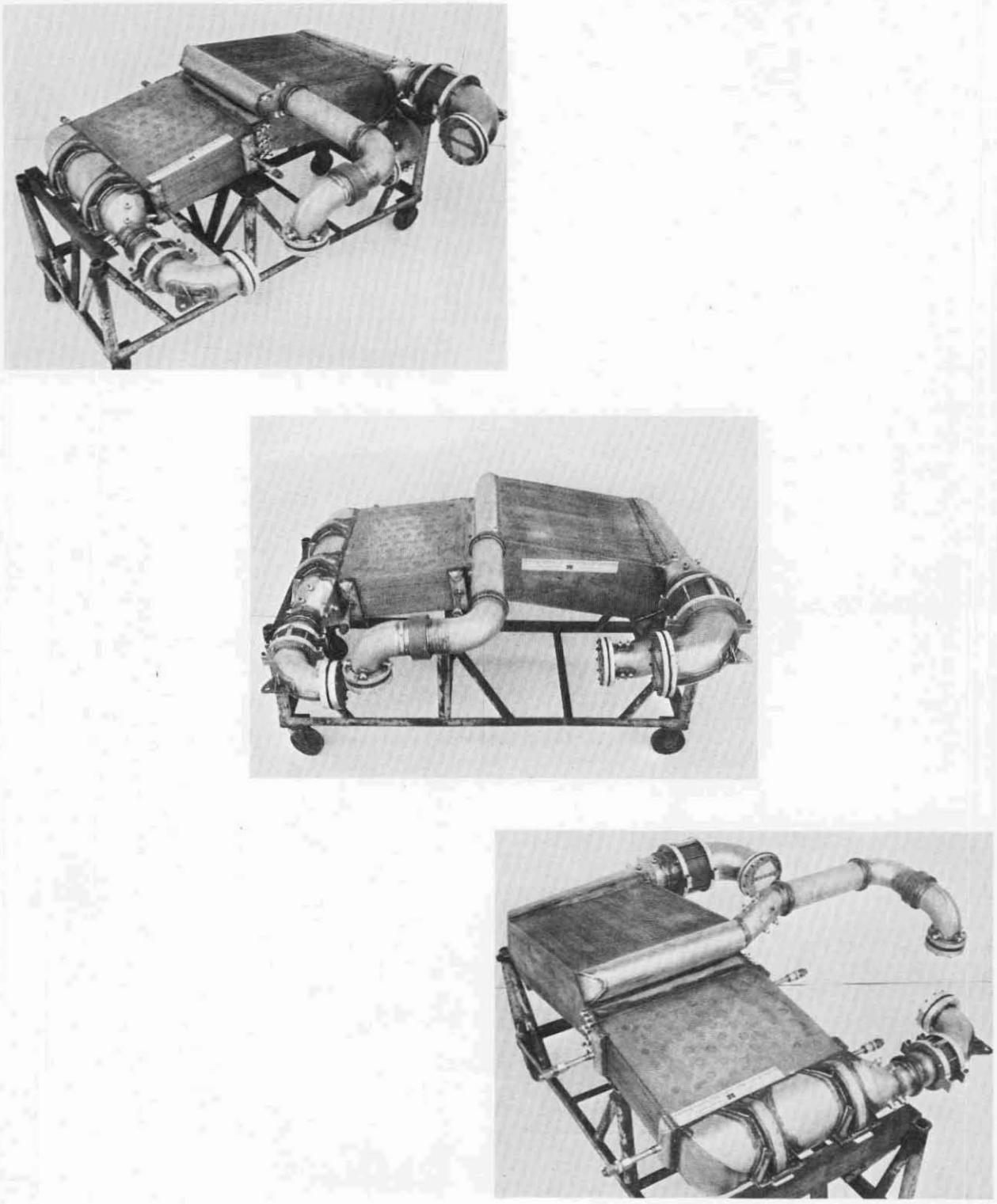

F-9668

Figure 1. Brayton Heat Exchanger Unit

TABLE 2

RECUPERATOR DESIGN SUMMARY

Counterflow Section	
Flow length	19.7 in.
Flow width	8.45 in.
Hot-side fins	
Height	0.153 in.
Fins per inch	16
Thickness	0.004 in.
Type	Offset rectangular
Cold-side fins	
Height	0.125 in.
Fins per inch	16
Thickness	0.004 in.
Type	Offset rectangular
Nominal plate thickness	0.008 in.
Number of sandwiches, each side	66
Stack height	19.8 in.
Side plate thickness	0.06 in.
Weight	178 lb
Triangular End Sections	
Height, hot end	3.85 in.
Height, cold end	1.3 in.
Ratio*, hot end	0.65
Ratio, cold end	0.55
Fin configuration	
Height	Same as counterflow section
Fins per inch	10
Thickness	0.004 in.
Type	Plain rectangular
Weight	23 lb

*Ratio of projected width of hot-side passage to core width. See Figure 6.

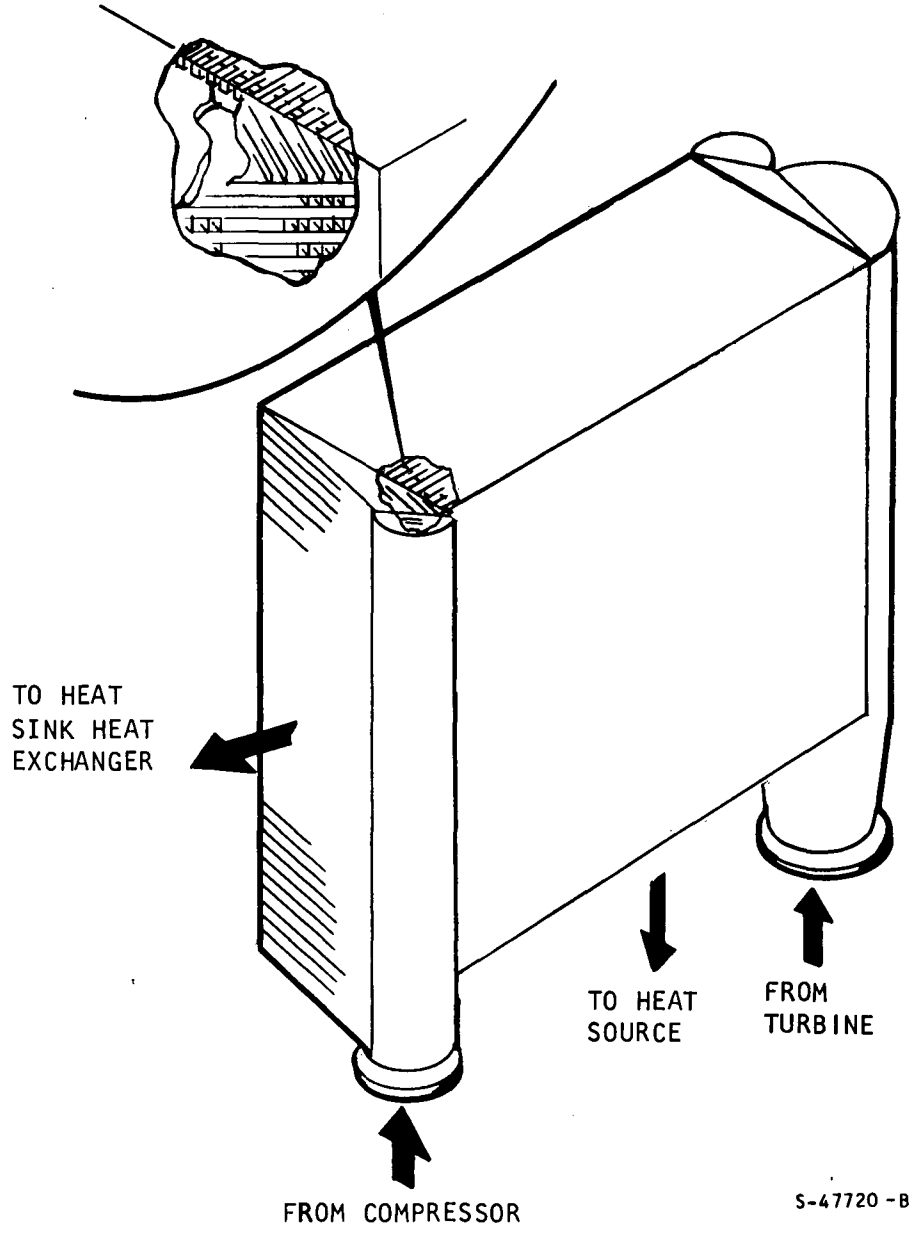

Figure 2. Brayton Cycle Recuperator

TABLE 3

HEAT SINK EXCHANGER DESIGN SUMMARY

Gas flow length	16.15 in.
Liquid flow length (per pass)	20.0 in.
Number of liquid passes	8
Gas-side fins	
Height	0.125 in.
Fins per inch	16
Thickness	0.004 in.
Type	Offset rectangular
Liquid-side fins	
Height	0.05 in.
Fins per inch	20
Thickness	0.002 in.
Type	Offset rectangular
Nominal plate thickness	0.010 in.
Number of gas sandwiches	31
Number of liquid sandwiches	32
Stack height	6.4 in.
Side plate thickness	0.06 in.
Weight (dry)	160 lb
Weight (wet)	174 lb

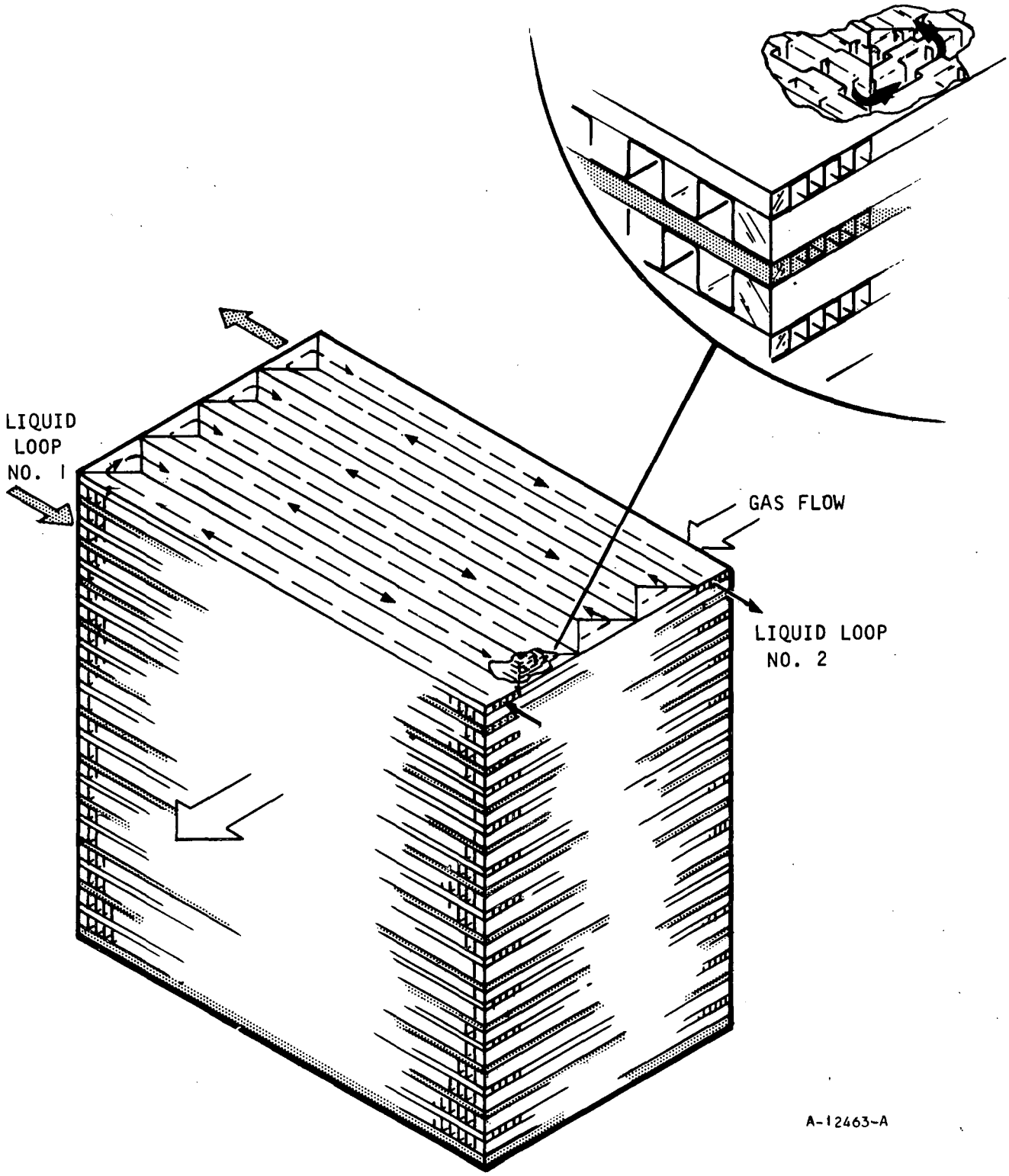

Figure 3. Eight-Pass, Cross-Counterflow, Plate-Fin Heat Exchanger with Two Liquid Loops

equal to the width of the liquid pass. Successive liquid passes within each sandwich are separated by 0.05 in. thick side strips. Header bars and side strips at the external faces of the core are 0.1 in. thick. The construction material is 347 stainless steel throughout the heat exchanger. As in the recuperator, tube plate thickness is increased in the regions adjacent to the side plates. Thus, a 0.016-in. thickness is used for the four plates nearest each side, whereas the remaining plates are 0.010 in. thick.

Between recuperator and heat sink exchanger is a short transition section that turns and distributes the gas flow from the recuperator low-pressure outlet into the heat sink exchanger. The transition section contains five turning vanes to ensure uniform flow at the heat sink exchanger inlet.

Gas manifolds are provided to collect and distribute all fluid flow through the recuperator and heat sink heat exchanger. Manifolds for the two heat exchangers are shown on Drawing 187370. These manifolds are shaped to obtain uniform flow distribution in the heat exchanger cores. In the case of the recuperator low-pressure inlet, the ideal manifold shape would involve a gas flow area that tapers in the gas-flow direction from maximum at the inlet to 10 percent of maximum at the far end. This taper is such that the small amount of friction pressure loss would be offset by momentum recovery, resulting in a static pressure profile at the recuperator inlet that is approximately constant and matches the (constant) static pressure profile in the transition section at the recuperator outlet. In actual practice, due to fabrication limitations, the low-pressure inlet manifold is tapered for only part of its length, resulting in a non-ideal static profile that results in some flow maldistribution. At the heat sink exchanger outlet, it is not possible to obtain uniform static pressure, since in this manifold both flow friction and increasing momentum tend to decrease static pressure in the direction of gas flow. This outlet manifold is sized such that the total static pressure loss along the manifold is approximately 10 percent of the pressure drop in the heat sink exchanger core. Inlet and outlet manifolds on the recuperator high-pressure side are sized such that the pressure rise profile in the inlet manifold (due to momentum recovery) matches the loss profile in the outlet manifold, resulting in equal static pressure differences for all flow paths through the heat exchanger.

Inlet and outlet liquid manifolds are provided for the two independent liquid circuits in the heat sink heat exchanger. These manifolds are sized for negligible liquid pressure drop.

Ducts for the gaseous working fluid connect the recuperator and heat sink heat exchanger manifolds to the BRU, the heat source, and the gas management system. (A section of ducting between the compressor outlet and the recuperator inlet is interchangeable with a section provided by NASA that contains an injection and vent valve which connects to the gas management system.) The duct from the recuperator to the turbine exhaust is Hastelloy X. All other ducts are 347 stainless steel. The duct diameters are as follows:

Compressor outlet duct - 3.5 in.

Recuperator high pressure outlet duct - 4.5 in.

Turbine outlet duct - 6 in.

Compressor inlet duct - 4 in., tapered to 3.5 in. at compressor inlet

Bellows are provided in the BHXU to accommodate differential thermal growth of the BRU and BHXU with minimum thermal loads. Bellows are located between the recuperator and the turbine, between the compressor and heat sink exchanger, and between the compressor and recuperator. The high-temperature bellows between turbine and recuperator is Hastelloy X, while the others are 347 stainless steel.

A lightweight mounting system is incorporated to support the BHXU and to minimize the growth differentials between the BHXU and BRU. The primary mounts support the BHXU at six locations, which are all positioned in one plane. Two are located on the transition section (between recuperator and heat sink exchanger), two on the recuperator high pressure outlet manifold, and two on the heat sink heat exchanger gas outlet manifold. Additional mounts on the ducts connecting to the BRU turbine outlet and compressor inlet are provided to react unbalanced pressure forces arising from the use of bellows.

Instruments are installed throughout the BHXU, as shown in Drawing 187370, Sheet 2, to monitor temperature and pressure during operation of the unit.

Flanges are attached to all ducts to form weldable connections with the mating equipment. The flanges used are the top and center ones of the three types shown on Drawing SK 51365. The flange shown in the center view is used on the duct sections immediately adjacent to the turbine and compressor. The flange in the top view is used for all other connections of the ducts to the manifolds, heat source, gas management system, and BRU. These flanges provide for simple and accessible connections for assembly and disassembly of components with reweldable characteristics.

Gas flow to the BHXU enters the recuperator low-pressure side from the turbine exhaust. This flow passes through the recuperator to the heat sink heat exchanger and is then ducted to the compressor inlet. The compressor discharge gas flows through the recuperator high-pressure side and exits to the heat source. Liquid coolant in the radiator loop flows from the radiator through one of the two independent liquid circuits in the heat sink heat exchanger and then back to the radiator.

PERFORMANCE

The performance of each of the two heat exchangers in the BHXU, based on the results of the performance and acceptance tests, has been estimated for the design and off-design conditions of temperature and flow listed in Table 4. The resultant performance map, representing the final performance estimate for the BHXU, is given in Table 5. A breakdown of the gas pressure drops in the heat exchangers, manifolds, and ducts, based on design calculations, is given in Table 6.

TABLE 4

DESIGN AND OFF-DESIGN CONDITIONS

Condition	Design	Off-design					
		Case I	Case II	Case III	Case IV	Case V	Case VI
Hot Side							
Gas flow rate, lb/sec	1.28	0.38	0.55	0.76	1.0	1.5	2.5
Recuperator inlet temperature, ^{0}R	1701	1709	1705	1701	1701	1701	1701
Recuperator inlet pressure, psia	24.1	6.86	9.95	13.9	18.1	27.2	45.3
Cold Side							
Recuperator inlet temperature, ^{0}R	738	740	739	738	738	738	738
Recuperator inlet pressure, psia	43.1	12.8	18.5	25.6	33.7	50.5	84.25

TABLE 5

DESIGN AND OFF-DESIGN PERFORMANCE

Condition	Recuperator Effectiveness*	Heat Sink Exchanger Effectiveness**	Gas Pressure Drop, Percent	Liquid Pressure Drop**, psi
Design	0.941	0.946	3.9	4.5
Off-design				
I	0.955	0.965	7.5	1.0
II	0.955	0.965	6.3	1.5
III	0.95	0.96	5.3	2.3
IV	0.945	0.955	4.8	3.2
V	0.935	0.94	3.9	5.3
VI	0.92	0.92	3.0	10.1

*Based on a cold-side flow rate equal to 99 percent of the hot-side flow.
**Based on a gas capacity rate equal to 87 percent of the liquid capacity rate.

TABLE 6

BHXU PRESSURE DROPS

		Pressure Drop, percent
Recuperator		1.86
Recuperator end sections		0.77
Heat sink exchanger		0.56
Manifolds		
Cold inlet	0.095	
Cold outlet	0.068	
Hot inlet	0.198	
Hot outlet	0.019	
Total manifolds		0.38
Ducts		
Hot inlet	0.16	
Hot outlet	0.16	
Cold inlet	0.13	
Cold outlet	0.09	
Total ducts		0.54
Total BHXU		4.11

FOLDOUT FRAME 1

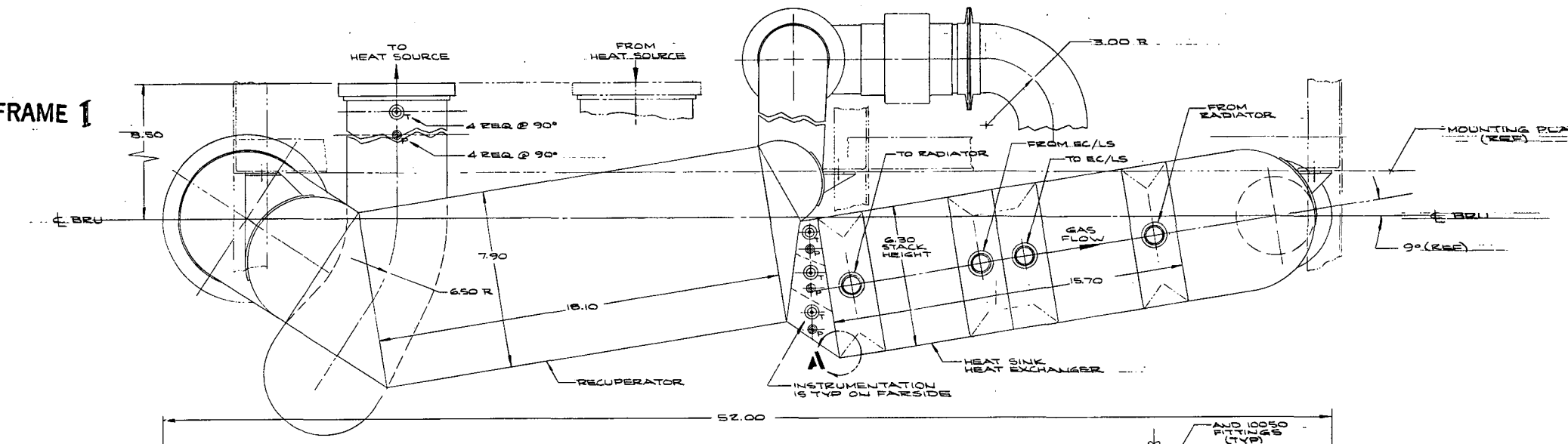

FOLDOUT FRAME II

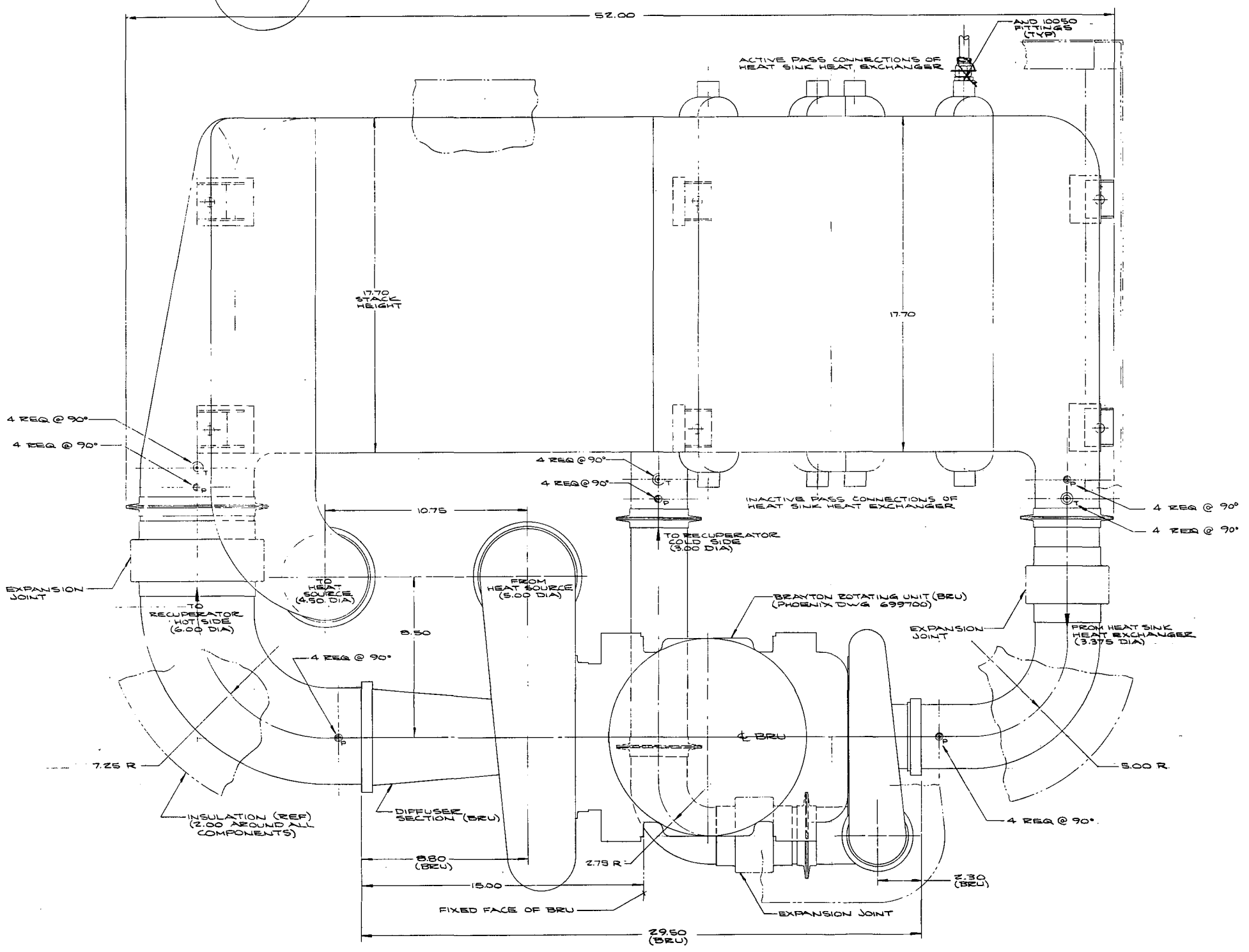

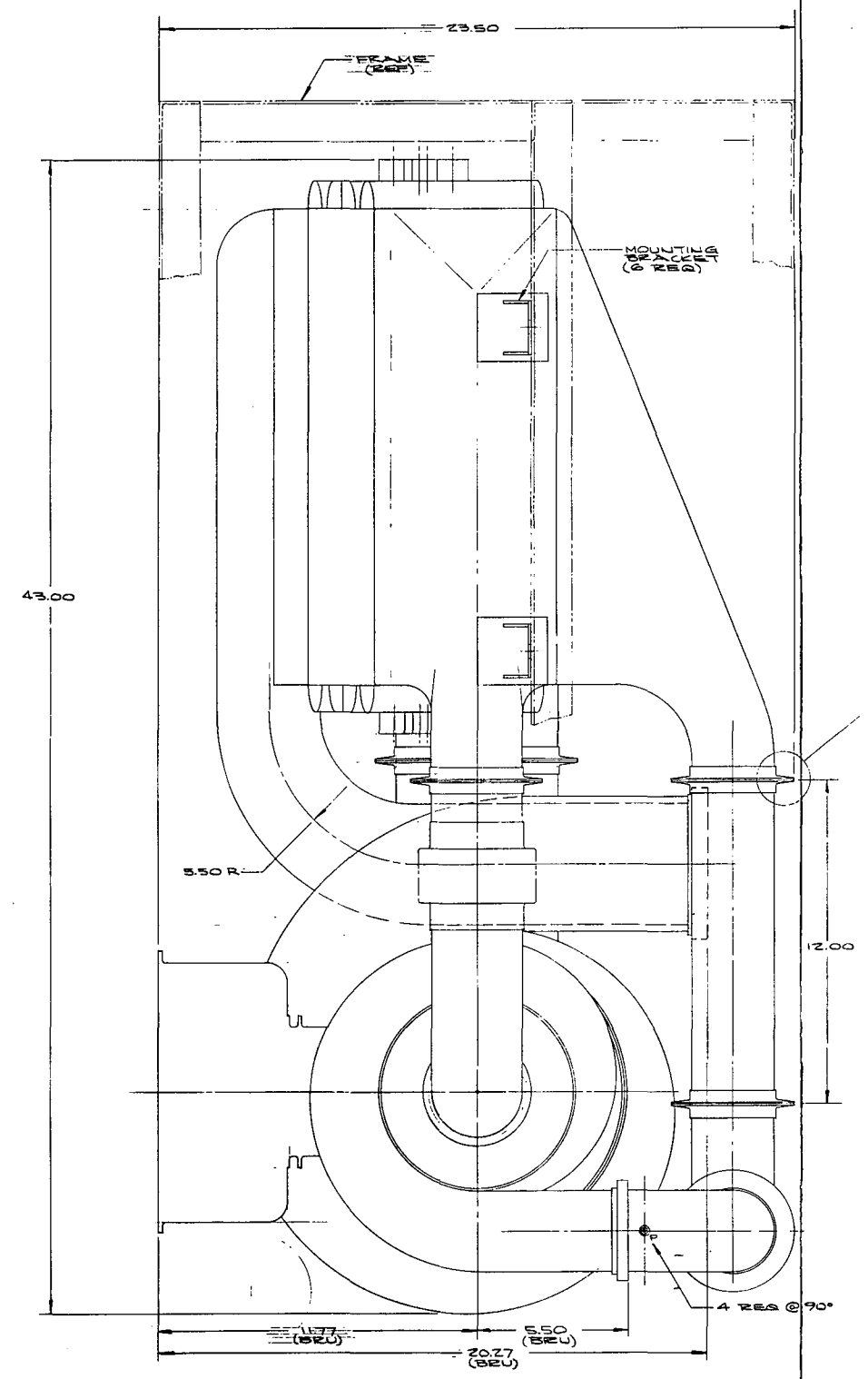

FOLDOUT FRAME III

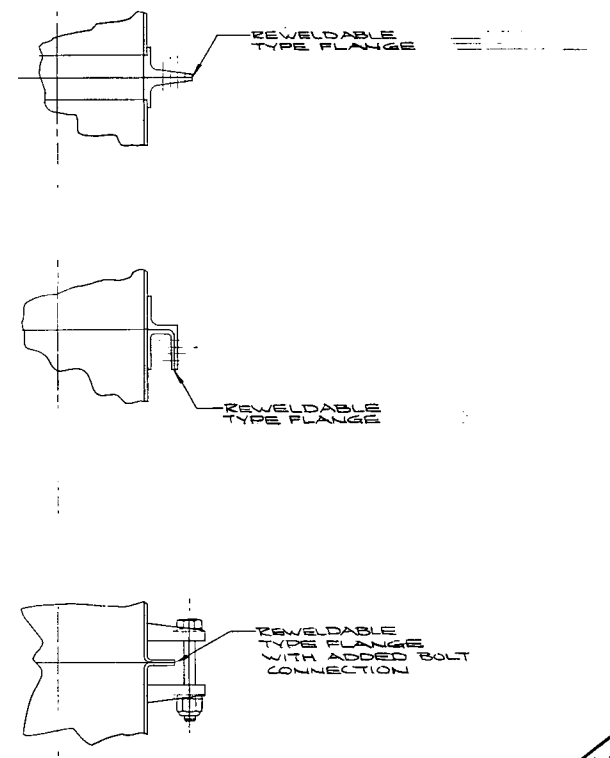

THE ABOVE THREE VIEWS SHOW VARIOUS FLANGE COMPINGURATIONS (TYP)
SCALE: 1/1

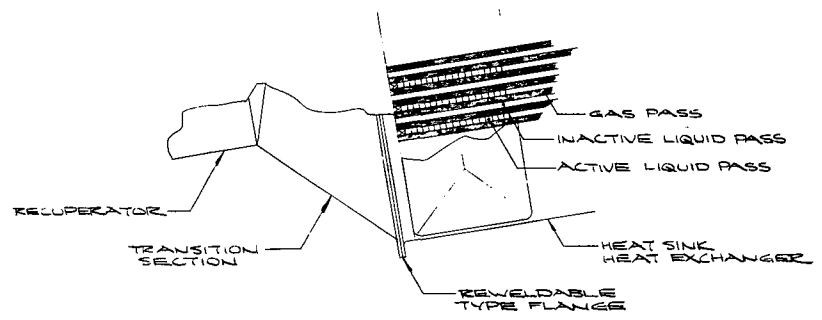

VIEW A
SHOWING RECUPERATOR TO HEAT SINK CONNECTION
SCALE: 1/1

2. INSTRUMENTATION LEGEND
PRESSURE TAPS INDICATED THUS ⊕
TEMPERATURE PROBES INDICATED THUS ⊕
1. FOR REFERENCE PURPOSES ONLY, DRAWING MAY BE SCALED FOR DIMENSIONS NOT SHOWN.

NOTES: UNLESS OTHERWISE SPECIFIED

REVISIONS				
SYM	ZONE	DESCRIPTION	DATE	APPROVED

ITEM NO.	PART NO.	SYM	DESCRIPTION	QUAN REQ'D	MATERIAL AND SPECIFICATION	SPEC
	ASSY		LIST OF MATERIAL			

UNLESS OTHERWISE SPECIFIED DIMENSIONS ARE IN INCHES
DIMENSIONS AND TOLERANCES PER MIL-STD-100
SURFACE ROUGHNESS PER MIL-STD-10A
DIMENSIONS APPLY AFTER PLATING
BASIC CONTROL PER SPEC SHEET

SIGNATURES	DATES
ANTHONY	7-17-67

HEAT TREATMENT PROCESS SPEC NO. SPEC

AiRESEARCH MANUFACTURING COMPANY OF CALIFORNIA

DESIGN STUDY RECOMMENDED LAYOUT BRAYTON HT. EX. UNIT

	70210	SK 51365

SCALE 1/4 WEIGHT SHEET 1 OF 1

Page intentionally left blank

Page intentionally left blank

SECTION 4

DESIGN STUDY

THERMAL DESIGN

Heat Transfer Data

Experimental heat transfer and friction loss data were used in the analysis of all heat exchanger types considered. Direct test data are available for the fin surfaces considered for the recuperator and the heat sink exchanger hot-side passage, whereas the performance of the fin surface used in the heat sink exchanger cold-side passage (20 fins per in., 0.05 in. high) was estimated from test data on a different fin set (20 fins per in., 0.1 in. high). The UA and pressure drop margins used for the plate-fin cores were consistent with the results of previous testing on the NASA solar Brayton cycle (argon-to-argon) recuperator. Recent data from Stanford on the 0.05 in. high sandwich indicate that actual heat transfer coefficients are between 20 and 25 percent less than what were estimated for this fin set during the design analysis. Since the ratio of liquid-side to gas-side conductance in the heat sink exchanger is quite high, this amount of change in the liquid-side coefficient caused a reduction of only 6 percent in overall UA, which was well within the original allotment of UA margin and thus did not require redesign of this exchanger. The data on the 0.05 in. high fins were all obtained from tests using air as the heat transfer fluid, however, and application of these data to liquid flow introduced an additional uncertainty in the design. Final UA margins incorporated in the designs for the two heat exchangers were 20 percent for the recuperator and 10 percent for the heat sink exchanger.

One of the candidate core geometries for the gas-to-liquid heat exchanger was the cross-counterflow tube-fin matrix, utilizing strip fins and a ring-dimpled tubing design. This matrix is the one considered by AiResearch for the NASA solar Brayton cycle heat sink heat exchanger (argon-to-liquid exchanger). Prior to the heat sink exchanger program, data did not exist for flow outside of this particular type of strip-finned matrix, nor was the small amount of data on liquid flow inside dimpled tubing sufficient for design purposes. During the design of the argon-to-liquid heat exchanger, AiResearch utilized f and j data, experimentally measured during a previous program, for flow across a disc-finned tubular matrix of similar geometry to the strip-finned matrix (i.e., same tube spacing, tube diameter, and number of fins per inch) and experimental data on gas flow inside dimpled tubes. Margins required on UA and pressure drop are somewhat higher than the margins required for plate-fin cores.

The following section of this report describes a parametric study of heat exchanger designs, utilizing AiResearch computer programs that are described in Appendix A. The heat exchanger weights generated during this phase of the

program were of a preliminary nature and substantially lower than final design weights. Specifically, final design heat exchanger sizes increased for two reasons. During final design, a new set of fluid properties was used for the xenon/helium mixture, based on data from the University of Iowa, with viscosity and thermal conductivity values predicted using the Chapman-Enskog theory. Use of these data caused a reduction of about 7 percent in estimated gas film coefficients (due primarily to a higher Prandtl number at elevated temperatures) and a consequent increase in heat exchanger sizes. In addition, during the detail design study the UA margins on heat exchanger performance were increased by 10 percent while gas pressure drops were decreased by about 10 percent.

Parametric Design Study

1. Recuperator

a. Configuration

During a previous study of recuperator designs for the NASA Solar Brayton Cycle System (Contract 3-2793), a number of heat exchanger configurations were studied extensively to determine minimum weight and size design solutions. The configurations studied were the following:

(a) Multipass cross-counterflow plate-fin

(b) Pure counterflow plate-fin

(c) Multipass cross-counterflow tubular

(d) Pure counterflow tubular

Applying the results of that study and the present one, several conclusions regarding the optimum heat exchanger configuration can be made. First, the pure counterflow tubular matrix can be eliminated from consideration as both one of the heaviest and one of the largest of the possible solutions. This occurs because of the relatively poor heat transfer coefficients obtained with flow parallel to tube bundles and because of the inherent low packing density of heat transfer surface in tubular as opposed to plate-fin matrixes. Secondly, of the two cross-counterflow units, plate-fin and tubular, the plate-fin matrix will generally result in heat exchanger configurations which are both heavier and more difficult to package than the tubular cores. The difficulty in packaging occurs because of the large no-flow dimension required to meet pressure drop limitations on both the multipassing and single-pass sides of the exchanger. The large no-flow requirement exists for the cross-counterflow tubular unit also, although it has been found that design solutions are available for this configuration through the use of folded or concentric ring packaging. Finally, comparing the pure counterflow plate-fin matrix with the cross-counterflow tubular matrix, the plate-fin unit will be more compact and simpler to package,

and may also result in the minimum-weight solution. From preliminary packaging studies it was found to be completely impossible to fit a tubular unit within the BHXU envelope provided by the problem statement (tubular units were three times the size of plate-fin units). For these reasons, the pure counterflow plate-fin heat exchanger geometry is considered exclusively for the gas-to-gas recuperator.

The following parametric study is based on the use of the pure counterflow plate-fin exchanger, with triangular, cross-flow end sections for introducing and removing the fluids from the core (see Figure 4).

b. Fin Set Selection

To determine the geometry for minimum recuperator weight, a series of recuperator designs was calculated using several different fin sandwich configurations. Single sandwich construction on each side was used in all cases. The designs are based on the use of 8-mil plates and 347 stainless as the material of construction throughout the core. The geometries of the fin sets used are given in Table 7. The fin efficiency was relatively high for all designs studied (87 percent was the minimum), so that the use of fins thicker than four mils was not considered. All fins used are geometries for which experimental curves have been obtained of friction factor, f, and Colburn modulus, j, as functions of Reynolds number.

TABLE 7

FIN SANDWICH GEOMETRY

Fin Number	Number of Fins per Inch	Fin Type	Plate Spacing, in.	Offset Length, in.	Fin Thickness, in.
1	20	Rect.	0.075	1/10	0.004
2	20	Rect.	0.100	1/8	0.004
3	16	Rect.	0.125	1/8	0.004
4	16	Rect.	0.153	1/7	0.004
5	12	Rect.	0.178	0.178	0.004

Figure 5 shows recuperator weight (counterflow section only) as a function of gas pressure drop for seven different combinations of the fin sets of Table 7. The curves were generated with the aid of the AiResearch counterflow plate-fin design program and include the effect of axial conduction of heat in the core. The effect of axial conduction on heat transfer matrix selection is to penalize the more compact surfaces in favor of the more widely spaced arrays, because, for a given gas pressure drop, the wider spacings

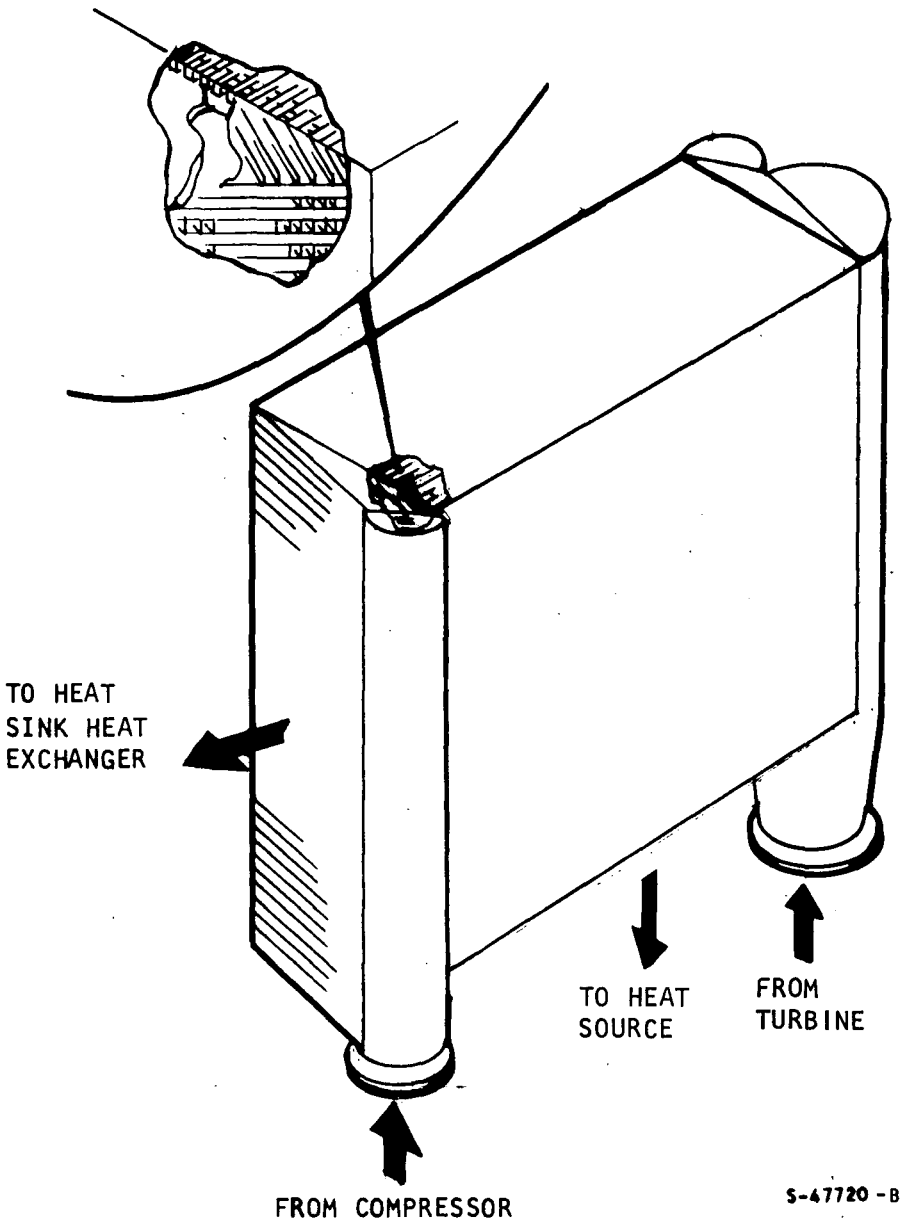

Figure 4. Counterflow, Plate-Fin Recuperator

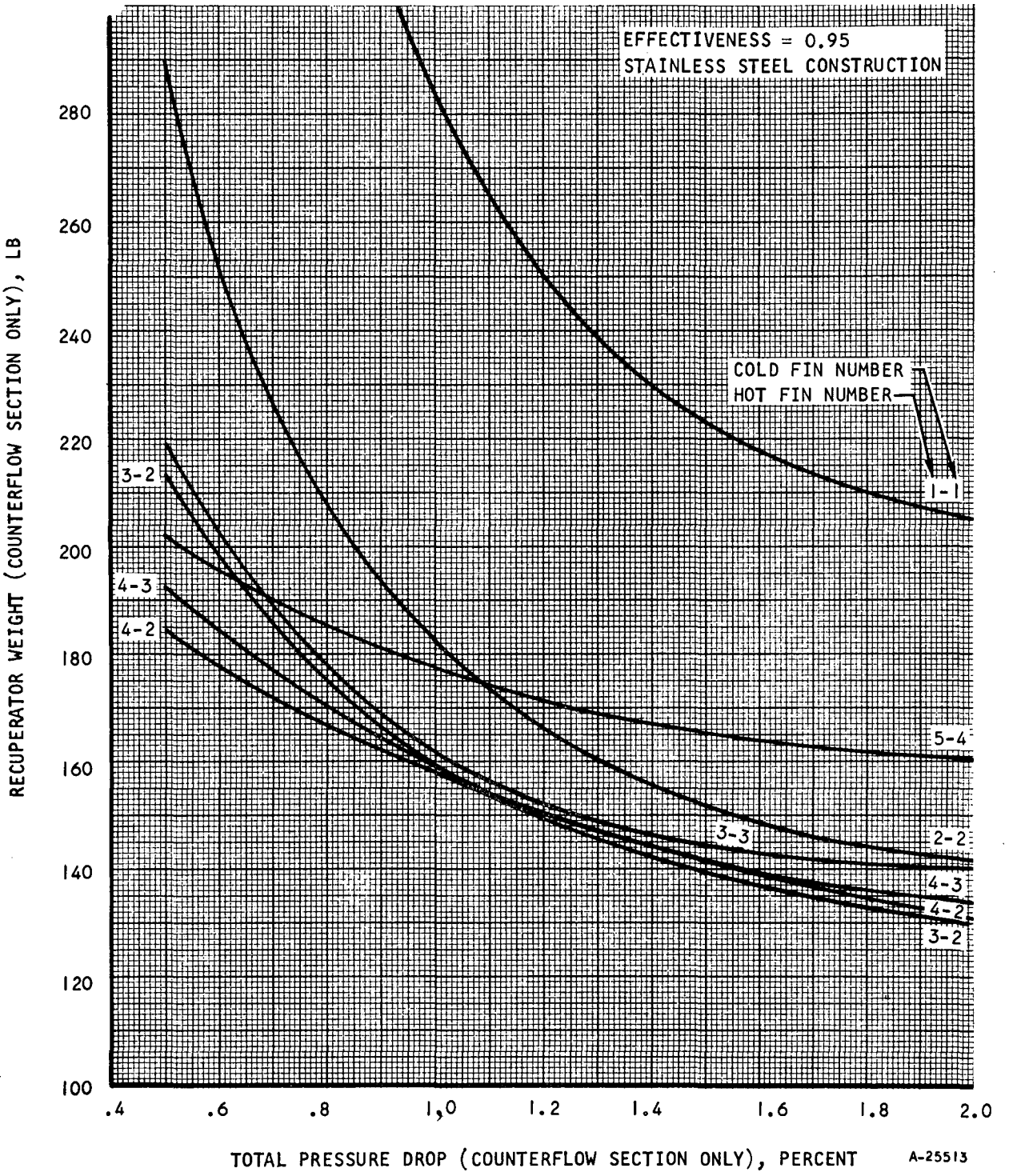

Figure 5. Variation of Recuperator Weight with Pressure Drop and Fin Sandwich Geometry

result in a larger gas flow length and thus a reduced temperature gradient for axial conduction. Over the pressure drop range shown, for example, the minimum weight solution would have been fin set 2-2 and the second best would have been fin set 3-2 if the effect of axial conduction had not been included in the calculations. Figure 5 also shows the trend toward less compact surfaces for minimum weight as the pressure drop (and thus the gas flow length) decreases.

Based on Figure 5, it was decided to include fin sets 3-2, 4-3, and 4-2 (hot fin number-cold fin number) in a further analysis including the triangular cross-flow end section design. A series of triangular end section designs was calculated for the cores corresponding to each of these fin sets, using the AiResearch end section design program. The parameters varied in these calculations were end section height, H, and ratio, X/Z, as defined in Figure 6 below. (For this parametric study, X/Z = Y/Z in all cases.)

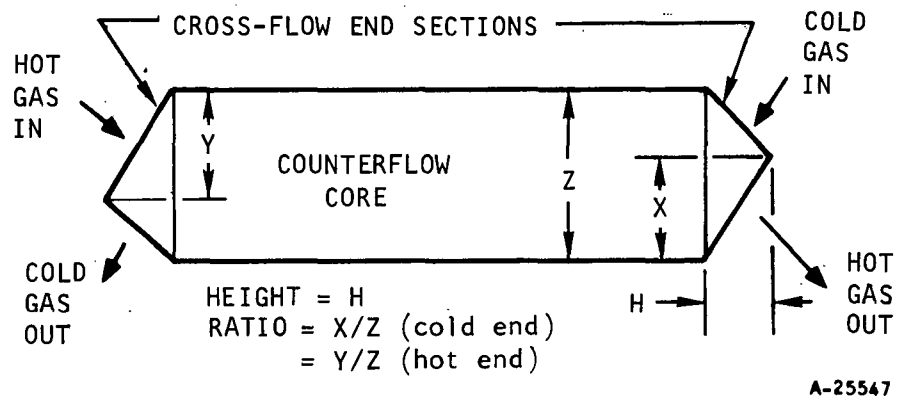

Figure 6. Recuperator Schematic

The end section fins used are plain rectangular, 10 fins per inch, in all cases. Ten fins per inch has been determined to be the minimum allowable based on fabrication limitations.

The end sections calculated in this portion of the study do not take into account the effect of end section design on core flow distribution and are simply an initial estimate of the tradeoff between weight and pressure drop for this component. The redesign of the end sections to ensure uniform core flow is described in a later section of this report.

It was determined that, with core fin sets 3-2 and 4-3, the optimum value of the end section ratio is approximately 0.7 for all cases, but that the pressure drop tradeoffs are such as to result in a relatively broad minimum weight region, so that values of the ratio from about 0.6 to 0.8 represent reasonable design solutions. These conclusions are illustrated in Figure 7, where the total of end section pressure drops, calculated as percentages of the respective gas pressure levels, is plotted as a function of end section ratio for heights of 2, 3, and 4 in. For core fin set 4-2, the lower ratio of cold-side flow area (0.100-in. passages) to hot-side flow area (0.153-in. passages) results in lower optimum ratios of about 0.6.

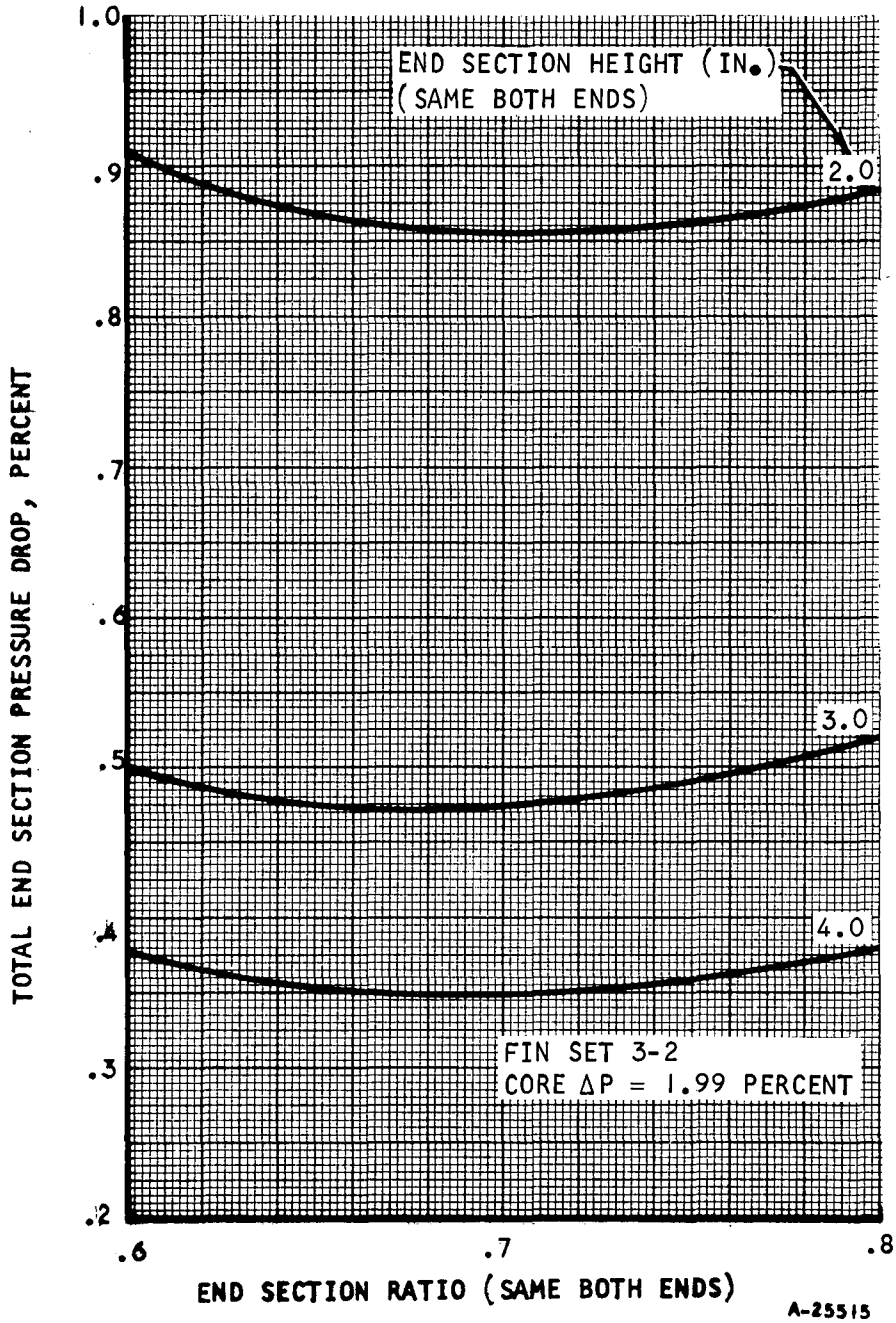

Figure 7. End Section Pressure Drop as a Function of End Section Geometry

Using a value of 0.7 for the end section ratios (0.6 for fin set 4-2), curves of total recuperator weight, including counterflow core and crossflow end sections, are now plotted as a function of combined core and end section pressure loss for each of several core pressure drops. The curves corresponding to core fin set 4-3 are shown in Figure 8. By drawing a curve tangent to each of the curves for fixed core pressure drop, the locus of minimum weight recuperator designs is achieved; i.e., each point on the dashed line in Figure 8 represents a recuperator with an optimized core/end section pressure drop split for the value of total pressure drop given by the abscissa.

Similar curves for the recuperators with core fin sets 4-2 and 3-2 are shown in Figures 9 and 10. In these figures (as in the preceding figure), the same end section height is assumed at each end of the recuperator. During final recuperator sizing, different heights and ratios are used at the opposite ends of the recuperator in order to match end section pressure drops and thus obtain improved flow distribution. As a result of this, the pressure drop split will vary somewhat from the "optimum" indicated by Figures 8, 9, and 10. A second modification may occur due to a change in the ratio of stack height to flow width for the recuperator core. The core designs assumed in Figures 8, 9, and 10 have height-to-width ratios of 2 to 1. As relative stack height is increased, the end section pressure drop decreases for a given end section height, resulting in a lower optimum value of end section pressure loss as well as a lower optimum end section height. It is convenient to adjust recuperator stack height to obtain a dimensional match between recuperator low pressure outlet face and the heat sink heat exchanger inlet face, as described in a later section.

Despite these two modifications which will occur during final sizing, the curves of Figures 8, 9, and 10 are useful for comparing recuperator designs and for examining the weight and pressure drop tradeoffs between the two heat exchangers in the BHXU system. A comparison of the three fin sets indicates that fin set 4-3 results in the lightest recuperators for the pressure drop range of 1.0 to 3.0 percent. There was found to be negligible variance in gas flow areas among the fin sets, and thus no relative advantages in terms of face area matching with the heat sink heat exchanger. Based on these factors, fin set 4-3 was selected for the remaining portions of the parametric study.

c. Fin Conductivity

The effect of fin conductivity on recuperator weight is shown in Figure 11. With a thermal conductivity in the range of 10 to 12 Btu/hr-ft-^{0}F for the recuperator operating temperature level, the 347 stainless used for the fins is seen to be about optimum. This optimum occurs as a result of the tradeoff between fin efficiency and heat exchanger axial conduction, both of which increase with increasing fin conductivity.

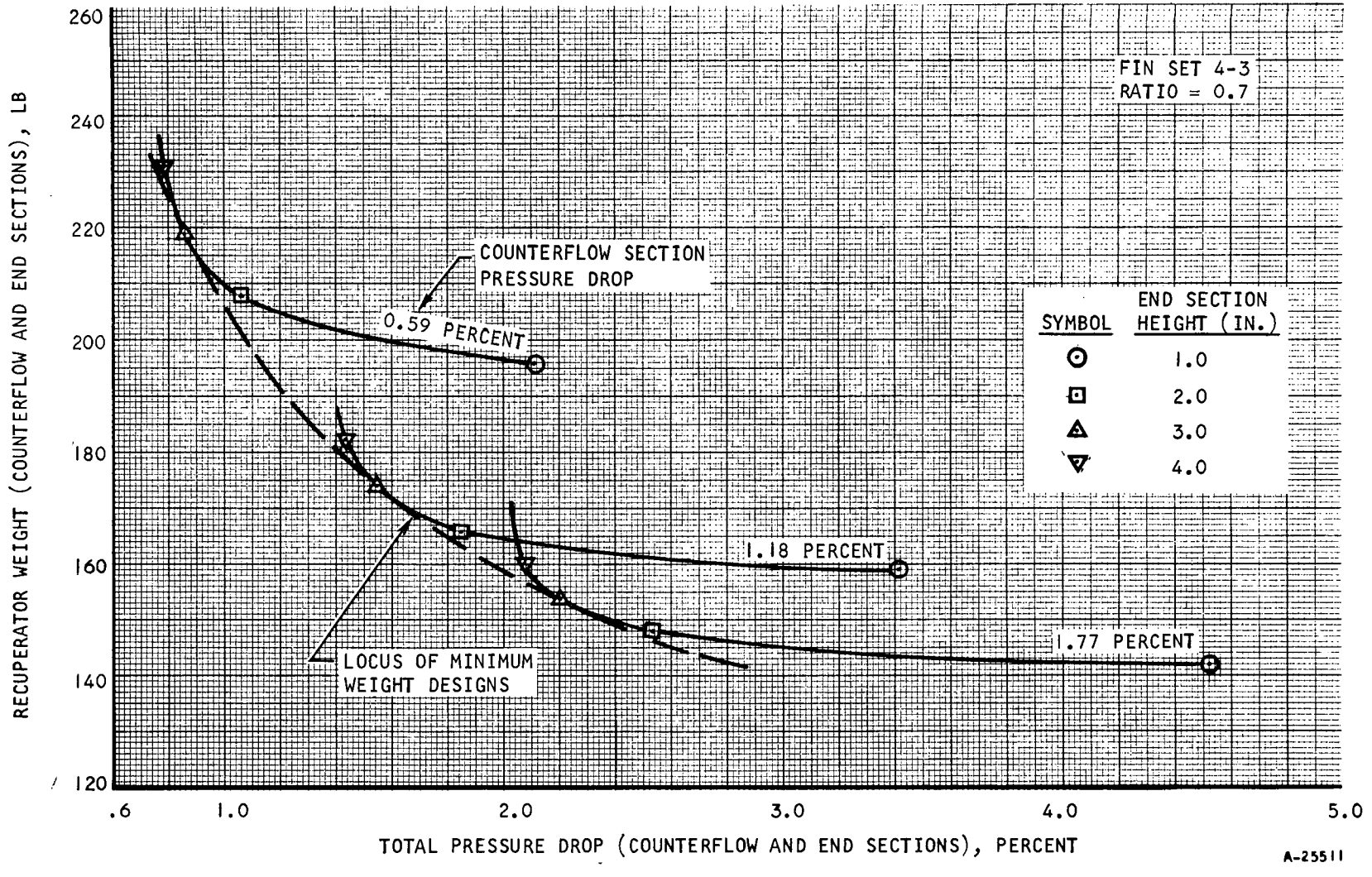

Figure 8. Recuperator Weight vs Total Pressure Drop, Fin Set 4-3

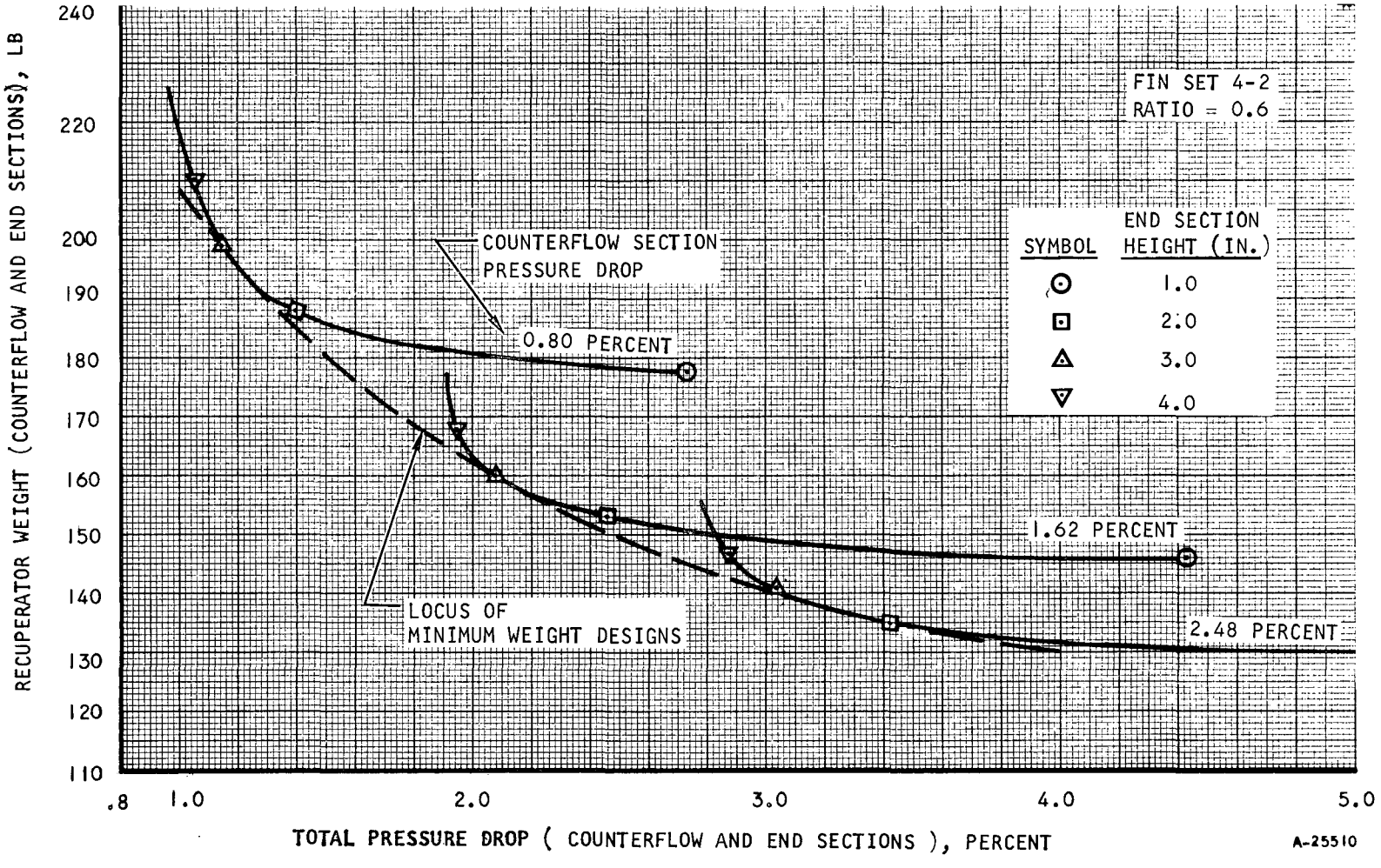

Figure 9. Recuperator Weight vs Total Pressure Drop, Fin Set 4-2

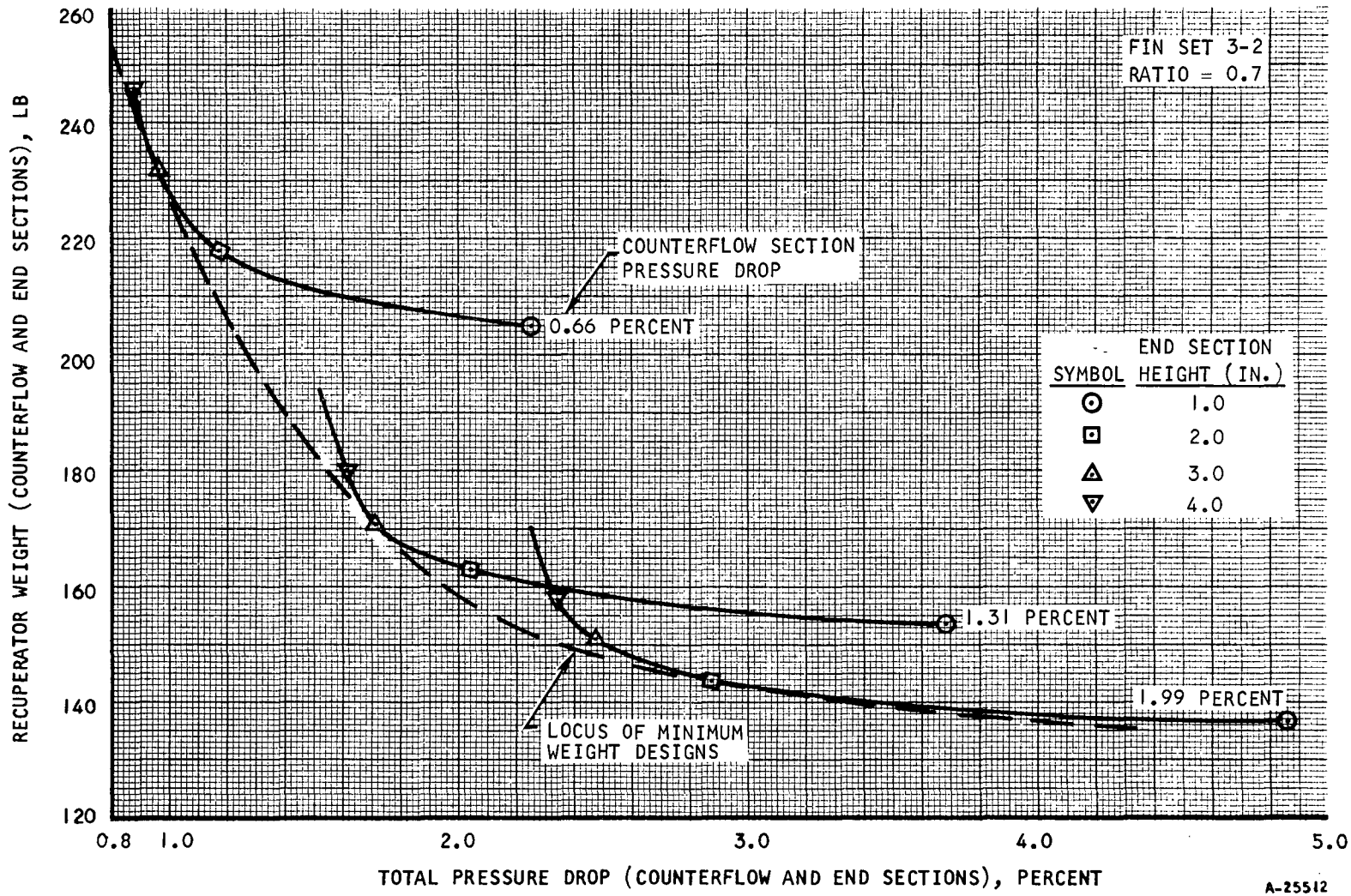

Figure 10. Recuperator Weight vs Total Pressure Drop, Fin Set 3-2

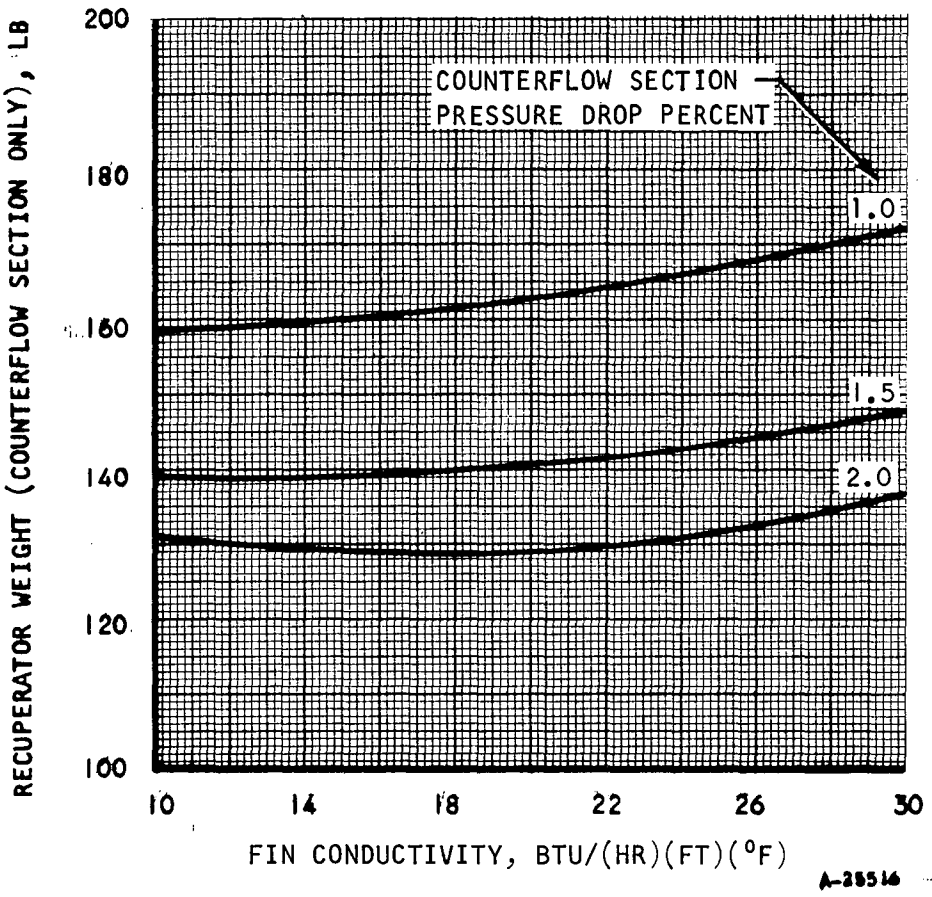

Figure 11. Variation of Recuperator Weight With Fin Conductivity

2. Heat Sink Heat Exchanger

a. Configuration

The following heat exchanger types have been considered as possibilities for the heat sink exchanger:

(a) Cross-counterflow tube-fin

(b) Counterflow plate-fin

(c) Cross-counterflow plate-fin

(d) Cross-counterflow tubular

Each of these configurations was analyzed to obtain initial comparisons of size and weight. These comparisons are made in the next subsection of this report, where the optimum gas pressure drop split between recuperator and heat sink exchanger and the resultant combined BHXU weight are obtained for each configuration. The following paragraphs discuss the heat exchanger geometry and flow configuration for each of the four exchanger types.

The cross-counterflow tube-fin heat exchanger utilizes serpentine tubes and strip fins that connect the tubes in each tube row (see Figure 12). The advantage of using strip fins, as opposed to disc fins, is that each of the two separate liquid loops in the core uses the same fin surface as gas-side heat transfer area, eliminating the duplication of area which would be required if separate disc fins were used on each tube. The designs considered utilize two tube rows per pass, with the operating and redundant loops arranged in one to two possible ways, as sketched in Figure 13. The sketch shows a single liquid pass in the heat exchanger core in each case, with the liquid flow direction being into the paper. In configuration (a) the active and redundant tubes are alternated in each tube row, while in configuration (b) alternate tube rows are active and redundant. Configuration (a) will have slightly better heat transfer performance for two reasons: (1) the gas-side heat transfer area is interrupted twice as frequently in the gas flow direction, resulting in a higher film coefficient and (2) the operating tube is centered in the fin, resulting in a slightly higher fin efficiency than obtained with the offset active tube positions of configuration (b). Neither of these considerations is strong enough to rule out the use of configuration (b), which has the advantage of requiring simpler manifolding arrangements than configuration (a).

Some of the features of the cross-counterflow tube-fin exchanger that make it a lightweight design candidate for this application are the following:

(a) The heat transfer area is interrupted in the gas flow direction, which essentially eliminates axial conduction as a problem in this core.

(b) Dual use is made of the metal in the core, since all of the core metal serves as gas-side heat transfer area and is effective during operation of either of the two liquid loops.

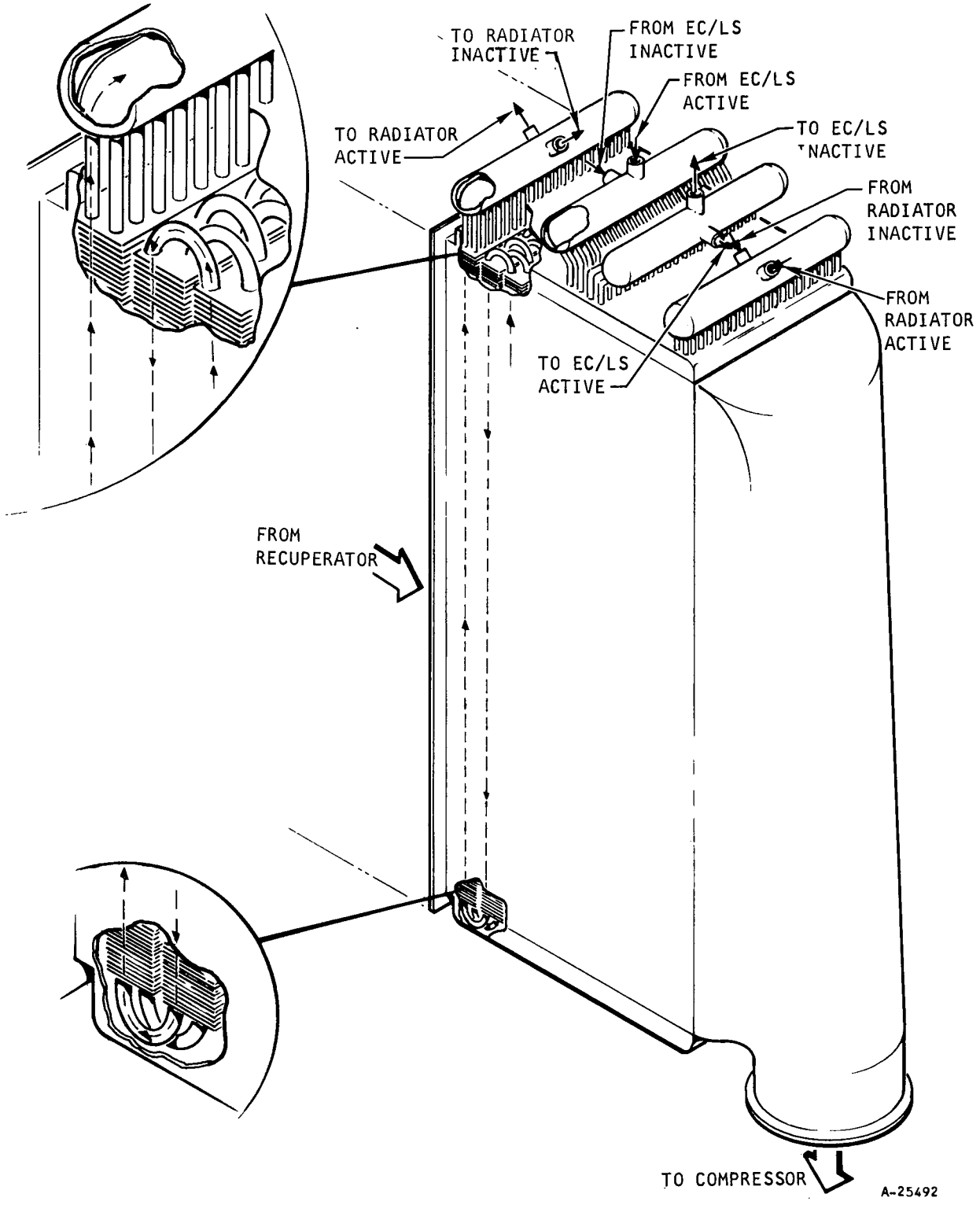

Figure 12. Cross-Counterflow Finned-Tubular Heat Exchanger with Two Liquid Loops

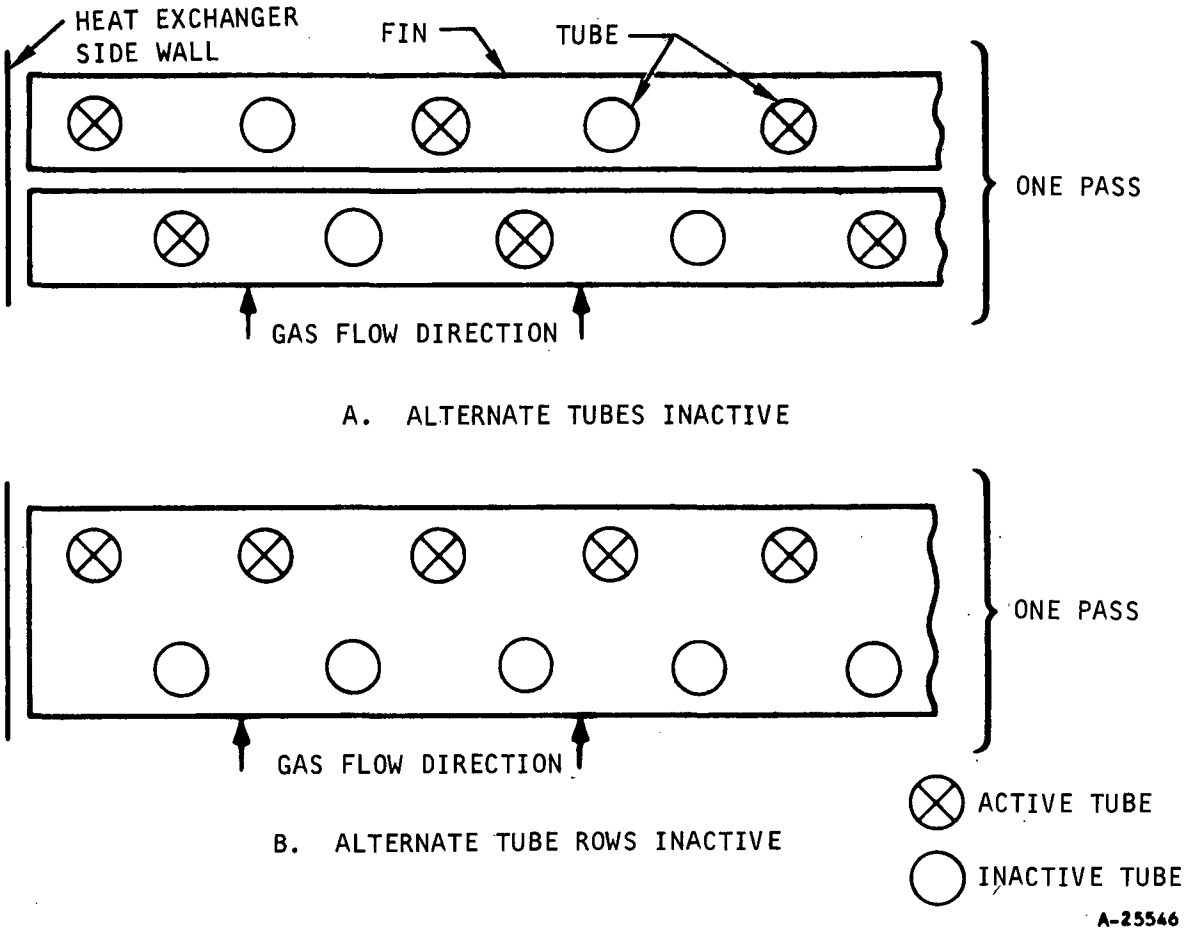

Figure 13. Tube/Strip Fin Arrangements

The plate-fin matrices are reliable and easy to fabricate but tend to be heavier than the tube-fin matrix. The high weight of plate-fin cores is attributable to (1) the high proportion of total heat transfer area provided by the plates, which must be relatively thick to meet fabrication requirements (6 to 8 mils is standard), (2) a relatively unfavorable geometry for achieving an optimum conductance ratio in a gas-to-liquid application, and (3) the degradation in heat transfer performance due to axial conduction of heat in the core. In the plate-fin designs, as in the tube-fin core, it is possible to integrate both liquid loops (active and redundant) into a single core and thus make dual use of the gas-side heat transfer area. This is done by alternating liquid passages in the core; i.e., the order of sandwiches in the heat exchanger is as follows: gas, liquid 1, gas, liquid 2, gas, liquid 1, etc.

Manifold arrangements for the pure counterflow plate-fin heat exchanger are depicted in Figure 14. The liquid loops enter through rectangular end sections, allowing the gas to make a straight pass into the core. The end sections required for introducing the liquids into the counterflow core represent a major disadvantage of the counterflow configuration, since the end sections both add substantial weight to the heat exchanger and make it virtually impossible to obtain constant liquid pressure across the flow width of the

exchanger. The latter effect occurs because the reduced liquid flow area in the cross-flow portion of the ends ensures an end section pressure loss which is comparable to the counterflow core loss and a resulting pressure gradient along the entrance face of the core. The resultant tendency for cross-flow in the core is prevented by the use of flow dividers, which add further to the weight of the exchanger.

The cross-counterflow plate-fin heat exchanger core is shown in Figure 15. This exchanger is easy to manifold though somewhat more difficult to construct than the counterflow unit, due to the turning sections required between each pass.

The cross-counterflow tubular heat exchanger could be one of the simplest types to construct. The use of serpentine tubes for this design would result in a minimum number of braze joints and thus inherent high reliability. However, the plain tubular unit is the heaviest core type for two reasons: (1) there is a large liquid inventory weight, amounting to about 42 percent of the dry weight in the designs studied, and (2) since the active and inactive tubes are not connected in any way, a separate core is required for each of the two liquid loops. In addition, the low packing density of heat transfer area in the tubular core has been found to result in high heat exchanger volume and difficult problems in packaging and matching to the recuperator. The use of serpentine tubing, because of minimum allowable tube bend radii, would require wide spacing of the tubes and a further decrease in heat transfer area per unit volume, to the point where the heat exchanger becomes very bulky.

b. Core Optimization

(1) Tube-Fin Cross-Counterflow Core

The effects of several parameters on the size and weight of the tube-fin cross-counterflow heat exchanger were studied parametrically. Figure 16 shows the variation of heat exchanger face area and heat exchanger weight with number of fins per inch. These curves are based on the following assumptions:

(1) A single fin strip per tube row, with a strip fin width of 0.300 in. and a spacing between tubes in a tube row of 0.340 in.

(2) A tube OD of 0.15 in. and a tube wall of 0.008 in. (ss)

(3) Ring-dimpled tubing

(4) Copper fins, 0.004 in. thick

(5) Performance as specified in the figure

Minimum heat exchanger weight is seen to occur at approximately 15 fins per inch. Using this same core geometry and 15 fins per inch, the effect of liquid pressure drop on core size and weight is illustrated in Figure 17. Weight was found to increase sharply as pressure drop was decreased below 10 psi, because the reduced liquid Reynolds numbers obtainable at the lower pressure drops dropped the flow into a region where the tube dimples were not effective in increasing the liquid film coefficient; i.e., essentially laminar flow prevailed.

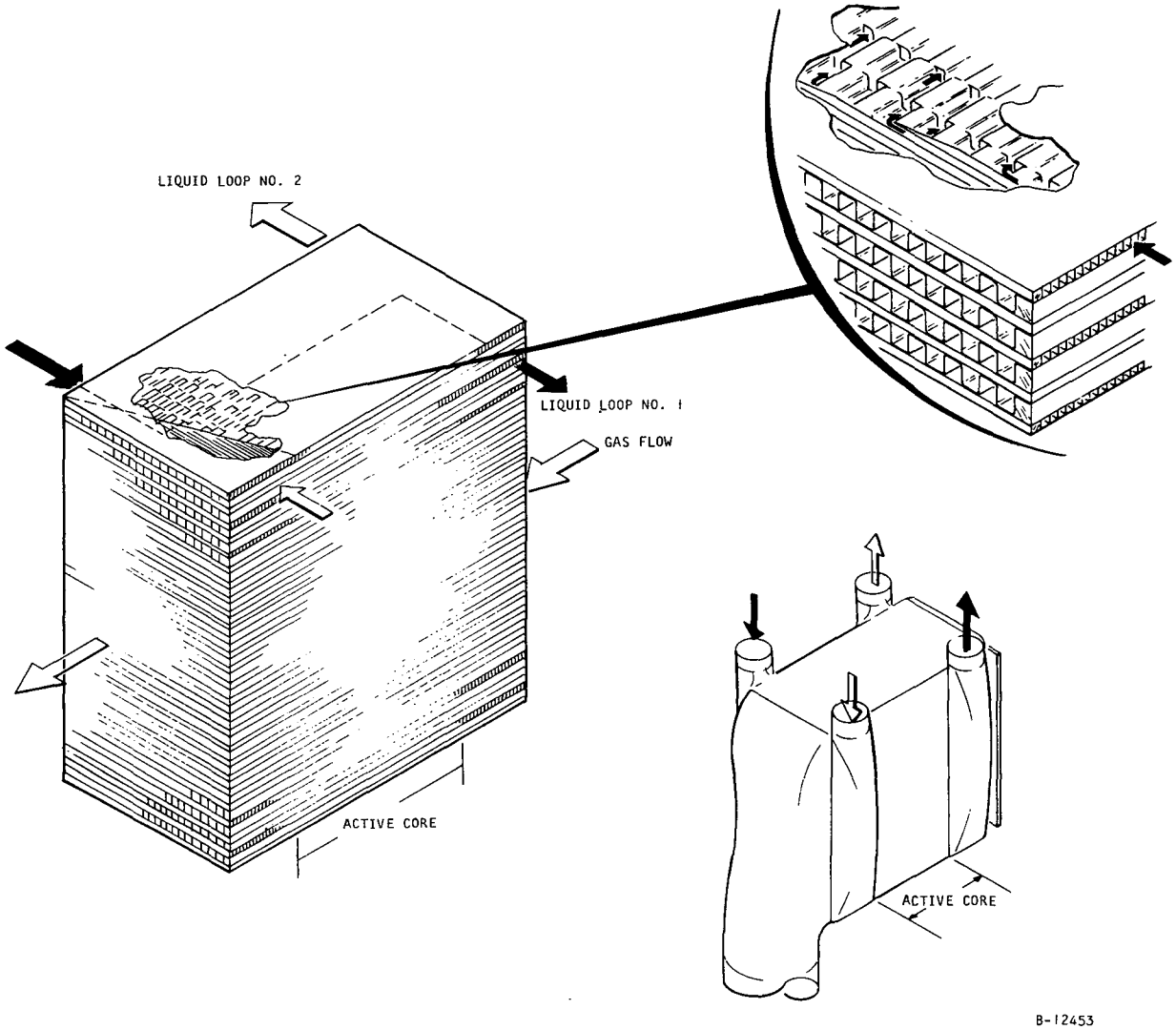

Figure 14. Counterflow Plate-Fin Heat Exchanger With Two Liquid Loops

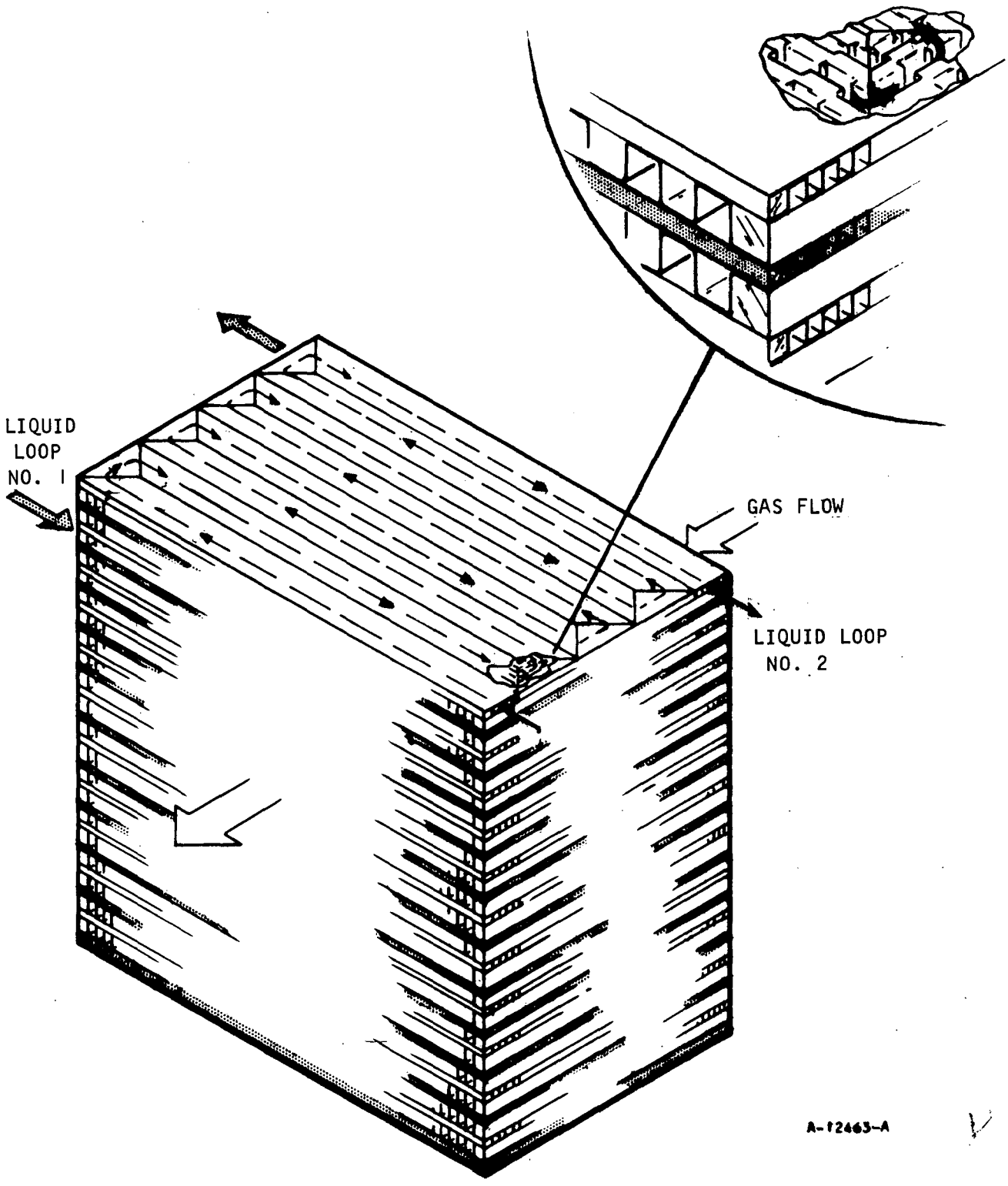

Figure 15. Eight-Pass, Cross-Counterflow, Plate-Fin Heat Exchanger with Two Liquid Loops

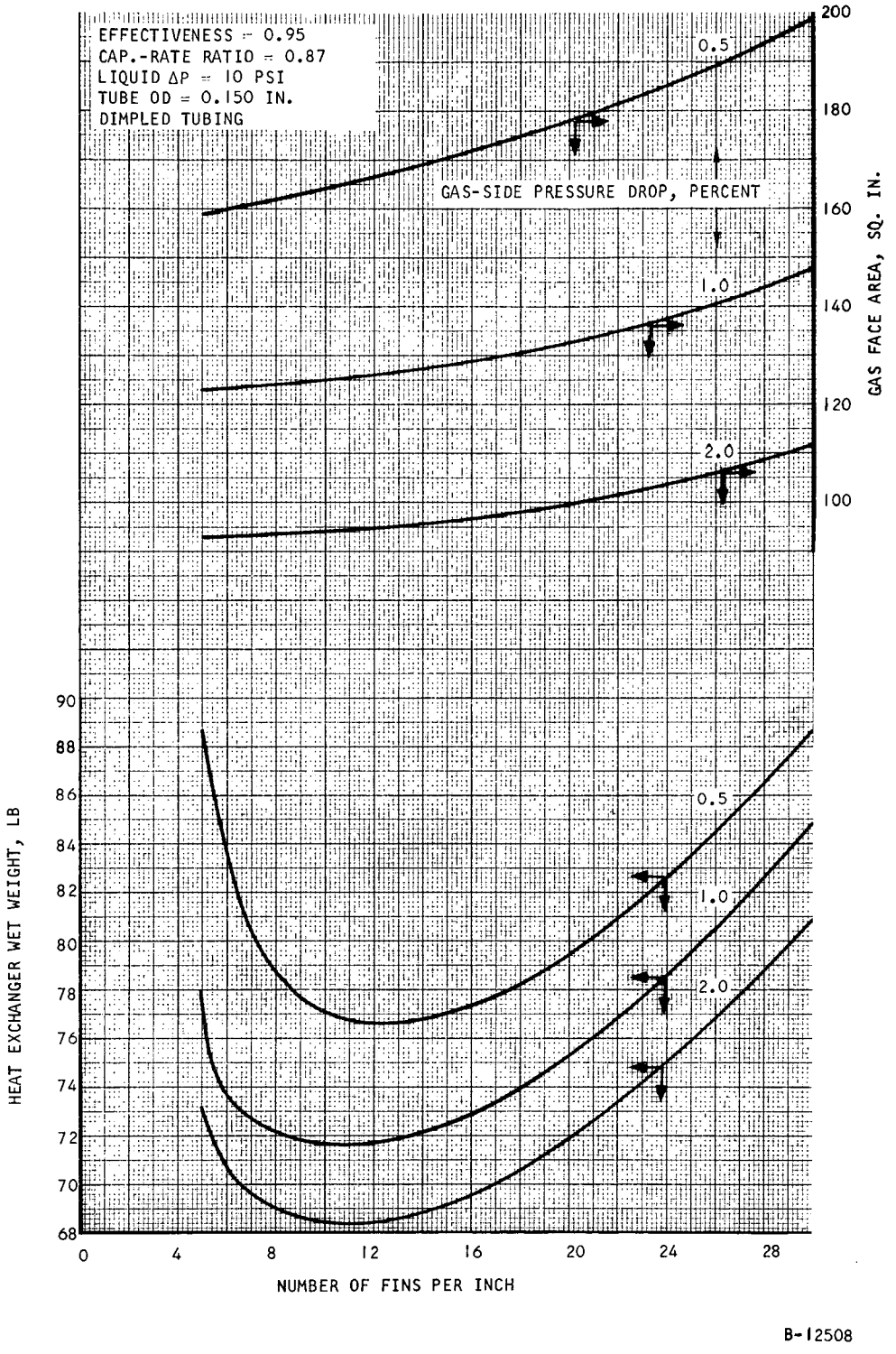

Figure 16. Variation of Finned-Tubular Heat Exchanger Face Area and Weight with Number of Fins per Inch

The effect of tube diameter on heat exchanger weight is shown in Figure 18 for tube-fin matrix number SPT4. The SPT4 matrix is of interest because it is the matrix used in the solar Brayton cycle heat sink heat exchanger design AiResearch performed for NASA. It has the following geometry:

(1) 30 fins per inch

(2) Fin width = 2.0 in. x (tube OD)

(3) Tube spacing (transverse to gas flow) = 2.35 in. x (tube OD)

(4) Fin thickness = 0.004 in. (copper)

(5) Ring-dimpled tubing

It may be noted that heat exchanger weight decreases with decreasing tube diameter to 0.125 in. This is consistent with previous AiResearch experience on this type of matrix, which has indicated generally improved performance with smaller tubes. The SPT4 matrix has a higher than optimum number of fins per inch, although the weight penalty is not as great as that shown in Figure 16 if the higher liquid pressure drop of 25 psi is used. The 25-psi pressure drop results in a higher liquid film coefficient and a higher optimum ratio of outside-to-inside heat transfer area, thus an optimum number of fins somewhat above 15 per in.

(2) Plate-Fin Cross-Counterflow Core

A number of fin sandwich geometries (fin height, fin thickness, and number of fins per inch) were studied to obtain a minimum-weight core design. A significant part of the optimization procedure involves calculating the effect on performance due to axial conduction of heat in the heat exchanger core. This calculation is accomplished with AiResearch Computer Program No. H2300 (see Appendix A), a nodal point analysis program that calculates the transient and steady-state performance of cross-counterflow plate-fin heat exchangers. To determine the effect of axial conduction, the program is run first with an option in which the conduction heat transfer between metal nodes is disregarded in the calculation, and then with the option in which conduction is included. The results from this program are then used to adjust the heat exchanger designs obtained from H0120, the plate-fin design program.

Results of the analysis are shown in Table 8.

In all cases, the cold-side (liquid) fin sandwich is 20 fins per in., 0.050 in. high, 0.0020 in. thick, and the hot-side fin thickness is 0.004 in. Computer results were obtained for axial conduction in Cases 2 and 3 cores, and the axial conduction effect was estimated from these results for Cases 1 and 4. On the basis of Table 8, the Core 2 fin set was chosen for the plate-fin cross-counterflow heat sink exchanger.

A brief study was made of the effect on heat exchanger size of the number of liquid-side passes. The selected number of passes is eight, for which the

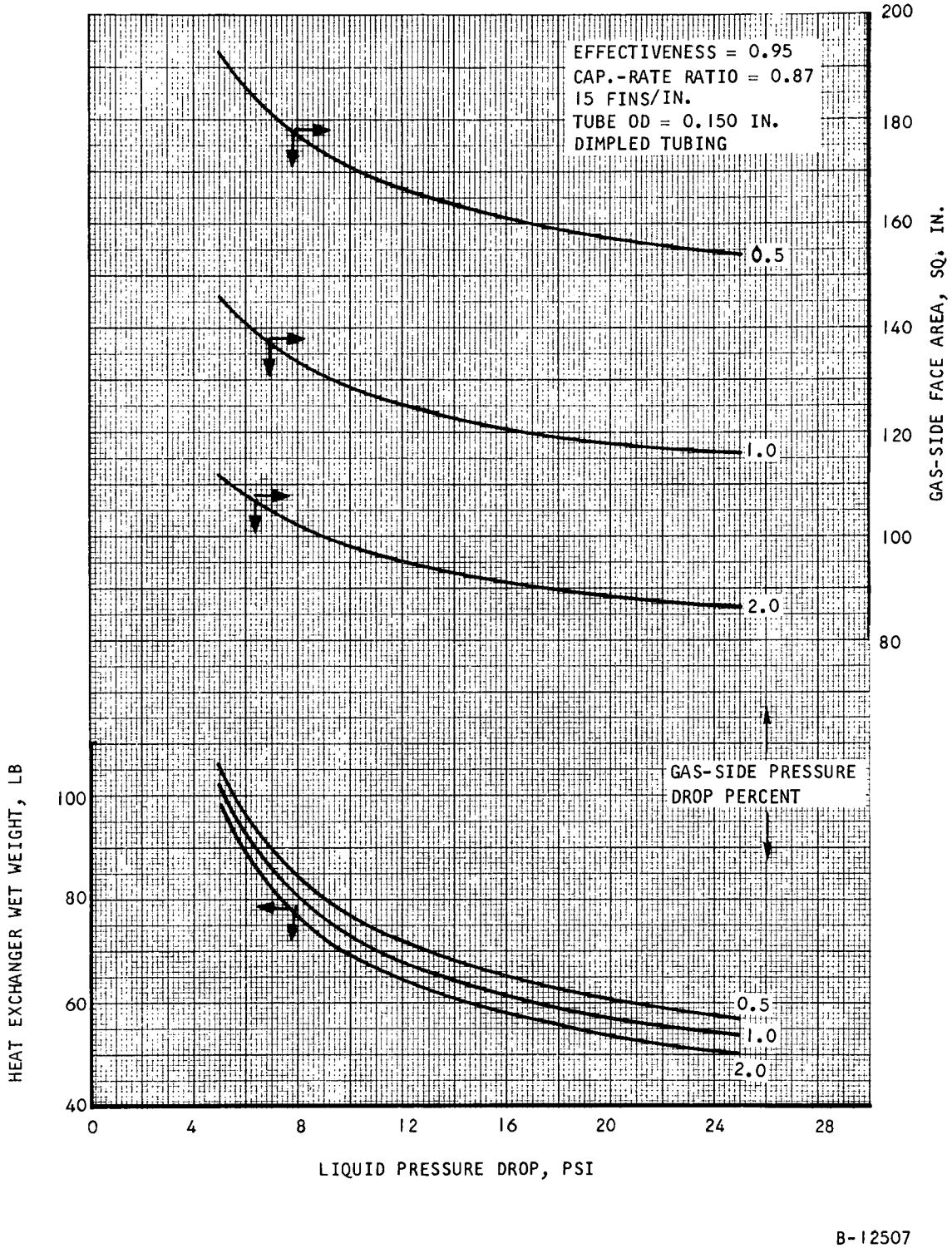

Figure 17. Variation of Finned-Tubular Heat Exchanger Face Area and Weight with Liquid Pressure Drop

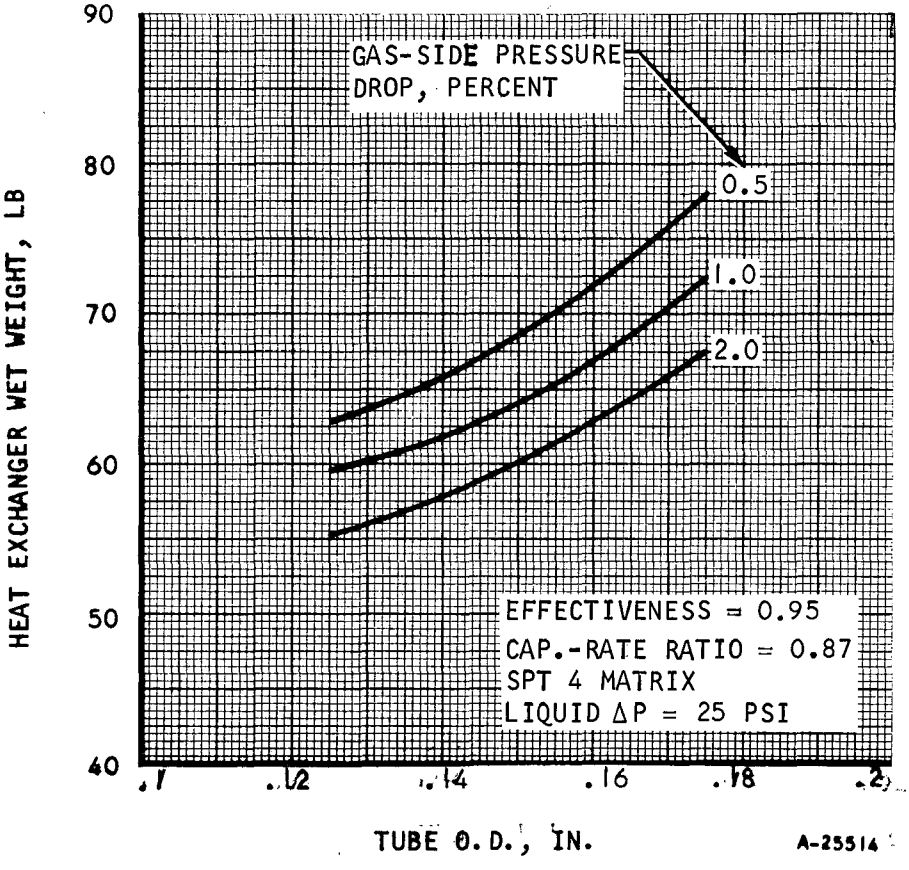

Figure 18. Variation of Finned-Tubular Heat Exchanger Weight with Tube Diameter

TABLE 8

COMPARISON OF FIN SETS FOR THE HEAT SINK EXCHANGER

Case	Hot-side Fin Sandwich Geometry			Core Wet Weight, lb	
	Fin Height, in.	Fins per in.	Gas Flow Length, in.	Axial Conduction Disregarded	Axial Conduction Included
1	0.153	16	20	98	100
2	0.125	16	16	90	97
3	0.100	20	11	81	104
4	0.100	16	24	94	109

UA requirement is 14 percent above the UA required for a pure counterflow configuration. The reduction in required UA obtained by increasing the number of passes above eight does not justify the added complexity of the design.

3. Design Point Selection

a. General

Selection of the design geometries for the two heat exchangers in the BHXU requires consideration of the face area match between low pressure recuperator outlet and heat exchanger inlet in addition to the reliability and weights of the individual units. Reliability, which is considered to be the most important design criterion for this program, enters the design process through its effect on heat exchanger matrix type selection, e.g., plate-fin vs tubular. For a given heat exchanger type, selection of the individual core parameters and the pressure drop split between recuperator and heat sink exchanger are based on (1) minimum BHXU weight and (2) the face area match between the two exchangers, as required to eliminate intermediate ducting pressure losses. In addition, each BHXU configuration must be checked to make sure it can fit within the envelope specified by the problem statement and further evaluated on the basis of the resultant configuration of the gas ducting.

b. Pressure Drop Split

The method by which minimum weight and the recuperator/heat sink match are obtained is shown for the candidate heat sink heat exchanger types by the curves presented in this section. The recuperator assumed in all cases is the counterflow plate-fin unit with fin set 4-3 (0.153-in. fins on hot side,

0.125-in. fins on cold side). Total pressure drop for the two exchangers was set at 3.5 percent, exclusive of manifold losses, leaving 1 percent available for manifolds and ducting external to the exchangers.

Figure 19 shows heat exchanger weights and frontal areas for the recuperator and the tube-fin (SPT4 matrix) heat sink exchanger. The weights include heat exchanger cores, end sections, and side plates, but do not include manifolds, ducting, and associated structure. Since total pressure drop is held constant, increasing recuperator pressure drop causes a decrease in heat sink heat exchanger pressure drop and a resultant increase in heat sink heat exchanger weight. The combination of increasing heat sink exchanger weight and decreasing recuperator weight results in a minimum combined weight at a pressure drop split of 3.0 percent for the recuperator and 0.5 percent for the heat sink exchanger. As may be seen from the face area curves, at this pressure drop split the heat sink exchanger frontal area is 160 sq in. and the recuperator low pressure outlet face is 110 sq in. By reducing the recuperator pressure drop to 2.5 percent, a face area match is obtained, with a weight penalty of only 3 lb. The 2.5-percent recuperator pressure drop was chosen as the design point for this BHXU combination, and the combined heat exchanger weight is 209 lb. It may be noted that once a face area match is obtained for the two heat exchangers, a dimensional match may be obtained by suitably adjusting the recuperator stack height to width ratio.

It should be noted that the recuperator curves for Figures 19 through 23 are all based on a recuperator end-section height of 2.0 in. (same at both ends) and a ratio of 0.7 (Figure 8). In final recuperator sizing, the end sections are adjusted to obtain the best possible gas flow distribution, as described in a following section of this report. The resultant end-section designs will cause slight variations in face area, weight, and pressure drop splits from those indicated by the curves of this section; but the variations are small and exact matches are not necessary.

c. System Comparisons

A comparison of the six BHXU configurations studied is shown in Table 9. Based on the results shown in this table and on considerations discussed in other sections this report, Configurations 1 and 6 appear to be the leading candidates for the BHXU system.

The configuration 1 tube-fin heat sink exchanger is slightly heavier than the Configuration 2 heat sink exchanger, but it has the following advantage: the smaller number of liquid passes in the Configuration 1 core (16 passes vs 20 passes in Configuration 2) provides greater simplicity and higher realiability because of the fewer interpass braze joints required.

Configuration 3 is heavier than Configuration 1 and has the further disadvantage of a large number of passes (26) required for the heat sink heat exchanger. Although the use of plain tubes is attractive from the standpoint of simplicity in fabrication, the use of dimpled tubes does not represent a reliability problem for this heat exchanger because of the low temperature gradients involved, the use of 8-mil tubing walls, and the freedom to expand thermally provided by the mechanical design. In determining reliability, the fewer number of braze joints required for the Configuration 1 design is believed to be a more important factor than dimpling.

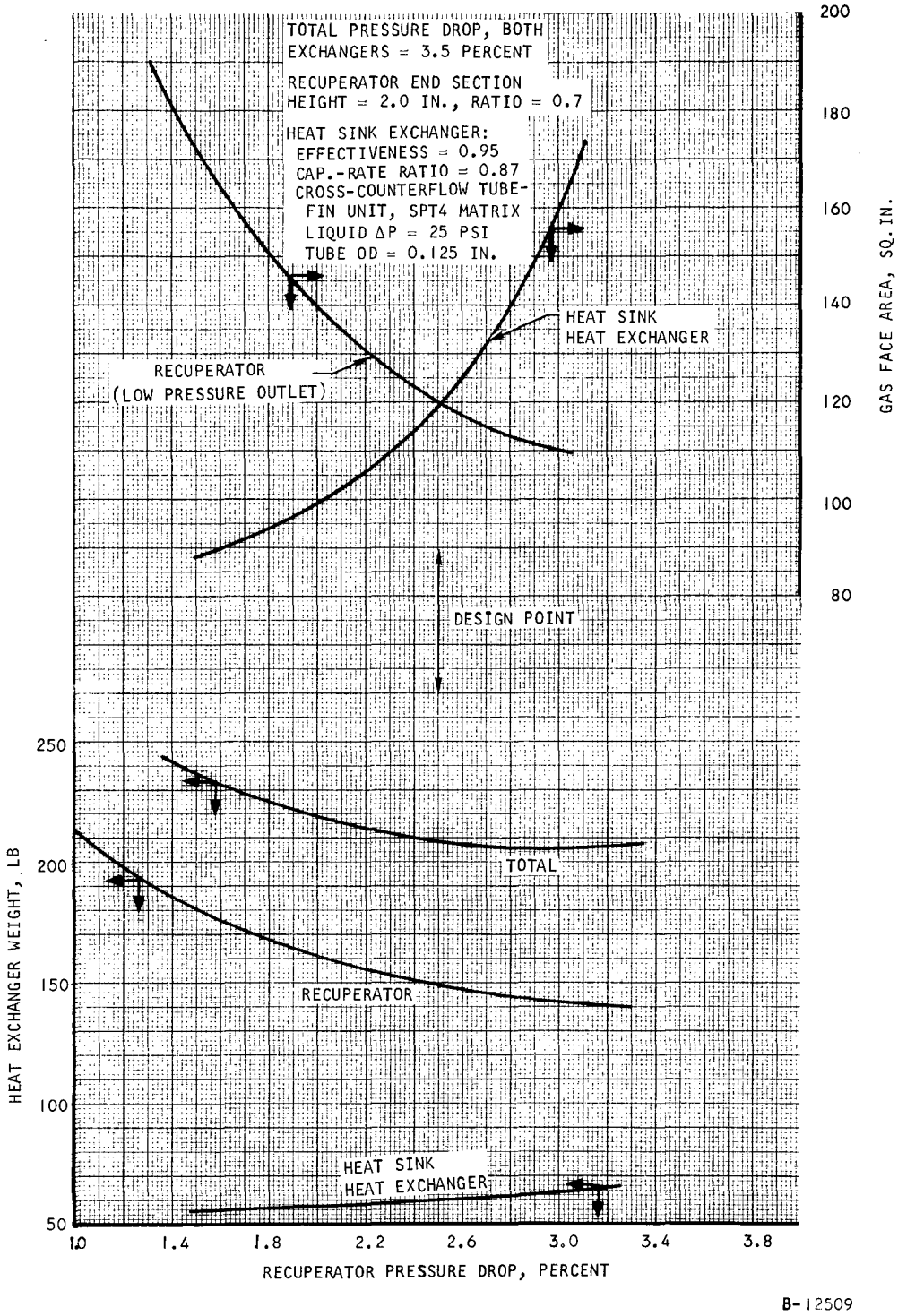

Figure 19. Design Point Selection Curves for Cross-Counterflow Finned-Tubular Heat Exchanger (SPT4 Matrix)

Figures 20 through 23 are similar design point selection curves for other heat sink heat exchanger core matrix configurations. Figure 20 is for the tube-fin heat exchanger with 15 fins per inch ("optimum," as per Figure 16). This heat sink exchanger, as the previous one, utilizes dimpled tubing to increase the liquid film coefficient. Design point pressure drop split for this BHXU is 2.6/0.9 (recuperator/heat sink exchanger), which is also close to the minimum weight point. Combined weight is 199 lb.

The design point selection curves for the plain tube (undimpled) tube-fin heat sink exchanger are shown in Figure 21. This matrix is exactly the same as the SPT4 matrix with the exception of the nondimpling of the tubes. Due to the poorer liquid film coefficients, the gas face area is larger and minimum weight occurs at a somewhat higher heat sink heat exchanger gas pressure drop. Recuperator/heat sink exchanger design pressure drop split for this BHXU is 2.3/1.2, and combined weight at this point is 228 lb. It may be noted that liquid-side pressure drop for the heat sink unit is only 10 psi for this matrix. Higher pressure drops resulted in excessively long tubes and thus could not be used.

Design curves for the cross-counterflow and pure-counterflow plate-fin units are given in Figures 22 and 23. In both cases, the maximum liquid-side pressure drops that could be utilized were less than the 25 psi allowable; and, in both cases, the heat transfer performance consequently suffers. In the cross-counterflow configuration, the limitation occurs because larger liquid pressure drops can only be obtained by increasing the liquid flow length. Since the liquid flow direction in the heat sink heat exchanger corresponds to one of the recuperator no-flow dimensions, the magnitude of this dimension is restricted by the recuperator design. The two possible orientations of the heat sink exchanger, corresponding to the two no-flow directions in the recuperator, are compared later. For the weight curves of Figure 22, a minimum stack height of 10 in. was assumed.

In the pure counterflow configuration, the liquid flow area and length are established by gas-side pressure drop limitations, and high liquid mass velocities cannot be obtained. In this configuration, as in the cross-counterflow configuration, a minimal fin height is used on the liquid side. Liquid pressure drops are still low.

Recuperator/heat sink exchanger pressure drop splits are 2.6/0.9 and 2.5/1, respectively, for the cross-counterflow and pure-counterflow plate-fin cores. Total weights are 237 lb for the cross-counterflow unit, and 278 lb for the counterflow unit. These figures are based on all-stainless construction for the heat sink exchangers. Axial conduction effects preclude the use of higher conductivity fins in this heat exchanger as in the recuperator, the axial conduction effect being approximately the same for the two exchangers.

It was impossible to obtain a plain tubular heat sink exchanger that was suitable for matching with the recuperator or fitting within the allowable envelope specified in the problem statement. Both weight and volume are high for this type of core in a gas-to-liquid application.

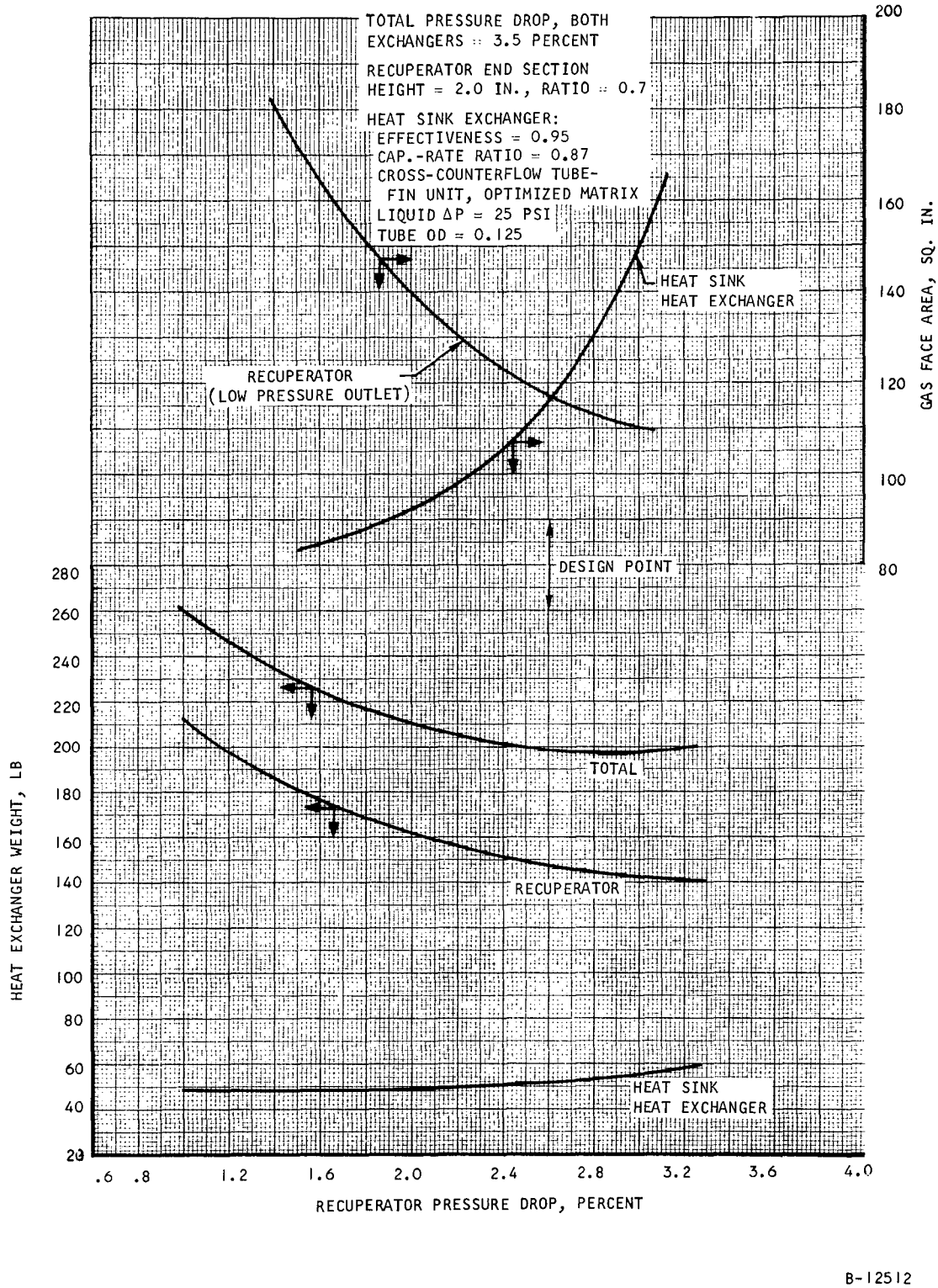

Figure 20. Design Point Selection Curves for Cross-Counterflow Finned-Tubular Heat Exchanger (Optimized Matrix)

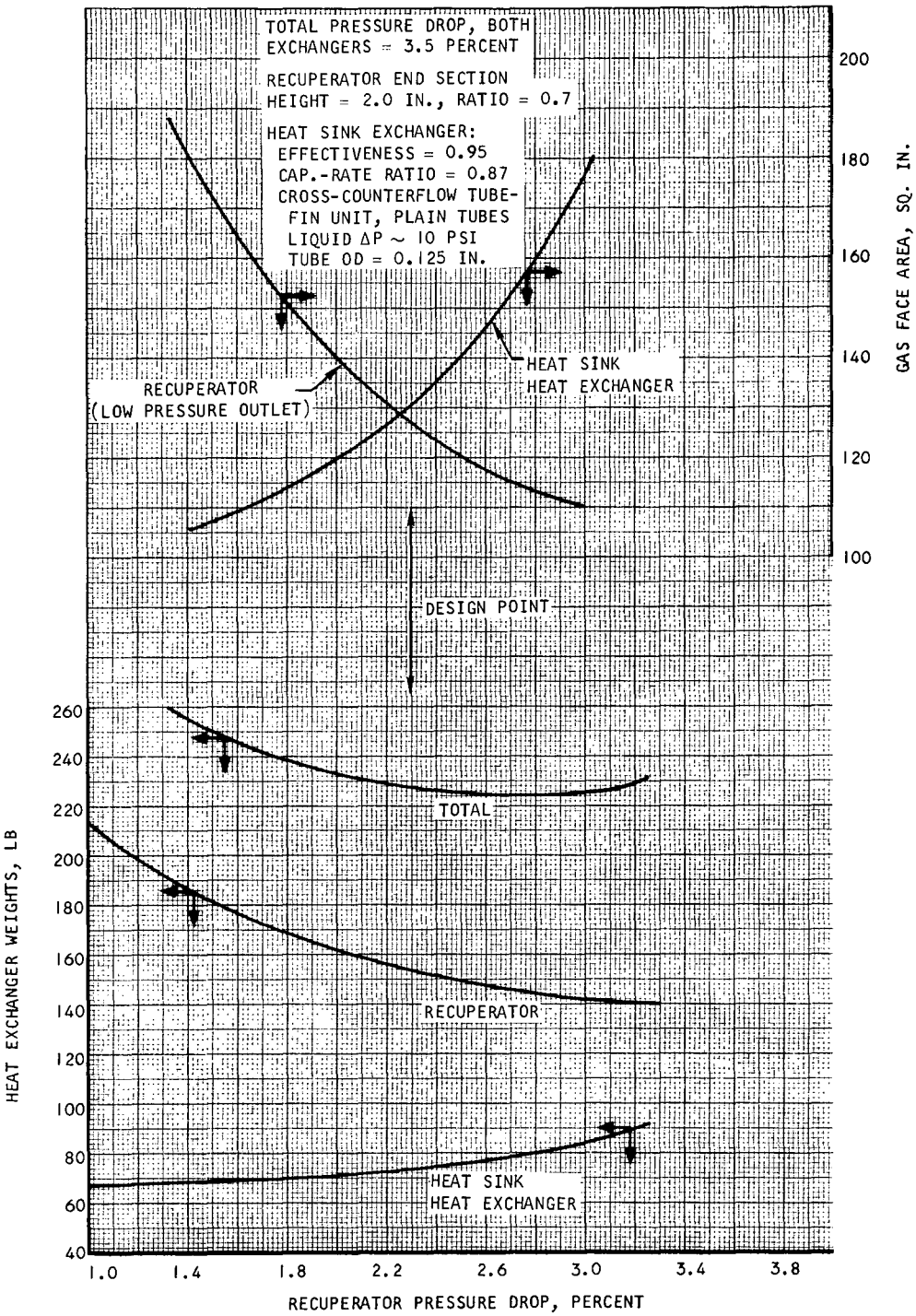

Figure 21. Design Point Selection Curves for Cross-Counterflow Finned-Tubular Heat Exchanger (Nondimpled Tubes)

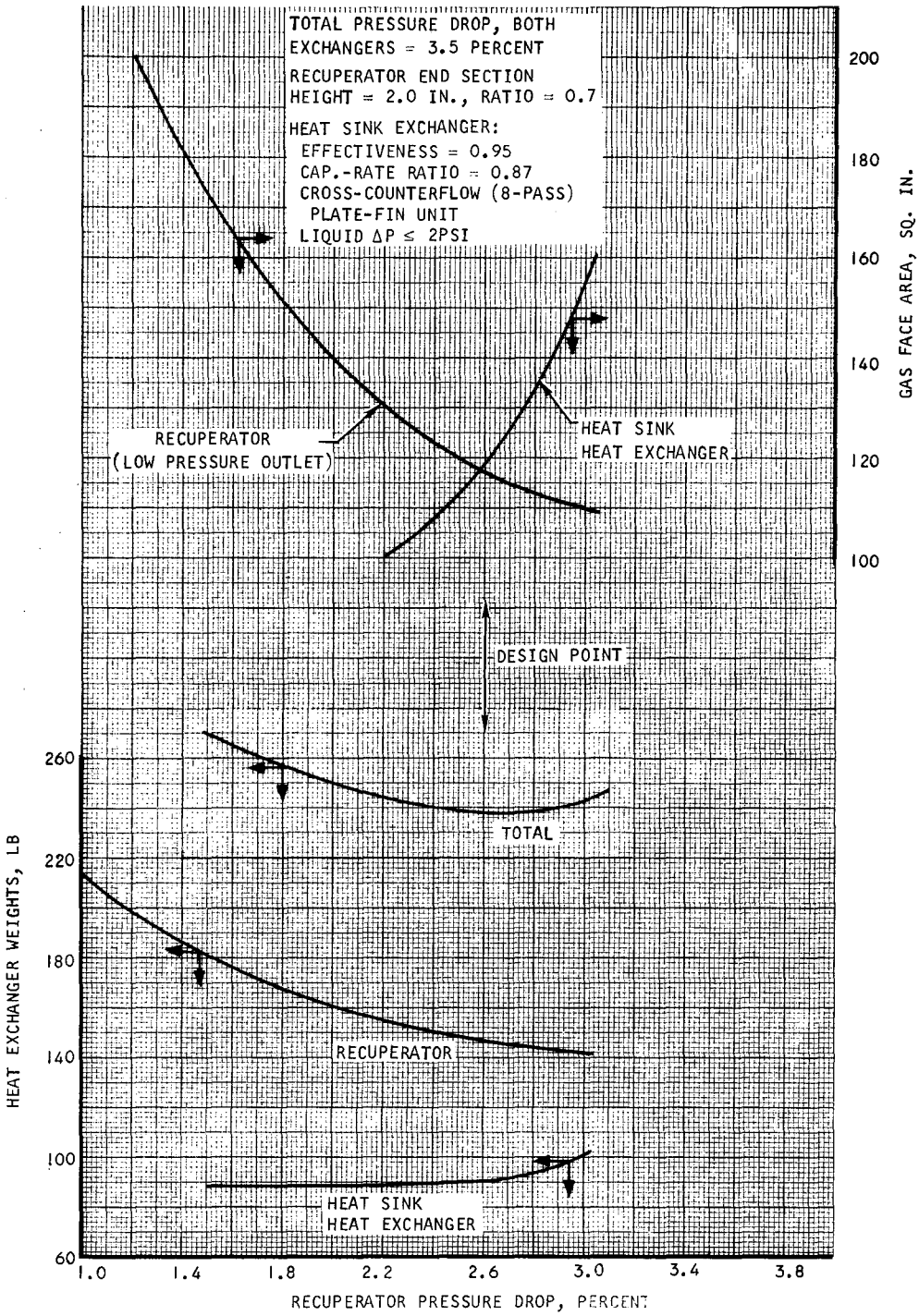

Figure 22. Design Point Selection Curves for Cross-Counterflow Plate-Fin Heat Exchanger

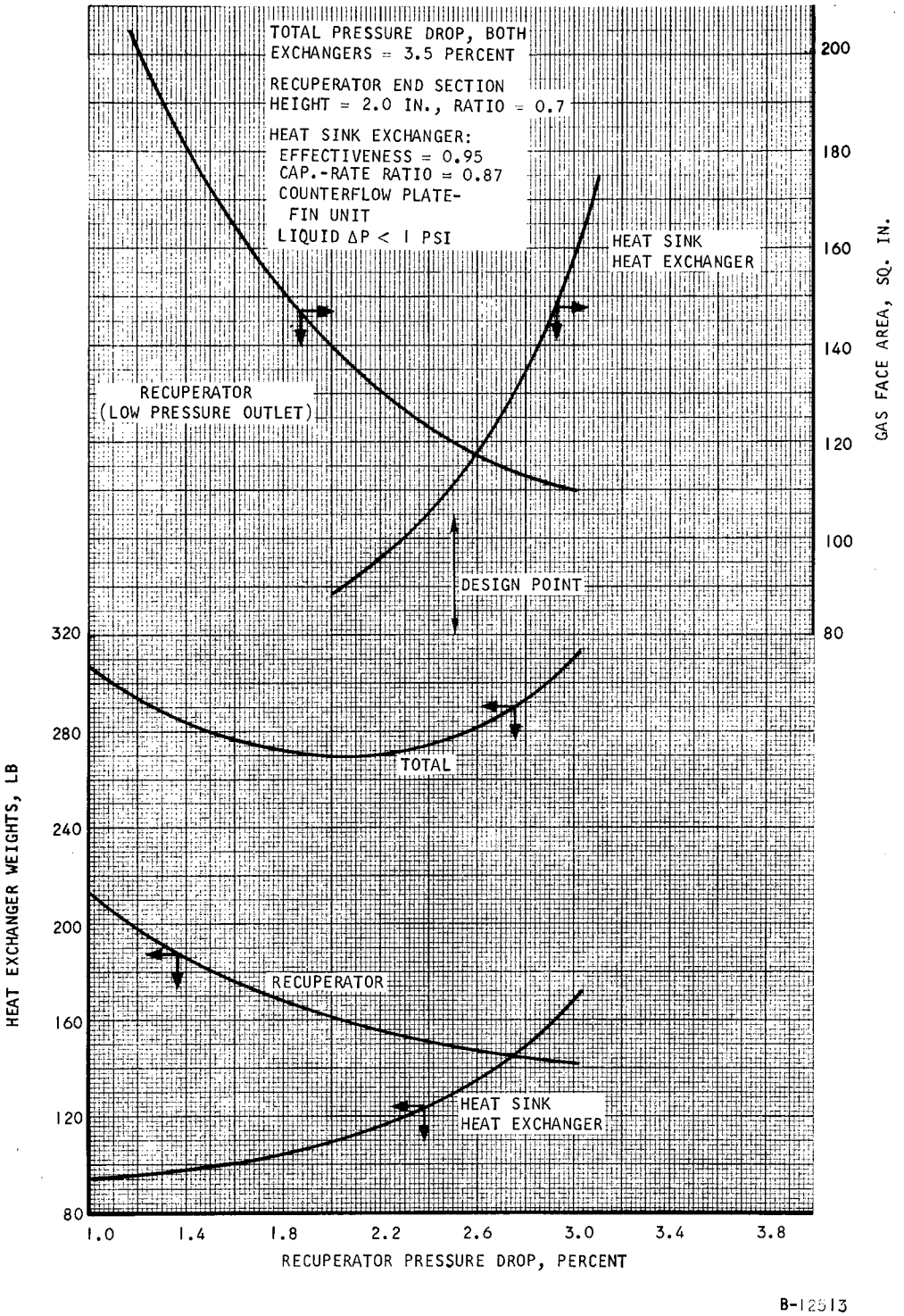

Figure 23. Design Point Selection Curves for Pure Counterflow Plate-Fin Heat Exchanger

Of the two plate-fin heat sink exchangers, the cross-counterflow unit is more attractive than the pure counterflow unit because (1) it results in a lighter package, and (2) it results in a smaller package, lacking the end sections required by the counterflow unit for liquid access to the core.

The plate-fin cross-counterflow geometry for the heat sink exchanger is more attractive for this application than it was for the NASA solar Brayton cycle system using low-pressure argon. The difference is attributable to two factors: (1) the lower pressure in the argon Brayton cycle system (about 6 psi) resulted in a shorter gas flow dimension in the heat exchanger and, consequently, a greatly increased axial conduction effect for the plate-fin designs; and (2) the poorer gas film coefficients and lower mass velocities obtainable with low-pressure argon (as opposed to high-pressure Xe-He) established a requirement for a high ratio of gas-side heat transfer area to liquid-side area, which is not easily obtainable in a plate-fin geometry.

A cross-counterflow plate-fin geometry allows two possible heat exchanger orientations: in the Configuration 5 orientation, the liquid flow direction is in the flow width direction referred to the recuperator; in the Configuration 6 orientation, the liquid flow direction is rotated 90 deg so that it is in the recuperator stack height direction. In the latter case, the stack heights of the heat sink exchanger and the recuperator lie in orthogonal directions. Both configurations are feasible to match with the recuperator; Configuration 6, however, represents a slightly better design. With the heat exchanger and recuperator stack-up directions orthogonal, the face area match can be based on a large recuperator stack height ($\sim$ 20 in.) and a low heat exchanger stack height ($\sim$ 6 in.), both of which are desirable. The large recuperator stack height (and corresponding small flow width) reduces end-section weight for a given end-section pressure drop. (This effect is not reflected in the weights of Table 9, since all recuperator weights are based on a 2.0-in. end-section height; thus, actual recuperator weight for Configuration 5 would be somewhat greater than shown.) The low stack height is beneficial to the heat sink exchanger design because it reduces the liquid flow area and increases the liquid film coefficient. The heat sink heat exchanger has increased reliability in this configuration because of the reduced number of fluid containment brazes, which is proportional to stack height.

Comparing the plate-fin and tube-fin heat sink exchangers (Configuration 6 vs Configuration 1), the tube-fin geometry appears to have a weight advantage over the plate-fin design. During the course of this study, however, small scale testing of the solar Brayton cycle (argon system) heat sink heat exchanger was concluded and results of that testing became available. The tests showed that the unit as originally designed was undersized by about 25 percent, due primarily to poorer than anticipated gas-side film coefficients. Applying these results to the Configuration 1 heat sink exchanger, which has the same core matrix as the referenced test core, would substantially reduce the weight difference between the Configurations 1 and 6 BHXU's. In addition, the weight associated with structural reenforcement of the core (not included in the weights of Table 9) is much greater for the tube-fin heat exchanger than for the plate-fin exchanger, which is an inherently rugged structure without reenforcement. It is estimated that final heat exchanger weights for the two

TABLE 9

COMPARISON OF BHXU CONFIGURATIONS

Configuration No.	Heat Sink Exchanger Core Matrix Geometry	Pressure Drop, percent		Weight, lb		
		Heat Sink HX	Recuperator	HSHX	Recuperator	Total
1	Cross-counterflow tube-fin, SPT4 matrix, 16 passes, dimpled tubes	1.0	2.5	60	149	209
2	Cross-counterflow tube-fin, optimized matrix (15 fins per inch) 20 passes, dimpled tubes	0.9	2.6	52	148	200
3	Cross-counterflow tube-fin, 15 fins per inch, tubes not dimpled, 26 passes	1.2	2.3	74	154	228
4	Pure counterflow plate-fin	1.0	2.5	129	149	278
5	Cross-counterflow plate-fin, 8 passes, stack height direction parallel to recuperator stack height	0.9	2.6	90	147	237
6	Cross-counterflow plate-fin, 8 passes, stack height direction perpendicular to recuperator stack height	0.9	2.6	85	147	232

core types would be virtually equal. On the basis of these results, in conjunction with the simplicity of the plate-fin construction and the extensive experience accumulated by AiResearch in the fabrication of plate-fin heat exchangers, the decision was to use the Configuration 6 BHXU.

Detail Design Study

1. Design Comparisons

Using the Configuration 6 BHXU geometry, as established during the parametric analysis, a further analysis was made to determine the effect on overall weight and system packaging due to variations in the recuperator design. Three variations in recuperator design were investigated, as specified in Table 10.

TABLE 10

RECUPERATOR DESIGN VARIATIONS

Design Study	Hot-side Fin Height, in.	Cold-side Fin Height, in.	Stack Height, in.
1	0.153	0.125	18
2	0.153	0.100	18
3	0.153	0.125	21

The first two design studies involved variations in the recuperator fin set while the third study was based on a different recuperator stack height. For all three cases, the pressure drop split between recuperator core and recuperator end sections was based on minimum weight, as established by curves similar to Figures 8 and 9, and the split between recuperator and heat sink exchanger was such as to give minimum weight plus an approximate face area match between the two exchangers. The optimization of the pressure drop split between recuperator and heat sink exchanger is shown in Figures 24, 25, and 26, based on a total pressure drop of 3.5 percent for the heat exchanger combination.

Results of the study are shown in Table 11. It can be seen that total weights are nearly equal for the three studies. The design study 3 BHXU can be eliminated from further consideration because it results in a slightly larger package dimension (in the stack-up direction) with no appreciable saving in weight. For design studies 1 and 2, the recuperator end sections were redesigned to obtain uniform core flow distribution, following the procedure described in a later section of this report. It was determined that the best end section design for both design studies involved an increase of about 50 percent in end section pressure drop over that shown in Table 11. A final

selection of the design study I BHXU was made for final design analysis because the greater length of the recuperator in this configuration results in a slightly more favorable arrangement of the BHXU ducting.

2. Final Design

Using the design study I BHXU of Table II, the designs of both heat exchangers were reexamined to determine their adequacy in meeting the heat transfer and pressure loss requirements of the problem statement. It was decided at this time to increase the margin on recuperator UA from 10 percent, which was used throughout the preliminary sizing studies, to a new value of 20 percent, strictly as a means of ensuring that the required performance of this unit would be met. Since preliminary analyses of the recuperator end section designs indicated that a 50-percent increase in end section pressure drop would result when the end sections were redesigned for uniform flow distribution, the recuperator UA was increased by increasing the unit stack height while maintaining a constant gas flow length. As a result, the redesign effected both a 10-percent increase in recuperator UA and a 15-percent decrease in counterflow section pressure drop. Similarly, the margin on heat sink exchanger UA was increased from essentially nil to 10 percent while the pressure drop through this unit was decreased by 10 percent.

An additional factor affecting the size of the two heat exchangers was the use at this time of a different set of fluid properties for the xenon-helium gas mixture. The values of viscosity and thermal conductivity now used are based on data received from the University of Iowa. The variation of these properties with temperature, which was predicted from the Chapman-Enskog theory, results in the use of a Prandtl number at operating temperatures that is about seven percent greater than was used during the preliminary design study.

Final designs of the two heat exchangers, as modified by the above factors, are described in Tables 2 and 3. Estimated final pressure drop allocations in the BHXU system are summarized in Table 6.

3. Recuperator End Section Design

The designs discussed in the preceding sections were based on the same cross-flow end section geometry at each end of the recuperator. Use of this end section symmetry in the final recuperator design would result in poor gas flow distribution because, although all flow paths followed by the fluids through these symmetrical end sections are of equal length, they do not result in equal pressure drops for given mass velocities. The nonuniformity in the flow-path pressure drops results in a nonuniform flow through the counterflow core, which has an adverse effect on heat exchanger performance.

The nonuniformity in pressure drops for equal flows along the parallel flow paths is due to the large change in density that occurs from the inlet to the outlet ends of the recuperator. Thus, the pressure drop along the long flow path in the inlet end triangular section is not equal to the pressure drop along the long flow path in the outlet end because the gas density differs

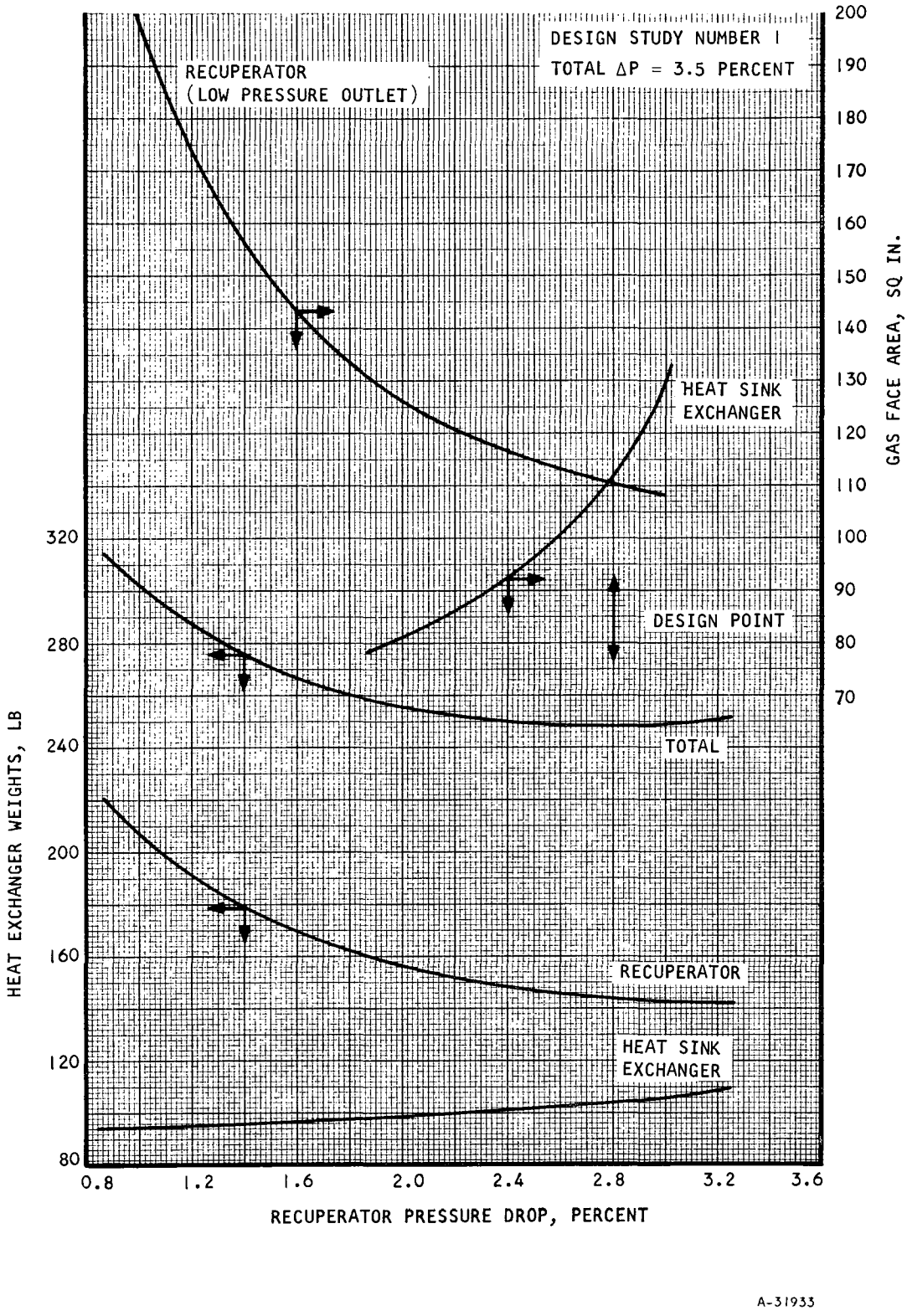

Figure 24. Design Point Selection Curves for Design Study No. 1

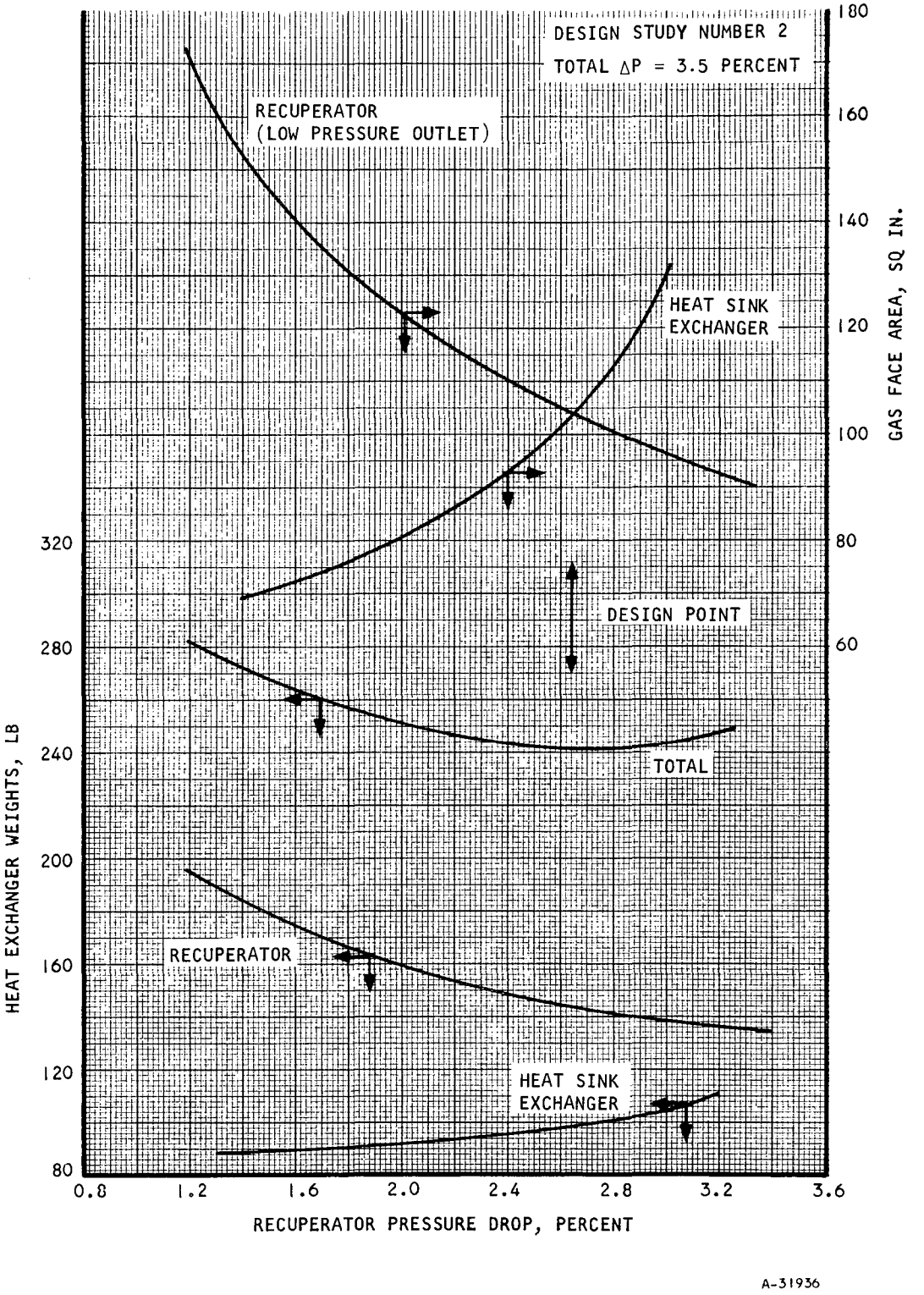

Figure 25. Design Point Selection Curves for Design Study No. 2

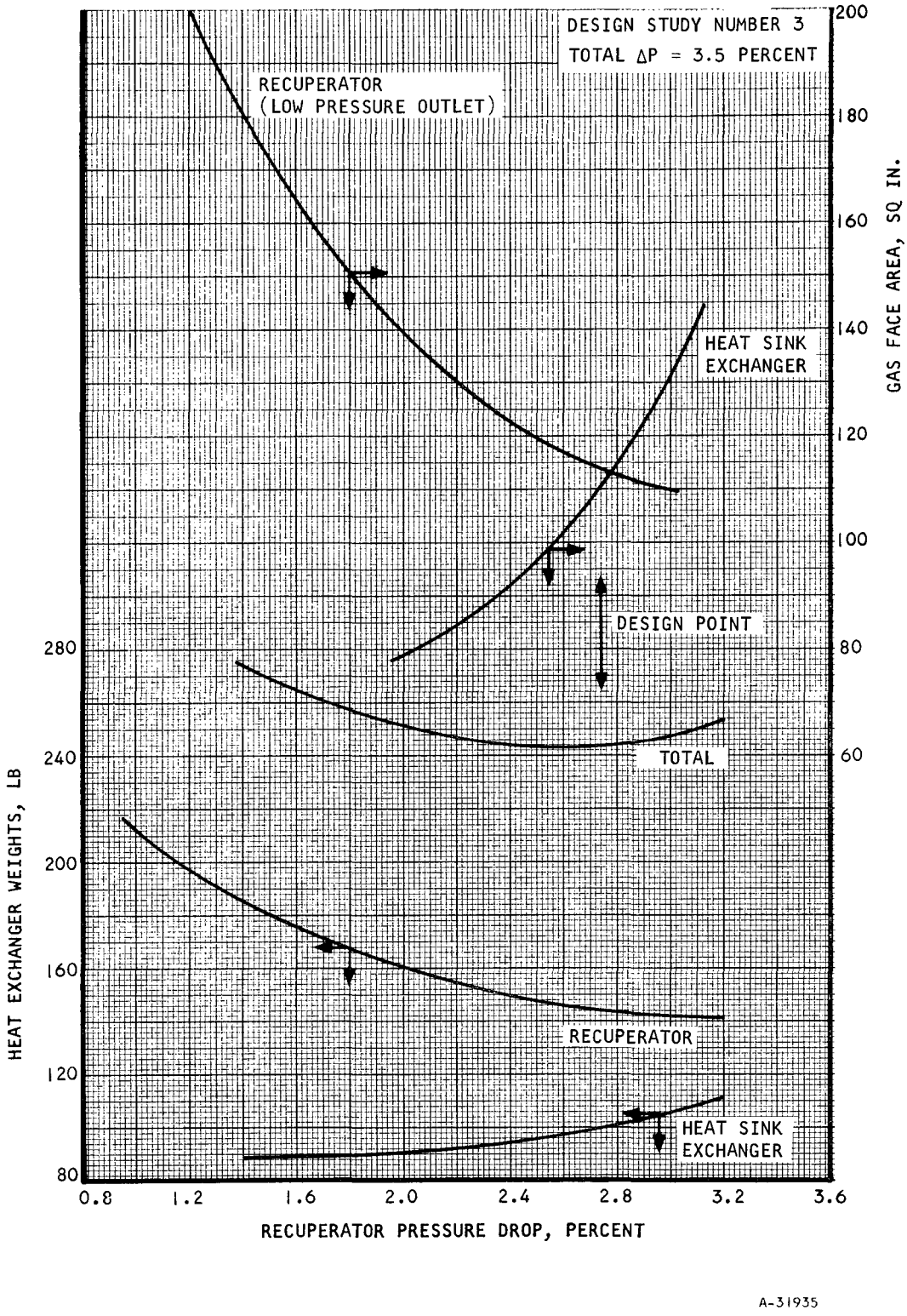

Figure 26. Design Point Selection Curves for Design Study No. 3

TABLE II

PRELIMINARY HEAT EXCHANGER DESIGNS

Design Study	1	2	3
Gas Pressure Drop, percent			
Recuperator Core	2.24	2.07	2.19
End Sections	0.56	0.58	0.56
Heat Sink Exchanger	0.70	0.85	0.75
Weight, lb			
Recuperator Total	144	144	144
Heat Sink Exchanger	104	98	100
Combined	248	242	244
Recuperator			
Height, in.	17.7	17.7	20.7
Length, in.	18.1	15.5	18.3
Width, in.	8.1	8.8	7.1
Heat Sink Exchanger			
Height, in.	6.1	6.1	5.5
Cold Length, in.	18.4	17.0	19.6
Hot Length, in.	15.0	16.0	15.5

substantially between the two ends. This effect can be minimized by reducing the height of the cold-end end section to the point where the pressure drops at opposite ends are equal. Reducing the height of the cold-end end section causes a reduction in the gas flow area in that section and thus an increase in the end-section pressure loss.

The end section geometries must be such that balanced pressure drops are obtained for both the high-pressure and low-pressure sides of the heat exchanger. Within this requirement, a number of design solutions exist, since for each geometry selected at one end of the exchanger there is in general a geometry at the other end (obtained by varying end section RATIO* and height) which size between the recuperator low pressure outlet and the heat sink exchanger inlet faces, since the initial sizing of these units was based on an assumed end section ratio of 0.7 at the cold end. Packaging studies show that the amount of mismatch obtained can be handled with a short transition section between the two exchangers, internally vaned to distribute the flow uniformly to the heat sink exchanger.

4. Manifold Design

The high-pressure recuperator manifolds are designed for uniform core flow using a "two-dimensional" flow model. The flow configuration is "U" flow and the header shape is rectangular. The sizing is based on obtaining matched static pressure profiles in the inlet and outlet manifolds, thus ensuring equal static pressure drops along all flow paths through the heat exchanger.

On the low-pressure side, the use of matched profiles is not sufficient, since the transition section between the two exchangers establishes essentially a uniform pressure profile at recuperator outlet and heat sink exchanger inlet. Constant static pressure drop on the recuperator low-pressure side is achieved with a tapered inlet manifold that provides a constant static pressure at the heat exchanger face. The taper of the manifold is ideally such that there is a slightly decreasing mass velocity in the flow direction, resulting in a small amount of momentum recovery to offset the pressure loss due to friction. At the heat sink exchanger outlet, the manifold is simply sized large enough to obtain an acceptable static pressure profile. As designed, the pressure drop along the low-pressure outlet manifold is about 10 percent of the pressure drop in the heat sink exchanger core.

Manifold pressure losses are summarized in Table 6.

5. Axial Conduction

Calculation of the effect of axial conduction of heat in the heat exchanger core is an important step in the design of plate-fin heat exchangers. The calculation of axial conduction in the recuperator is discussed in Appendix B. The effect of axial conduction, which is calculated by the counterflow design program, is to reduce recuperator equivalent UA by about 8 percent. Axial conduction in the heat sink exchanger was calculated using the H2300 nodal point analysis program (see Appendix A) and amounted to about 8 percent for this unit also.

*See Figure 6.

results in uniform flow on both sides. A number of such solutions were obtained for the final recuperator design and are summarized in Table 12. The procedure by which these solutions are obtained is shown in Figures 27 through 31. In these figures, the average frictional pressure drop for each side of each end section is plotted as a function of end section height. The design points marked on the curves occur where (1) the pressure drops at the inlet and outlet are equal, for both sides of the exchanger, and (2) there is a match between low-pressure and high-pressure side heights at both ends of the exchanger. At these points, the frictional pressure drops along all parallel flow paths in the end sections (summed for both ends of the recuperator) are equal. Since the fluid velocity head is the same for all paths, other losses associated with the end sections (turning, expansion, and contraction) are equal and thus total pressure drops are equal. This analysis neglects minor variations in velocity head due to heat transfer in the end sections.

Use of the balanced end-section design, in conjunction with flow dividers that run the length of the counterflow core and prevent fluid cross-flow, ensures equal pressure losses for equal flow rates along parallel fluid paths and thus uniformity in the distribution of flow.

TABLE 12

END SECTION DESIGNS FOR BALANCED PRESSURE DROPS

Case	Ratio*		Height, in.*		End Section ΔP, Percent	End Section Weight**, lb
	Hot End	Cold End	Hot End	Cold End		
1	0.65	0.55	3.75	1.185	0.774	15.3
2	0.7	0.55	4.35	1.19	0.749	17.1
3	0.7	0.6	2.425	1.075	1.003	10.8
4	0.75	0.575	4.3	1.185	0.780	17.0
5	0.75	0.6	3.4	1.155	0.801	14.2

*See Figure 6
**Plates and fins only

From Table 12 it may be seen that a tradeoff exists between end section pressure drop and weight in the selection of an end section design. Case 1 was chosen for the recuperator final design as representing the best compromise solution. One result of this selection is that there is now some mismatch in

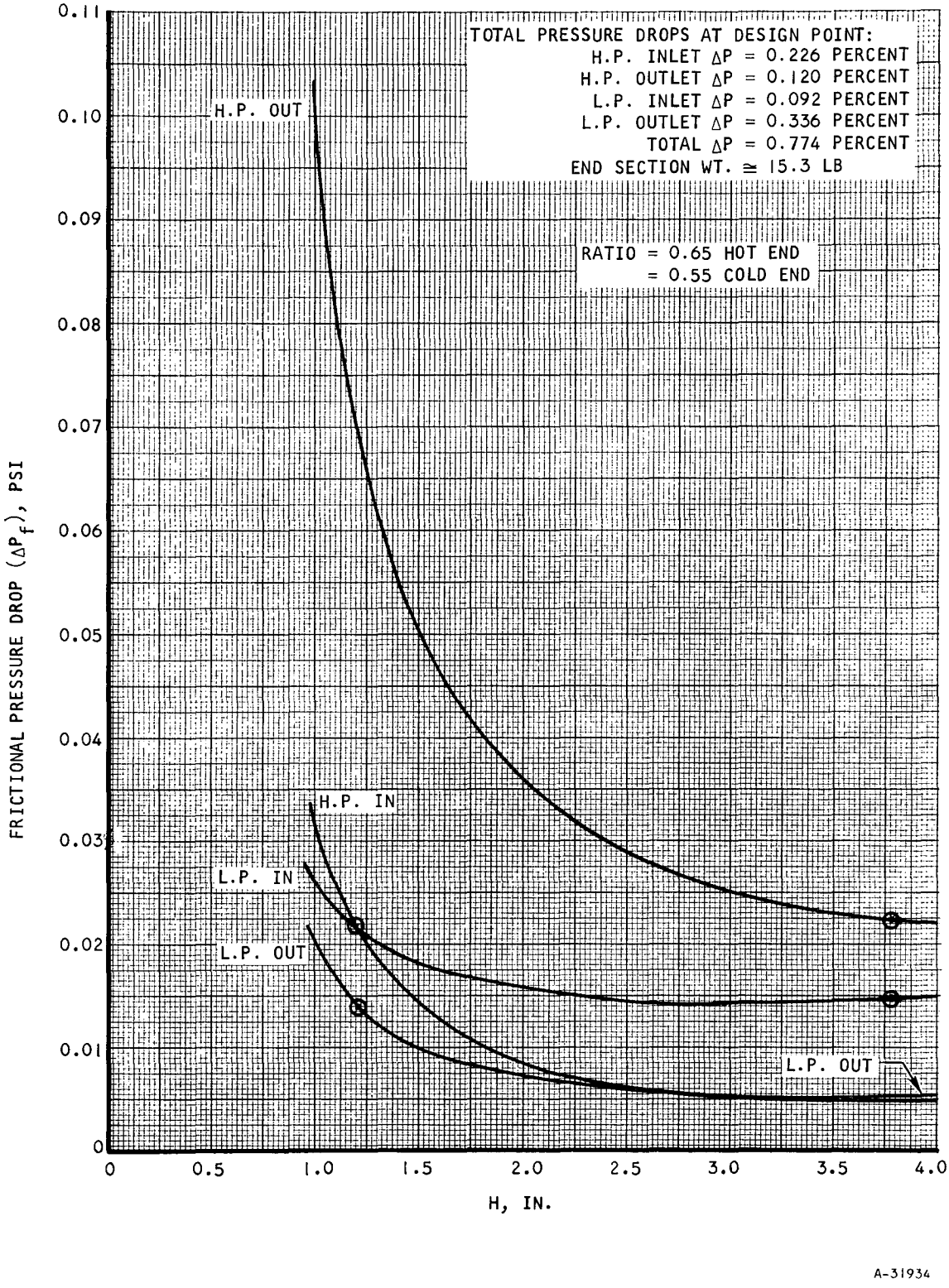

Figure 27. Friction Pressure Loss vs End Section Height, Case I

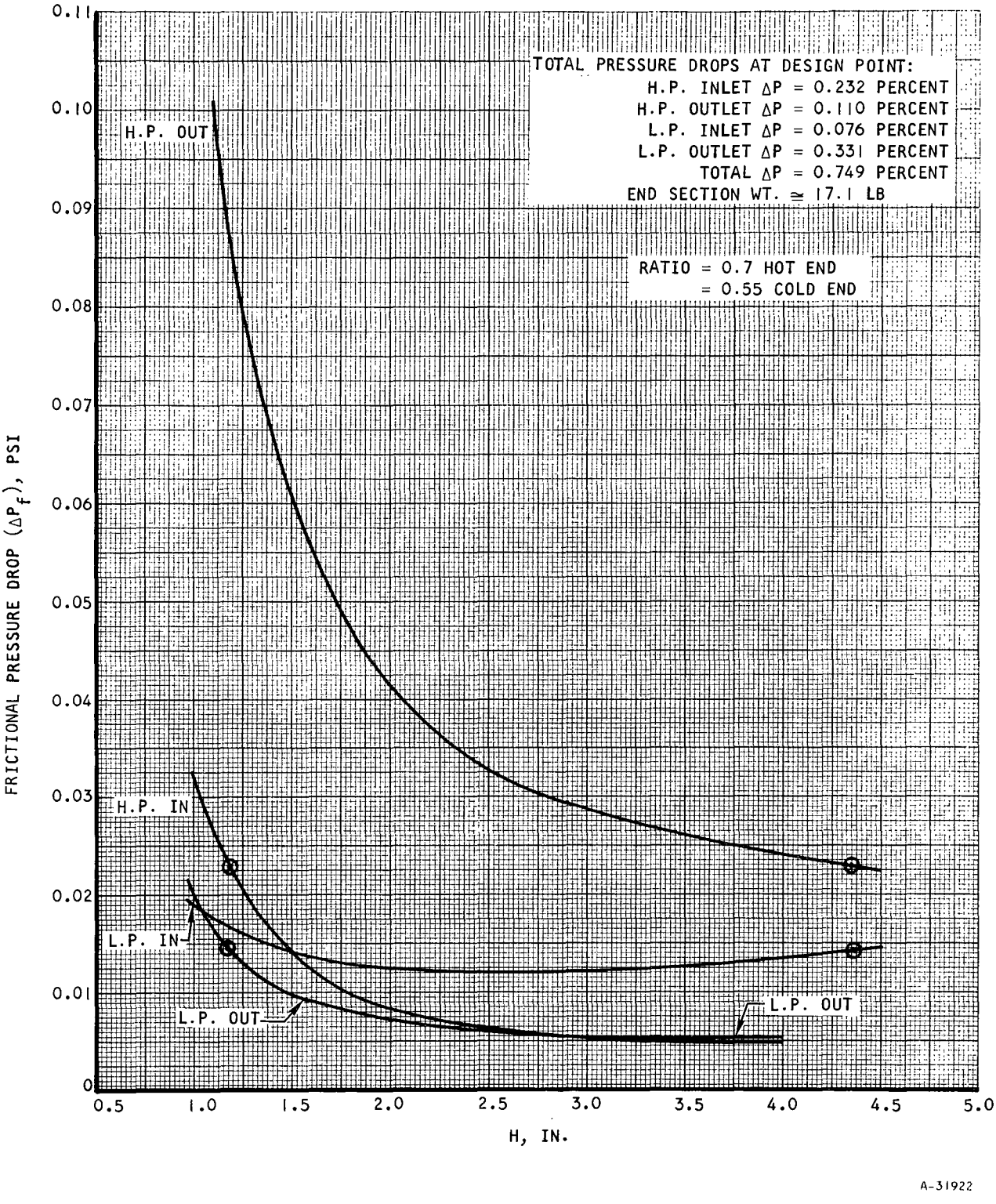

Figure 28. Friction Pressure Loss vs End Section Height, Case 2

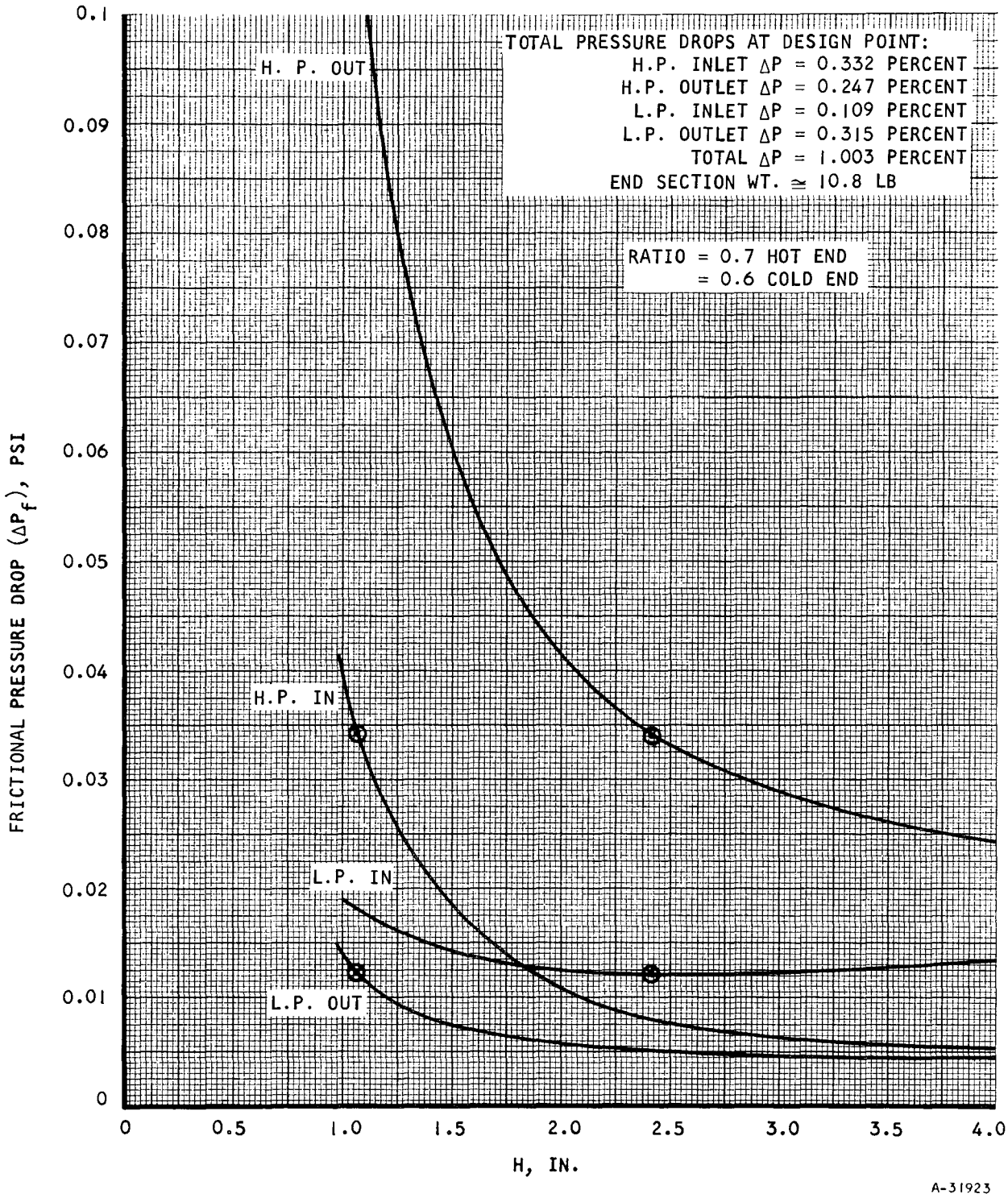

Figure 29. Friction Pressure Loss vs End Section Height, Case 3

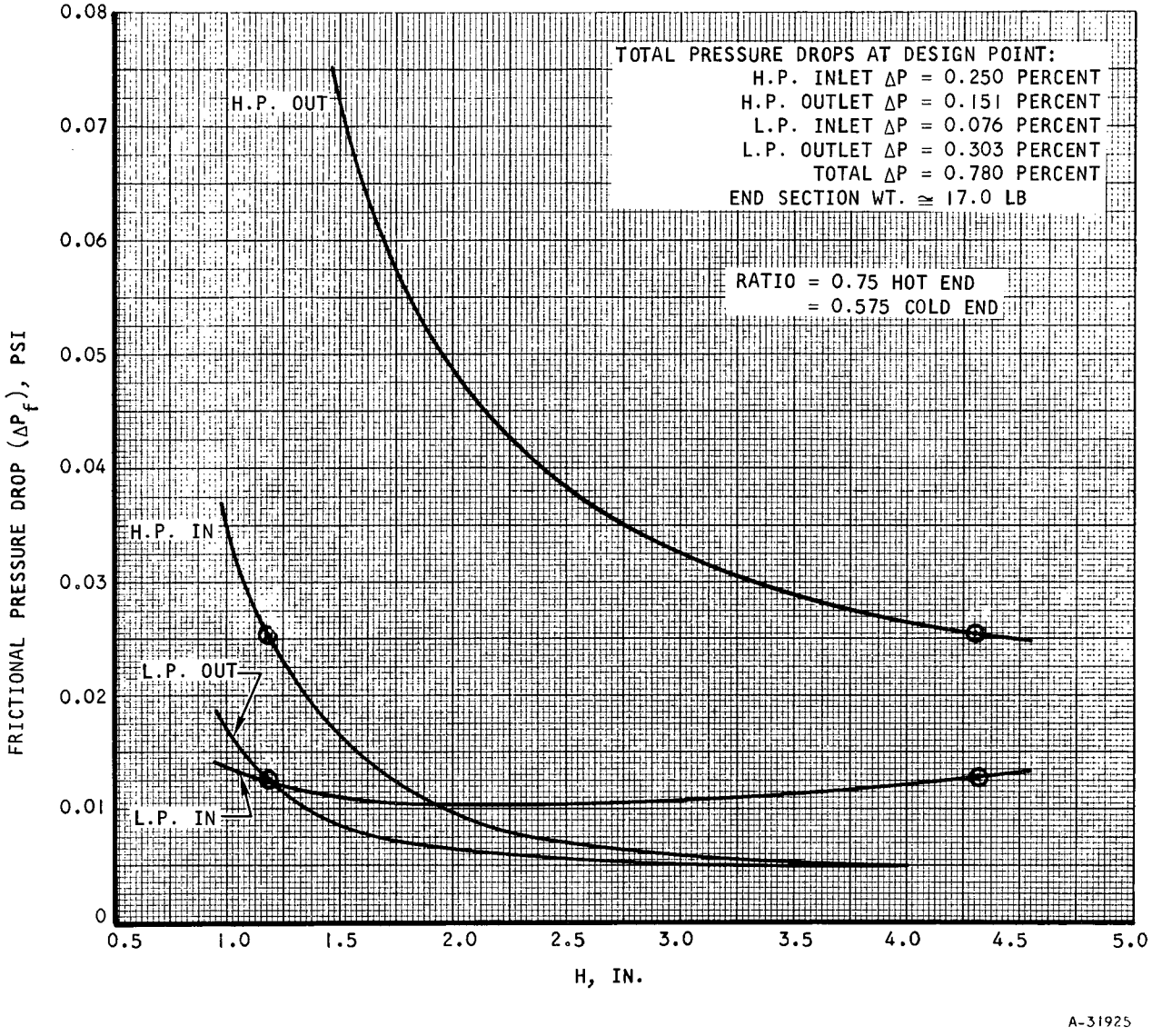

Figure 30. Friction Pressure Loss vs End Section Height, Case 4

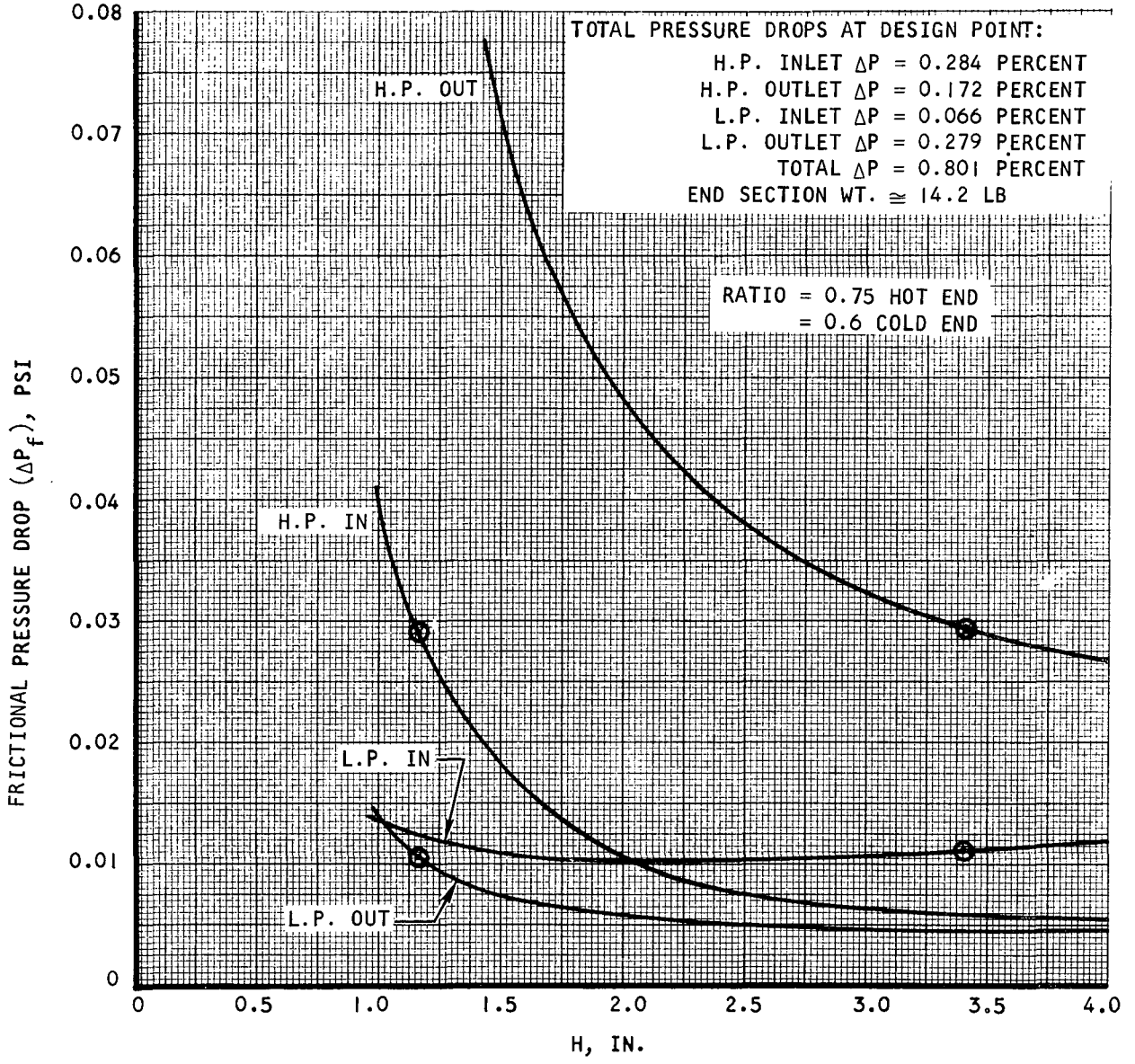

Figure 31. Friction Pressure Loss vs End Section Height, Case 5

6. Variable Specific Heat

During design of the heat sink heat exchanger for the NASA Engine A Brayton cycle system, it was discovered that there would be a serious error in the prediction of exchanger effectiveness if the variation in specific heat of the liquid coolant with temperature were not accounted for in the design calculations. The increase in specific heat with temperature for Dow Corning fluid (or other possible liquid coolants) causes a reduction in the mean temperature difference between hot-side and cold-side fluids and a resultant decrease in exchanger heat transfer performance. This effect occurs because the liquid specific heat is lowest at the liquid inlet and highest at the outlet, resulting in a liquid side temperature profile that rises more steeply near the inlet end of the exchanger and more gradually near the outlet end, thus approaching more closely the gas side temperatures as compared with the profile for a fictitious liquid with constant specific heat.

A computer program was written to determine the effect of variable liquid specific heat on heat exchanger performance for cross-counterflow tubular exchangers. In this program, the performance of each crossflow pass is computed separately, based on average fluid properties within each pass, and the results are synthesized to obtain overall heat exchanger effectiveness. An iterative procedure is required to obtain the correct temperature distribution throughout the heat exchanger, meeting the requirement that, within each pass, the heat transferred match the enthalpy change in the fluid streams. Since the variation in specific heat within each pass is relatively small, this method gives an accurate evaluation of exchanger heat transfer performance.

Using this program, it was found that fluid properties variations in the Engine A Brayton cycle heat sink exchanger caused a reduction of about 1.25 percent in effectiveness, which was equivalent to 12 percent in heat exchanger UA.

Due to the similarity of the problem statements for that heat exchanger and the BHXU heat sink exchanger, it is possible to use these results to estimate the effect of variable fluid properties on the BHXU exchanger. This effect is estimated to be a 12-percent reduction in equivalent UA and has been accounted for in all heat sink exchanger designs.

Heat Sink Exchanger Capacity-Rate Ratio

An analysis was made of the effect on the BHXU of varying the heat sink heat exchanger capacity-rate ratio. Capacity-rate ratios of 0.73, 0.8, and 0.95 were analyzed. For each case, the pressure drop split between recuperator and heat sink exchanger was adjusted so as to obtain an approximate face area match between the recuperator low-pressure outlet and the heat sink exchanger inlet. Curves showing the face areas and resultant pressure drop splits for the heat exchangers are presented in Figure 32. It can be seen that increasing capacity-rate ratio causes the design pressure drop split to move in the direction of lower recuperator pressure drop and higher heat sink exchanger pressure drop. Resultant weights for the individual exchangers and the combination of two exchangers are shown in Figure 33. Results of the analysis are summarized in Table 13. It should be noted that the weights shown are preliminary design estimates and would require upward revision of the same magnitude as the difference between final and preliminary design weights for the reference BHXU, i.e., about 33 percent for each heat exchanger.

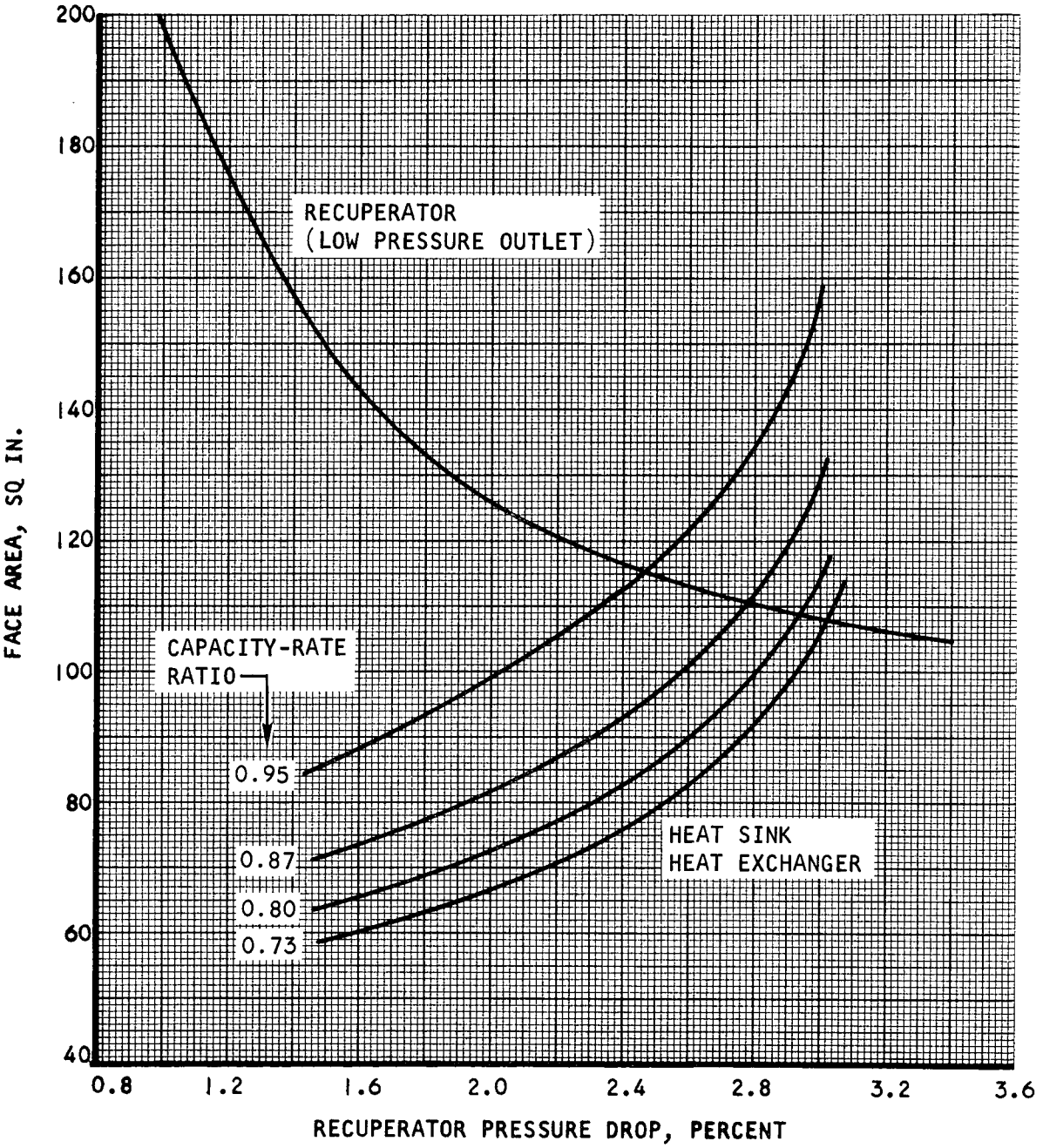

Figure 32. Design Point Selection Curves For Several Capacity-Rate Ratios

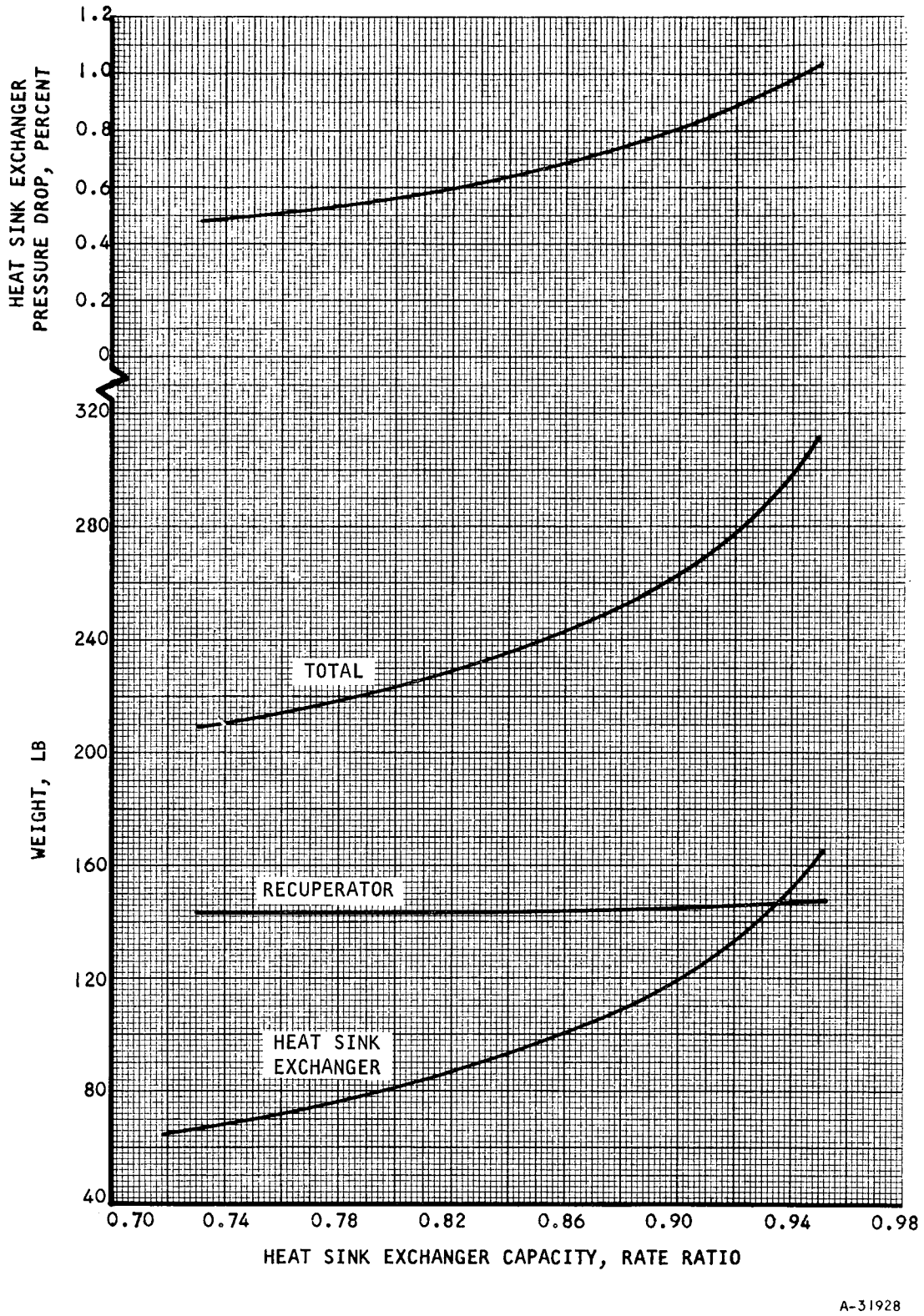

Figure 33. Heat Exchanger Weights and Pressure Drop Split as a Function of Capacity-Rate Ratio

TABLE 13

BHXU DESIGNS AT SEVERAL CAPACITY-RATE RATIOS

Heat Sink HX Capacity-rate Ratio	Pressure Drop, percent		Weight, lb		
	Heat Sink HX	Recuperator	Heat Sink HX	Recuperator	Total
0.73	0.48	3.02	66	143	209
0.8	0.56	2.94	81	144	225
0.87	0.72	2.78	104	144	248
0.95	1.03	2.47	164	148	312

EC/LS Heating

To establish the feasibility of extracting liquid from the heat sink exchanger for the purpose of providing heat to an environmental control and life support system at one or more discrete temperature levels, a calculation was made of the interpass temperatures of the Dow Corning fluid in the heat sink exchanger. Figure 34 shows the liquid temperatures that exist at the interpass locations. It would be inconvenient to extract liquid from between the first and second passes (interpass location 1-2) or from between the seventh and eighth passes (location 7-8) because, at these locations, extraction of the active loop fluid would be from the same face at which the redundant loop fluid enters or exits the core. Extraction of liquid from the other locations would require only a minor modification of the heat exchanger design.

One of the possible requirements, as indicated by NASA, is to provide heat at a temperature level of 250°F or above. Figure 35 shows the amount of heat available above 250°F from the liquid stream exiting the heat sink exchanger as a function of the heat exchanger capacity-rate ratio. This curve is based on the assumption of no heat removal from the liquid at lower temperatures. Removal of heat at lower temperatures would reduce the liquid outlet temperature from the heat exchanger and thus the heat available above 250°F. From Figure 35 it can be seen that approximately 12,300 Btu/hr is available at the design capacity-rate ratio of 0.87.

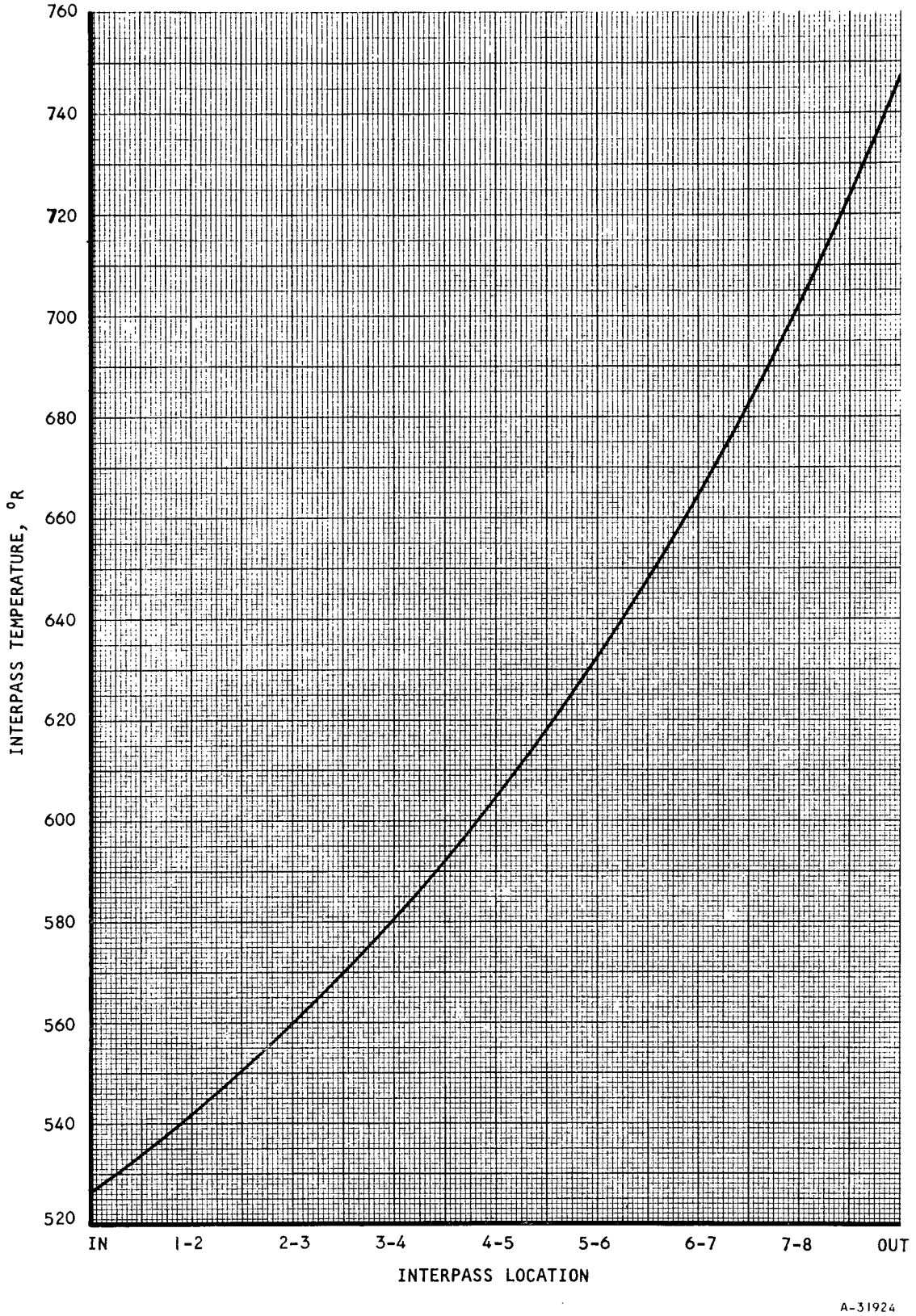

Figure 34. Dow Corning Fluid Interpass Temperatures in Heat Sink Exchanger

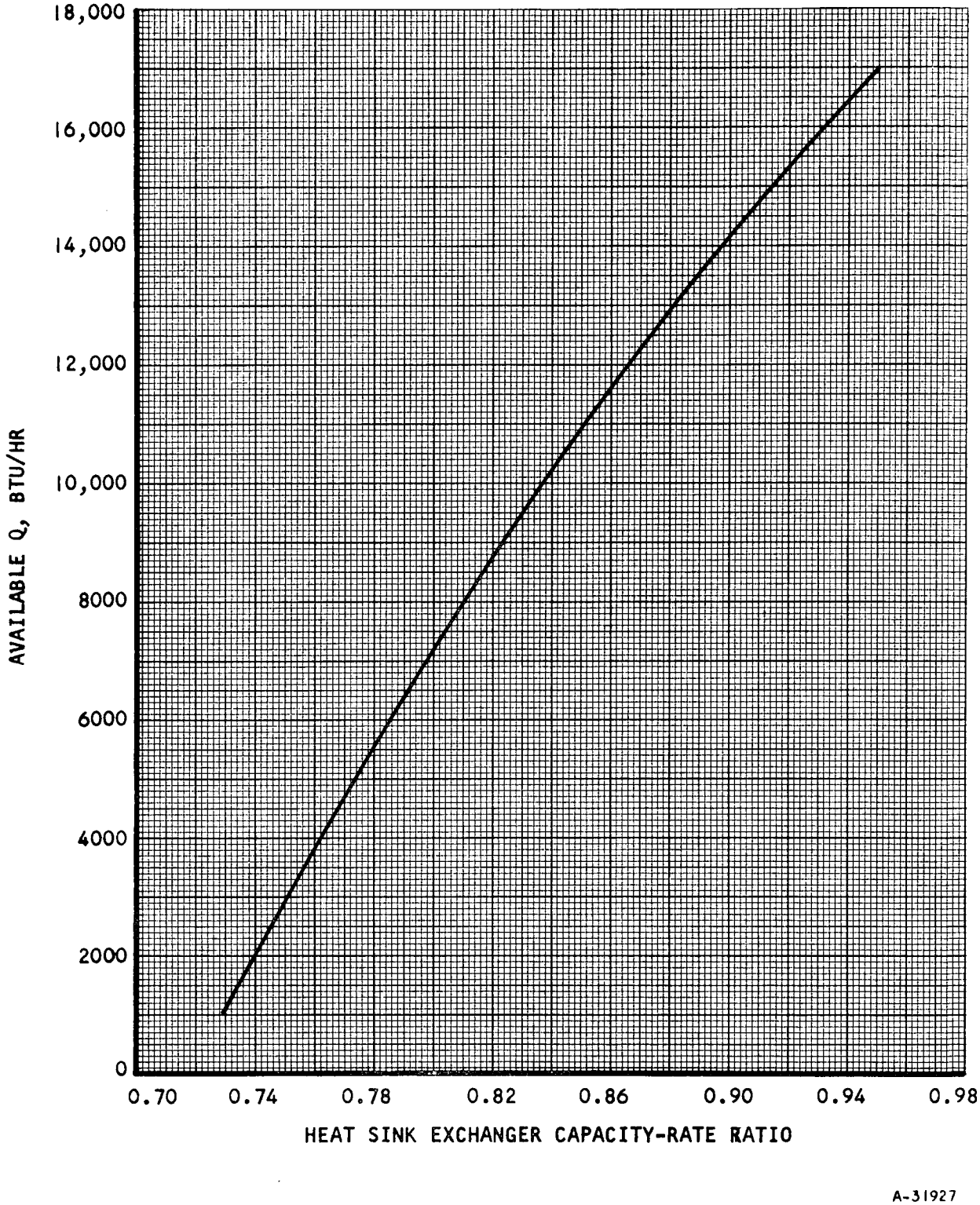

Figure 35. Heat Available Above 250°F From Heat Sink Exchanger Liquid Outlet

Start-Up Temperature Transients

1. Mounting Brackets

The transient temperature distribution in the BHXU mounting brackets under start-up conditions was analyzed using AiResearch computer program H2361, a nodal point thermal analysis program. The first calculation was made for a bracket mounted on the recuperator side plate at the hot end of the recuperator. Figure 36 shows the two-dimensional bracket geometry assumed for the calculation and the calculated temperature history for some typical nodal points of this geometry. The basic assumptions governing the calculation are listed below.

(a) The bracket geometry is two-dimensional, as shown in Figure 36, with a reinforcement plate thickness of 0.375 in., a reinforcement plate width of 6 in., and a total bracket height of 2.8 in.

(b) The bracket is perfectly insulated so that the only heat transfer is between recuperator side plate and bracket.

(c) The bracket material is 347 stainless steel.

(d) The heat exchanger side plate in contact with the bracket maintains a temperature equal to the core hot passage metal temperature during the transient, i.e., the side plate temperature in the vicinity of the bracket is not assumed to be depressed due to the heat flow into the bracket.

(e) At start-up, gas at 1701^{0}R enters the recuperator hot inlet and the recuperator, initially at 0^{0}F, starts heating up with a 15-sec time constant.

Due to the fast response of the recuperator and consequent rapid rise in side plate temperature, the temperature differentials are seen to be quite large for a bracket mounted on the recuperator side plate. A second calculation was made for a bracket located on one of the recuperator hot-end manifolds. The bracket geometry assumed is essentially that of Figure 36, with two reinforcement plate thicknesses considered - a thickness of 0.47 in. to simulate a bracket designed for a soft-mounted BHXU and a thickness of 1.12 in. for a bracket designed for hard-mounted BHXU. The bracket geometries and nodal point locations are shown in Figure 37.

Temperature histories of the two brackets are shown in Figures 38 and 39. Temperature differentials encountered are much less than those obtained with a bracket mounted on the recuperator side plate because of the slower response of the manifold to the inlet gas temperature. A film coefficient of 8 Btu/hr-ft^{2}-^{0}F was used for heat transfer between the gas and the manifold.

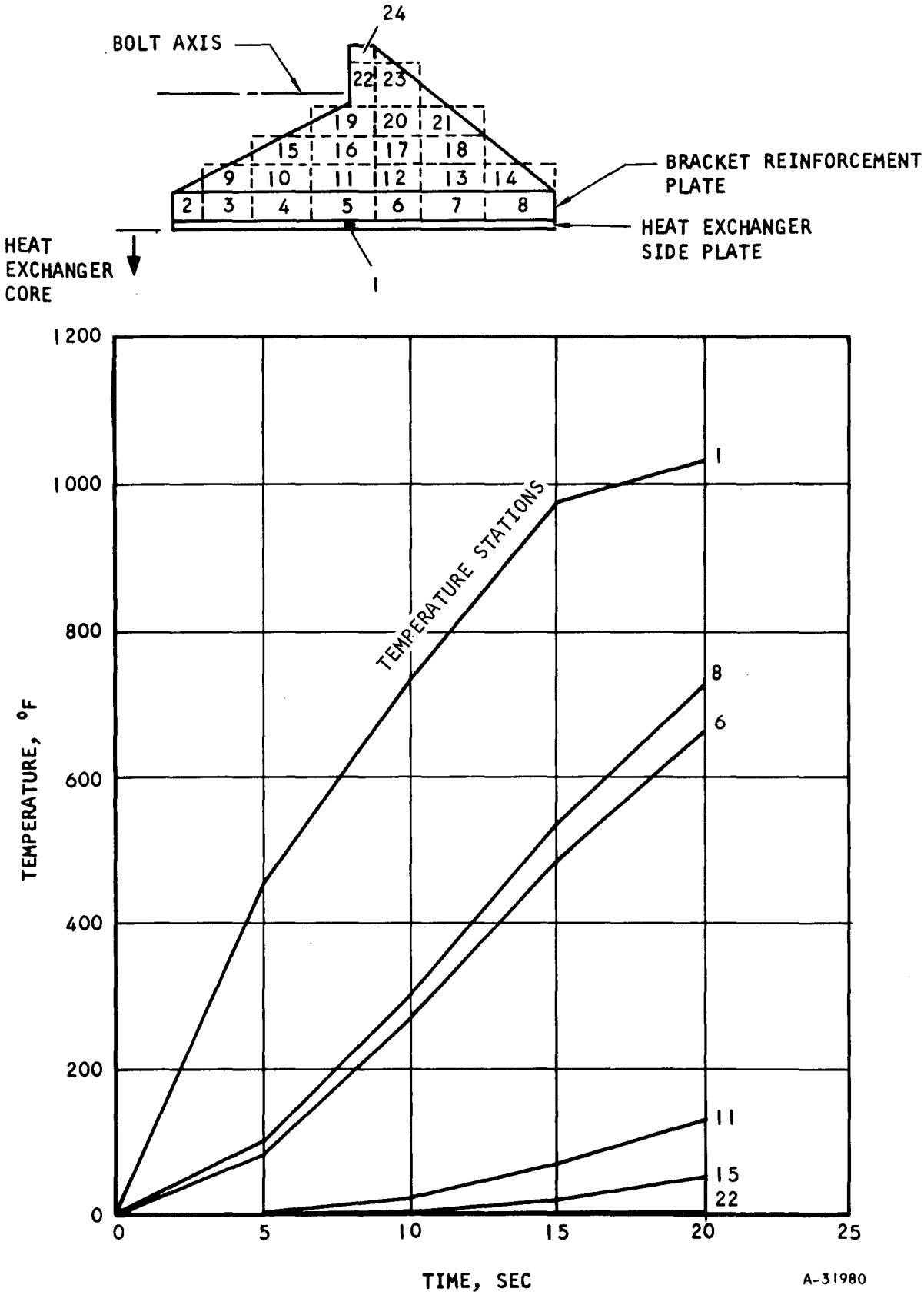

Figure 36. Temperature vs Time from Startup for Bracket Mounted on Recuperator Side Plate

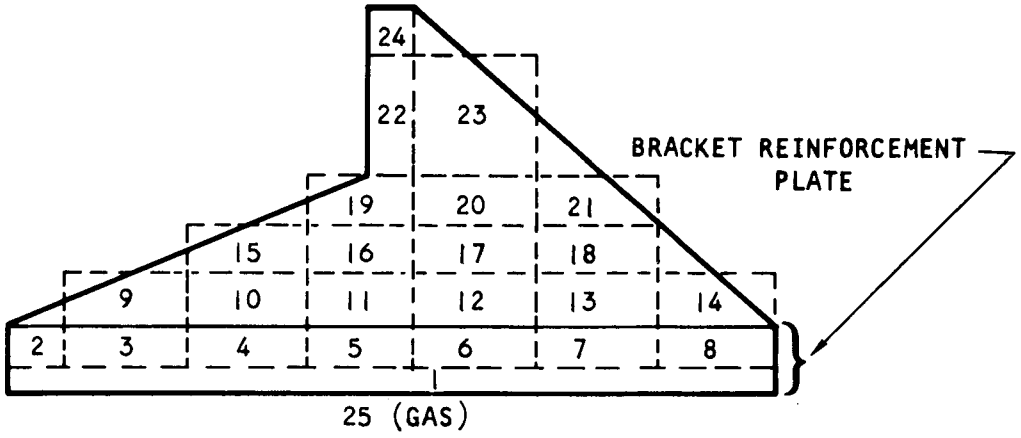

a. BRACKET GEOMETRY FOR BHXU SOFT MOUNT

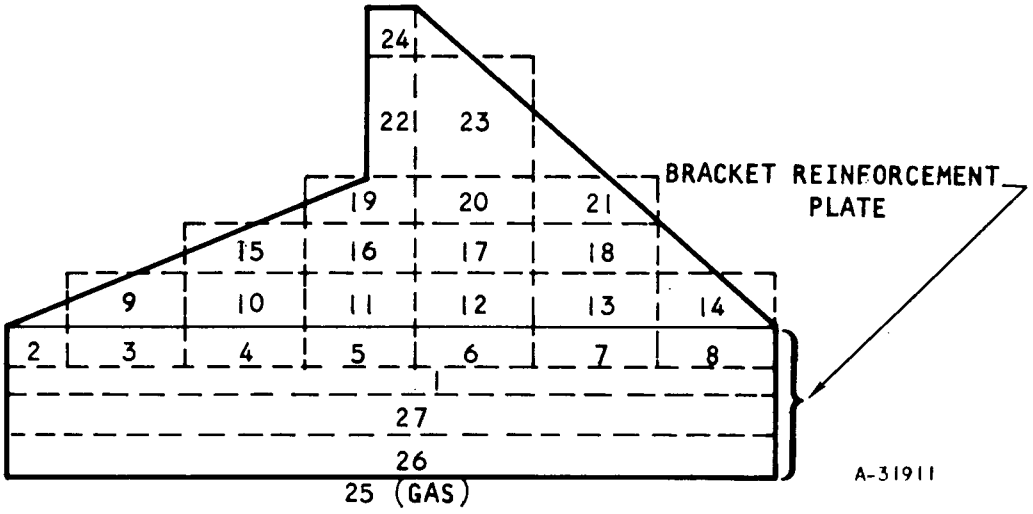

b. BRACKET GEOMETRY FOR BHXU HARD MOUNT

Figure 37. Geometry of Manifold-Mounted Brackets

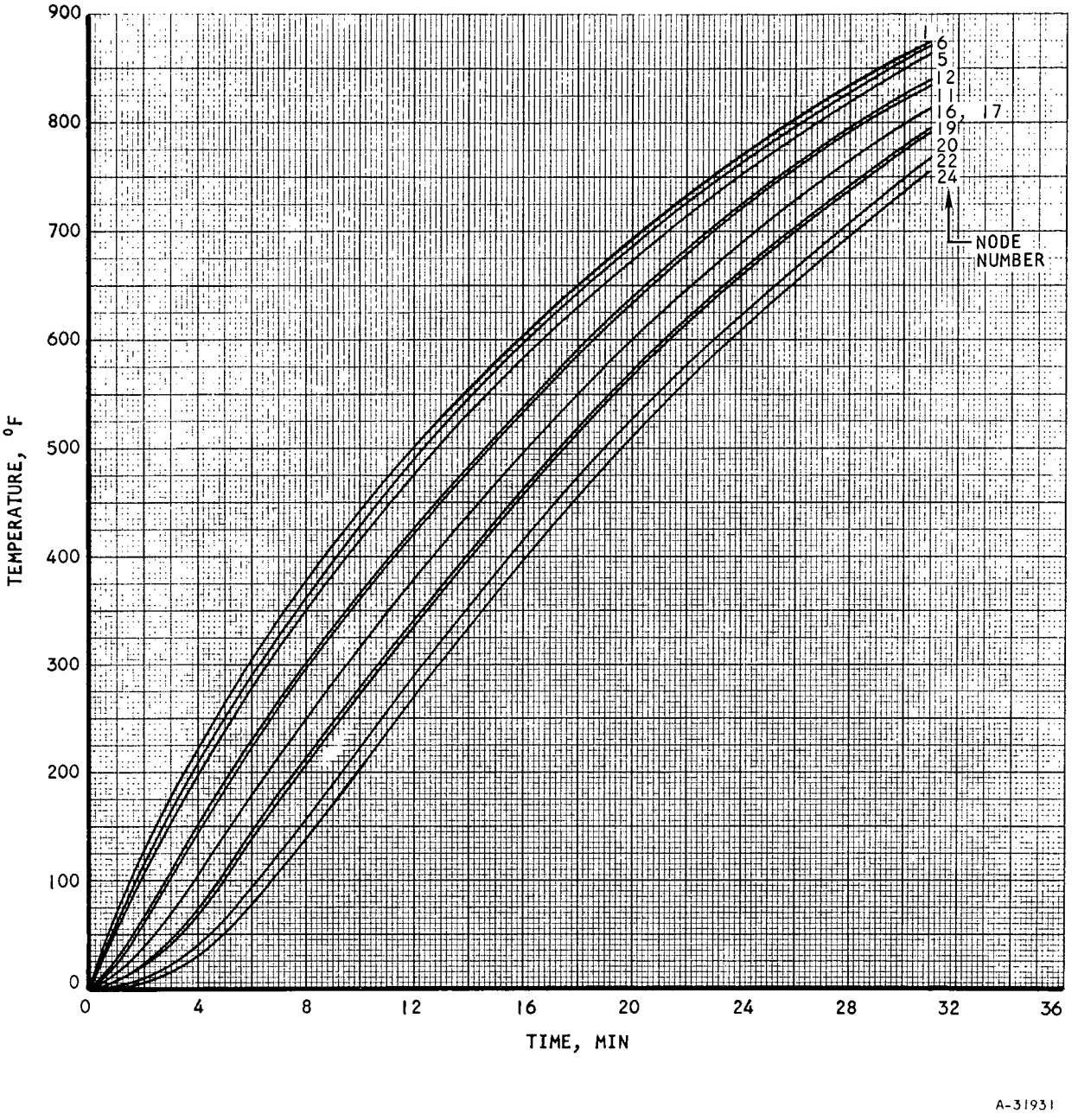

Figure 38. Temperature vs Time From Startup for Manifold-Mounted Bracket Based on BHXU Soft Mount

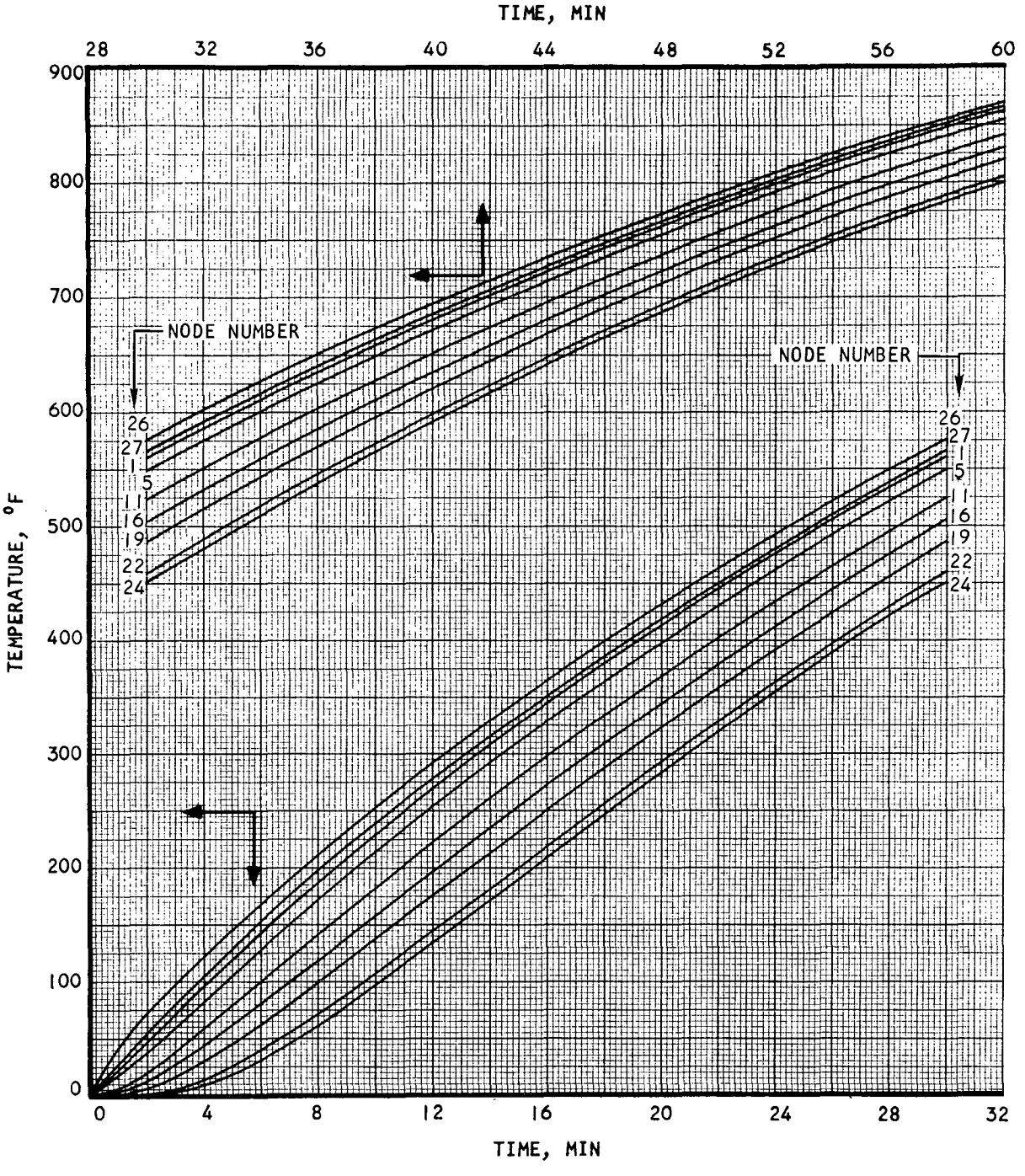

Figure 39. Temperature vs Time From Startup for Manifold-Mounted Bracket Based on BHXU Hard Mount

2. BHXU Thermal Growth

The temperature histories of the recuperator and the turbine exhaust duct during startup were determined. This information is used to size the bellows in the turbine outlet duct to allow for differential thermal expansion between BHXU and BRU, as discussed in the next section of this report. Average recuperator temperature and turbine exhaust duct temperature are plotted as a function of time in Figure 40.

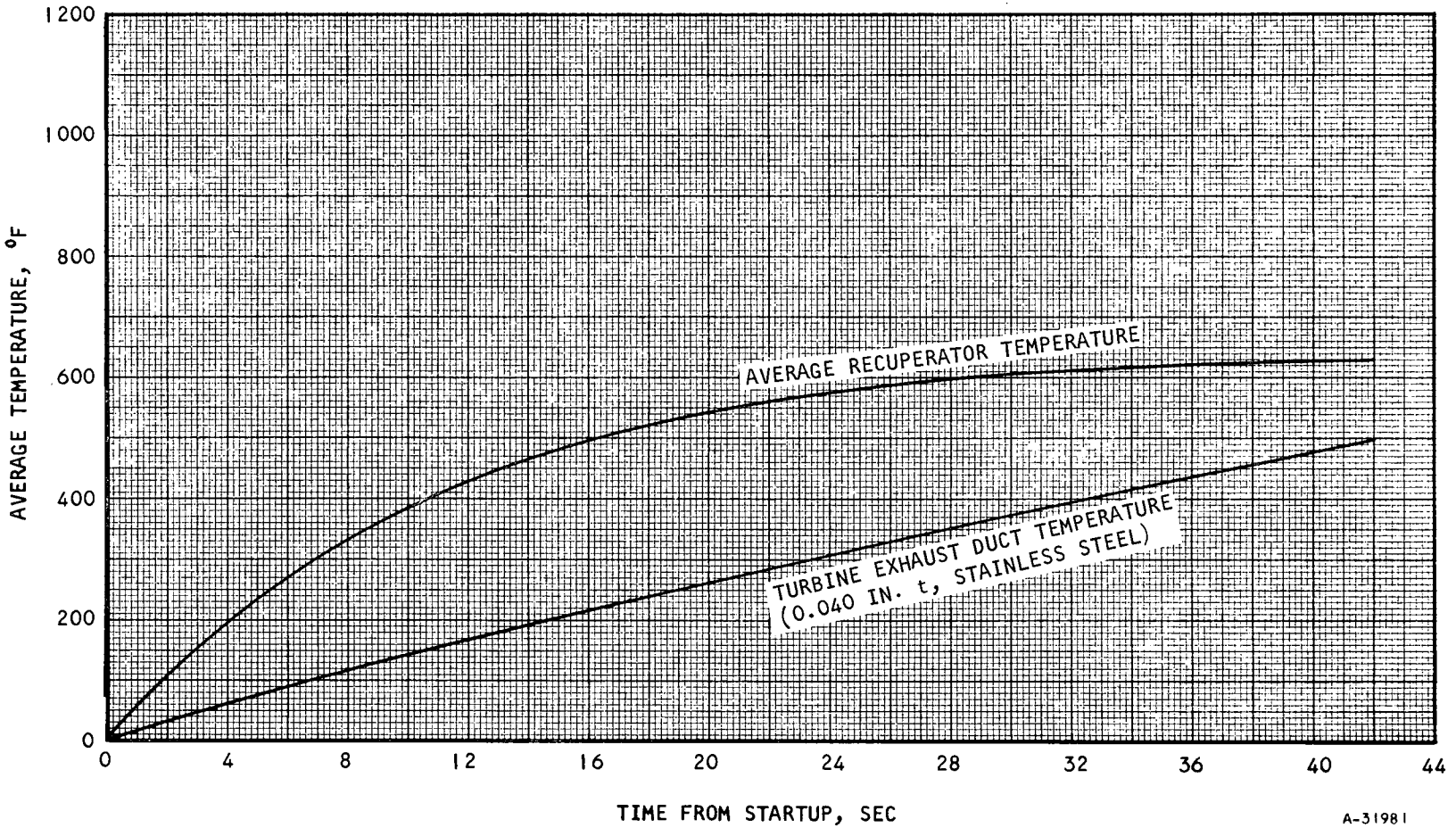

Figure 40. Temperature Rise During Startup for Calculating Elongation of Recuperator and Hot Side Duct

STRUCTURAL DESIGN

This section treats the various structural aspects related to the detailed design of the BHXU. Although the BHXU consists of two separate heat exchangers, the recuperator and the heat sink heat exchanger are rigidly joined to form an integral structural element with respect to environmental loads, support bracketry, and interconnecting ducts to the BRU and heat source heat exchanger. In addition, the recuperator and heat sink heat exchanger are each designed to provide adequate structural integrity for pressure containment loads and thermal stresses to satisfy the required reliability objectives.

Summary

1. Design Criteria

The operating conditions for the BHXU package include a maximum operating temperature of 1701°R (1241°F) in the recuperator for a design life of 5 years (about 44,000 hr). The short-time material properties were used for temperatures below 800° to 900°F. For sustained operations at higher temperatures, the 1 percent creep and stress rupture properties for 50,000 hr at temperature were used. The design of the heat sink heat exchanger is based on material properties at 325°F.

It was further specified that a 100-cycle life is required for this unit. A typical cycle is defined to be startup of the unit, operation at design temperatures and pressures, and shutdown. This requirement applies primarily to thermal loads due to temperature gradients and differences in the system. Thermal stresses exceeding the material yield strength cannot be completely avoided due to the rapid startup condition. Structural performance was evaluated by considering the relation between accumulated plastic strain per cycle and number of cycles to failure. The results of the analysis presented below indicate that a cycle life considerably in excess of the 100-cycle requirement will be achieved.

2. Material Selection

Type 347 stainless steel was selected for the recuperator and heat sink heat exchanger based on its suitability for the design operating conditions and AiResearch experience with this material in similar applications. Hastelloy X was used for the hot duct and in the high temperature section between the BRU turbine outlet and the BHXU high temperature inlet manifold flange. The transition from Hastelloy X to Type 347 steel is accomplished in the flange between the bellows and the recuperator pan to place the thermal expansion loads in a region away from the more sensitive BRU and recuperator core matrix.

3. Heat Exchanger Core Design

The heat exchanger core utilizes standard AiResearch fin and plate geometry and presents no serious structural design problems for the desired operating conditions. Table 14 shows the operating conditions, fin geometry and associated minimum safety margin. The minimum tube plate thickness is 0.008 in. and minimum side plate thickness is 0.060 in.

4. Manifold and Duct Design

The heat exchanger manifold configurations were selected based on fabricability considerations and the desire to achieve a lightweight design. The recuperator high pressure outlet and heat sink gas outlet pans are of circular cross section with an included angle greater than 180 deg. This design places the greater portion of the shell under direct membrane stress which produces the lightest weight configuration. The recuperator high and low pressure inlet pans are essentially semicircular with short flat sections mating to the core. This design is somewhat less efficient than a circular shape. However, the flat area is small on the low pressure inlet and space limitations preclude use of a complete circular shape on the high pressure inlet.

5. Bellows Design

Expansion bellows were required in each of the three ducts connecting the BHXU to the BRU. These bellows isolate the BHXU thermal movements so that duct loads applied to the BRU scrolls would be within acceptable limits. Preliminary thermal movements at the three bellows were estimated and this information, along with other specific design requirements, was submitted to several bellows manufacturers to obtain proposed configurations. AiResearch then performed a stress analysis of each candidate bellows configuration. Finally, double-ply, formed bellows manufactured by Aeroquip Corporation were selected for all three ducts based on the most accurate accommodation of the problem statement.

6. Mounting System Design

A six-point mounting system was selected based on requirements to: (1) minimize thermal expansion differences between the BHXU and BRU, (2) minimize bracket and heat exchanger loads and (3) minimize thermal stresses in the recuperator due to transient temperature gradients which occur due to differential heating (or cooling) of components with different thermal masses. The brackets are mounted on manifolding to eliminate the possibility of severe thermal stresses in the core (particularly in the fins) which would arise during transient conditions.

The six-point system is designed to allow for free thermal growth of the recuperator about a fixed point which is located on the recuperator-to-heat sink transition piece near the BRU. Pairs of brackets were located on the recuperator high pressure outlet pan, transition piece and heat sink gas outlet pan to provide a lightweight support bracketing system. Particular consideration was given to minimizing thermal expansion differences in

TABLE 14

OPERATING CONDITIONS, FIN GEOMETRY, AND MINIMUM SAFETY MARGIN

Unit	Circuit	Operating Conditions		Fin Geometry				Minimum Margin of Safety
		Max Temp, °F	Max Pressure, psi	Fins Per in.*	Fin Height, in.	Fin Offset, in.	Fin Thick, in.	
Recuperator	Low pressure	1241	30.5	16RO	0.153	1/7	0.004	+1.01
				10R	0.153	-	0.004	+0.24
	High pressure	1194	56.0	16RO	0.125	1/8	0.004	+0.53
				10R	0.125	-	0.004	-0.09**
Heat Sink	Gas side	325	30.5	16RO	0.125	1/8	0.004	+11.8
	Liquid side	300	100	20RO	0.050	1/10	0.002	+3.80

*R, plain rectangular(triangular end sections);
RO, rectangular offset
**This fin has a 90°F overtemperature capability rather than the design criteria of 100°F.

the plane of the attach points on the brackets and maximum deflection differences of less than 0.005 in. were achieved for the entire operating cycle of the BHXU.

Detailed bracket design was based on the use of an isolation mounting arrangement which will limit the BHXU maximum load to 24 g in the spacecraft axis and 20 g lateral to the spacecraft axis. A comparison of an isolation mounting vs a hard mount system for solid supports showed that a large weight penalty is sustained in the BXHU brackets for the hard mount case. In addition, core reinforcement would be required to transmit the loads to the brackets. The actual bracket supports are box-structures which are more efficient than solid rings for transferring the loads from the brackets to the cores.

The mounting approach recommended by AiResearch for the BXHU-BRU package consists of a frame, hard mounted to the BHXU and BRU (with internal thermal expansion provisions), which is in turn mounted on isolators. The entire mount frame and Brayton cycle subsystem therefore acts as a single unit within the spacecraft or test facility. The structural analysis and design considerations required to integrate the frame structure with the present equipment are further amplified later in this section.

Structural Design Criteria

A variety of load conditions, stress conditions, and types of failure mode possibilities will be experienced by the BHXU during its five-year service life. The detailed set of design criteria discussed below was used to design the various BXHU components.

1. Allowable Stresses for Internal Pressure Design

The standard design practice employed by AiResearch is to design the pressure carrying structure for proof pressures of 1.5 times the working pressures and for burst pressures of 2.5 times the working pressures. The structure must not yield at proof pressure or rupture at burst pressure. This implies that the proof pressure is the governing design condition if the ratio of yield stress to ultimate stress is less than 0.6 and that the burst pressure will govern if the ratio is greater than 0.6. The allowable stress at working pressure is, therefore, the lesser of the following:

$$\sigma_{all} = (f_{tu})/2.5 \qquad (1a)$$

$$\sigma_{all} = (f_{ty})/1.5 \qquad (1b)$$

When the limiting stress is due to bending, a small amount of yielding can be allowed in the outermost fibers which leads to a modified stress distribution through the thickness. The ideal plastic bending moment is 1.5 times the computed elastic bending moment for the same peak stress. Accordingly, the allowable indicated elastic stress due to bending loads is taken to be 1.5 times the allowable values in Equation (1).

At elevated temperature, the above conditions must be satisfied, and in addition, the component must be satisfactory for long time creep effects. A set of criteria for creep must be comparable to those for the short time loading. Accordingly, limitations based upon stress-to-rupture and stress-to-one percent creep must be established. The rated design life of the unit is five years and it will be designed for sustained pressure operation at maximum operating temperature throughout the entire design life. Allowable stresses at working pressure must be the lesser of the following:

$$\sigma_{all} = [(\text{1-percent creep stress})_{50,000\ hr}]/1.2 \qquad (2a)$$

$$\sigma_{all} = [(\text{creep-rupture stress})_{50,000\ hr}]/1.5 \qquad (2b)$$

Material properties at elevated temperatures are very sensitive to temperature. For the candidate materials, an increase in temperature of $100^{0}F$ typically leads to a decrease of approximately 33 percent in creep and stress rupture strengths. Therefore, an allowance must be made to account for the possibility of overtemperature. The design temperature used to establish allowable stresses is taken to be the maximum operating temperature plus $100^{0}F$.

One modification of the above will be made for bending load designs which will be governed by the material creep properties. When the limiting pressure stress is caused by bending load, the steady creep stresses are substantially lower than those indicated by an elastic analysis. By using the plastic hinge moment analogy, an allowable creep bending stress can be used that is 1.5 times the stated values from Equation (2). Stated slightly differently, the actual sustained creep stress due to bending is taken to be 0.667 times the indicated elastic stress.

2. Allowable Stresses for Inertia Loads

Inertia loads may be experienced during any phase of the operating cycle of the unit. The mounting brackets must, therefore, be designed to carry the inertia loads at elevated temperature. Since the maximum loads occur for a relatively small time duration during vehicle launch, the short time material properties will be used.

The design allowable stress used for the inertia loads will be governed by Equation (1) for direct stresses and modified by a 1.5 factor for bending as discussed above. It should be noted that this will lead to a conservative bracket design because the above criteria allows for simultaneous application of the various inertia loads discussed below. In practice, these loads will not occur simultaneously and the peak loads experienced by the mounting system may be considerably less than the quoted combined maximum values. For example, application of the shock load and vibration load at different times would produce maximum bracket loads at about 50 percent of the design load capability.

3. Allowable Thermal Fatigue Stresses

The magnitude of thermal stress due to temperature differences developed during the rapid heat-up cycle of the system results in plastic deformations in various components, particularly in the hot operating regions. The minimum operating life requirement of the unit is 100 thermal cycles. A minimum design life of 400 cycles would be used to ensure that the 100-cycle life is achieved. The required analyses were based on the accumulated plastic strain approach for estimating fatigue life. The number of cycles to failure N is determined from the formula:

$$N = \frac{2C^2}{(\epsilon_p)^2_{1-2} + (\epsilon_p)^2_{4-5}} \qquad (3)$$

where N = cycles to failure

ϵ_p = plastic strain

C = material ductility constant

The ductility constant is based upon the material reduction of area property, RA, and the formula recommended by S. S. Manson of NASA Lewis Research Center is

$$C = 0.79 \ln \left(\frac{100}{100 - RA}\right)$$

The ductility constant is determined from material properties, and the plastic strain is estimated from a typical load cycle for the material. Two examples of loading sequences are shown in Figure 41 with the associated expressions for determining ϵ_p. Cumulative effects for different load cycles during the material life are handled by a fatigue damage rule similar to Miner's rule. In addition, since both creep and fatigue are occurring simultaneously, the effects of the two material damage phenomena are important.

Material Properties

The physical and mechanical properties of Type 347 SS and Hastelloy Alloy X are shown in Tables 15 and 16, respectively. The references used in computing the tables are included. The design allowables for 347 steel are shown in Table 17 for sustained and short-time operation under direct and bending stresses.

Core Analysis

1. Pressure Containment, Recuperator

Calculations are presented for stresses in the fins and plates of the recuperator core structure. The core geometry will consist of 0.004-in. thick

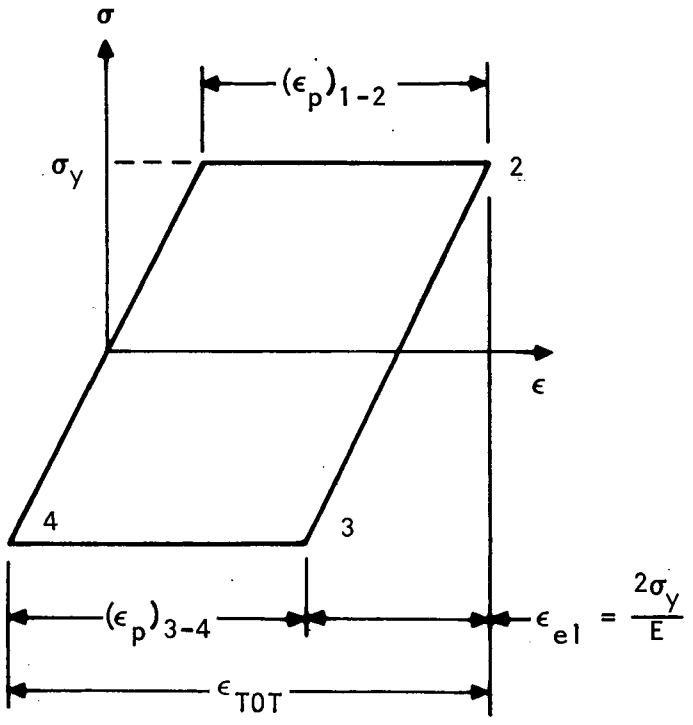

a. CYCLE WITHOUT CREEP

$$(\epsilon_p)_{1-2} = \epsilon_{TOT} - \frac{2\sigma_y}{E}$$

$$(\epsilon_p)_{3-4} = \epsilon_{TOT} - \frac{2\sigma_y}{E}$$

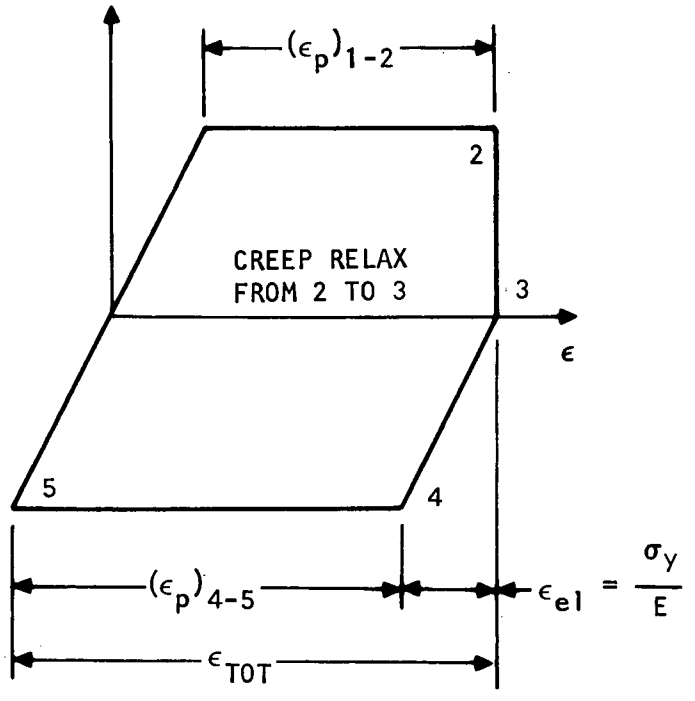

b. CYCLE WITH CREEP

$$(\epsilon_p)_{1-2} = \epsilon_{TOT} - \frac{2\sigma_y}{E}$$

$$(\epsilon_p)_{4-5} = \epsilon_{TOT} - \frac{\sigma_y}{E}$$

A-30679

Figure 41. Typical Ideal Elastic - Plastic Load Cycles

TABLE 15

TYPE 347 SS MATERIAL PROPERTIES

Temp, °F	σ_{tu}, psi	σ_{ty}, psi	1 Percent Creep 50,000 hr, psi	Stress Rupture in 50,000 hr, psi	Elastic Modulus, 10^6 psi	Thermal Expansion, 10^{-6} in./in./°F	RA, Percent
70	90,000	36,000			28.0	8.60	65
200					27.2	9.10	70
300					26.6	9.25	
400	78,000	34,000			26.0	9.40	74
500					25.4	9.50	
600	71,000	32,000			24.8	9.65	72
700					24.2	9.75	
800	65,000	30,000			23.6	9.85	70
900			39,000		23.0	9.95	
1000	60,000	28,000	29,000	34,000	22.4	10.10	65
1100	56,000	26,000	18,000	23,000	21.8	10.25	
1200	51,000	24,000	12,000	15,000	21.2	10.45	67
1300	43,000	22,000	6,000	8,000	20.6	10.65	
1350	39,000	21,000	4,300	6,000	20.3	10.75	
1400	35,000	20,000	2,800	4,100	20.0	10.9	70
1500	26,000	18,000					

Data Obtained From:

1. Armco stainless steels, Armco Steel Corporation, Copyright 1963
2. Carpenter stainless and heat resistant steels, The Carpenter Steel Co., Copyright 1965
3. Aerospace Structural Metals Handbook, Syracuse University, March 1963 rev. March 1964
4. U.S. Steel

TABLE 16

HASTELLOY X MATERIAL PROPERTIES

Temperature, ^{0}F	σ_{tu}, psi	σ_{ty}, psi	1 Percent Creep in 50,000 hr, psi	Stress to Rupture in 50,000 hr, psi	Elastic Modulus, 10^{6} psi	Thermal Expansion, 10^{-6} in./in./^{0}F
70	114,000	52,000			28.6	
200	111,000	51,000			28.1	7.70
400	107,000	48,000			26.9	7.82
600	103,000	46,000			25.8	7.90
800	98,000	44,000			24.6	8.15
1000	94,000	42,000			23.4	8.39
1200	83,000	40,000	13,000	18,400	22.3	8.56
1300	73,000	39,000	9,800	12,500		
1400	63,000	38,000	8,400*	10,200*	21.1	8.81
1600	37,000	26,000			19.9	9.02

*1350^{0}F

Reference - "High Temperature High Strength Nickel Base Alloys" The International Nickel Company Inc., 67 Wall Street, New York, N.Y., 10005, Copyright 1964

TABLE 17

347 STEEL ALLOWABLE DESIGN STRESSES

Maximum Operating Temperature, °F	Allowable Stress for Sustained Operation			Allowable Stress for Short-Time Operation		
	Design Temperature, °F	Direct Stress, psi	Bending Stress, psi	Design Temperature, °F	Direct Stress, psi	Bending Stress, psi
70	70	24,000	36,000	70	24,000	36,000
350	350	23,000	34,000	350	23,000	34,000
1200	1300	5,000	7,500	1200	16,000	24,000
1250	1350	3,600	5,400	1250	15,300	23,000

rectangular offset and plain fins and 0.008-in. thick plates. The rectangular offset fin spacing is 0.0625 in. (16 fins/in.) and the triangular end fin spacing is 0.10 in. (10 fins/in.)

Fin tensile stress due to internal pressure is computed from the following formula:

$$\sigma_{fin} = \frac{p}{f}\left(\frac{b_{fin} - t_{fin}}{t_{fin}}\right)$$

where p = internal pressure

b_{fin} = fin spacing

t_{fin} = fin thickness

f = fin strength efficiency factor

Fin strength efficiency factors have been found to range from 0.25 to 0.50 based upon actual test results on a wide variety of plate and fin configurations. The 0.25 factor will be used in high temperature designs to reflect the uncertainty in the long-life material properties and 0.50 will be used in low temperature situations. The strength efficiency factor is defined as the ratio of actual burst pressures to burst pressures as calculated from ultimate stress properties. The apparent reduction in strength is attributable to nonuniform load distribution across the fins which arises due to inequality in fin height. The taller fins actually buckle during the braze operation and as a consequence the shorter fins carry the bulk of the pressure containment forces. Since the fins are never perfectly straight, pressure loads will also cause fin bending stresses. Finally, the fins cannot be formed with perfectly square corners, and stress concentrations will actually occur at the fin to plate braze fillet joints. This strength reduction factor is based upon the performance of successfully brazed heat exchangers, i.e., the failure mode at burst is tensile rupture of the fins. For poorly brazed heat, exchangers (incomplete braze joining of the fins and plates), the pressure containment capability of the plate fin structure is drastically reduced. For this reason, all heat exchangers are subjected to a proof pressure test at 150 percent of working pressure. This proof test is expected to cause a failure in defective cores, and conversely, a unit that passes the proof test is expected to achieve the required pressure capability.

For the given core geometry, the maximum fin stress, in the triangular ends, is

$$\sigma_{fin} = \frac{p}{0.25}\left(\frac{0.10 - 0.004}{0.004}\right) = 96\ p$$

The triangular fin stress in the high pressure side which has a 1300°F design temperature is therefore

$$\sigma_{fin} = (96)(56) = 5400 \text{ psi}$$

Similarly the stress in the triangular low pressure side (30.5 psi) is 2900 psi. The allowable stresses of 5000 and 3600 psi, respectively, are listed above for 347 stainless steel. The fin stress on the high pressure side exceeds the allowable stress by 400 psi. This indicates that the overtemperature capability of this fin set is only 90°F (σ_{all} at 1290°F equals 5400 psi). The recuperator fin stress summary (Table 14) shows that the other fin geometries have excess strength for the 100°F overtemperature requirement.

Maximum plate bending stress is given by the following formula for a fixed ended plate under uniform normal pressure:

$$\sigma_{plate} = \frac{p}{2}\left(\frac{b_{fin} - t_{fin}}{t_f}\right)^2$$

where t_f = plate thickness

The calculated bending stress for a 25.5 psi (56 - 30.5) pressure differential across the plate is

$$\sigma_{plate} = \frac{25.5}{2}\left(\frac{0.10 - 0.004}{0.008}\right)^2$$

$$\sigma_{plate} = 1800 \text{ psi}$$

Type 347 stainless steel is a satisfactory material for this design. Higher pressure differentials will be experienced by the outer plates, however, they are 0.060 in. thick to prevent damage from handling or other external causes. The side plates also carry the manifold pressure loads as well as the acceleration loads into the core.

2. Pressure Containment, Heat Sink Heat Exchanger

The plate-fin heat sink heat exchanger uses a spacing of 0.0625 in., a 0.153-in. fin height and a 0.004-in. thickness on the gas side. The maximum design pressure is 30.5 psi. On the liquid side the geometry is 0.002-in. fin thickness with an 0.050-in. fin spacing. The design pressure on the liquid side is 100 psi. The maximum expected temperature in this unit is 325°F.

The fin tensile stress on the high pressure side is

$$\sigma_{fin} = \frac{p}{0.50}\left(\frac{b_{fin} - t_{fin}}{t_{fin}}\right)$$

$$\sigma_{fin} = \frac{100}{0.50}\left(\frac{0.050 - 0.002}{0.002}\right)$$

$$\sigma_{fin} = 4800 \text{ psi}$$

This is well below the allowable stress for Type 347 stainless steel at 325°F (σ_{all} = 23,000 psi).

The maximum plate bending stress occurs for a pressure differential of 100 psi assuming loss of gas side pressure. For 0.008 in. thickness plates,

$$\sigma_{plate} = \frac{100}{2}\left(\frac{0.050 - 0.002}{0.008}\right)^2$$

$$\sigma_{plate} = 1800 \text{ psi}$$

3. Core Thermal Stresses

Core thermal stresses were minimized in the design by placing the mounting brackets on the pans, rather than on the side plates, and by increasing sheet thickness in the passages adjacent to the side plates. Sheet thicknesses of 0.012, 0.016, and 0.020 in. were used to transition from the 0.008 in. plates in the interior to the 0.06 in. side plates. This design approach reduces the transient temperature differentials between the side plates and the adjacent sheets and it improves the area ratios between sheets to give better load distribution. Of the two effects the improved load distribution may give the largest reduction in sheet thermal strain. For example, when the side plate is significantly stronger in load carrying ability than the adjacent sheet, the weaker sheet is deformed to nearly the full thermal strain potential, i.e.,

$$\epsilon = \alpha\Delta T$$

However, when the balance between the sheets is optimum the strain level in each sheet will be

$$\epsilon = \alpha\Delta T/2$$

To achieve balance, adjacent sheet thickness greater than the side plate thickness would be required, however, the use of 0.020-in. rather than 0.008-in. plates will give a significant thermal strain reduction.

Manifold and Duct Design

A summary of the gas side pan designs is shown in Table 18. The maximum internal pressure stresses, allowable stresses and external (buckling) pressure capabilities are included. An external pressure strength of 1 atm is required due to a requirement for helium leak checks which are accomplished by evacuating the core. Two basic configurations were used: a circular pan with an included angle greater than 90 deg (balloon shape) and a semicircular pan with flat sides joining to the core. Figures 42 and 43 show the two types of designs along with free body diagrams and equations for determining the various discontinuity loads relevant to each shape.

The high pressure outlet and low pressure outlet pans are circular shape to achieve the most effective design for these pans. For example the high pressure outlet would be greater than 0.080 in. thick for the same flow area if a combination of semi-circle and flat sides were used. This would be an increase in weight of over 25 percent over the sizes used. In addition, the transfer of inertia loads across the flat section would also require extra reinforcing as compared to the circular shape.

The low pressure inlet pan has a varying height along its length which is accommodated by using a varying height flat section. The flat section is preferable to a varying radius circular shape due to relative ease of fabrication. The small weight penalty associated with using the flat sections rather than a full circle does not warrant the added compelxity. The high pressure inlet pan also has a flat portion adjacent to the core since space limitations precluded use of the more efficient circular shape. The pan is of relatively small size and operates at relatively low temperatures so the weight penalty associated with using a non-optimum shape is not significant.

The analysis of pan stresses assumed the pans fixed to the recuperator and heat sink heat exchanger. The maximum discontinuity bending stresses occur at the core attachment and generally exceeded membrane stresses in the pans. A discontinuity analysis was also performed on the high pressure outlet between the pan, doubler and mounting bracket ribs. This analysis is shown in Figure 44. Figure 45 shows the analysis of the side pan on the transition ducting between the recuperator and heat sink heat excahnger.

A summary of the stresses in the ducting system connecting the BHXU and BRU is shown in Table 19. The stresses in the pipe bends due to internal pressure are also shown. The allowable stresses shown in the table exceed the applied stresses in all cases.

Bellows Design

It was determined during the conceptual stage of the BXHU program that expansion bellows would be required in each of the three interconnecting ducts between the BHXU and the BRU. In this way, the BHXU thermal movements were isolated from the BRU thermal response such that the resulting ducting forces and bending moments applied to the BRU scrolls were held within acceptable

TABLE 18

PAN DESIGN AND STRESS SUMMARY

Pan	Maximum Temp, ^{0}F	Buckling* Pressure, psi	Internal Pressure, psi	Maximum Stress, psi	Allowable Stress, psi	Design Stress
Low Pressure Inlet	1241	28	30.5	6100**	5400	Bending due to internal pressure
High Pressure Inlet	278	131	56.0	17,500	34,000	Bending due to internal pressure
Low Pressure Outlet	80	15	30.5	6,200	24,000	Buckling due to 15 psi external pressure
High Pressure Outlet	1194	51	56.0	7,600	7,500	Bending due to internal pressure

*$P_{cr} = \frac{3EI}{R^3}$ gives the critical buckling pressure for a cylinder of infinite length. The buckling pressures shown are conservative since buckling strength is greatly increased above the values shown by using a short cylinder. An external pressure of one atmosphere is applied during acceptance testing.

**This stress is above the allowable, however, this is a conservative estimate since the flat section (L) tapers to zero at the opposite end and the strength of the transition duct mating to the end of the pan is not included in the analysis.

PAN CONFIGURATION

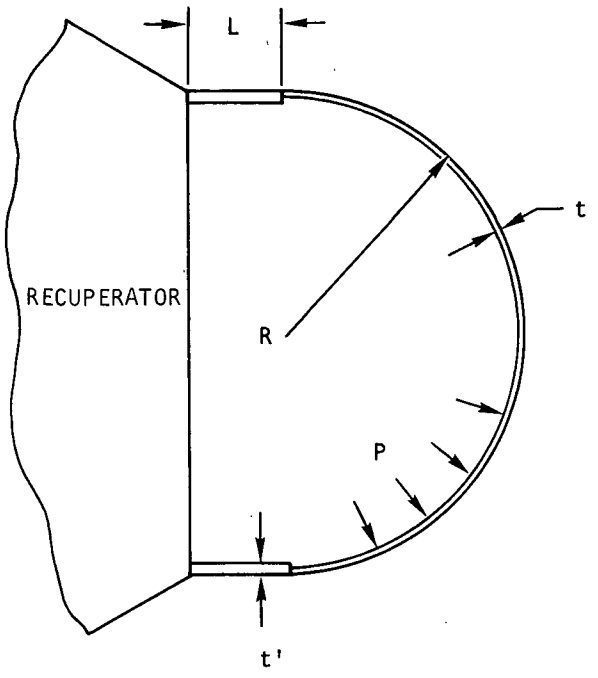

	Low Pressure Inlet	High Pressure Inlet
R	3.395 in.	1.85 in.
L	1.53 in.	0.93 in.
t	0.060 in.	0.05 in.
t'	0.120 in.	0.05 in.
P	30.5 psi	56.0 psi
E	20.3×10^6 psi	26.6×10^6 psi
μ	0.3	0.3

FREE BODY DIAGRAMS

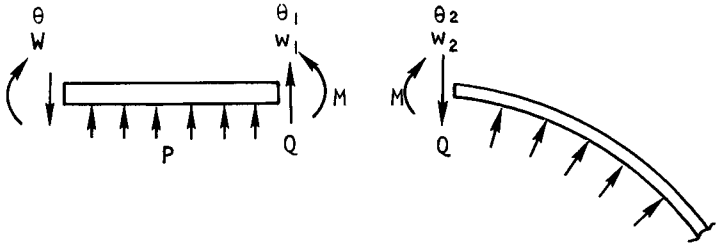

ROTATION AND DEFLECTION EQUATIONS FOR OBTAINING THE DISCONTINUITY FORCES AND MOMENTS, Q AND M

$$\theta_1 = \frac{ML}{EI} + \frac{QL^2}{2EI} + \frac{PL^3}{6EI}$$

$$w_1 = -\frac{ML^2}{2EI} - \frac{QL^3}{3EI} - \frac{PL^4}{8EI}$$

$$\theta_2 = \frac{2\beta^2}{Et} Q - \frac{4\beta^3}{EtR} M$$

$$w_2 = \frac{2\beta R}{Et} Q - \frac{2\beta^2}{Et} M - \frac{\left(1 - \frac{\mu}{2}\right) PR^2}{Et}$$

$$I = \frac{t'^3}{12}$$

$$\beta = \sqrt[4]{3(1-\mu^2)\left(\frac{R}{t}\right)^2}$$

BOUNDARY CONDITIONS

$$\theta = 0$$

$$w = 0$$

$$\theta_1 = \theta_2$$

$$w_1 = w_2$$

A-31937

Figure 42. Low Pressure and High Pressure Inlet Pan Configurations

PAN CONFIGURATION

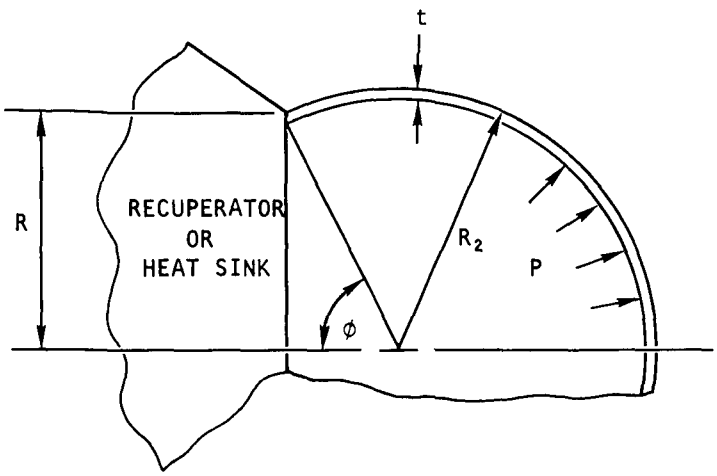

	Low Pressure Outlet	High Pressure Outlet
R_2	3.91 in.	2.80 in.
R	3.31 in.	2.47 in.
t	0.050 in.	0.060 in.
ϕ	$57^0 50'$	$61^0 54'$
P	30.5 psi	56.0 psi
E	28×10^6 psi	20.7×10^6 psi
μ	0.3	0.3

FREE BODY DIAGRAM

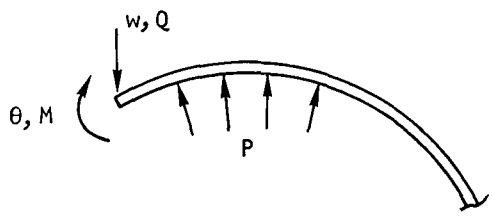

ROTATION AND DEFLECTION EQUATIONS FOR DETERMINING THE DISCONTINUITY FORCES AND MOMENTS, Q AND M

$$\theta = \frac{3PR_2}{2EtTAN\phi} + \frac{2\beta^2 SIN\phi}{EtK_1} Q - \frac{4\beta^3}{EtR_2K_1} M$$

$$w = \frac{-\left(1 - \frac{\mu}{2}\right)PRR_2}{Et} + \frac{\beta R_2 SIN\phi}{Et}\left(K_2 + \frac{1}{K_1}\right) Q - \frac{2\beta^2 SIN\phi}{EtK_1} M$$

$$K_1 = 1 - \frac{1 - 2\mu}{2\beta}$$

$$K_2 = 1 - \frac{1 + 2\mu}{2\beta}$$

$$\beta = \sqrt[4]{3(1-\mu^2)\left(\frac{R_2}{t}\right)^2}$$

BOUNDARY CONDITIONS

$$\theta = 0$$

$$w = 0$$

A-31938

Figure 43. Low Pressure and High Pressure Outlet Pan Configurations

CROSS SECTIONAL VIEW

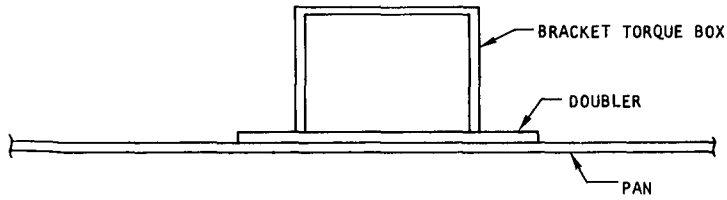

FREE BODY DIAGRAMS

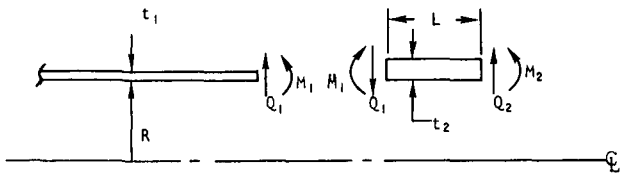

A-31939

$p = 56.0$ psi

$t_1 = 0.060$ in.

$t_2 = 0.110$ in.

$L = 0.50$ in.

$R = 3.91$ in.

$E = 20.7 \times 10^6$ psi

ROTATION AND DEFLECTION EQUATIONS FOR SEMI-INFINITE CYLINDER

$$\theta_1 = \frac{1}{2\beta_1^2 D_1} Q_1 - \frac{1}{\beta_1 D_1} M_1$$

$$w_1 = \frac{\left(1 - \frac{\mu}{2}\right) pR^2}{Et_1} + \frac{1}{2\beta_1^3 D_1} Q_1 - \frac{1}{2\beta_1^2 D_1} M_1$$

ROTATION AND DEFLECTION EQUATION FOR SHORT CYLINDER

$$\theta_1 = \frac{Y}{2\beta D} M_2 - \frac{S}{2\beta D} M_1 + \frac{K}{2\beta^2 D} Q_2 + \frac{B}{2\beta^2 D} Q_1$$

$$w_1 = \frac{K}{2\beta^2 D} M_2 - \frac{B}{2\beta^2 D} M_1 + \frac{V}{2\beta^3 D} Q_2 + \frac{L}{2\beta^3 D} Q_1 - \left(1 - \frac{\mu}{2}\right) \frac{PR^2}{Et_2}$$

$$\theta_2 = \frac{S}{2\beta D} M_2 - \frac{Y}{2\beta D} M_1 + \frac{B}{2\beta^2 D} Q_2 + \frac{K}{2\beta^2 D} Q_1$$

$$w_2 = -\frac{B}{2\beta^2 D} M_2 + \frac{K}{2\beta^2 D} M_1 - \frac{L}{2\beta^3 D} Q_2 - \frac{V}{2\beta^3 D} Q_1 - \left(1 - \frac{\mu}{2}\right) \frac{PR^2}{Et_2}$$

where $D_1 = \frac{Et_1^3}{12}$

$$D = \frac{Et_2^3}{12}$$

$$\beta_1 = \frac{\sqrt[4]{3(1-\mu^2)}}{\sqrt{Rt_1}}$$

$$\beta = \frac{\sqrt[4]{3(1-\mu^2)}}{\sqrt{Rt_2}}$$

K,B,S,Y,L and V are the short cylinder influence coefficients

BOUNDARY CONDITIONS

θ_1 (semi-infinite cylinder) = θ_1 (short cylinder)

w_1 (semi-infinite cylinder) = w_1 (short cylinder

$\theta_2 = 0$

$w_2 = 0$

RESULTING MOMENTS AND SHEARS

$M_1 = -3.2741$ in.-lb/in.

$M_2 = 9.7284$ in.-lb/in.

$Q_1 = -20.3672$ lb/in.

$Q_2 = -34.8404$ lb/in.

MAXIMUM COMBINED STRESS

$$\sigma_{max} = \pm \frac{6M_1}{t_1^2} + \frac{PR}{2t_1} = 7282 \text{ psi}$$

ALLOWABLE STRESS

$\sigma_{all} = 7500$ psi

Figure 44. High Pressure Outlet Pan Discontinuity Analysis

SIDE PLATE CONFIGURATION

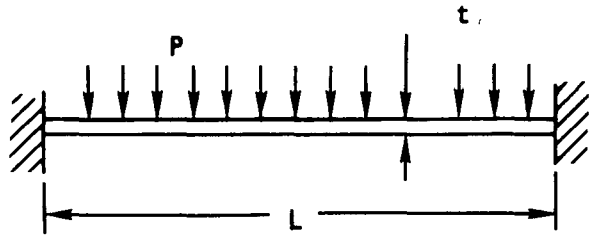

A-31940

$L = 2.9$ in.

$t = 0.080$ in.

$p = 30.5$ psi

$$M_{max} = \frac{PL^2}{12} = \frac{30.5\ (2.9)^2}{12} = 21.4 \text{ in.-lb/in.}$$

$$\sigma = \frac{6M}{t^2} = \frac{6(21.4)}{(0.08)^2} = 20{,}040 \text{ psi}$$

$\sigma_{all} = 23{,}000$ psi

Figure 45. Transition Duct Analysis

TABLE 19

DUCTING STRESSES

Material	Pipe	R, in.	R', in.	t, in.	P* cr, psi	Direct** Stresses, psi			Bending*** Stresses, psi		
						Hoop	Axial	Allowable	Hoop	Axial	Allowable
Hastelloy X	Low Pressure Inlet	3.00	6.0	0.050	25	1830	920	5,000	920	2750	7,500
347 steel	High Pressure Inlet	1.75	3.5	0.035	53	2800	1400	23,000	1400	4200	34,000
347 steel	Low Pressure Outlet	2.00	5.0	0.035	37	1740	872	24,000	872	2320	36,000
347 steel	High Pressure Outlet	2.25	4.84 6.50	0.050	57	2520	1260	5,000	1260	3620 3190	5,000 5,000

NOTES: * $P_{cr} = \frac{3EI}{R^3} = \frac{Et^3}{4R^3}$ (This equation is for infinitely long cylinders, therefore, these numbers will be very conservative. The design external pressure is 15.0 psi.)

**Direct Stresses: Hoop Stress = $\frac{PR}{t}$ Axial Stress = $\frac{PR}{2t}$

***Bending Stresses (assuming a complete torus): Hoop = $\frac{pR}{2t}$ Axial = $\frac{pR}{t}\left(\frac{2R'-R}{2R'-2R}\right)$

R' = bend radius (average)

limits. Each component (i.e., the BHXU and BRU) is separately attached to a mounting frame to withstand environmental loads due to launch and flight into orbit. Since each unit will undergo an appreciable temperature increase to reach operating temperature and must be tied down at a single mount point, the remaining supports must be selected to absorb applied loads and yet allow free thermal expansion.

Wherever a decision is made to employ bellows, it is incumbent upon the designer and user to satisfy four important sequential steps. These are:

Step 1--Develop an accurate estimate of thermal movements. In rapid startup equipment, the transient relative motions for a bellows occasionally far exceed the steady-state movement. In addition, accurate data must be obtained regarding operating pressures and temperatures.

Step 2--With the data collected from Step 1, a specification must be generated for use by the prospective bellows manufacturers. This specification must be complete and explicit. For elevated temperature applications it is necessary to define stress limits for both pressure and thermal displacements to ensure attainment of a satisfactory component.

Step 3--A careful verification should be made of the proposed bellows configurations. While almost all of the well established bellows manufacturers are able to construct and deliver good components, many of them depend upon highly empirical techniques to arrive at their designs. When faced with nonstandard or difficult design problems, the actual performance of these bellows in terms of spring rate or stress per unit motion can be much different than what is indicated by the bellows vendor. Discrepancies by as much as a factor of four between vendor analysis results and AiResearch results have occurred. Numerous actual bellows have been checked by comparing the AiResearch computer analysis with load compression test data, and the results have been found to agree within ±20 percent.

Step 4--During installation of the bellows into ducting and then into the final assembly, great care must be taken to protect them from being damaged. The bellows will usually be tolerant of small amounts of misalignments during final assembly, but, unless specifically designed for tolerance buildups, the bellows should not be used to take up large deviations from proper fit up.

I. Bellows Procurement and Selection

Initially, AiResearch prepared and submitted a preliminary specification to several bellows manufacturers. This specification included preliminary thermal movements, spring rates (based on acceptable BRU scroll loads), operating temperatures and pressures. In addition, operating and cyclic life

were specified. Three companies responded with single-ply formed bellows which would have utilized standard tooling to form the convolutions. AiResearch then performed a stress analysis on each of the proposed bellows to determine stresses due to pressure containment and thermal movements.

Subsequent to this submittal of bellows design, further analysis was performed on the BHXU to assess different mounting concepts for their influence on bracket design and duct thermal movements. A thermal transient analysis was also completed which permitted a more realistic calculation of BHXU, BRU and interconnecting duct thermal movements during the startup process (The BHXU plate-fin structure responds rapidly to temperature rise wheras the BRU, the interconnecting ducts and the BHXU pans respond much more slowly during startup.). This calculation revealed that the relative thermal movements during the transient period were much greater than at the steady-state final movement for the high temperature (turbine outlet) 6 in. dia bellows. In addition the cold bellows diameters were increased from 3 and 3.5 in. to 3.5 and 4 in., respectively. Accordingly, revised bellows specifications were prepared, and these were resubmitted to the manufacturers. The revised specifications, shown in Tables 20, 21, 22, also included the requirement for two-ply bellows which provide two important advantages over single-ply bellows: increased leakage reliability (the main concern being the longitudinal seam welds) and reduction in bellows spring rate (for the same pressure containment capability), hence lower duct loads. Upon receipt of the modified proposed designs from the manufacturers, a detailed analysis of stresses due to thermal movement and pressure containment was carried out using an AiResearch computer program that had been used previously and verified on another program. The computed stresses and bellows spring rates were then compared to the allowable values and a selection was made, with NASA concurrence.

Of the three manufacturers that responded to the procurement request, designs from only one, Aeroquip Corp., was found to satisfy all design objectives. Accordingly, Aeroquip Corp. was selected to supply the set of three bellows for the BHXU. The details of the selected bellows configurations are presented in Table 23.

2. Bellows Thermal Movements

An isometric sketch depicting the physical arrangement of the BHXU and the BRU is provided in Figure 46. This drawing shows the fixed mounting point for each unit and the location of the three bellows. The figure also shows the set of reference coordinate axes that have been used to describe the thermal motions at each bellows.

The thermal movement directions for the 3-1/2 in. compressor bellows are shown in Figure 47. The thermal movements, composed almost entirely of slow heatup motions, are summarized in Table 24. The thermal motion at each end of the bellows and the net relative movement, the algebraic difference between movements at each end, are presented.

TABLE 20

BHXU 3-1/2 IN. DIA BELLOWS

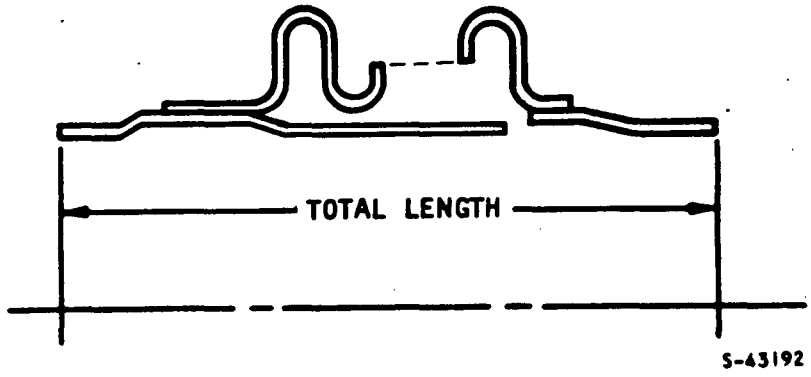

MATCHING DUCT SIZE = 3.50 IN. OD X 0.035 IN. WALL
TOTAL LENGTH = 4.00 IN. MAXIMUM, ACTIVE LENGTH = 2.50 IN. MAXIMUM
LINER REQUIRED
LINER ID TO BE 3.43 IN.
OPERATING TEMPERATURE = 300°F
MATERIAL: TYPE 347 STAINLESS STEEL OR 321 STAINLESS STEEL
WORKING PRESSURE = 56 PSI
REQUIRED MOVEMENTS
AXIAL = 0.00 IN.
LATERAL = 0.040 IN.
SHEAR FORCE TO DEFLECT BELLOWS LATERALLY $\leq$ 300 LB
CYCLE LIFE $\geq$ 1000
BELLOWS TO BE AT LEAST 2 PLY CONSTRUCTION
BELLOWS MUST BE BRAIDED TO REACT INTERNAL PRESSURE FORCE
PROOF PRESSURE = 84 PSI
BURST PRESSURE = 140 PSI
HELIUM LEAKAGE AT 56 PSI TO BE LESS THAN 1 X 10^{-6} ATMOSPHERIC CC/SEC

REFERENCE: AIRESEARCH SOURCE CONTROL DRAWING 183444

TABLE 21

BHXU 4-IN. DIA BELLOWS

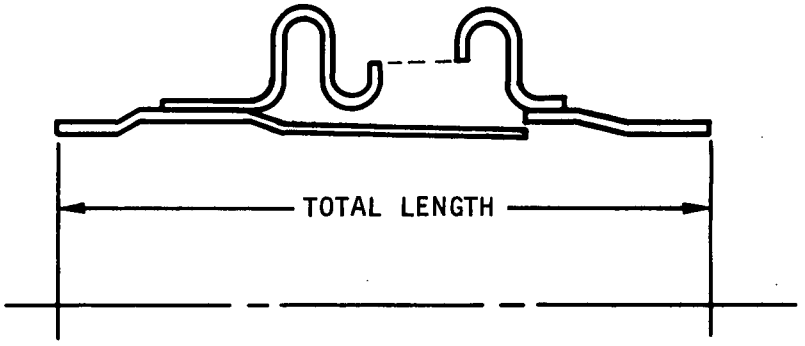

MATCHING DUCT SIZE = 4.00 IN. OD X 0.035 IN. WALL
TOTAL LENGTH = 4.00 IN. MAXIMUM, ACTIVE LENGTH = 2.5 IN.
LINER REQUIRED
LINER ID = 3.93 IN.
OPERATING TEMPERATURE = ROOM TEMPERATURE
REQUIRED MOVEMENT
AXIAL DEFLECTION = 0.040 IN.
LATERAL DEFLECTION = 0.030 IN.
SHEAR FORCE TO DEFLECT BELLOWS LATERALLY $\leq$ 300 LB
CYCLE LIFE $\geq$ 1000
BELLOWS MUST BE AT LEAST 2 PLY CONSTRUCTION
MATERIAL: TYPE 347 STAINLESS STEEL OR 321 STAINLESS STEEL
WORKING PRESSURE = 30.5 PSI
PROOF PRESSURE = 46 PSI
BURST PRESSURE = 76.5 PSI
HELIUM LEAKAGE AT 30.5 PSI TO BE LESS THAN 1×10^{-6} ATMOSPHERIC CC/SEC

REFERENCE: AIRESEARCH SOURCE CONTROL DRAWING 183442

TABLE 22

BHXU 6-IN. DIA BELLOWS

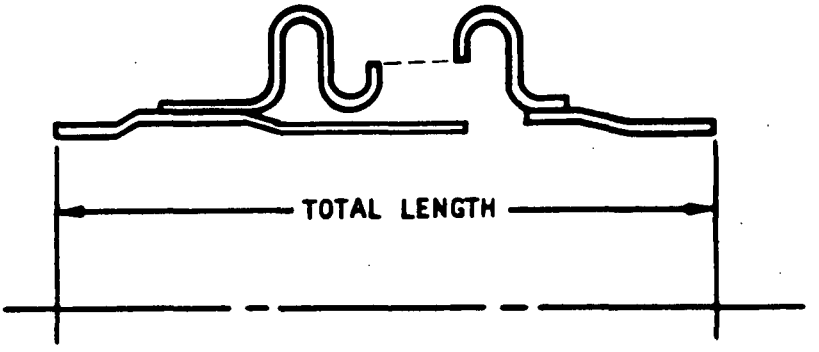

S-43191

MATERIAL: HASTELLOY X
MATCHING DUCT DIAMETER = 6.00 IN. OD X 0.035 IN. WALL
TOTAL LENGTH = 5.50 IN. MAXIMUM, ACTIVE LENGTH = 4.0 IN.
LINER REQUIRED
LINER ID = 5.93 IN.
OPERATING TEMPERATURE = 1240°F
DESIGN LIFE = 5 YEARS
WORKING PRESSURE = 30.5 PSI
REQUIRED MOVEMENTS
    AXIAL DEFLECTION = 0.250 IN.
    LATERAL DEFLECTION = 0.130 IN.
SHEAR FORCE TO DEFLECT BELLOWS LATERALLY ≤ 300 LB
    (USE HIGH TEMPERATURE MODULUS OF ELASTICITY)
BELLOWS TO BE AT LEAST 2 PLY CONSTRUCTION
ALLOWABLE STRESSES
    MAXIMUM HOOP STRESS DUE TO INTERNAL PRESSURE = 10,200 PSI
    MAXIMUM PRESSURE BENDING STRESS = 15,300 PSI
    COMBINED STRESS DUE TO APPLIED MOVEMENTS ≤ 80,000 PSI
      (USE RT ELASTIC MODULUS)
HELIUM LEAKAGE AT 30.5 PSI TO BE LESS THAN 1×10^{-6} ATMOSPHERIC CC/SEC

REFERENCE: AIRESEARCH SOURCE CONTROL DRAWING 183443

TABLE 23

BELLOWS DIMENSIONS AND STRESSES

	Low Pressure Recuperator Inlet	Low Pressure Heat Sink Outlet	High Pressure Recuperator Inlet
Nominal diameter, in.	6	4	3.5
Total length, in.	4	4	4
Convolute details:			
Length, in.	3.75	1.50	1.50
Height, in.	0.46	0.31	0.31
Pitch, in.	0.175	0.231	0.231
No. of convolutions	22	7	7
Thickness/ply, in.*	0.010	0.006	0.006
Pressure bending stress, psi	15,100	14,400	25,700
Thermal motion stress, psi/in.	79,500	236,000	233,000
Spring rate performance			
K_{axial}, lb/in.	233	311	285
$K_{lateral}$, lb/in.	1160	4310	3140
Lateral force, lb**	151	130	126

*All bellows are two-ply
**BRU scroll-duct load restrictions were that lateral loads on the turbine and compressor scrolls would not exceed 150 and 300 lb, respectively.

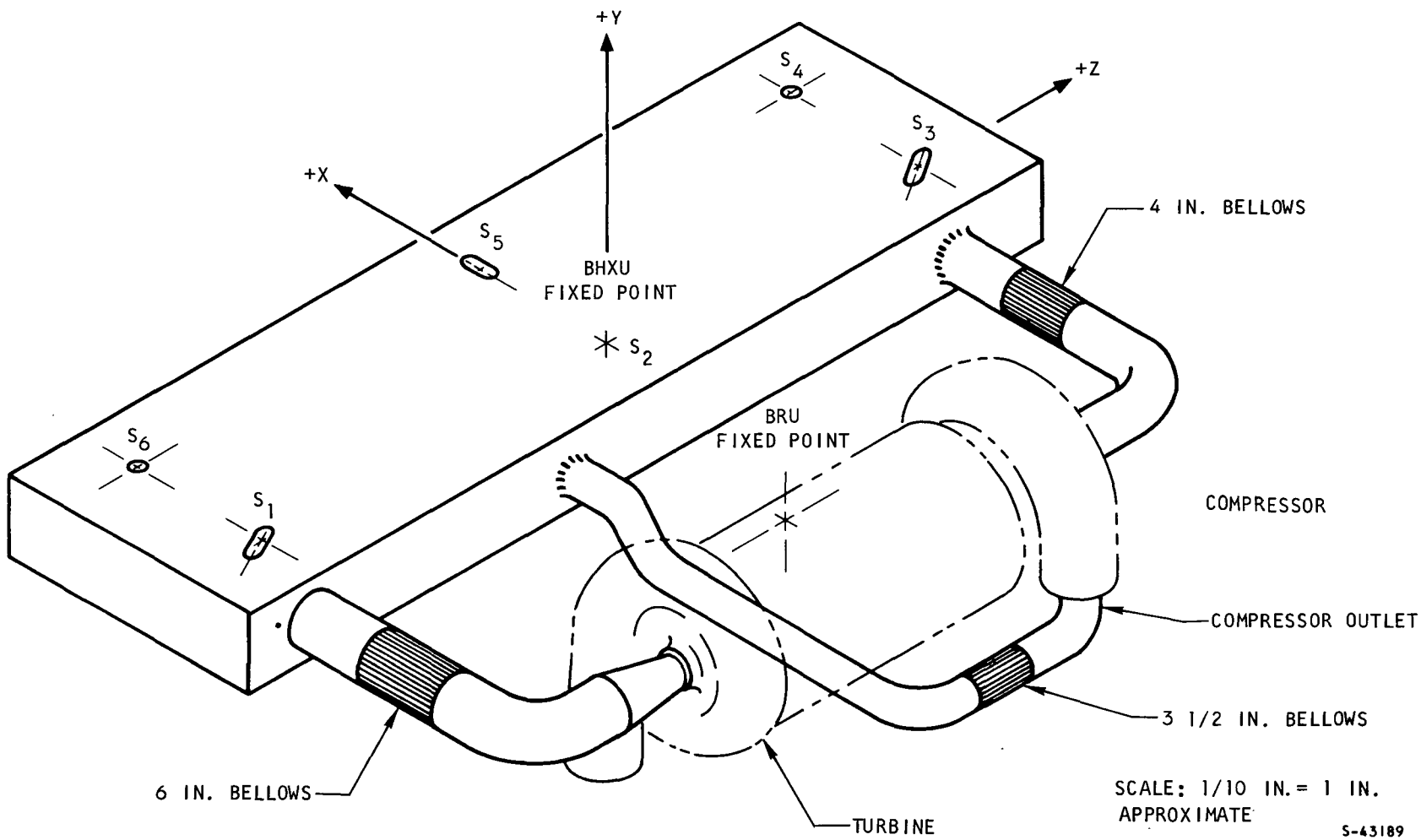

Figure 46. BHXU-BRU Arrangement

The ducting between the BHXU and the BRU compressor inlet carries ambient temperature gas. The only movements on the bellows are due to BHXU thermal expansion from its fixed mount point to the BHXU duct outlet flange and thermal movements of the BRU from its fixed mount point. The BHXU end of the bellows responds rapidly while the BRU response is slow. For axial motion, the transient component of response, 0.013 in. occurs rapidly, and this eventually builds up to its maximum value of 0.037 in. at steady state. The lateral movement, ΔZ, consists of a rapid response component of 0.023 in. and a slow component of response that tends to reduce the net movements. Since lateral motion causes much more stress than axial movement, the maximum condition consists of a combined movement of 0.013 in. axial with 0.023 lateral. The thermal movement directions for the 4-in. bellows are shown in Figure 48 and the thermal movements, composed almost entirely of the slow heatup motion, are summarized in Table 25.

The thermal motion directions for the 6-in. turbine outlet bellows are shown in Figure 49 and the thermal motions are summarized in Table 26. The transient response history is of great importance in establishing the net relative movements on this bellows. The motions summarized in Table 26, combined with estimates of the response behavior (Figure 40 for example), are thenused to determine the repeating cycle conditions shown in Figure 50. The maximum repeating cycle conditions occur during the repeating full cycle (Figure 50) giving an axial movement of 0.131 in. and a lateral movement of 0.128 in.

3. Bellows Performance Analysis

a. Compressor Outlet Bellows (3-1/2 in.)

The equivalent axial movement due to combined axial and lateral movement is obtained from the formula:

$$\delta_{equiv} = \delta_{axial} + 6\delta_{lateral}\left(\frac{R}{\ell}\right)$$

where R is the mean convolute radius and ℓ is the convolution length. The applied motions are $\delta_{axial} = 0.010$ in. and $\delta_{lateral} = 0.023$ in. The equivalent motion is

$$\delta_{equiv} = 0.010 + (6)(0.023)\left(\frac{2.030}{1.500}\right) = 0.197 \text{ in.}$$

Thermal motion stress from the computer solution was found to be equal to 233,000 psi/in. of movement. Therefore, thermal motion stress for the bellows is

$$\delta_{th} = 233{,}000 \times 0.197 = 46{,}000 \text{ psi}$$

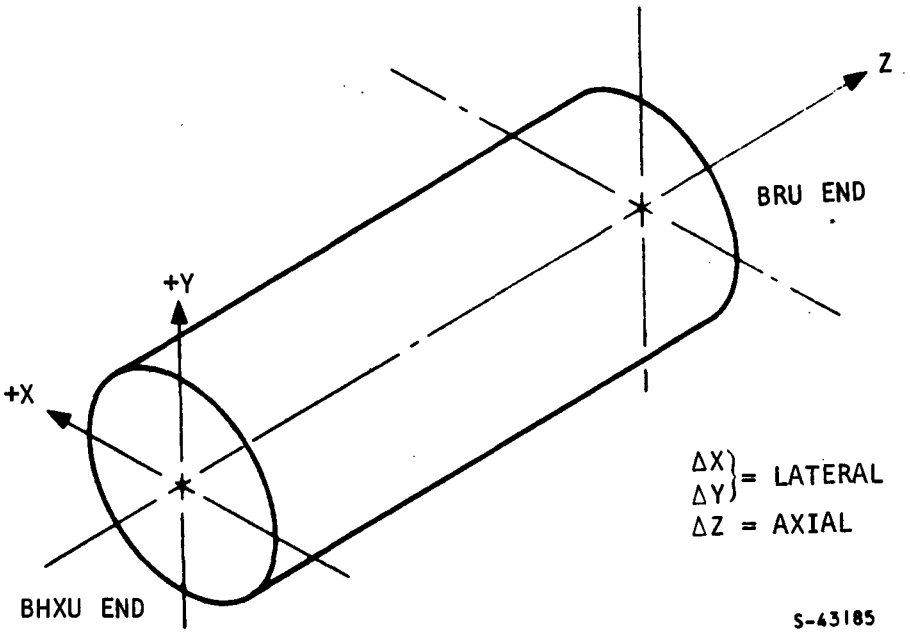

Figure 47. Thermal Movement Directions for 3-1/2 in. Compressor Outlet Bellows

TABLE 24

THERMAL MOTION SUMMARY, 3-1/2 IN. BELLOWS

	ΔX, in.	ΔY, in.	ΔZ, in.
BHXU end	-0.046	-0.024	+0.010
BRU end	-0.024	-0.018	+0.000
Net motion	-0.022	-0.006	+0.010

Net lateral motion = $(\Delta X^2 + \Delta Y^2)^{1/2}$ = 0.023 in.

Net axial motion = ΔZ = 0.010 in.

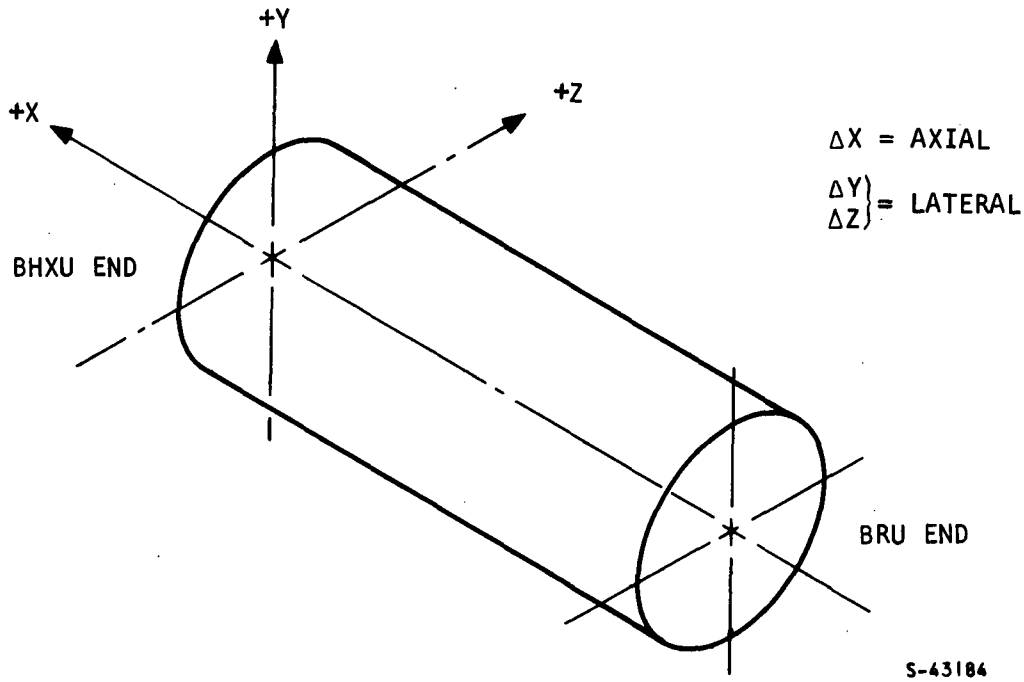

Figure 48. Thermal Movement Directions for 4-in. Compressor Inlet Bellows

TABLE 25

THERMAL MOTION SUMMARY FOR 4-IN. BELLOWS

	ΔX, in.	ΔY, in.	ΔZ, in.
BHXU (rapid heatup)	+0.013 (due to bowing)	0.00	+0.023
BRU (slow heatup)	-0.024	0.00	+0.010
Steady-state net motion	+0.037 (extension)		+0.013

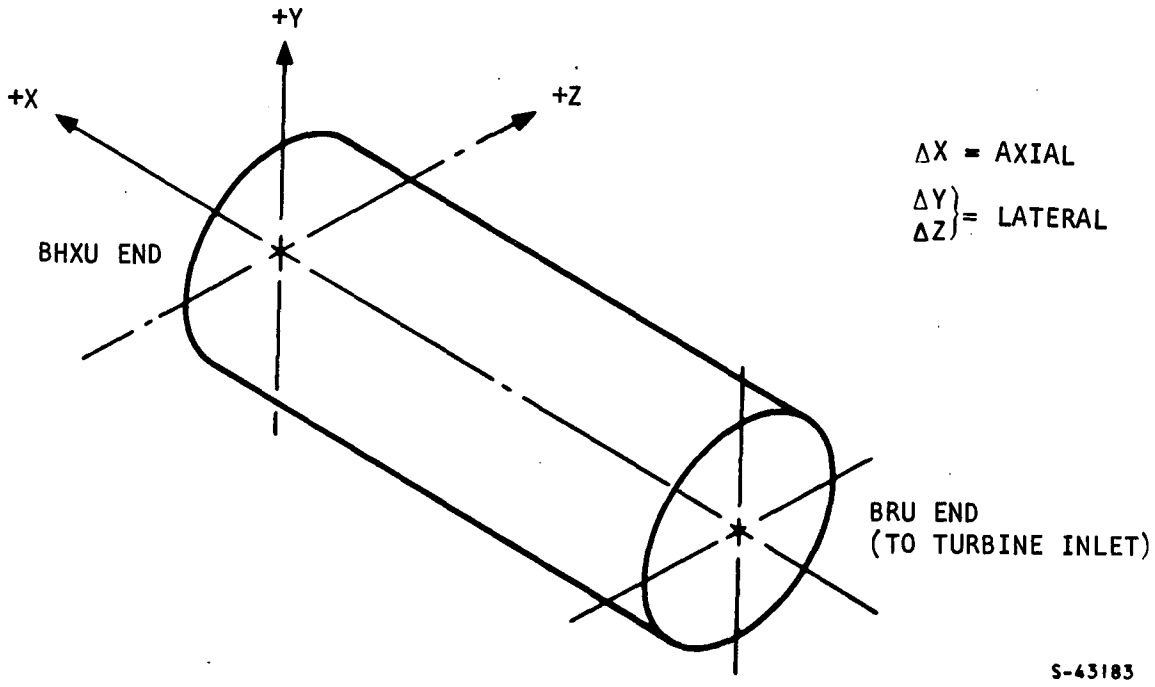

Figure 49. Thermal Movement Directions for 6-in. Turbine Outlet Bellows

TABLE 26

THERMAL MOTION SUMMARY FOR 6-IN. BELLOWS

	ΔX, in.	ΔY, in.	ΔZ, in.	Element
BHXU end rapid heatup	-0.060 (bending)	-0.070	-0.148	Core
BHXU end slow heatup	-0.112	0	-0.036	Ducting
BRU end slow heatup	-0.024	-0.010	-0.130	BRU
BRU end slow heatup	+0.103	-0.012	-0.104	Ducting
Steady-state motion	-0.251	-0.048	+0.050	

The maximum repeating cycle conditions are:

$$\text{Lateral motion} = (\Delta y^2 + \Delta Z^2)^{1/2} = 0.128 \text{ in.}$$

$$\text{Axial motion} = 0.131 \text{ in.}$$

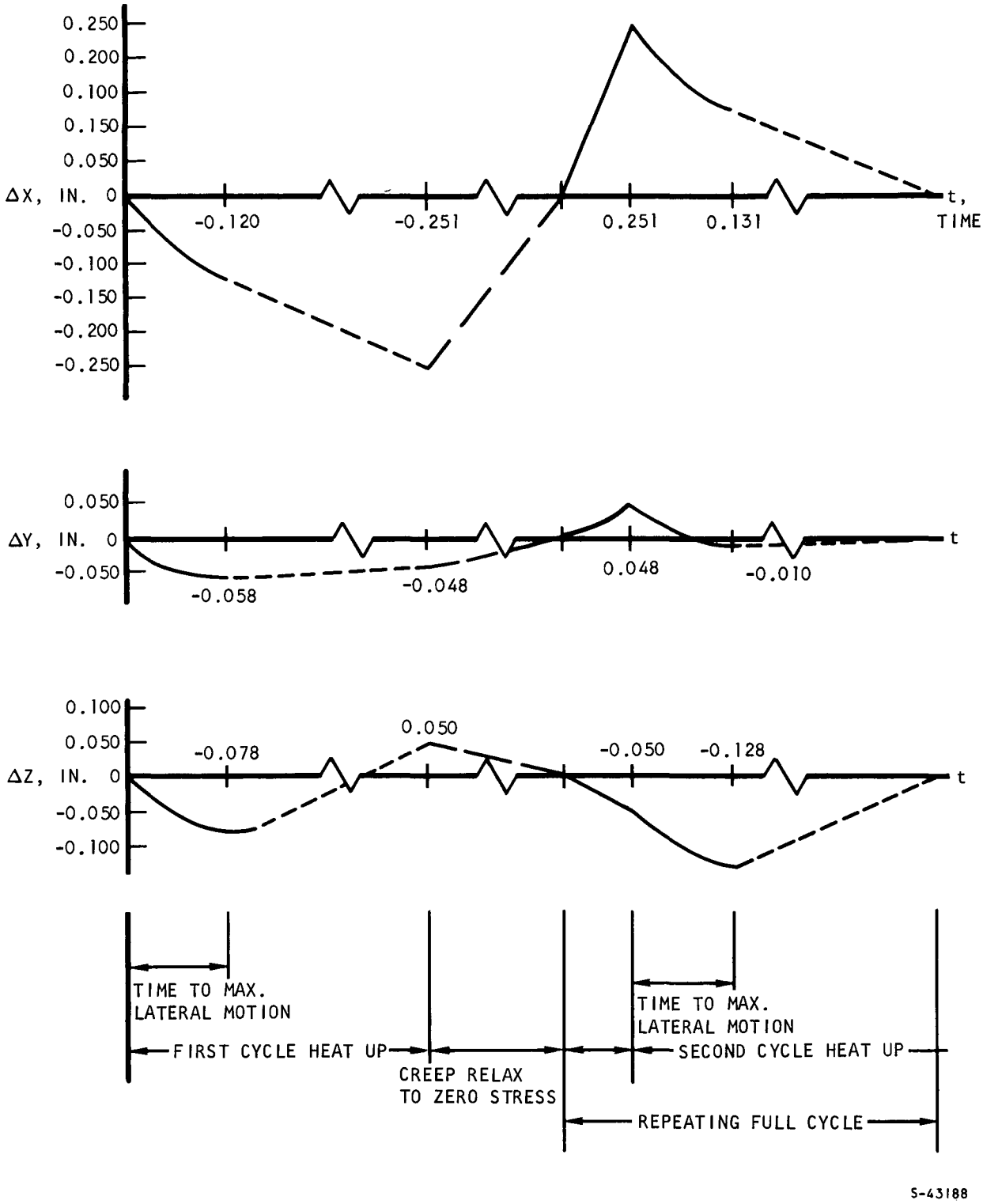

Figure 50. Transient Motions Imposed on the 6-in. Bellows During the First and Subsequent Operating Cycles

The pressure bending stress was computed to be 25,700 psi, and this was satisfactory when compared to the allowable of 27,500 psi.

The combined stress due to pressure and thermal motion is 25,700 + 46,000 = 71,700 psi. The plastic strain/cycle is

$$\Delta\epsilon_p = \frac{\sigma_{total} - 2\sigma_y}{E} = \frac{(71,700 - 2 \times 27,500)}{29 \times 10^6}$$

$$\Delta\epsilon_p = 0.00057 \text{ in./in.}$$

Using the prescribed strain concentration factor of 2.0 (equivalent to a safety factor of four on cycle life), the plastic strain range is 0.00114 in./in. Also using the ductility constant of 0.500 and placing these numbers into the low cycle fatigue formula

$$N = \left(\frac{C}{\Delta\epsilon_p}\right)^2 = \left(\frac{0.500}{0.00114}\right)^2 = 192,000 \text{ cycles}$$

this is a predicted life well in excess of the required 100 cycles.

b. Compressor Inlet (4-in. Bellows)

The applied thermal motions are $\delta_{axial} = 0.013$ in. and $\delta_{lateral} = 0.023$ in. The equivalent movement is

$$\delta_{eq} = 0.013 + (6)(0.023)\left(\frac{2.281}{1.50}\right) = 0.223 \text{ in.}$$

Thermal motion stress was computed to be 236,000 psi/in. of movement. Thermal motion stress for this bellows is

$$\sigma_{th} = (236,000)(0.223) = 52,600 \text{ psi}$$

The pressure bending stress was computed to be 14,400 psi which is well within the allowable value of 32,400 psi.

The combined stress due to pressure and thermal motion is 14,400 + 52,600 = 67,000 psi. The plastic strain range is

$$\Delta\epsilon_p = \frac{67,000 - (2)(32,400)}{29 \times 10^6} = 0.00008 \text{ in./in.}$$

The computed number of cycles to failure is

$$N = \left(\frac{0.500}{0.00016}\right)^2 = 9 \times 10^6 \text{ cycles}$$

c. Turbine Outlet (6-in. Bellows)

The computed thermal motions are $\delta_{axial} = 0.131$ in. and $\delta_{lateral} = 0.128$ in. The combined equivalent motion is

$$\delta_{eq} = 0.131 + (6)(0.128)\left(\frac{3.40}{3.75}\right)^2 = 0.827 \text{ in.}$$

The computed thermal motion stress was 79,500 psi/in. of axial movement. Thermal motion stress for this bellows is

$$\sigma_{th} = 79,000 \times 0.827 = 65,700 \text{ psi}$$

This is within the 80,000 psi stress limitation. For Hastelloy C at room temperature, the yield strength is 57,000 psi which indicates that the yielding will be extremely small on successive cycles.

The computed elastic pressure bending stress was found to be 15,100 psi. The Hastelloy C 13,000 psi stress limit for 1 percent creep in 50,000 hr at 1350°F indicates that the full 100°F overtemperature is not available. An overtemperature of 70°F gives an allowable stress of 15,100 psi.

A small amount of plastic flow will occur during removal of internal pressure and cooldown. Since thermal stresses are assumed to be at or nearly zero, the plastic flow during cooldown is

$$\Delta\epsilon_p = \frac{(65,700-57,000)}{28.6 \times 10^6} = 0.0003 \text{ in./in.}$$

Using a strain concentration factor of 2.0 and a ductility constant of 0.48 (RT reduction of area of 40 percent), the calculated number of cycles for failure is

$$N = \left(\frac{0.48}{0.0006}\right)^2 = 640,000 \text{ cycles}$$

Cyclic fatigue is therefore not an important factor in the life of the bellows.

Mounting System

1. BHXU Mount System Selection

The BHXU support system was selected to give a lightweight, reliable arrangement consistent with overall thermal expansion requirements, operating time-temperature history and specified inertia loadings. The initial task performed to meet these objectives was the selection of mount point locations on the BHXU. Additional work was carried out to select a system mounting philosophy consistent with the loads outlined in the environmental specification (Specification No. P1224-1). Consideration was given to two system mounting approaches which lead to significantly different load requirements for the BHXU bracketing; an isolation mounting system and a rigidly mounted system. The isolation system approach assumes that elastic mounts with at

least 10 percent of critical damping capacity are introduced between the BHXU and the input source so that the shock load is reduced and resonances within the BHXU above the isolation frequency are greatly attenuated. The isolation system approach, therefore, results in considerably lower design loads as compared to the hard mount system where only internal structural damping limits resonant amplifications. A comparison of bracket sizes and weights and resulting heat exchanger core loads was performed. The weight comparison indicated that the isolation system is preferred and this type of mounting was assumed for the BHXU detailed design. Further considerations supporting this approach are additional weight increases in the core required to transmit loads to the bracketry and inherent design complications associated with welding relatively large metal components to the brazed core assembly.

A preliminary structural analysis was performed early in the study on tasks related to mounting bracket design and location. A six-point mount system was selected as shown in Figure 51. As discussed below, the BHXU fixed point is at Point B on the sketch with the other five brackets having provisions for BHXU thermal movement (in the plane of the paper).

Prospective bracket locations were limited to pan areas based on the assumption that fin thermal stresses would be excessive for bracket side plate locations. The bracket size required to distribute the inertia loads over some reasonable number of fins would ensure a temperature gradient at startup approximately equal to the core temperature increase. Bowing of the bracket under such a temperature gradient would introduce very high fin loads.

With the assumption that the brackets would be placed at pan locations, the following general criteria were used for the selection of bracket locations:

(a) Minimum relative thermal deflections to be accommodated by the bellows in the hot inlet duct to the BHXU.

(b) Minimum bracket loads to achieve lightweight design.

(c) Minimum heat exchanger bending moment at the recuperator to heat sink heat exchanger joint.

The specific results expected from this analysis were:

(a) Selection of fixed point of BHXU relative to the BRU in both the x^1 and z^1 directions.

(b) Selection of number of brackets.

(c) Selection of bracket locations.

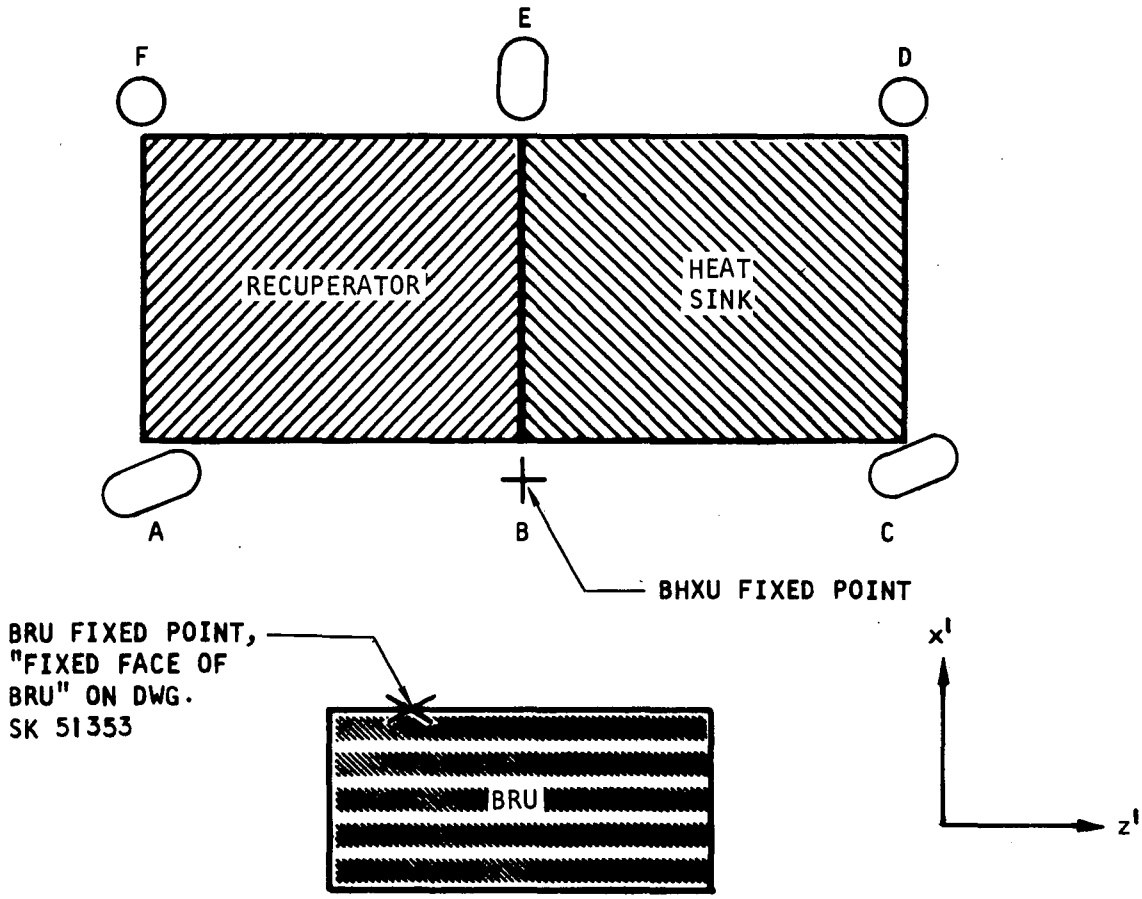

Figure 51. BHXU Bracket Locations

The results of the preliminary thermal movement analysis indicated that the minimum hot end bellows extension would be achieved by fixing the BHXU relative to the BRU at Point B. In addition, the load analysis indicates that supports on the lines AF and CD are needed to minimize bracket loads and BHXU bending moment at the joint between the recuperator and heat sink heat exchanger. The results may be summarized as follows:

(a) The fixed reference in the z^1 axis is taken to be on the line EB.

(b) The fixed reference in the x^1 axis is taken to be on the line ABC.

(c) The six-point mount system was selected with two brackets each on BHXU hot pan, the BHXU - heat sink transistor plate and the heat sink outlet pan.

2. Inertia Load Analysis

The bracket loads were calculated for a six-point mounting system using the final detailed design dimensions. Figure 52 shows a sketch of the six-point mounting system with the loading assumptions and a summary of dimensions, and Figure 53 shows the load distribution in the z^1-axis. The bracket loads, P_i, were related to the inertia forces, F_i, by the matrix relation

$$AF = P$$

The dimensionless coefficients in the 3 by 3 matrix, A, give the geometrical relation between the load vectors (1 by 3 matrixes) F and P (units of the components are pounds). The A matrices are tabulated for each mount in Table 27. The applied forces, F_i, and the bracket design loads, P_i, are summarized in Table 28 for the isolating mounting condition using an approximate total BHXU weight of 375 lb. The BHXU coordinate system (x^1, y^1, z^1) was used in the bracket design that follows. The spacecraft system (x, y, z) is assumed to be in line with the BRU axis and the difference between the two coordinate systems is less than 4 deg in any axis. Therefore, the loads shown in Table 2 are sufficiently accurate for the bracket design.

3. Thermal Expansion Analysis

a. Mounting Plane Location

The bracket mounting plane (x^1, z^1) was selected so as to achieve minimum thermal loads on the brackets due to steady state and transient thermal movements normal to the plane. In addition the choice as to which side of the BHXU (either side is possible from a thermal growth standpoint) the brackets should be placed was made to (1) reduce bracket weights, (2) reduce pan reinforcement weights (i.e., rings) and (3) place the brackets in the lowest temperature environment consistent with placement on the manifolding. For example, the cooler hot end pan with its smaller radius pan was used and the bracket on the transition piece achieves a very direct path to the core for the highest loads. Figure 54 shows a layout of the heat exchanger unit with the mounting plane and bracket attachment points.

ASSUME: S_1 TAKES LOADS IN X' AND Y'
S_2 TAKES LOADS IN X', Y', AND Z'
S_3 TAKES LOADS IN X' AND Y'
S_4 TAKES LOADS IN Y'
S_5 TAKES LOADS IN Y' AND Z'
S_6 TAKES LOADS IN Y'

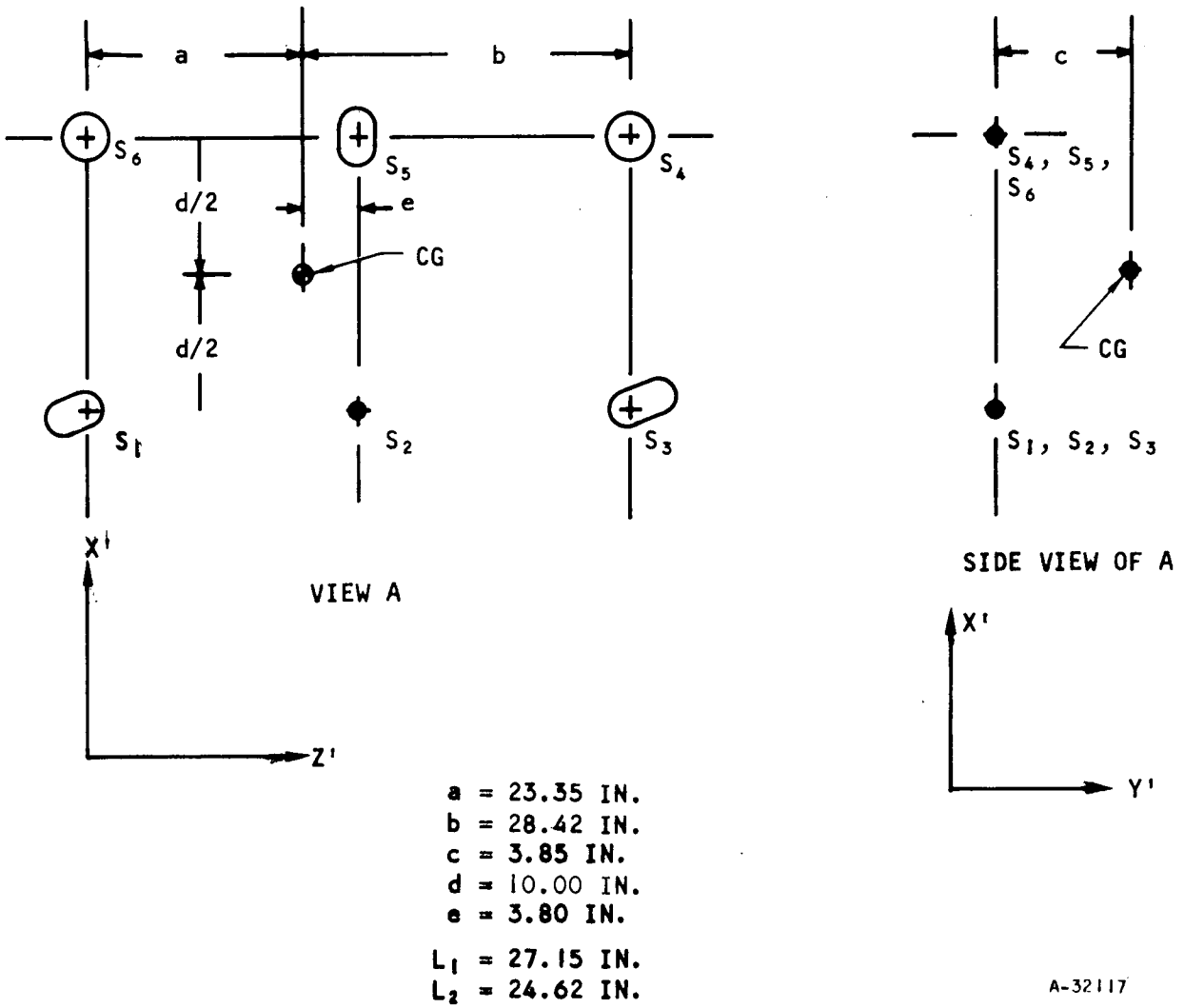

a = 23.35 IN.
b = 28.42 IN.
c = 3.85 IN.
d = 10.00 IN.
e = 3.80 IN.

L_1 = 27.15 IN.
L_2 = 24.62 IN.

A-32117

Figure 52. Sketch of Six Point Mounting System

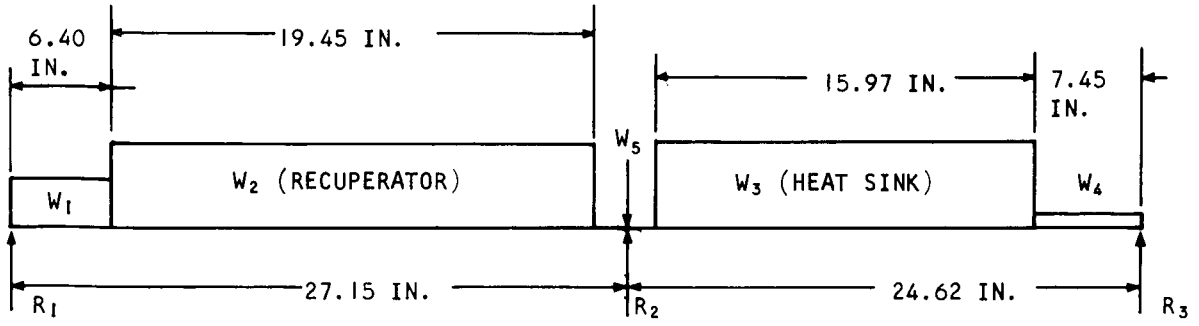

W_1 = 42.05 LB
W_2 = 170.58 LB
W_3 = 141.02 LB
W_4 = 10.50 LB
W_5 = 10.85 LB

a. BHXU Weight Distribution Along the Z^1 - Axis

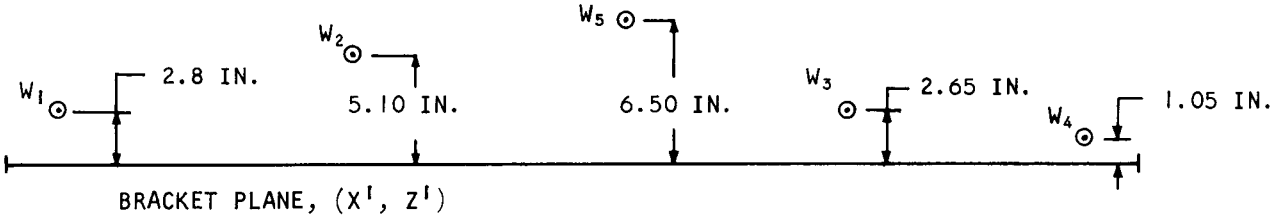

b. BHXU Weight Distribution Along the Z^1 Axis for Loads in the Y^1-Direction

A-32118

Figure 53. Loading Diagram for CG Determination

TABLE 27

RELATION BETWEEN BRACKET LOADS AND INERTIA FORCES

BRACKET S_1

$$\begin{bmatrix} 0.222 & 0 & 0 \\ 0.052 & 0.113 & 0.036 \\ 0.060 & 0 & 0 \end{bmatrix} \begin{bmatrix} F^I_x \\ F^I_y \\ F^I_z \end{bmatrix} = \begin{bmatrix} P^I_x \\ P^I_y \\ P^I_z \end{bmatrix}$$

BRACKET S_2

$$\begin{bmatrix} 0.684 & 0 & 0 \\ 0.333 & 0.338 & 0 \\ 0.100 & 0 & 0.500 \end{bmatrix} \begin{bmatrix} F^I_x \\ F^I_y \\ F^I_z \end{bmatrix} = \begin{bmatrix} P^I_x \\ P^I_y \\ P^I_z \end{bmatrix}$$

BRACKET S_3

$$\begin{bmatrix} 0.094 & 0 & 0 \\ 0 & 0.049 & 0.036 \\ 0.040 & 0 & 0 \end{bmatrix} \begin{bmatrix} F^I_x \\ F^I_y \\ F^I_z \end{bmatrix} = \begin{bmatrix} P^I_x \\ P^I_y \\ P^I_z \end{bmatrix}$$

BRACKET S_4

$$\begin{bmatrix} 0 & 0 & 0 \\ 0 & 0.049 & 0.036 \\ 0 & 0 & 0 \end{bmatrix} \begin{bmatrix} F^I_x \\ F^I_y \\ F^I_z \end{bmatrix} = \begin{bmatrix} P^I_x \\ P^I_y \\ P^I_z \end{bmatrix}$$

BRACKET S_5

$$\begin{bmatrix} 0 & 0 & 0 \\ 0.333 & 0.338 & 0 \\ 0 & 0 & 0.500 \end{bmatrix} \begin{bmatrix} F^I_x \\ F^I_y \\ F^I_z \end{bmatrix} = \begin{bmatrix} P^I_x \\ P^I_y \\ P^I_z \end{bmatrix}$$

BRACKET S_6

$$\begin{bmatrix} 0 & 0 & 0 \\ 0.052 & 0.113 & 0.036 \\ 0 & 0 & 0 \end{bmatrix} \begin{bmatrix} F^I_x \\ F^I_y \\ F^I_z \end{bmatrix} = \begin{bmatrix} P^I_x \\ P^I_y \\ P^I_z \end{bmatrix}$$

TABLE 28

BRACKET DESIGN LOADS

Force Matrix:

$$F_{x_1} = 375\ (20\ g) = 7500\ lb$$

$$F_{y_1} = 375\ (20\ g) = 7500\ lb$$

$$F_{z_1} = 375\ (24\ g) = 9000\ lb$$

or:

$$F_i = \begin{bmatrix} 7500 \\ 7500 \\ 9000 \end{bmatrix}$$

BRACKET LOAD MATRICES (forces in pounds)

$$S_1: \quad P_i = \begin{bmatrix} 1665 \\ 1562 \\ 450 \end{bmatrix} \qquad S_2: \quad P_i = \begin{bmatrix} 5130 \\ 5033 \\ 5250 \end{bmatrix}$$

$$S_3: \quad P_i = \begin{bmatrix} 705 \\ 692 \\ 300 \end{bmatrix} \qquad S_4: \quad P_i = \begin{bmatrix} 0 \\ 692 \\ 0 \end{bmatrix}$$

$$S_5: \quad P_i = \begin{bmatrix} 0 \\ 5033 \\ 4500 \end{bmatrix} \qquad S_6: \quad P_i = \begin{bmatrix} 0 \\ 1562 \\ 0 \end{bmatrix}$$

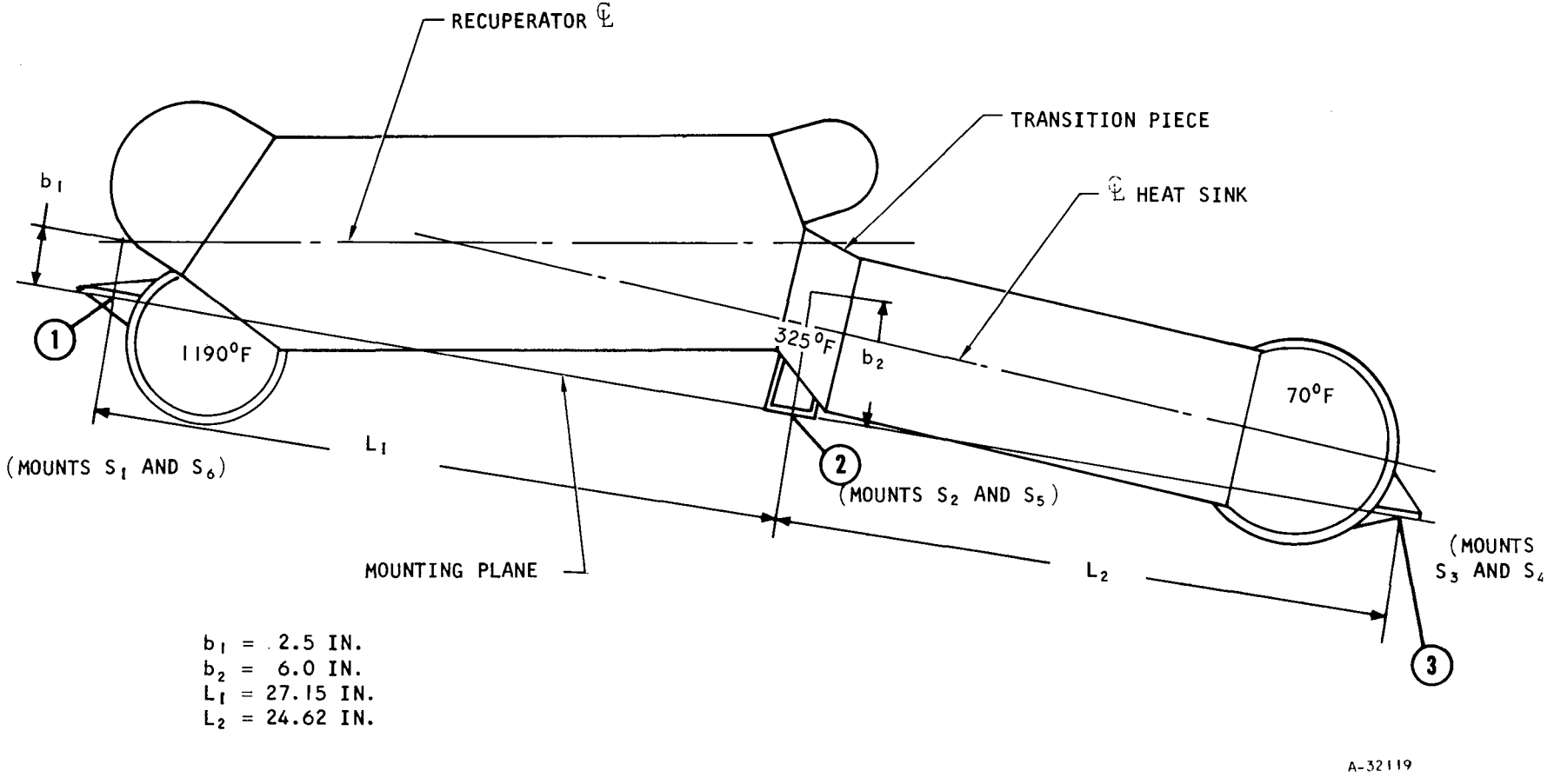

Figure 54. Mounting Plane Location

In selecting the desired $x^1 - z^1$ plane, the distance, b_2, at point 2 (Figure 54) was initially established by the minimum size requirements for brackets S_2 and S_5. The distance, b_1, was then calculated by minimizing the out-of-plane thermal growth using the deflection at Point 2 relative to Points 1 and 3. The deflection at Point 2 is

$$\delta_2 = \delta_{21} + \delta_{22} + \delta_{23}$$

where δ_{21} is the thermal growth at Point 2 relative to the thermal growth at Point 1, etc. The relative growths can be expressed as a function of geometry (Figure 54), temperature difference, ΔT, and mean coefficient of thermal expansion, α. Since the ΔT at point 3 is zero (80^0F operations at all times), δ_2 is

$$\delta_2 = \delta_{21} + \delta_{22} + 0 = \frac{\alpha, \Delta T_1, b_1 L_2}{L_1 + L_2} + \alpha_2 \Delta T_2 b_2$$

Analysis of the BHXU heat conditions was performed and b_2 was established to give a maximum out-of-plane movement of 0.005 in. Insignificant loads would occur in the BHXU or a mounting frame due to this movement.

b. Thermal Movement in the Plane of the Mounting Brackets

A summary of the thermal growth in the plane of mounting brackets is shown in Table 29. Brackets located on the circular pans utilized two bolts and both values are given. Figure 55 shows the bracket locations and hole sizes required to allow heat exchanger movement during the heatup and cooldown cycles. The angles shown at mounts S_4 and S_6 indicate the direction of heat exchanger movement; the bolt holes are oversize at these mounts to provide free movement in the x^1, z^1 - plane. Additional brackets (not shown) were provided on the low pressure ducts between the BRU and BHXU to react bellows unbalance pressure forces.

4. Bracket Analysis

The brackets for mount locations S_1 through S_6 were designed for the 20 g lateral and 24 g axial inertia loads. Three configurations were used, one pair each for the recuperator high pressure outlet pan, the transition section between the recuperator and heat sink, and the heat sink low pressure outlet pan. Each pair was designed for the maximum combined loading, listed in Table 28, for either of the two mount points (i.e., S_1 loads for S_1 and S_6, etc.). A stress analysis was performed for each configuration and the support system will be satisfactory for the applied inertia loads.

TABLE 29

THERMAL GROWTH SUMMARY AT BRACKETS (x^1, z^1 PLANE)

Bracket	δ_{x^1}, in.	δ_{z^1}, in.	$\vec{\Sigma}\delta$
S_1 (A)	-0.028	-0.187	0.189
(B)	-0.070	0.187	0.200
S_2	0	0	0
S_3 (A)	0.012	0.029	0.031
(B)	0.012	0.029	0.031
S_4 (A)	0.012	0.029	0.031
(B)	0.012	0.029	0.031
S_5	0.023	0	0.023
S_6 (A)	0.093	-0.187	0.209
(B)	0.051	-0.187	0.194

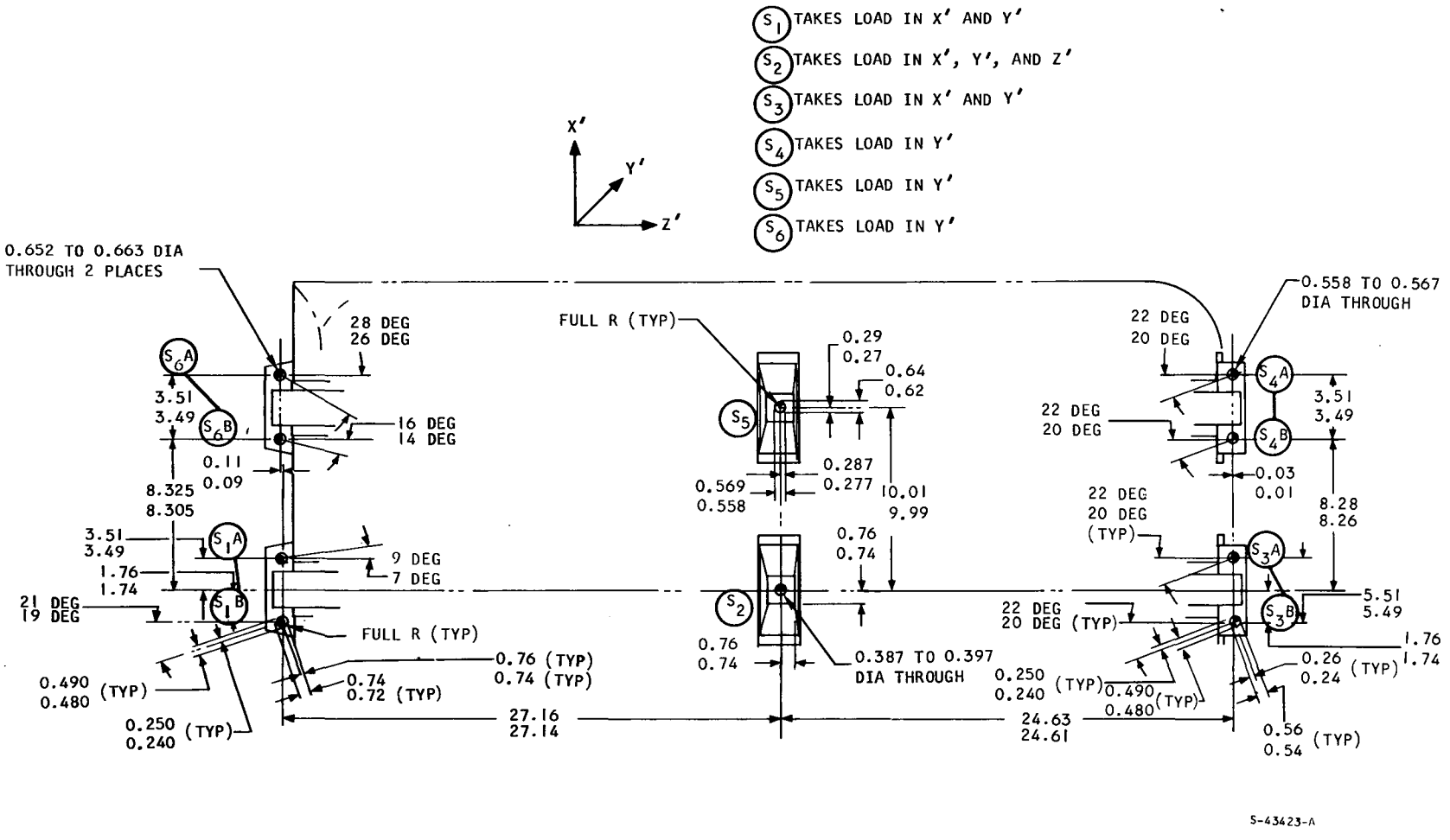

Figure 55. Six Point Mounting System

The brackets located on the circular pans (S_1, S_6, S_3, S_4) consist of a doubler and variable cross-section torque box to transmit the bolt loads to the core. A computer program available to AiResearch was used to analyze the frame as several finite elements with varying section properties. The geometry of the hot end (1194°F) brackets, S_1 and S_6, is shown in Figure 56 and the heat sink outlet pan bracket configuration (80°F operating temperature) is shown in Figure 57. Brackets S_2 and S_5, located on the transition section, are shown in Figure 58. These transition brackets, S_2 and S_5, operate at a maximum temperature of 350°F.

5. External Mount System Definition

An external mounting frame is required for mounting the BHXU-BRU package within a spacecraft or in a test facility where the design shock and vibration spectra will be applied. The frame will be mounted on isolators to restrict the inertia load levels in the BHXU and BRU. The specific design criteria governing the mounting system would be consistent with the BHXU design criteria as discussed previously. The structural analytical approach is outlined in appendix C, including calculations relating to the design of a feasible frame and definition of the desired isolator properties.

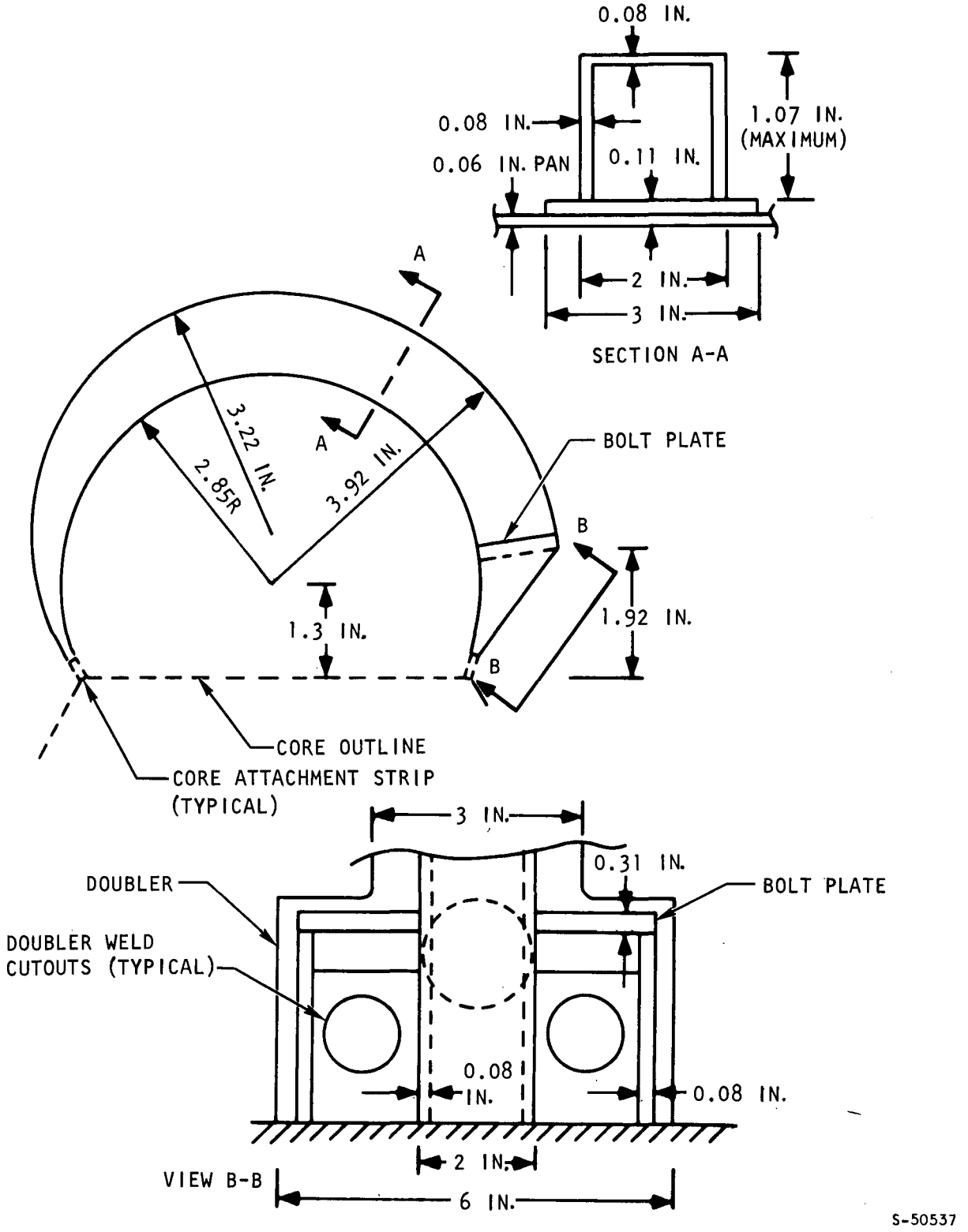

Figure 56. High Pressure Outlet Pan Mounting for Brackets S_1 and S_6

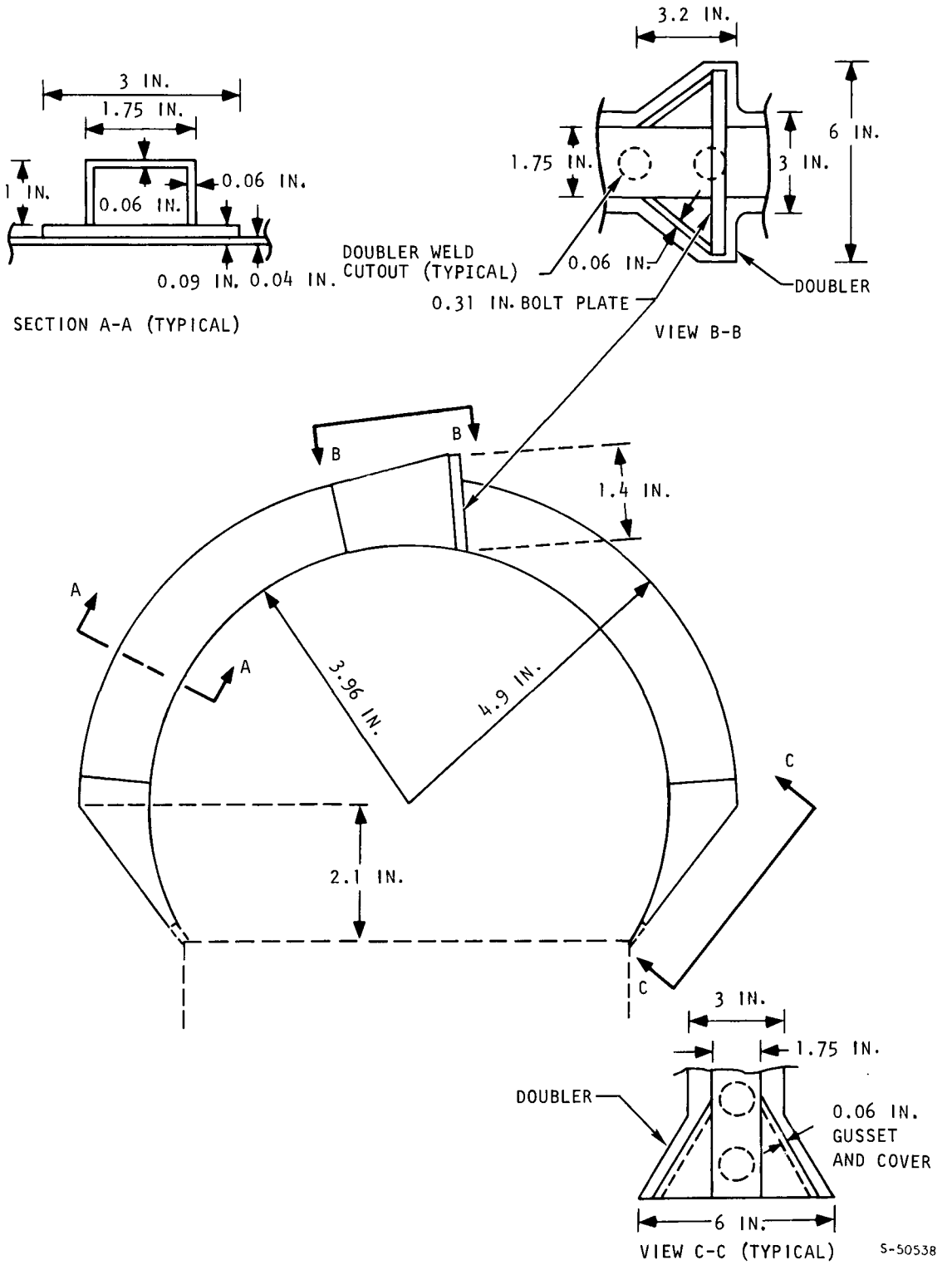

Figure 57. Low Pressure Outlet Pan Mounting for Brackets S_3 and S_4

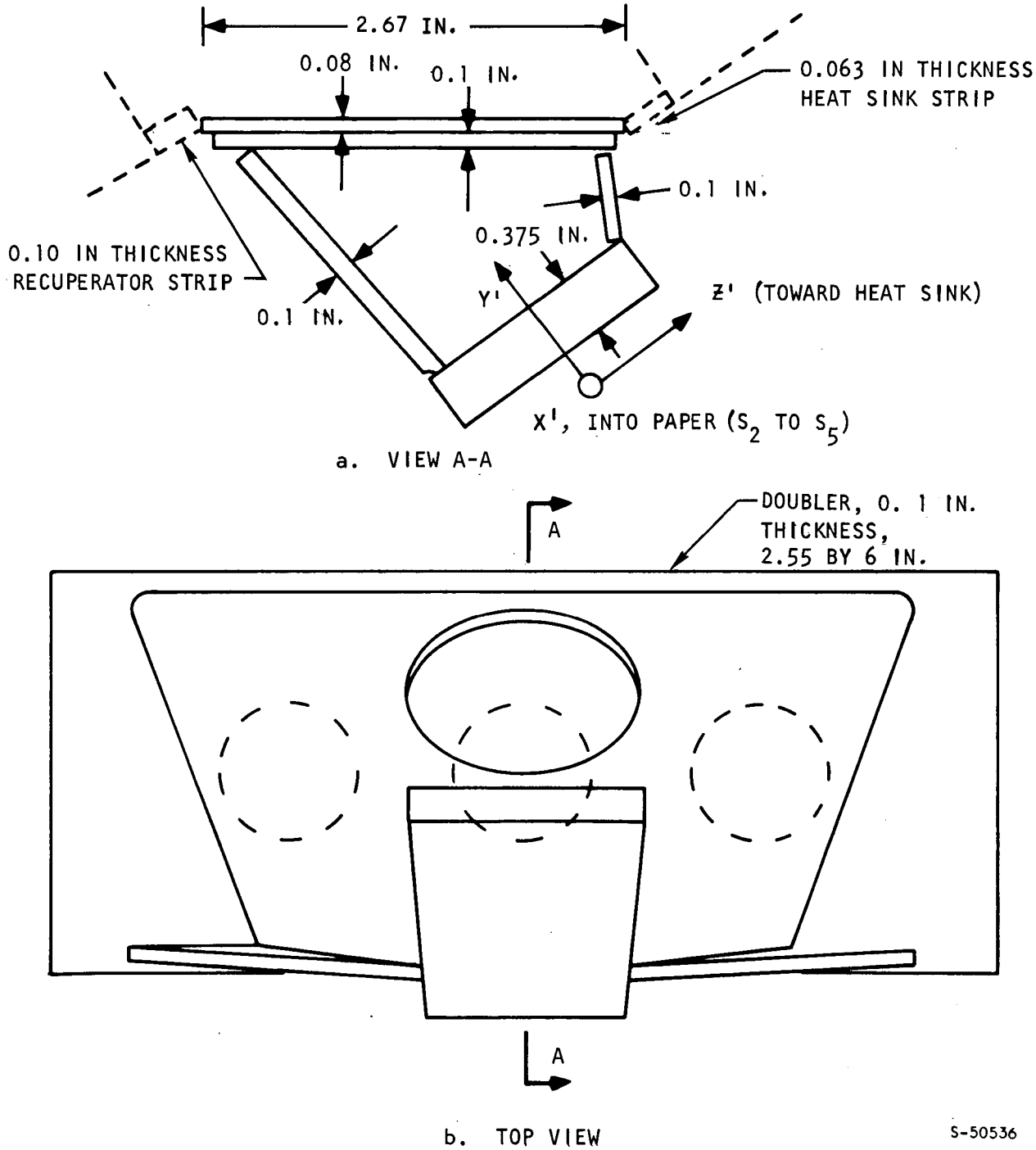

Figure 58. Transition Brackets, S_2 and S_5

SECTION 5

FABRICATION

Fabrication of three heat exchanger units that met the thermodynamic, structural, and leakage requirements of the work statement was accomplished. To achieve the successful fabrication of the heat sink heat exchangers, a fabrication development program was required. In this fabrication development program, the gas-to-gas recuperators were fabricated using established state-of-the-art procedures.

FABRICATION DEVELOPMENT

The initial fabrication procedures for the heat sink heat exchanger were state-of-the-art techniques. The first heat sink heat exchanger cores brazed did not meet the structural or leakage requirements. Evaluation of the cores indicated that the header bars for the liquid passes should be modified from single-piece formed headers to multiple headers. The quality of the braze joints also indicated that the braze cycle time was too long, allowing an increase in the braze temperature that resulted in under-brazed joints. To improve the quality of the braze joints, the outermost layers of the heat sink heat exchanger were prebrazed as modules with a relatively short braze cycle. The prebrazed modules were then incorporated into a heat sink heat exchanger core which was brazed using a shortened braze cycle to ensure satisfactory brazing.

The use of modules and the shortened braze cycle resulted in cores that met the structural requirements but did not satisfy the leakage level required between the gas and liquid passages. To satisfy the leakage requirement, thicker tube sheet material was used. The 0.008-in. tube sheet material that was used initially was changed to 0.016 in. for the modules and 0.010 in. for the remaining tube sheets. Heat sink heat exchanger No. 1 was fabricated with the thicker tube plate material, but it had one leak between a gas and liquid passage. The liquid pass that leaked was sealed off and the core was used in BHXU No. 1. The source of the leak in the heat sink core was thought to be a local spot weld used in fabrication. Therefore, spot welding was eliminated from the fabrication sequence. Heat sink heat exchanger cores No. 2 and No. 3 were fabricated using the modified procedure with no difficulties.

FABRICATION SEQUENCE

The fabrication sequence in building the Brayton cycle heat exchanger units was to fabricate the details and braze the cores for a BHXU. Upon completion of the cores being brazed, each was checked by performing a proof pressure test (1.5 times working pressure) and a helium leak check. This procedure was followed for the gas-to-gas recuperator and the gas-to-liquid heat sink heat exchanger. The recuperators were brazed in pairs to provide a larger base-area-to-height ratio as a means of maintaining the desired geometry. After the initial braze and successful completion of the proof

pressure test, the cores were subjected to a second braze where all exposed exterior braze joints were re-alloyed. The second braze was implemented to ensure good filleting on all exterior joints to improve reliability in meeting the long life, low leakage requirements of this hardware.

The heat sink heat exchanger was fabricated, after a period of investigation, with the outermost liquid passages of each circuit prebrazed as modules. The four modules were then included in the stack up and the core brazed. Upon completion of this braze cycle and the proof pressure test, the heat sink heat exchanger was also subjected to an exterior alloying and braze cycle to meet the requirements of life and leakage.

The next step in the fabrication sequence was the assembly of the two cores. Because of the tolerance control desired on the interface locations, a progressive buildup was used on the BHXU starting with the transition section between the cores. After the gas manifolds were welded in place the assembly was stress relieved and the mounting pads machined.

The final ducting was attached following the progressive trim and weld procedure. After the ducting was complete, the entire BHXU was subjected to a helium leak check prior to being tested.

BHXU 1

In following the indicated sequence for unit 1, no difficulties were experienced with the recuperator. In fabricating the heat sink heat exchanger, a series of design and procedure changes were required to produce the first heat sink heat exchanger core. The core obtained for the first unit required 1 of the 32 liquid sandwiches that form two liquid circuits to be sealed off before reaching the desired helium leak requirements.

During the assembly of the first unit, an internal leak in the heat sink heat exchanger developed. Several attempts to locate the passage which contained the leak were unsuccessful.

This unit was shipped with the 15-liquid sandwich circuit helium tight but the 16-liquid sandwich circuit was not recommended for operation.

BHXU 2

The recuperator for the second unit had been brazed simultaneously with the recuperator for the first unit. The heat sink heat exchanger for BHXU 2 was brazed following the same procedure as the heat sink heat exchanger in unit 1. BHXU 2 proceeded through the assembly with no difficulties, was acceptance tested, and was shipped exceeding all leakage requirements.

BHXU 3

Two recuperator cores were brazed for BHXU 3 and based upon exterior appearance one core was selected. The selected core was processed and no difficulties were experienced. The heat sink heat exchanger for this unit was fabricated in the same manner as the heat sink heat exchanger for BHXU's 1 and 2. No difficulties were experienced in the assembly of BHXU 3 and this unit was shipped exceeding all leakage requirements, after being subjected to the acceptance test.

SECTION 6

TESTING

TEST OBJECTIVES AND PROCEDURES

Two series of tests were conducted to evaluate performance of the three BHXU's:

(a) Performance tests of unit 1 to gain data relating to the effectiveness and pressure drop characteristics of the BHXU design

(b) Acceptance tests of each of the three units delivered

Testing was conducted at the AiResearch Los Angeles facility. The performance test series consisted of three separate heat transfer and pressure loss tests on BHXU 1:

(a) A performance test of the recuperator at conditions simulating the reference design point

(b) A performance test of the heat sink exchanger at conditions simulating the design point

(c) A performance test of the combined heat exchanger unit at conditions simulating the design point and at conditions simulating each of the off-design conditions (included for reference as Table 30).

The acceptance test series conducted on each unit included a single-unit heat sink heat exchanger test (recuperator nonoperative) and several BHXU combined-unit tests simulating operating points within the range of the design and off-design conditions of Table 30. The purpose of running a separate, single-unit test of the heat sink exchanger was to obtain a higher end-to-end temperature difference through the unit than was possible during the combined-unit tests. During the combined unit tests, the simulation of the recuperator operating points resulted in a relatively low air inlet temperature to the heat sink exchanger (in the range of 120^0 to 170^0F). With this low inlet temperature, the end-to-end temperature difference through the heat sink exchanger was insufficient to provide accurate heat transfer data on this unit.

Table 31 shows the performance test conditions that were specified in the test plan and obtained with only minor variations during the actual testing. Conditions for test 1, in which only the recuperator was operative, were established on the basis of obtaining the reference design point Reynolds number on both sides of the exchanger and obtaining a balance of end-section pressure losses on both sides, as predicted by the same analysis as was used in designing the end sections for uniform flow. The hot air inlet temperature

TABLE 30

BHXU OFF-DESIGN CONDITIONS

		Case I	Case II	Case III	Case IV	Case V	Case VI
Hot Side	XeHe flow rate (lb/sec)	0.38	0.55	0.76	1.0	1.5	2.5
	Recuperator inlet temperature (^{o}R)	1709	1705	1701	1701	1701	1701
	Recuperator inlet pressure (psia)	6.86	9.95	13.9	18.1	27.2	45.3
Cold Side	Recuperator inlet temperature (^{o}R)	7.40	739	738	738	738	738
	Recuperator inlet pressure (psia)	12.8	18.5	25.6	33.7	50.5	84.25

TABLE 31

PERFORMANCE TEST CONDITIONS

Parameter (units)	Test (1)	Test (2)	Test (3)						
			Design	I	II	III	IV	V	VI
Hot air flow (lb/sec)	0.680	0.900	0.680	0.202	0.292	0.404	0.531	0.796	1.33
Cold air flow (lb/sec)	0.673	-	0.673	0.200	0.289	0.400	0.526	0.788	1.32
Liquid flow (lb/sec)	-	0.400	0.365	0.108	0.157	0.217	0.285	0.427	0.714
Hot air inlet temperature (^{0}F)	730	335	730	730	730	730	730	730	730
Cold air inlet temperature* (^{0}F)	70	-	70	70	70	70	70	70	70
Liquid inlet temperature (^{0}F)	-	30	30	30	30	30	30	30	30

*Ambient air temperature

was set at 730°F to avoid potential oxidation problems associated with the use of air as the test medium. Conditions for test 2, in which only the heat sink exchanger was operative, were established to obtain the reference design point Reynolds number on the gas side and a Reynolds number on the cold side that was as close to the design point Reynolds number as possible, within the requirement that the liquid outlet temperature should be sufficiently below the gas inlet temperature to yield an accurate evaluation of exchanger overall thermal conductance (UA). If the Dow Corning fluid were run at the design point Reynolds number, the cold-side effectiveness of the heat sink exchanger would be too high to yield an accurate measure of heat transfer performance. For this reason, the Dow Corning fluid flow rate was increased to the point where the heat exchanger capacity-rate ratio was of the order of one, and the cold-side inlet temperature was decreased to 30°F to compensate partially for the higher flow rate. The temperature of 30°F is the lowest that could be used without incurring the possibility of ice formation on the air side.

In test 3, the test of the combined heat exchanger unit, it was impossible to obtain the reference design point Reynolds numbers in the two heat exchangers simultaneously. This situation occurred because of the lower recuperator temperatures and the different relationship between recuperator and heat sink exchanger viscosities in the air test than exist during normal operation with xenon/helium. Thus, for the design point run, the gas flow rate was the same as in test 1, resulting in a correct simulation of recuperator performance and an inexact simulation of heat sink exchanger performance. It was preferred to use a correct simulation in the recuperator rather than in the heat sink exchanger because this results in a correct balance of the recuperator end-section pressure losses. For the test runs simulating the unit off-design conditions, the airflow rate was varied in proportion to the xenon/helium flow rates as specified in Table 30.

The acceptance tests on BHXU 1 comprised four additional test runs within the range of conditions of test 3 in Table 31. The acceptance tests on BHXU's 2 and 3 included a test 2 test point with each of the liquid loops active plus several runs in the test 3 test range.

The test results using air as the heat medium at simulated test conditions are not directly convertible to a performance prediction for XeHe at design conditions. However, the performance and acceptance tests were used to verify the analytical procedures employed by AiResearch and to verify the basic heat transfer data used in the analysis. To accomplish this verification, an analytical prediction of performance was made for each test point in Table 31 based upon the known heat exchanger configuration and the indicated test conditions. The analytical procedure used was identical to that used for the design of the BHXU, so that the comparison of predicted values using air to test values using air could be used to establish the correlation between predicted BHXU performance for XeHe and what the actual performance would be if the BHXU were tested with XeHe.

TEST SETUP

Figure 59 is a schematic of the test setup indicating test equipment and instrumentation locations. Temperature measurements were made with iron-constantan and chromel-alumel thermocouples. Two types of temperature readout were utilized: (1) a direct reading potentiometer, used for monitoring test conditions and providing a data sheet record of the test points, and (2) a stamping Brown recorder, for providing a permanent and continuous record of test temperatures. Pressures and liquid pressure drops were measured with gages, whereas air pressure drops were measured with water manometers. Airflow rates were determined from pressure drop measurements across standard orifice sections. Liquid flow rates were measured with a Cox turbine-type flowmeter, calibrated for the Dow Corning test fluid prior to the test. Table 32 provides a summary of the type, accuracy, and calibration of the instrumentation used.

Figure 60 is a photograph of BHXU 1 as instrumented and installed in the test facility prior to testing. Figure 61 is a photograph of the same unit after testing. These photographs are typical of all three BHXU's, although there was some reduction in the amount of active instrumentation on BHXU's 2 and 3. All units were completely covered with insulation during the actual testing. Figure 62 shows part of the instrumentation readout area of the test stand.

TEST RESULTS

Unit 1 Performance Tests

The reduced data on recuperator heat transfer performance are plotted in Figure 63. Averages of the hot- and cold-side temperature effectiveness and airflow rates are used to obtain a single plot of effectiveness vs flow rate for this unit. Capacity-rate ratios for the actual test points varied from 0.944 (hot-side minimum) to 0.974 (cold-side minimum). The test points plotted include the recuperator single-unit test, the BHXU design point run, and the six BHXU off-design points. Comparing test performance with the predicted performance for this unit, shown by the dashed line in Figure 63, the ratio of test UA to predicted UA varies from 83 percent at 12.5 lb/min to 90 percent at 80 lb/min. At the simulated design flow of 41 lb/min, test UA is 86 percent of predicted.

The heat sink exchanger performance is shown in Figure 64. The points shown are the single-unit performance test, the BHXU design point test, and the BHXU off-design test points. In plotting the test data, the average temperature effectiveness is used and the airflow rate at each test point is corrected to an equivalent flow corresponding to the average of the hot- and cold-side capacity rates. The result is a single curve of effectiveness vs flow rate for the operating condition of equal hot and cold capacity rates. Actual test capacity-rate ratios for the BHXU tests varied from 0.90 to 0.99 (cold-side minimum in all cases). In the single-unit heat sink exchanger test, the cold-side capacity rate was 83 percent of the hot-side capacity rate. The single-unit performance test is considered to be the most reliable of the test points because it involved the highest temperature differential between inlet fluids (301°F) and is therefore least sensitive to thermocouple errors. For

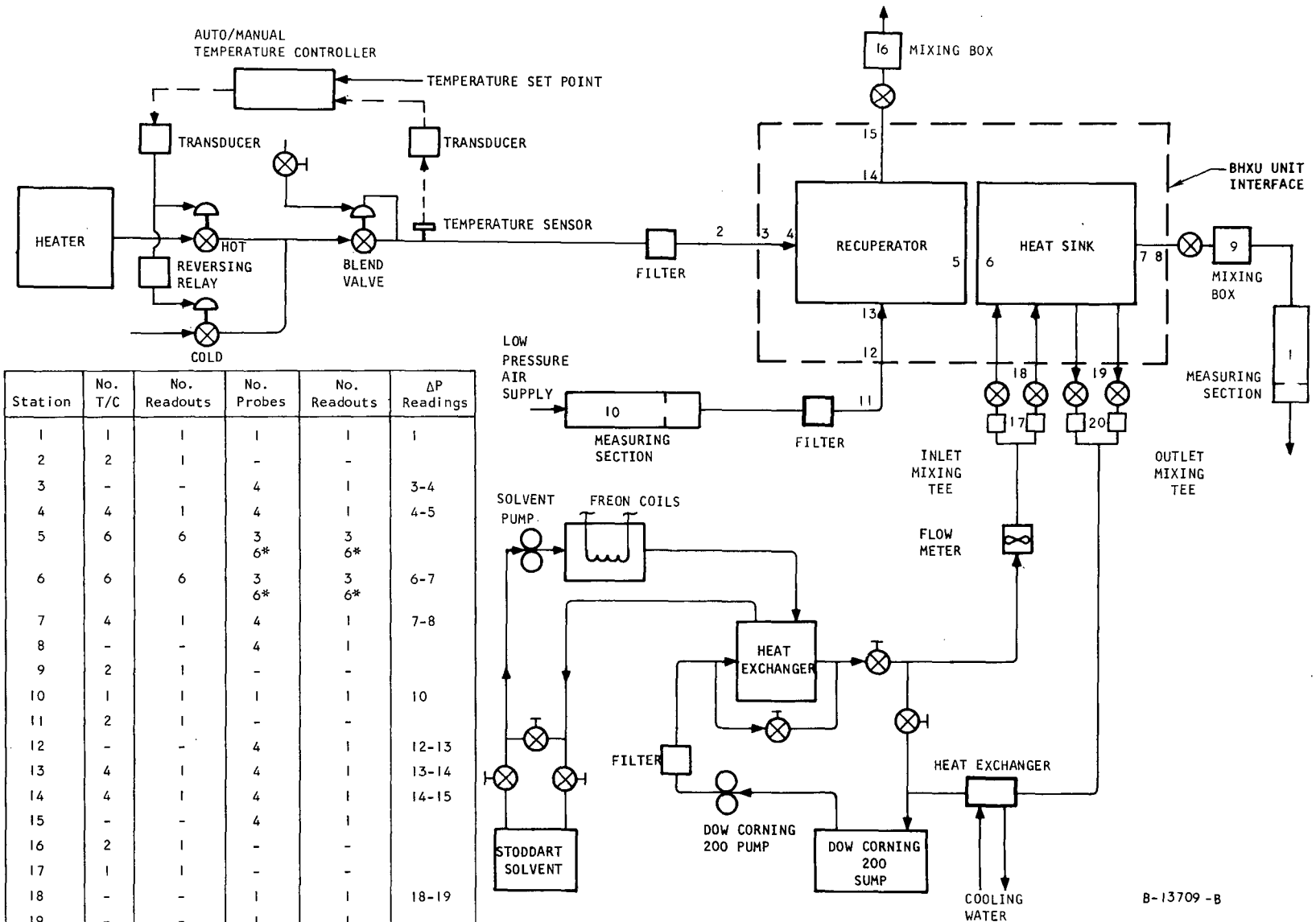

Station	No. T/C	No. Readouts	No. Probes	No. Readouts	ΔP Readings
1	1	1	1	1	1
2	2	1	-	-	
3	-	-	4	1	3-4
4	4	1	4	1	4-5
5	6	6	3 6*	3 6*	
6	6	6	3 6*	3 6*	6-7
7	4	1	4	1	7-8
8	-	-	4	1	
9	2	1	-	-	
10	1	1	1	1	10
11	2	1	-	-	
12	-	-	4	1	12-13
13	4	1	4	1	13-14
14	4	1	4	1	14-15
15	-	-	4	1	
16	2	1	-	-	
17	1	1	-	-	
18	-	-	1	1	18-19
19	-	-	1	1	
20	1	1	-	-	

*Total Pressure Probes, BHXU No. 1 Only

Figure 59. Test Setup

TABLE 32

TEST INSTRUMENTATION

1. Temperature Measurements

   Iron-Constantan and Chromel-Alumel thermocouples

   Record continually (stamping Brown), 24 channels

   Class 15 Honeywell direct reading potentiometer
   Accuracy ±1/2 percent
   Calibration every 4 months

2. Pressure Measurements

   (a) Gages

   Ashcroft, U.S. gage
   Accuracy ±1/2 percent
   Range 0-15, 0-30, 0-60, 0-100 psi
   Calibration every 3 months

   (b) Manometers

   Merriam
   Accuracy 0.05 in. of liquid
   Range 0-30, 0-60 in. H_2O and in. Hg

3. Differential Pressure Measurements

   (a) Manometers

   Merriam
   Accuracy 0.05 in. of fluid
   Range 0-60 in. H_2O
   Calibration every 2 months

   (b) Gages (ΔP)

   Barton
   Accuracy 1/2 percent
   Range 0-50 psi
   Calibration every 3 months

4. Flow Rate Calibration

   (a) Air

   Standard orifice section
   Accuracy 1/2 percent
   Calibration every 6 months, dimensional check

   (b) Liquid

   Cox turbine - type flow meter that registers the output in cycles per second on a counter. These readings are converted to flow rate from a calibration curve. The flow meter is calibrated for the specific fluid in the test temperature range by the weight-time method prior to test.
   Accuracy 1/2 percent
   Calibration every year

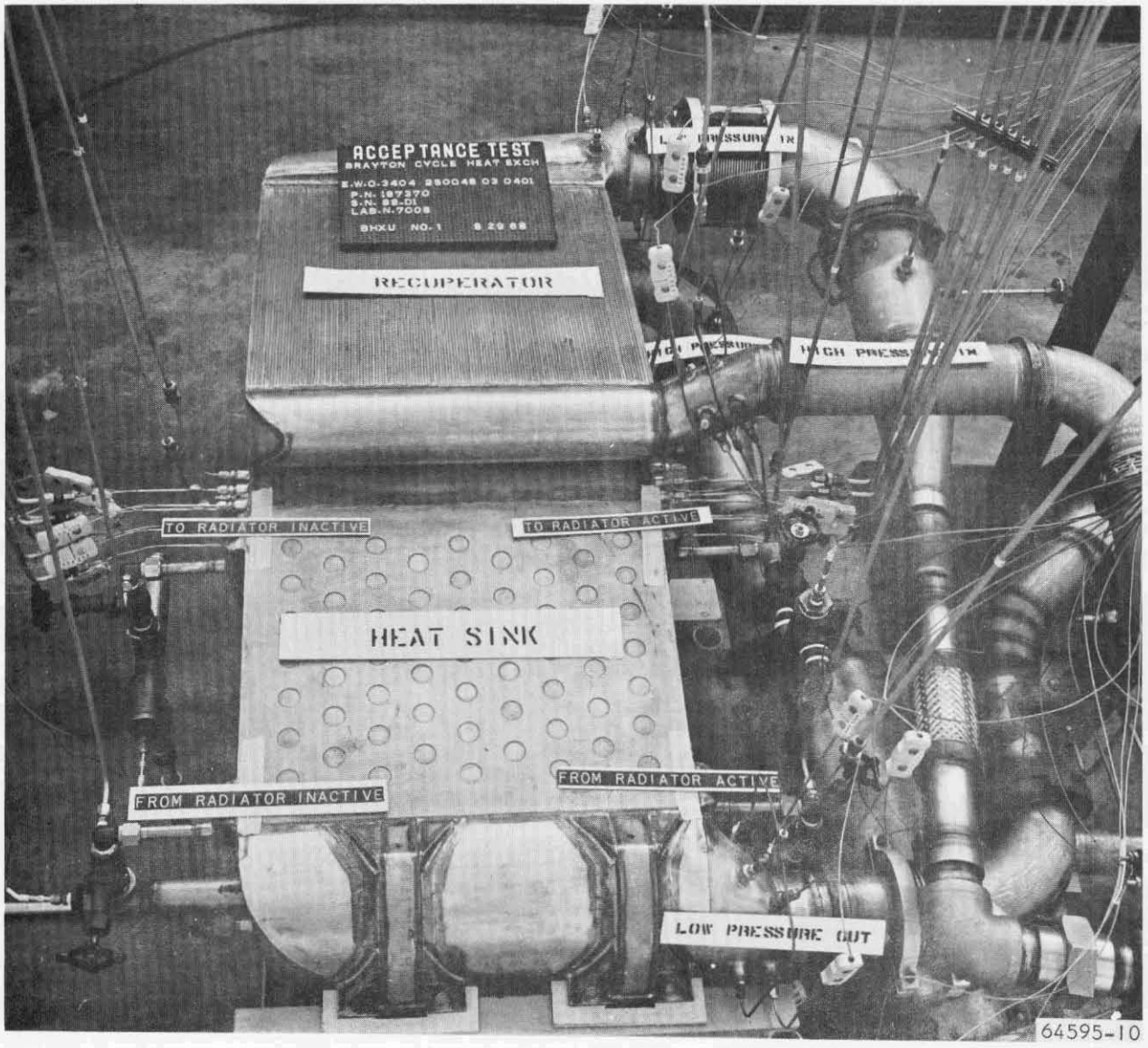

Figure 60. BHXU I Before Testing

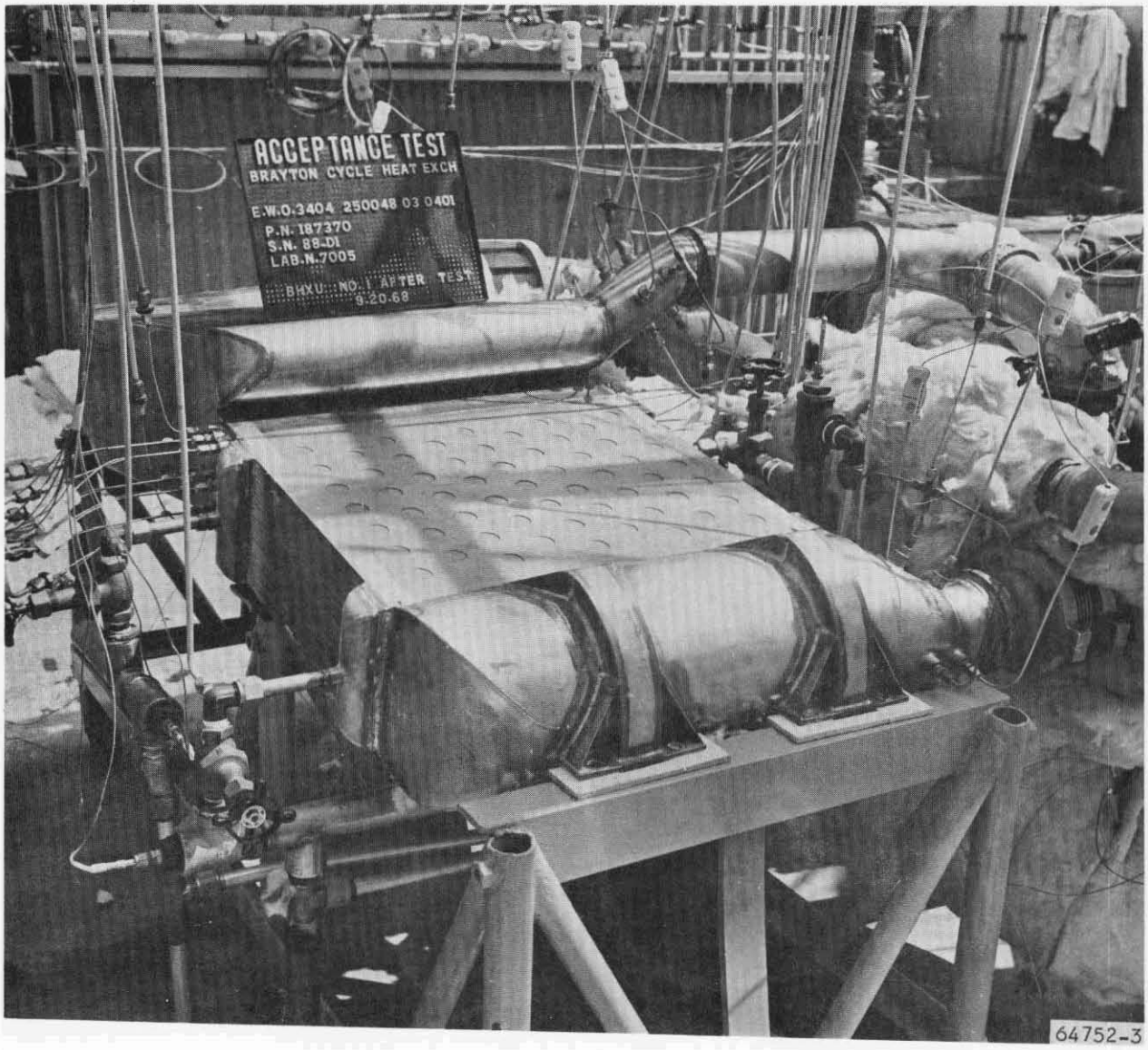

Figure 61. BHXU I After Testing

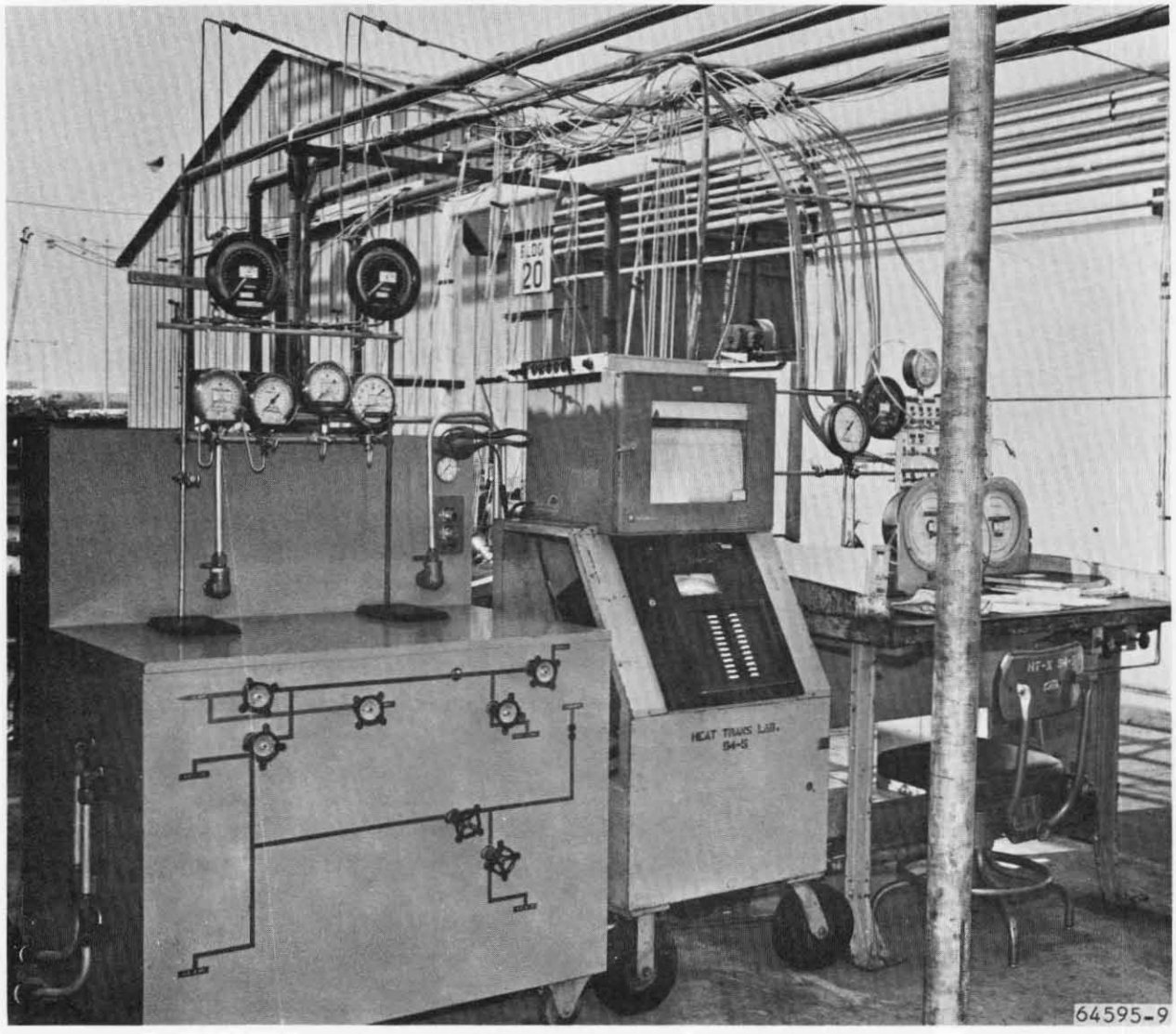

Figure 62. Instrumentation Readout Area of Test Stand

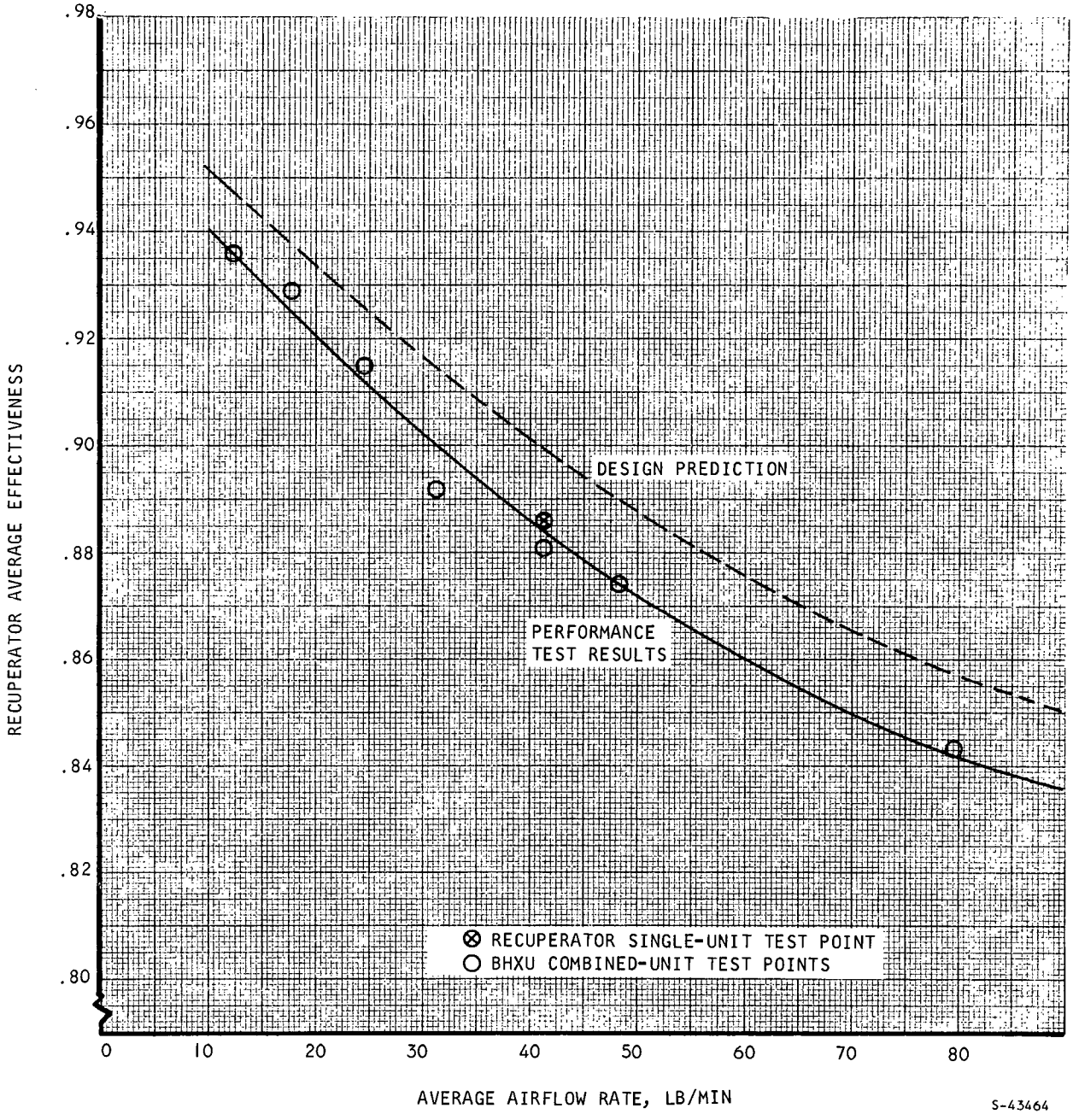

Figure 63. Recuperator Performance Test Results, BHXU I

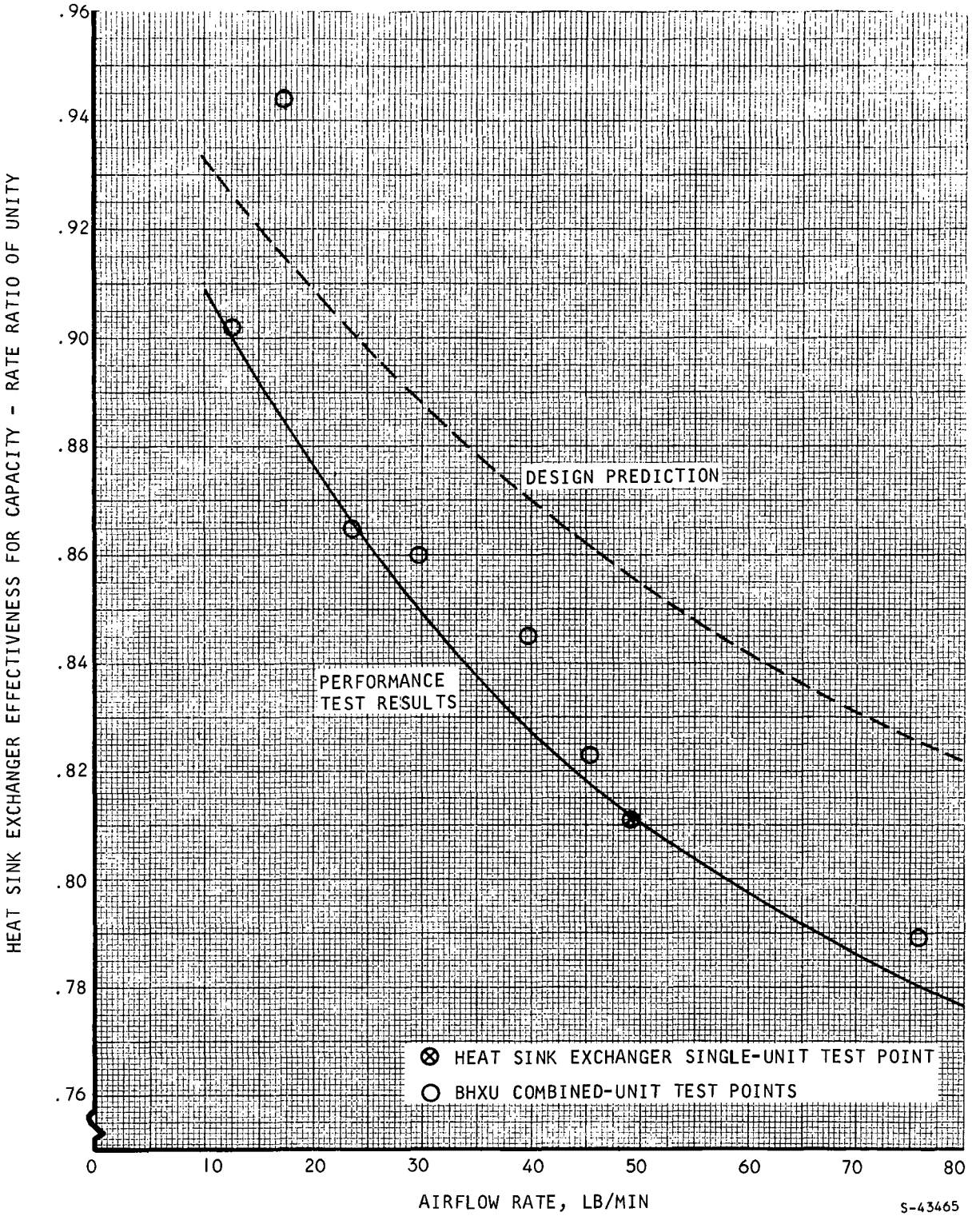

Figure 64. Heat Sink Heat Exchanger Performance Test Results, BHXU I

the combined BHXU tests, the temperature difference between inlet fluids varied from 92°F at 12.5 lb/min airflow to 145°F at 80 lb/min. Resultant errors range from about 1.1 to 0.7 percentage points in effectiveness per degree Fahrenheit error in a fluid temperature measurement. With the possible exception of the test point at 17.5 lb/min, the data scatter shown in Figure 64 can be fully accounted for by instrumentation accuracy.

Comparing test performance with predicted performance for the heat sink exchanger, the ratio of test UA to predicted UA varies from 65 percent at 12.5 lb/min airflow to 74 percent at 80 lb/min. At the simulated design point of 49 lb/min, the test UA is 70 percent of predicted. It should be noted that these tests were conducted with one (of a total of 16) of the liquid passages blocked off to prevent leakage from that passage.

Air pressure drop data for the unit are shown in Figure 65. These data are static pressure differentials corrected for differences in velocity head between inlet and outlet ducts to give change in total pressure through the unit (flange to flange). At the BHXU simulated design point, the high-pressure side pressure drop is 111 percent of predicted and the low-pressure side pressure drop is 86 percent of predicted. The new estimate of XeHe pressure drops based on these test results is shown by the dashed lines in Figure 65.

At the heat sink exchanger simulated design point, the Dow Corning pressure drop was 12.3 psi, which may be compared with a predicted value of 6.2 psi.

The degree of flow maldistribution in the recuperator is shown by the readings from the thermocouple array in the low-pressure side transition section between recuperator and heat sink exchanger. Figure 66 shows the temperature map at this location for the BHXU simulated design point run. Each thermocouple in the array was positioned in the center of a gas flow area approximately 1.9 in. wide by 5 in. high. Comparing the averages of the temperature readings at each horizontal position, it appears that the recuperator end sections were providing good flow distribution in the recuperator flow width direction, since the average temperatures in the outer areas are both 148°F. The average temperatures at the vertical locations show a trend of increasing temperature with height, which is indicative of higher low-pressure side mass velocities at the top of the recuperator than at the bottom. This result is consistent with an expected momentum recovery at the top of the low-pressure inlet manifold because the inlet manifold, for manufacturing and structural reasons, does not taper to zero flow area at the top as would be required for perfect flow distribution.

Unit I Acceptance Tests

Results of the acceptance tests on unit I are shown in Figures 67 through 69. It can be seen that the results of these tests verify the performance curves established by the performance tests. As in the case of the performance tests, the heat transfer results for the heat sink exchanger show a great deal

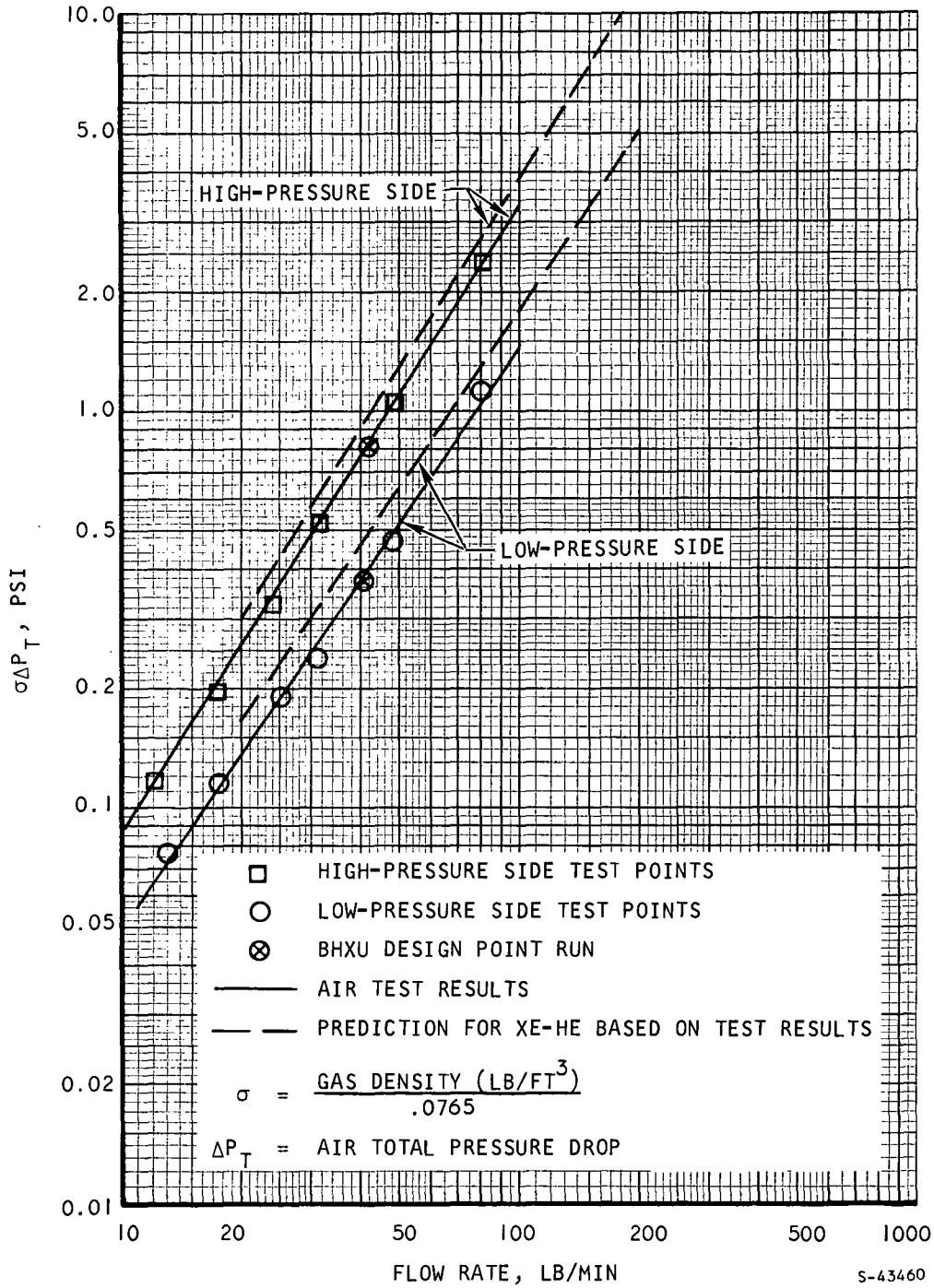

Figure 65. Gas Side Pressure Drop, Performance Test Results, BHXU I

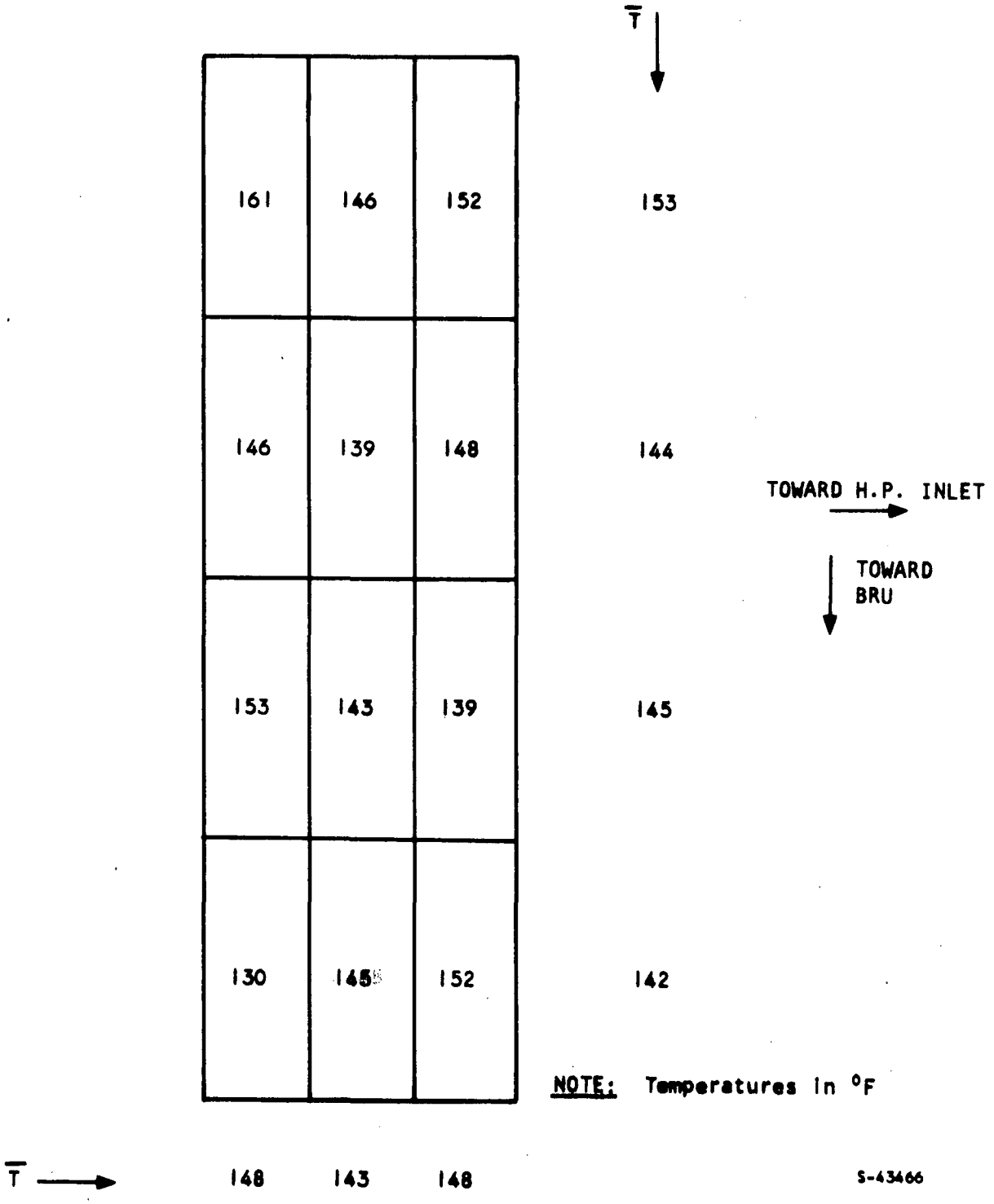

Figure 66. Transition Section Temperature Map, BHXU I Design Point Run

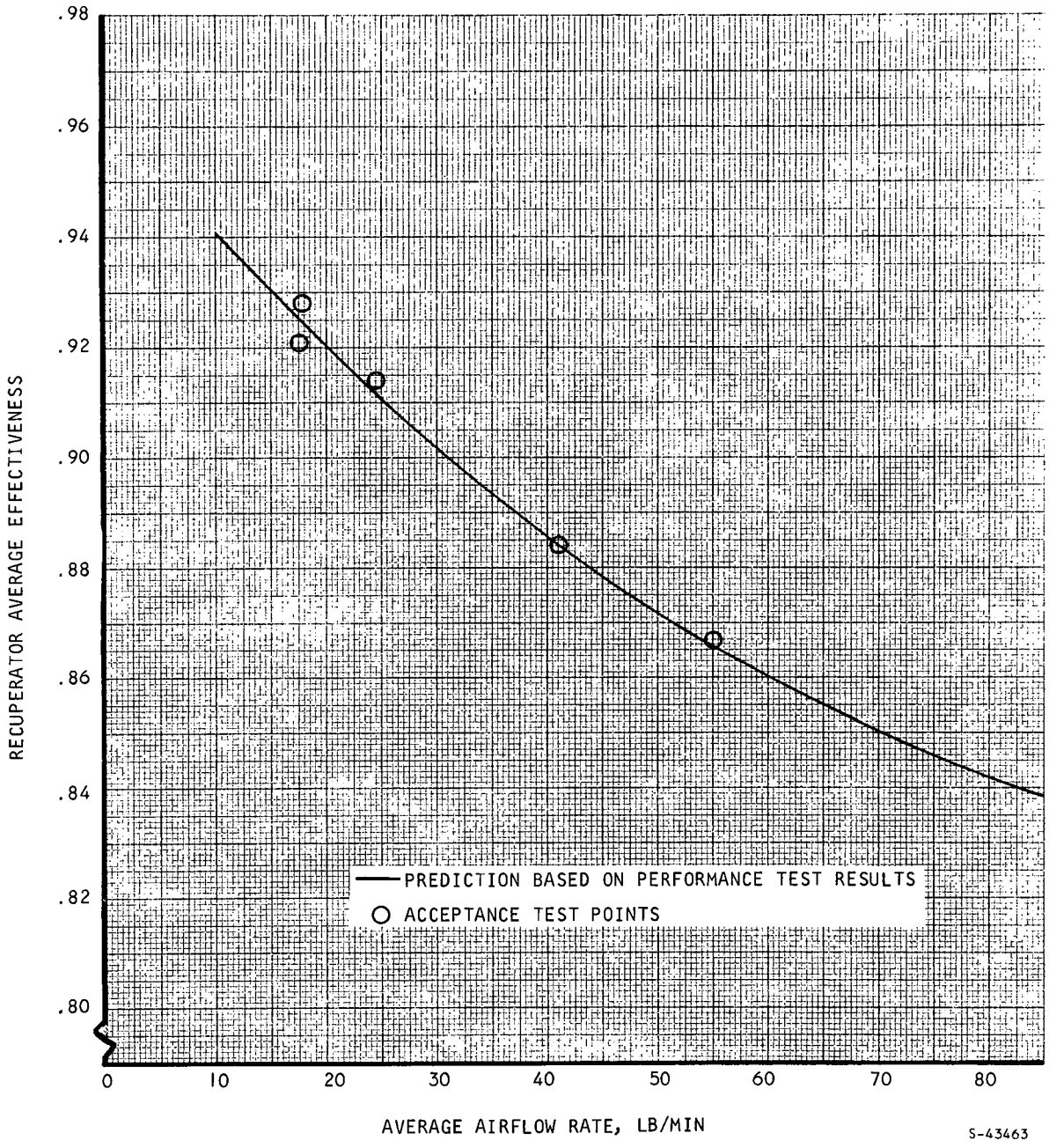

Figure 67. Recuperator Acceptance Test Results, BHXU I

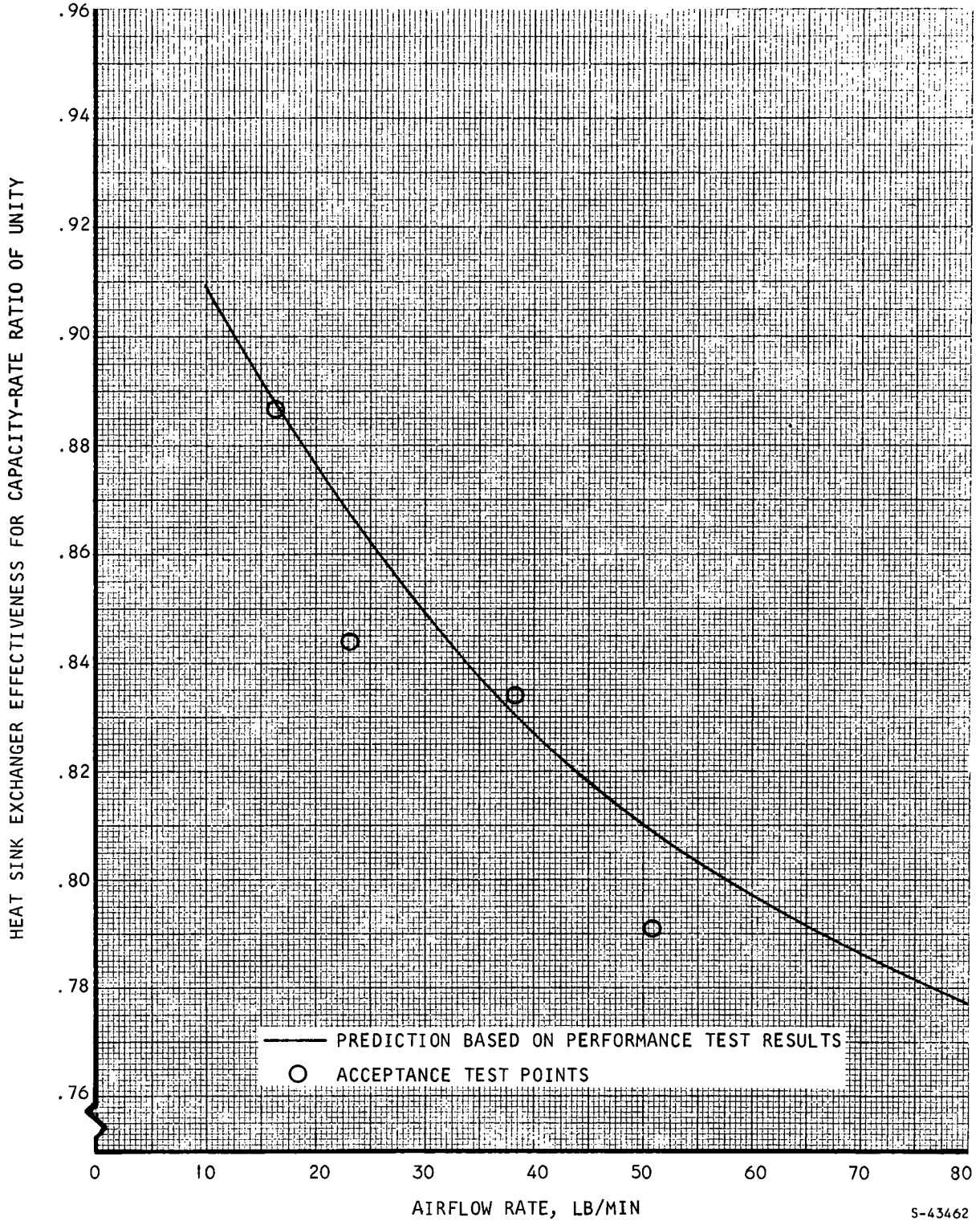

Figure 68. Heat Sink Heat Exchanger Acceptance Test Results, BHXU 1

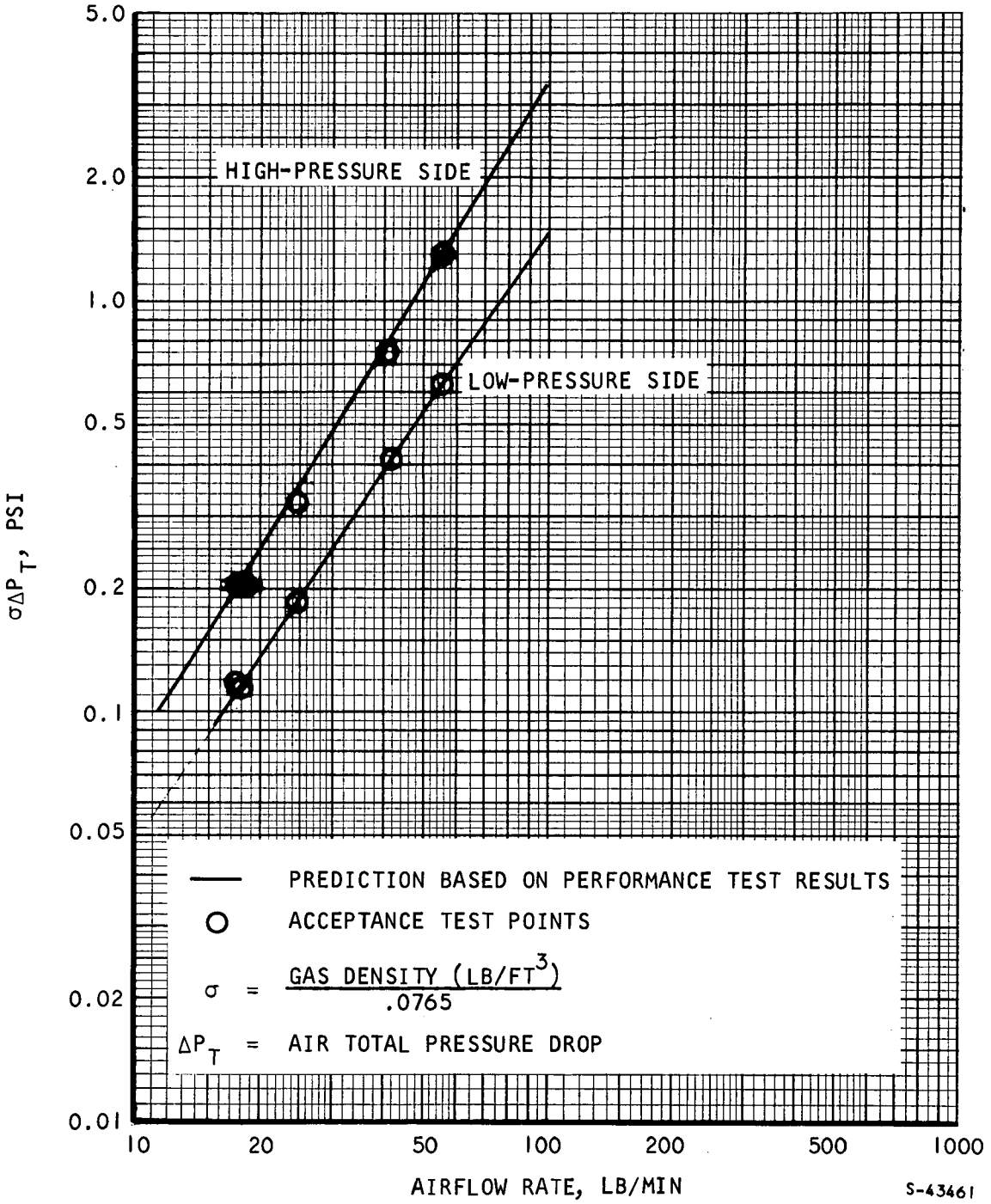

Figure 69. Gas Side Pressure Drop, Acceptance Tests, BHXU I

of scatter, this being attributable to the small end-to-end ΔT across the unit and the resultant sensitivity of the effectiveness measurements to thermocouple errors.

Liquid pressure drop is not directly verified by the acceptance tests because the new liquid pressure drop prediction was established by the results of the individual heat sink exchanger test rather than the combined BHXU tests. The individual test was used because this test more closely approximates the end-to-end ΔT encountered during heat sink exchanger operation with XeHe. Liquid pressure drops measured during the acceptance tests, however, were close to the pressure drops measured in the combined BHXU performance tests, which were about 30 percent above design prediction.

Unit 2 Acceptance Tests

A total of seven test points were run, including two BHXU simulated design point runs, three off-design runs, and two heat sink exchanger single-unit tests (one with each Dow Corning loop active). The data on recuperator heat transfer performance are shown in Figure 70 and compared with the effectiveness curve obtained from the BHXU I performance test series. The test data are seen to verify the previously obtained performance curve within the limits of instrumentation accuracy.

The data on heat sink exchanger heat transfer performance are shown in Figure 71. Also shown in the figure are the effectiveness curve obtained from the BHXU I performance test series and the curve based on the original design prediction of effectiveness for this unit. This unit performs much better than unit 1, which had one of 16 liquid-side flow passages blocked. The curve drawn in the figure as the best interpretation of the test data is not the best fit of all the data points, because more importance is attached to the single-unit test points than to the BHXU combined-unit points. The single-unit tests involved a higher temperature differential between inlet fluids and therefore resulted in a more accurate determination of temperature effectiveness than is available from the combined-unit tests.

Comparing test performance with predicted performance for the unit 2 heat sink exchanger, the ratio of test UA to predicted UA varies from 92 percent at 12.5 lb/min airflow to 94 percent at 80 lb/min. At the simulated design point of 49 lb/min, the test UA is 93 percent of predicted.

Air pressure drop data for BHXU 2 are shown in Figure 72 and compared with the pressure drop prediction based on the BHXU I performance tests. The high-pressure side pressure drops are slightly below predicted and the low-pressure side pressure drops are slightly above predicted.

Dow Corning fluid pressure drops in the single-unit heat sink exchanger tests were about 75 percent of the pressure drop measured during the single-unit performance test of BHXU I.

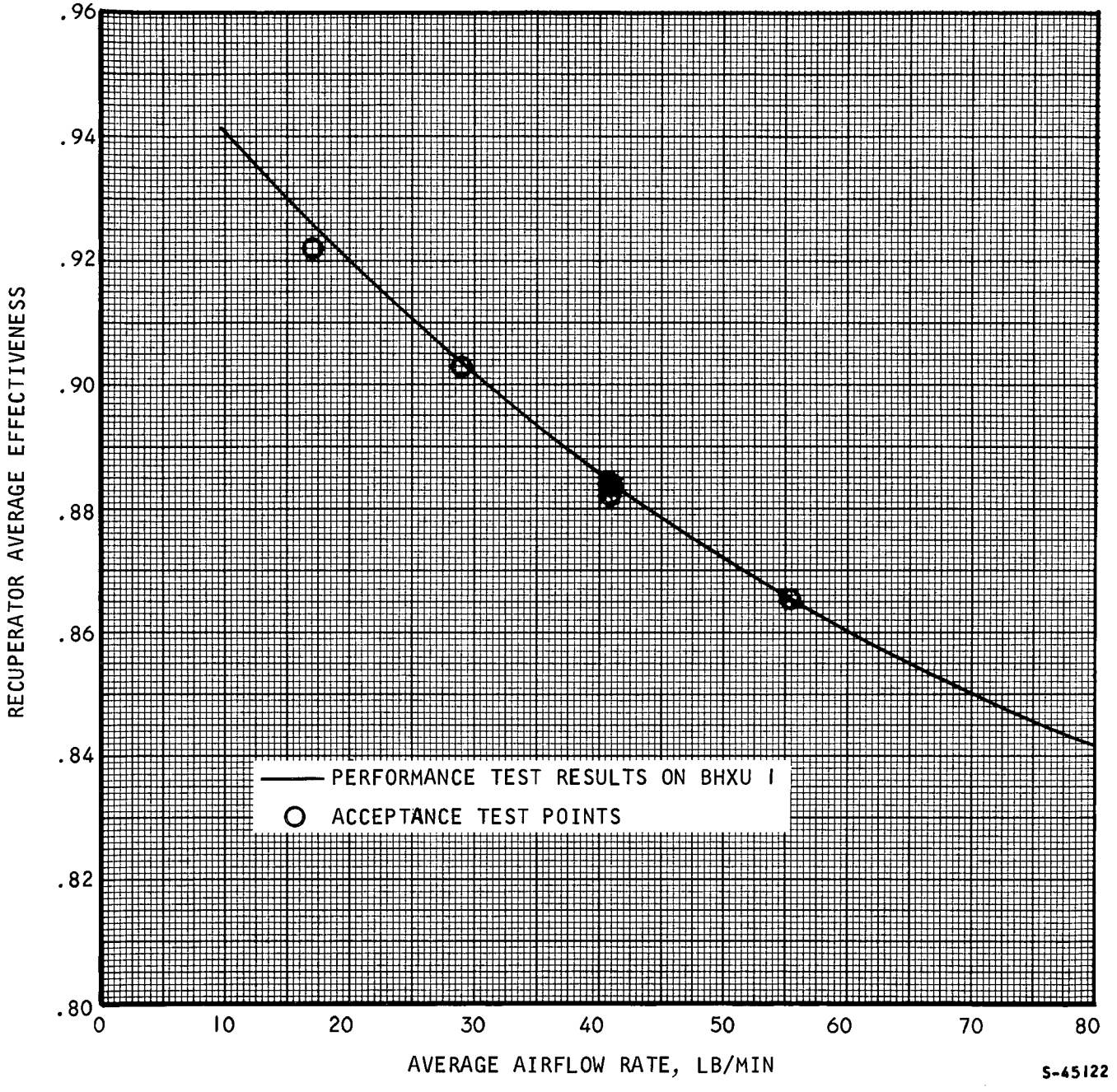

Figure 70. Recuperator Acceptance Test Results, BHXU 2

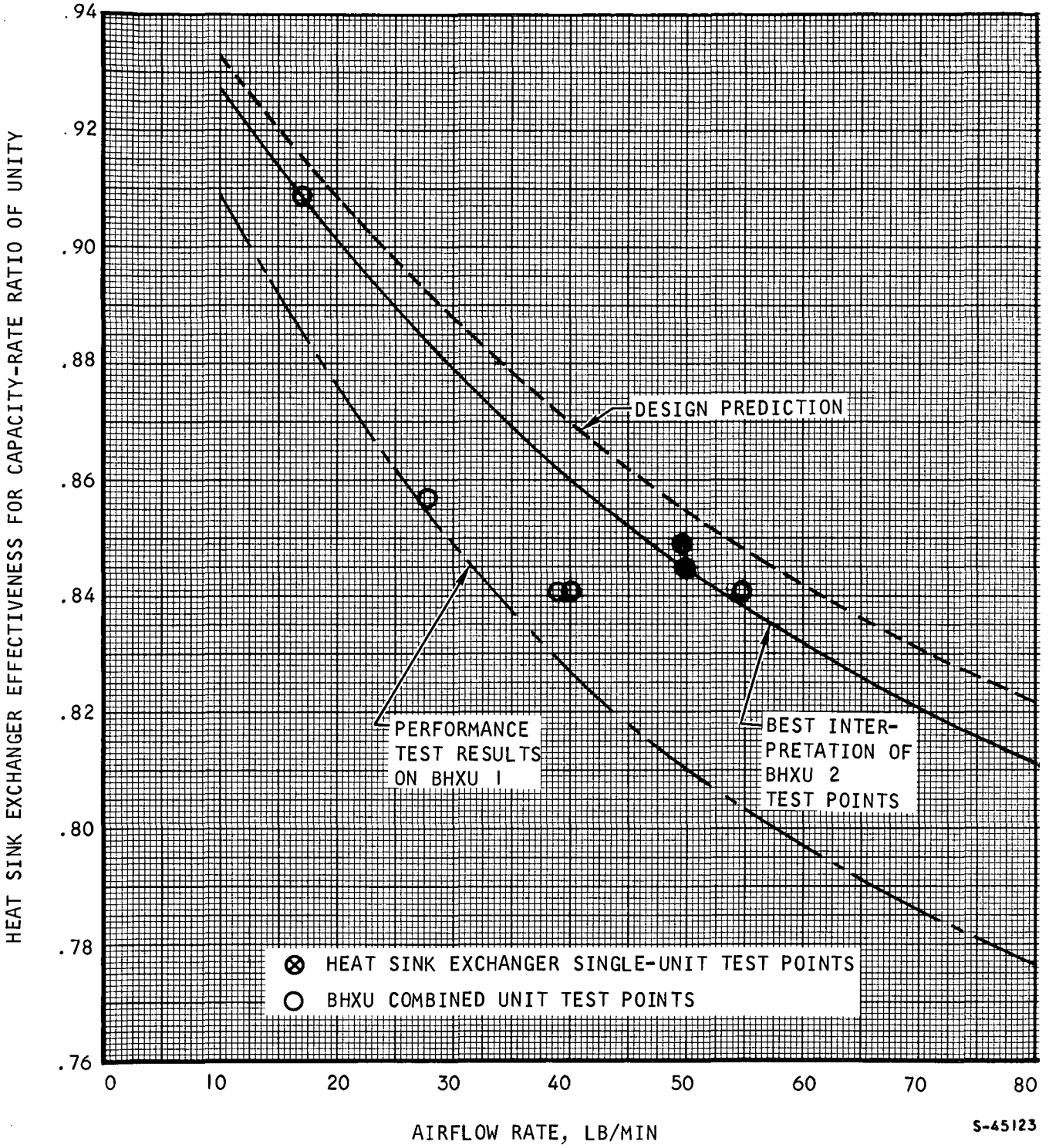

Figure 7.1. Heat Sink Exchanger Acceptance Test Results, BHXU 2

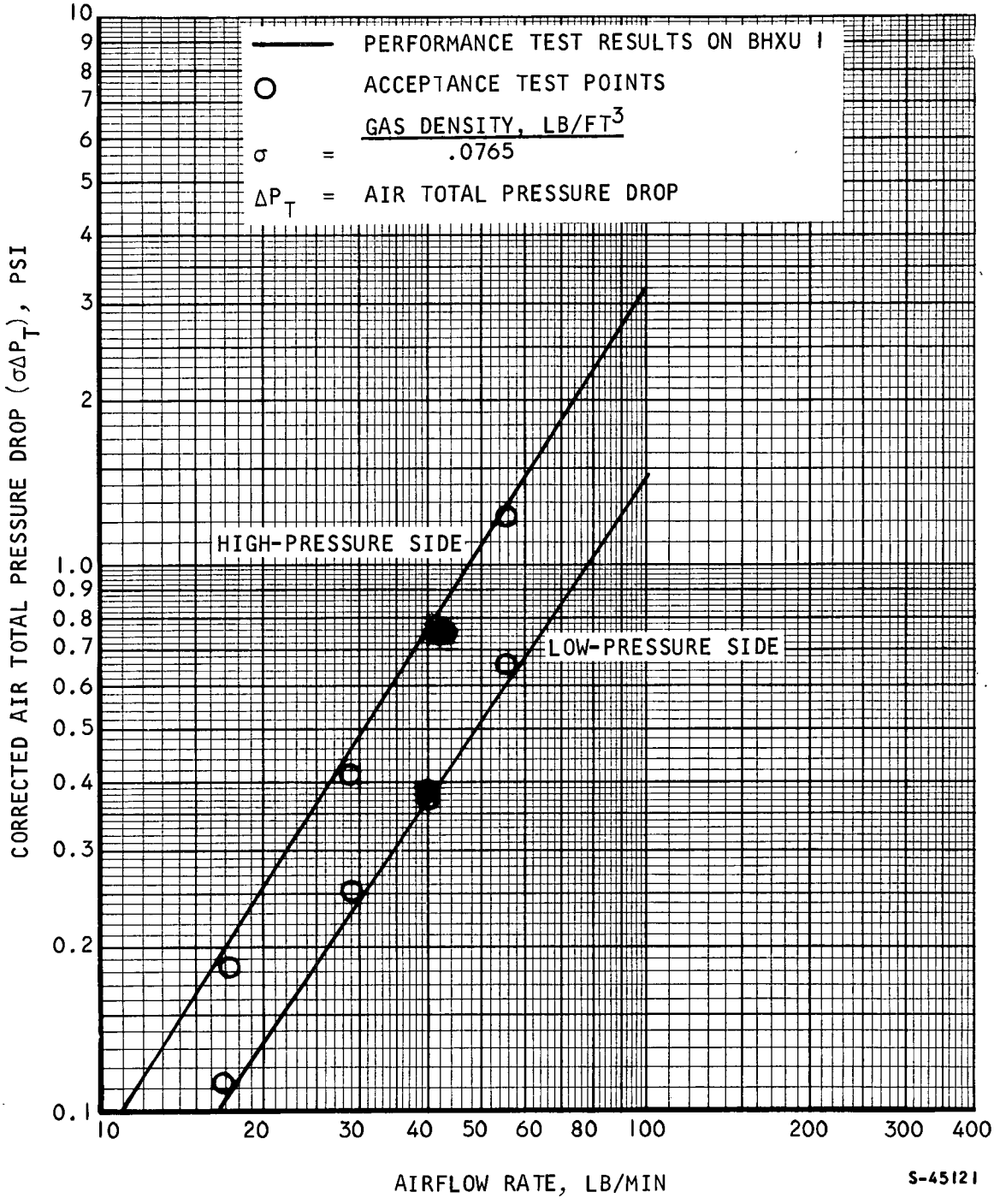

Figure 72. Pressure Drop vs Airflow, BHXU 2 Acceptance Tests

Unit 3 Acceptance Tests

Six test points were run, including four BHXU combined-unit runs and two heat sink exchanger single-unit tests (one with each Dow Corning loop active). The data on recuperator heat transfer performance are shown in Figure 73. The test data verify the previously obtained performance curve within the limits of instrumentation accuracy. The test point at 55 lb/min showed the poorest heat balance (4.4 percent discrepancy between hot and cold stream heat rates) and is therefore considered to be the least accurate of the test points.

The data on heat sink exchanger heat transfer performance are shown in Figure 74 and compared with the effectiveness curve obtained from the BHXU 2 acceptance test series. The latter curve represents a good interpretation of the BHXU 3 test data because of the greater importance attached to the single-unit test points than to the BHXU combined-unit points, as explained previously.

Air pressure drop data for BHXU 3 are shown in Figure 75. In comparison with the predicted pressure loss curves (based on the BHXU 1 performance tests), the high-pressure side pressure drops are slightly below predicted and the low-pressure side pressure drops are slightly above predicted.

Dow Corning fluid pressure drops in the single-unit heat sink exchanger tests were about 65 percent of the pressure drop measured during the single-unit performance test of BHXU 1.

BHXU PERFORMANCE WITH XE-HE

Based on the results of the performance tests, a new performance map for BHXU operation with XeHe was established. The estimated performance for BHXU 1 is shown in Table 33 for the design point and six off-design operating conditions. The test results on the recuperator indicate that the actual UA will be 86 percent of the analytically predicted design UA. Applying this factor to the predicted UA at the XeHe design point, the recuperator effectiveness is reduced from the design objective of 95 percent to 94.1 percent. Similarly, the heat sink exchanger UA is reduced to 70 percent of the original design prediction, resulting in a new heat sink exchanger effectiveness of 92.0 percent. This performance for the heat sink exchanger applies when the active liquid circuit is the one in which one of the 16 liquid-side flow passages is blocked. In estimating off-design effectivenesses for the two units, the ratio of actual to predicted UA is assumed to vary with XeHe flow rate in the same manner as actual to predicted UA was found to vary with airflow rate in the performance tests. The heat sink exchanger effectiveness is based on a constant capacity-rate ratio of 0.87.

To estimate XeHe pressure drops for unit 1, the ratios of test to predicted air pressure drops at the BHXU simulated design point were applied to the predicted XeHe pressure drops at the BHXU design point with XeHe. Off-design pressure drops were determined by drawing the $\sigma\Delta P_T$ curves for XeHe parallel to the $\sigma\Delta P_T$ curves for air. This is possible because the air and

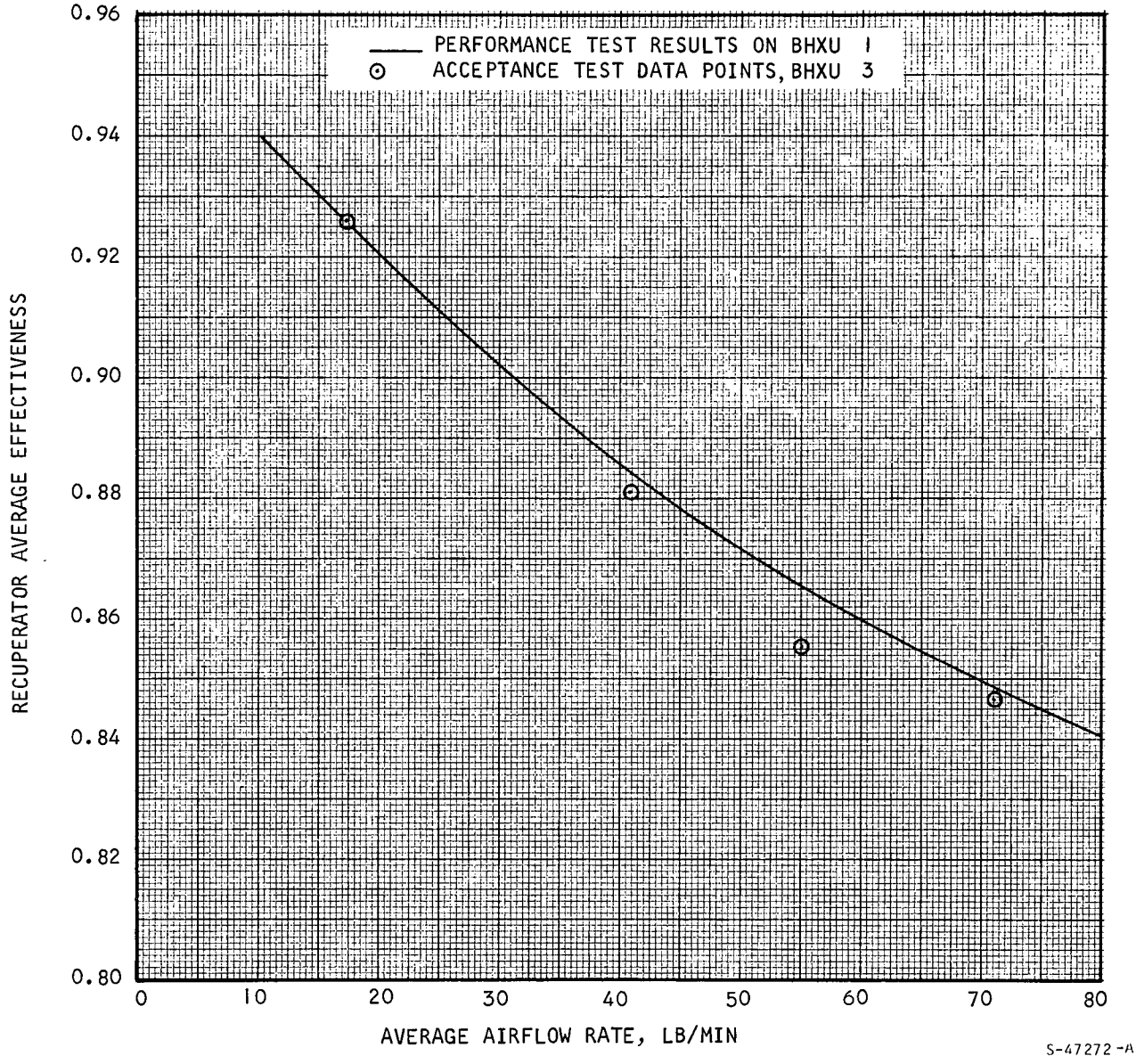

Figure 73. Recuperator Acceptance Test Results, BHXU 3

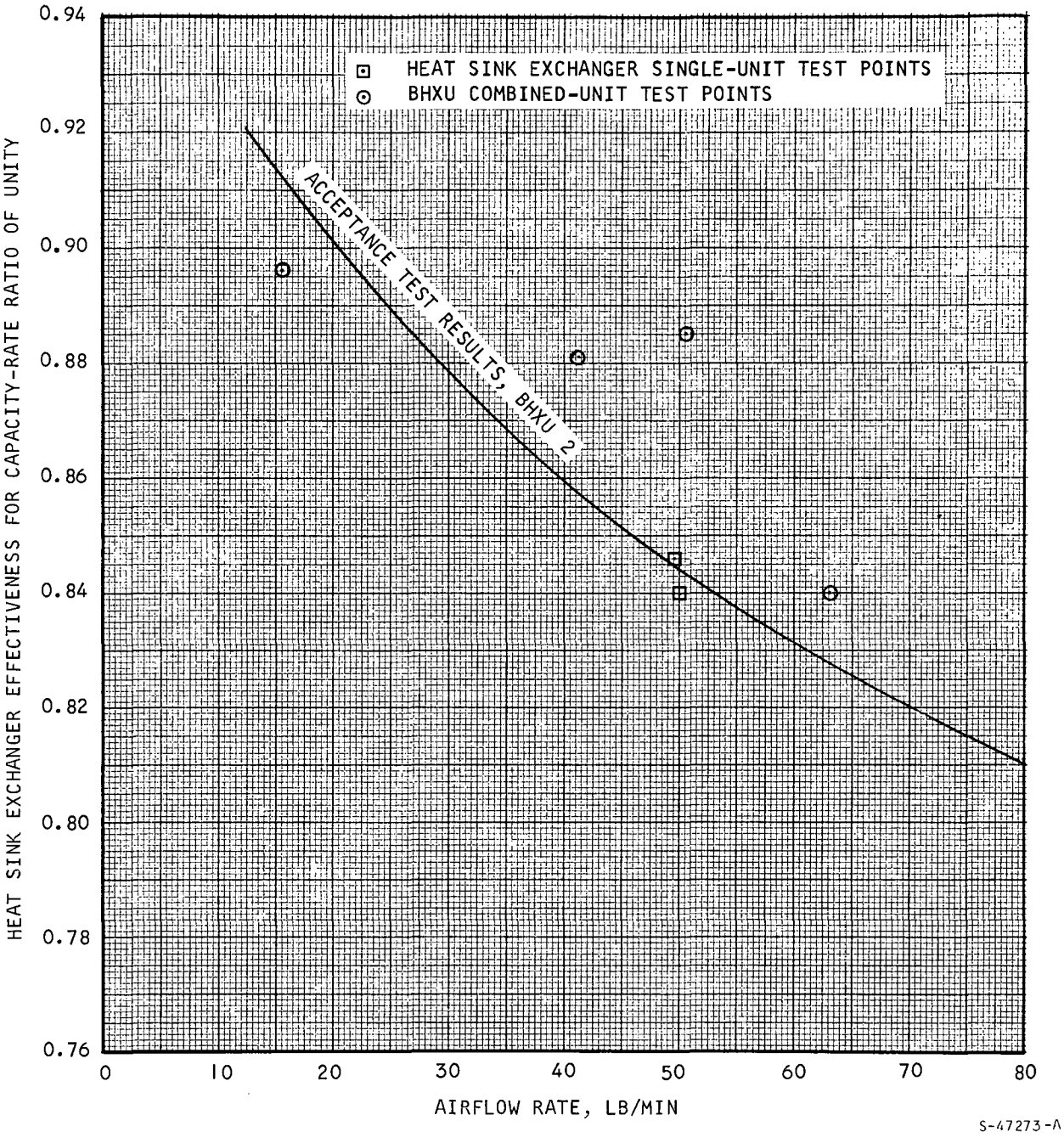

Figure 74. Heat Sink Exchanger Acceptance Test Results, BHXU 3

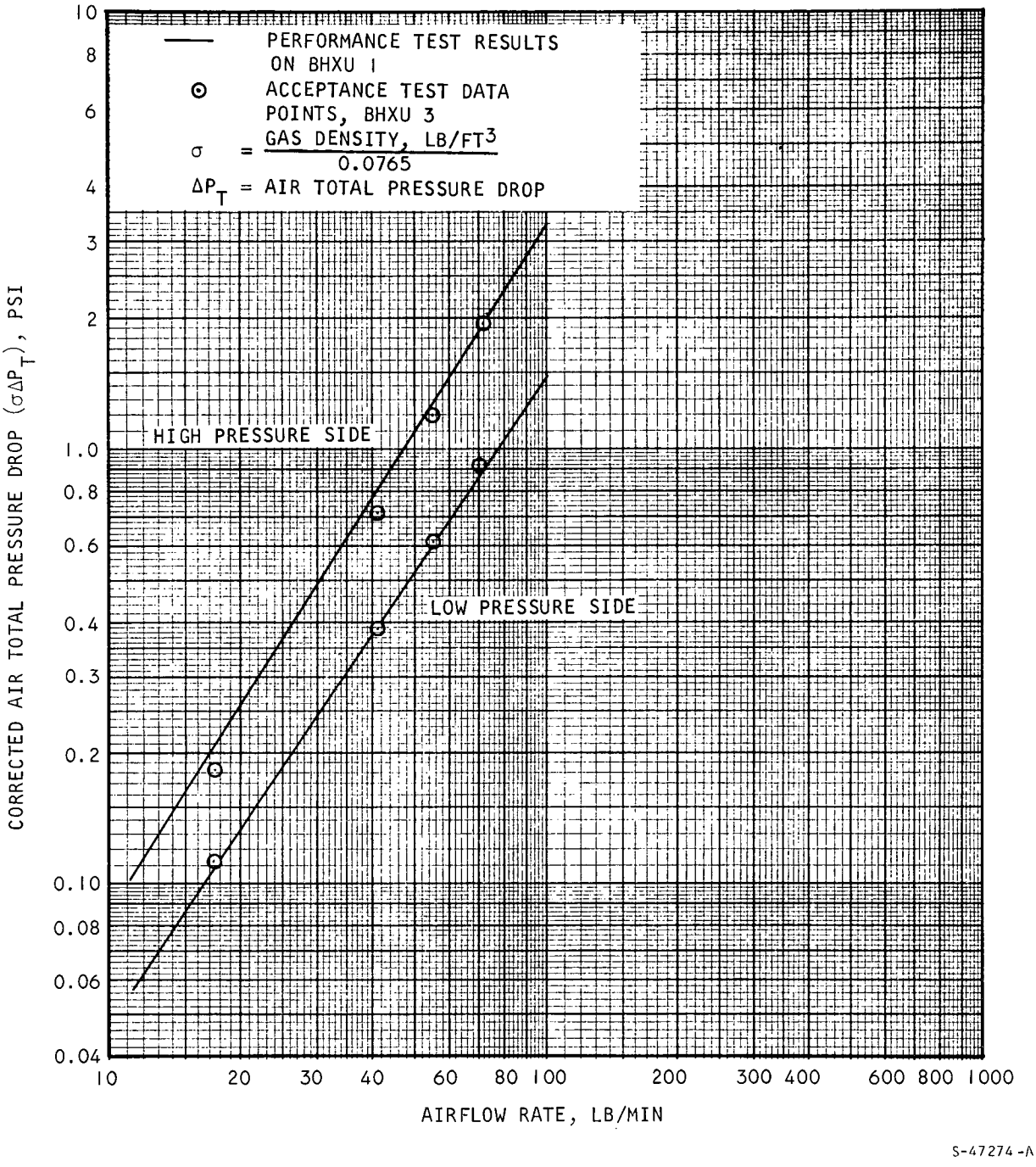

Figure 75. Pressure Drop vs Airflow, BHXU 3 Acceptance Tests

TABLE 33

BHXU I PERFORMANCE WITH XE-HE 83.8

Condition	Recuperator Effectiveness	HSHX Effectiveness*	Gas Pressure Drop, percent	Liquid Pressure Drop, psi
Design	0.941	0.920	3.9	6.0
Off-design				
I	0.955	0.95	7.5	1.3
II	0.955	0.945	6.3	2.0
III	0.95	0.94	5.3	3.0
IV	0.945	0.93	4.8	4.3
V	0.935	0.915	3.9	7.1
VI	0.92	0.89	3.0	13.4

*Based on a capacity-rate ratio of 0.87

XeHe curves extend over essentially the same Reynolds number range and should therefore have the same slope of pressure drop vs flow rate. The estimated $\sigma\Delta P_T$ curves for XeHe are shown by the dashed lines in Figure 65.

Based on the performance test results, predicted Dow Corning fluid pressure drops for unit I for the design and off-design conditions were increased by a factor of 2 from the original design predictions.

The acceptance tests indicated that BHXU's 2 and 3 have the same performance as BHXU I, with the exception that the heat sink exchanger in units 2 and 3 has a higher effectiveness and lower pressure drop than the heat sink exchanger in unit I. The estimated performance with XeHe for units 2 and 3 is shown in Table 34. The heat sink exchanger performance at the design condition is based on a UA equal to 93 percent of the original design prediction. The off-design effectivenesses are based on a UA variation with flow rate assumed to be the same as the variation of test UA with airflow in the acceptance tests.

Estimated liquid pressure drops for units 2 and 3, based on the unit 2 acceptance tests, are increased by 50 percent from the original design predictions. This may be considered to be slightly conservative for unit 3, since the acceptance test results for this unit indicated about a 30 percent increase in liquid pressure drop over the original prediction.

TABLE 34

BHXU'S 2 AND 3 PERFORMANCE WITH XE-HE 83.8

Condition	Recuperator Effectiveness	HSHX Effectiveness*	Gas Pressure Drop, percent	Liquid Pressure Drop, psi
Design	0.941	0.946	3.9	4.5
Off Design				
I	0.955	0.965	7.5	1.0
II	0.955	0.965	6.3	1.5
III	0.950	0.96	5.3	2.3
IV	0.945	0.955	4.8	3.2
V	0.935	0.94	3.9	5.3
VI	0.92	0.92	3.0	10.1

*Based on a capacity-rate ratio of 0.87.

APPENDIX A

AIRESEARCH HEAT EXCHANGER COMPUTER PROGRAMS

A brief description of several computer programs which AiResearch utilized in conducting the preliminary design study is presented below.

GAS-TO-LIQUID, MULTIPASS-CROSSFLOW PLATE-FIN HEAT EXCHANGER DESIGN PROGRAM (PLATE-FIN 5)

Plate-fin 5 is used to design crossflow or cross-counterflow plate-fin heat exchangers, with single or multipass construction on either the hot or the cold side, and with mixing of the fluids between passes and no mixing of the fluids within each pass. Calculations are made from separate f and f/j Lagrangian interpolation tables for each fin as functions of Reynolds number when the required performance, fluid properties, fin information, and heat exchanger details are given. An iterative procedure is required. Core dimensions and weights are calculated. The basic surfaces can be scaled to other geometrically similar surfaces.

Perfect gas behavior is assumed for the gas side, and all properties are evaluated at the bulk average temperature on each side. Gas density for friction pressure drop is the reciprocal of the average specific volume. Each side of the heat exchanger is designed separately, and then the sides are combined together. Thermodynamically impossible problems and core and duct gas Mach numbers are checked. Duct and core end losses are included as fixed multiples of the pertinent velocity head. Return pan pressure drops are neglected. Fin effectiveness is determined by iteration.

Required performance parameters in the input include gas and liquid weight flows, gas inlet total temperature, pressure and total-to-total pressure drop, liquid inlet temperature, and the heat transfer rate. Liquid pressure drop is not a design requirement for the heat exchanger, but it is calculated for each solution.

Required fin and heat exchanger information includes material, thicknesses, number of cross-counterflow passes, and duct diameters. The gas- and liquid-side fins are specified for the heat transfer surface combination to be investigated. Different heat exchangers are then calculated, with the specified fin surfaces, from all combinations of the input values of thermal conductance ratio and the number of liquid passages (tubes). The user of the program then picks the best solution for this problem on the basis of factors such as weight, dimensions, practicability, and liquid pressure drop.

COUNTERFLOW PLATE-FIN HEAT EXCHANGER DESIGN PROGRAM (PLATE-FIN 7B)

Plate-fin 7B designs pure counterflow heat exchanger cores. The effect of the inlet and outlet crossflow sections, which are necessary to distribute the gas flows into and out of the counterflow section, on the size and performance

of the unit is not calculated. Since these end sections are not considered, the shape of the gas face has no effect on the size of the effective heat transfer core. As a result, the dimensions of the core are not used to guide the program "search" for fin surface combinations yielding minimum-weight cores. Instead, the user can specify a dimension of the gas face (height or width) or its aspect ratio, and the program will calculate the dimensions and weight of the resulting heat exchanger. A separate operational program calculates pressure drop and weight of the end sections.

In counterflow, the designer loses a degree of freedom. Since the flow widths and lengths must be equal for the two sides of the heat exchanger, all the available pressure drop will be utilized only in the controlling side of the heat exchanger, if the program is restricted to the use of production fin surfaces arranged in practical configurations for manufacture. Normally, the gas side will be controlling. Therefore, after the heat exchanger is sized, the pressure drop actually used on the other side of the heat exchanger is calculated.

COUNTERFLOW PLATE-FIN END SECTION PRESSURE DROPS (H 1400)

The preceding description of AiResearch computer program plate-fin 7B describes the design procedure used for pure counterflow plate-fin heat exchangers. This description further states that no allowance is made for the pressure drop, weight, and volume required for the introduction and removal of the fluids from the counterflow core. In order to determine the effect of the end sections required for this purpose on the performance of the heat exchanger, Program H 1400 was written.

As in counterflow heat exchangers the flow face area is common to both fluids; simple manifolds are not sufficient to accomplish the fluid distribution. Two prime design concepts are available to accomplish the required flow distribution: triangular and rectangular end sections. Where the pressure drop available is low, the triangular-shaped ends are generally preferred, but if pressure drop is not limited, then the rectangular design may be preferred. For both design concepts, the ends are fabricated as an integral part of the heat transfer matrix. The plates used throughout cover the entire flow passage areas, but the fins used in the end sections need not necessarily have the same configuration as the fins in the counterflow core. Only the fin height must be maintained throughout. In most cases, as the temperature differences in the ends are small and as the flow is almost entirely crossflow, the heat transfer in these sections is negligible (or is assumed negligible to give extra "safety margin" to the design).

Program input required includes counterflow core geometry, inlet and outlet fluid conditions, and the overall configurations of the end sections to be considered. For each specified end section configuration, all end section pressure losses are calculated. When these are added to the pressure drops of plate-fin 7B, realistic overall heat exchanger pressure losses are achieved.

MULTIPASS TUBULAR HEAT EXCHANGER DESIGN PROGRAM (H 0424)

In this program multipass cross-counterflow and multipass cross-parallel-flow, tubular two-fluid heat exchangers are designed by an iteration procedure. Any combination of liquids and gases can be utilized. As in the plate-fin programs, the friction factor and Colburn modulus data for both inside and outside tubes are available in the form of Lagrangian tables. The outside of the tubes can either be plain or have circular disc fins or continuous-strip fins. The inside of the tubes can be plain, have turbulators, have internal fins, or be dimpled. A wide range of friction factor and Colburn modulus data is available for all these types of surfaces. The majority of the data used is actual test data obtained in tests conducted by AiResearch.

Input parameters required include heat transfer rate, inlet and outlet temperatures and pressures, and the weight flow rates of the fluids. Fluid properties are evaluated at average film temperature. Allowances for shock and turning losses are made as specified multiples of the core velocity pressure. Momentum pressure losses are calculated. Gas density is usually calculated on the basis of the perfect gas law, but compressibility factors (Z) can also be utilized, although in the subject study compressibility effects are not significant.

Multipassing can be accomplished either inside or outside of the tubes. Surface input information required includes the tube and fin diameters, the number of fins, the number of passes, all material thicknesses and the overall flow configuration. Options are available as to the type of overall heat exchanger configuration required. The dimensions, volume, and weight of a rectangular tube bundle are calculated but in addition to this, there is the option of arranging the tube bundle in a large annulus.

MULTIPASS CROSS-COUNTERFLOW TUBULAR PERFORMANCE (H 0415)

This program calculates pressure drops, thermal conductances, effectiveness, and outlet temperatures for any two single-phase fluids or for a single-phase fluid and condensing fluid. Manifold and tube-bundle pressure drops are separately calculated. Friction factor and Colburn modulus vs Reynolds number tables are available for many geometries. Input fluid properties, available for many fluids, are specific heat, dynamic viscosity, compressibility factor, Colburn modulus, and fluid properties are the same as for the tubular design program H 0424.

Heat exchanger geometry inputs are

(a) Number of passages and multipassing fluid

(b) Tube O.D., wall thickness, and thermal conductivity

(c) Tube-bundle dimensions and number of tubes

(d) Turbulator thickness and thermal conductivity

(e) Fin thickness, O.D., number per inch, and thermal conductivity

(f) Tube spacing and arrangement (center-to-center spacing in two directions, staggered or in-line arrangement)

(g) Manifold area and 90 deg-turn loss coefficient

Operating condition inputs are

(a) Margins for UA and both pressure drops

(b) Inlet temperature for both fluids

(c) Inlet or outlet pressure for both fluids

(d) Flow rate for both fluids

Fluid properties, except for the specific heats in the heat balance, are evaluated at a film temperature which is the arithmetic average between the mean wall temperature and the mean fluid bulk temperature. Core fluid velocity is evaluated at the bulk average temperature. Allowance for inside and outside tube entrance and exit losses is made as specified multiples of core velocity head. Momentum pressure losses are calculated. Manifold pressure drop is based on local density in each manifold.

Assumptions include

(a) Flow is completely mixed between passes and unmixed within a pass.

(b) UA per unit volume and specific heat are constant throughout the heat exchanger.

(c) Boundaries are adiabatic.

(d) Flow distribution is uniform.

(e) No heat leak will result due to conduction or radiation.

MULTIPASS CROSSFLOW PLATE-FIN TRANSIENT PERFORMANCE PREDICTION PROGRAM (HXTI)

The potential uses of this program are the following:

(a) Determination of steady-state operating points including the effects of axial heat conduction in the exchanger core.

(b) Determination of thermal stresses in the core due to rapid changes in inlet flow rates and temperatures.

(c) Prediction of the transient response of plate-fin exchangers, with the capability of including the program in system transient programs.

Heat exchanger configuration may be crossflow, cross-counterflow, or cross-parallel flow. The number of passes in the heat exchanger core is essentially unlimited; the present program storage limit is 15.

The program will allow fluid mixing in return pans or streamline turning; fluids are assumed unmixed in the core. Fluids may be either liquids or gases.

The normal output includes several tables giving input and calculated data on the core and quantities used in the computation. This is followed by tabled output of the computation results including fluid inlet and outlet temperatures, flow, pressures, etc. vs time. In addition, as optional output, any or all fluid and metal temperatures within the core can be obtained.

The program uses forward (or explicit) finite difference technique. In its present form, the exchanger can be divided into 900 total nodes. However, it is expected that approximately 50 to 60 nodes will give excellent results for most exchanger configurations.

The program considers both longitudinal and lateral heat conduction in the core; optionally, one may disregard such conduction by the appropriate setting of an input index.

Heat transfer coefficients and fluid properties are determined at each time step at average fluid temperatures; optionally, fluid properties and heat-transfer coefficients may be allowed to vary with temperature by computing such quantities at each node, at each time step. This is under the control of an input data index.

Time step data, as determined by numerical stability criteria, are automatically calculated by the program. The user of the program need not be concerned with what time value should be used as the program will normally use the largest time value which is stable. If a smaller time value is desired for greater accuracy, the program will accept such data from input. The program will also automatically adjust the size of the finite difference elements if those read in are too large.

Boundary data may be read in in the form of single values for those variables which are constant with time or as tables vs time for those quantities which are functions of time.

Initial-condition temperatures (of the core and both fluids) may be completely filled in by the program user, or from a minimum amount of input data (one value); the program will cyclically fill in all required initial temperature data.

Velocity profiles of both fluids are normally uniform; optionally, either or both fluids may have non-uniform velocity profiles. This is handled by either a velocity profile equation of general form which is built into the program and for which the user must read in coefficients, or velocity profiles data may be entered by tables.

The thermal capacitance of heat exchanger side bars can be considered. Fluids, of course, may be gases or liquids.

APPENDIX B

AXIAL CONDUCTION IN COUNTERFLOW HEAT EXCHANGERS

In all heat transfer devices, temperature gradients exist in the structure of the device. In any material where such a temperature gradient exists, there is a flow of heat from the high temperature portion of the structure towards the low temperature section. In many heat transfer devices, this leakage of heat through the heat exchanger material is very small and is generally ignored in the design of heat exchangers. In heat exchangers where high effectiveness is required, it is generally necessary to use some form of pure counterflow device, and the temperature gradient that exists in the material structure is at a maximum value, as the hot end of the heat exchanger is essentially at maximum fluid temperature and the low end is at minimum fluid temperature. The flow of heat through the metal in this type of situation results in a loss of heat from the hot end and addition of heat to the cold end, both of which have adverse effects on heat exchanger performance. In order to compensate for the reduced temperature difference at both ends of the heat exchanger, the heat exchanger size must be increased.

To determine exactly the necessary increase in heat exchanger size to account for the effects of axial conduction, it is necessary to conduct an energy balance over the entire heat exchanger, and a rigorous mathematical analysis is required to permit the accurate evaluation of these effects. Papers by H. W. Hahnemann (Reference 1) and by G. D. Bahnke and C. P. Howard (Reference 2) presented two methods of analysis. Both papers are sufficiently general to permit their adaption to the specific problem of axial conduction in a pure counterflow plate-fin heat exchanger. In addition to considering the information presented in these references, AiResearch has conducted an analysis to obtain a simple closed-form solution to the problem. This analysis is presented below.

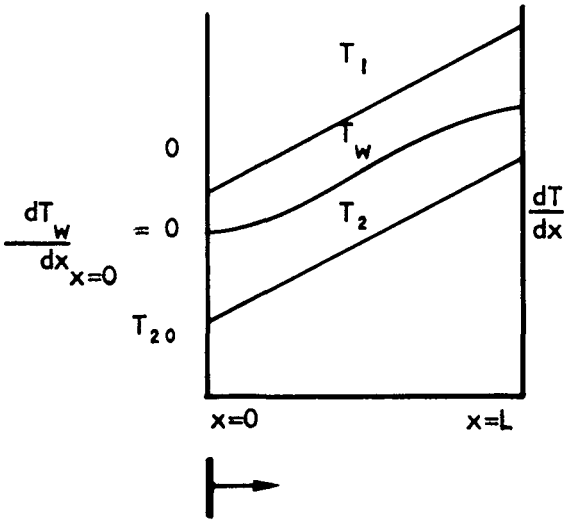

A-32208

T_1, T_2 — temperature of hot, cold fluid

T_W — wall temperature of surface separating hot and cold fluids

C_{p1}, C_{p2} — specific heat of hot, cold fluid

h_1, h_2 — film heat transfer coefficient on hot, cold side

W_1, W_2 — flow rate of hot, cold fluid

L	heat exchanger length
A_m	metal area available for heat conduction in direction of flow
$(hA)_1 (hA)_2$	heat transfer conductance on hot, cold side
k	metal thermal conductivity

The conditions of steady state, constant specific heats, and constant film heat transfer coefficient were assumed. Also, the thermal resistance of the metal surface separating the hot and cold fluids was assumed to be negligible compared to that of the fluid films. In other words, $\partial T_w / \partial y = 0$. The problem thus becomes one-dimensional.

For a differential length Δx of the heat exchanger, energy balance equations may be written for the hot and cold fluids and for the surface separating them. By allowing $Dx \rightarrow 0$, one obtains the differential equations of temperaure distributions:

$$A(T_1 - T_w) = \frac{dT_1}{dx}$$

$$B(T_w - T_2) = \frac{dT_2}{dx}$$

$$D(T_w - T_2) - C(T_1 - T_w) = \frac{d^2 T_w}{dx^2}$$

where $A = \dfrac{(hA)_1}{W_1 C_{p1} L}$

$B = \dfrac{(hA)_2}{W_2 C_{p2} L}$

$C = \dfrac{(hA)_1}{k A_m L}$

$D = \dfrac{(hA)_2}{k A_m L}$

By introducing $dT_w/dx = u$, the above equations are changed into four first-order differential equations. This is, in matrix notation

$$\{T'\} = [M]\{T\}$$

$$\{T\} = \begin{Bmatrix} u \\ T_1 \\ T_2 \\ T_w \end{Bmatrix}$$

and $$[M] = \begin{bmatrix} 0 & -C & -D & (D + C) \\ 0 & A & 0 & -A \\ 0 & 0 & -B & B \\ 1 & 0 & 0 & 0 \end{bmatrix}$$

Seeking solutions of the form

$$\{T\} = \{K\} e^{\mu x}$$

leads to the characteristic equation

$$\mu \left[\mu^3 - (A - B)\mu^2 - (AB + D + C)\mu + AD - BC\right] = 0$$

If μ_2, μ_3, and μ_4 are the nonzero, real and distinct roots of the expression in brackets above, then the solution of the differential equations is

$$\{T\} = \{K_1\} + \{K_2\} e^{\mu_2 x} + \{K_3\} e^{\mu_3 x} + \{K_4\} e^{\mu_4 x}$$

where $$\{K_i\} = \lambda_i \begin{Bmatrix} \mu_i \\ \dfrac{A}{A - \mu_i} \\ \dfrac{B}{B + \mu_i} \\ 1 \end{Bmatrix}$$

The coefficients λ_i are determined from the equations that result from the substitution of the boundary conditions into the solution above. Hahnemann (Reference 1) carried this through and then proceeded to find an explicit expression for the heat exchanger temperature effectiveness. His results are rather lengthy and, therefore, will not be repeated here. However, it must be pointed out that when the characteristic equation has multiple roots, the solution above must be modified according to well-established rules. Multiple roots occur, for instance, when A/B = C/D or when A = B and C = D.

The heat exchanger temperature effectiveness was found for the case when A = B and C = D, that is, when $W_1 C_{p1} = W_2 C_{p2} = WC_p$ and $(hA)_1 = (hA)_2$. It is

$$E = 1 - \frac{(NC_m + 1)}{(1 + N - \Psi)}$$

Where $C_m = \frac{kA_m}{L W C_p}$

$$N = NTU = \frac{(UA)}{WC_p}$$

$$\Psi = \frac{1}{2p}\left[\frac{\phi + 1}{1 - p} + \frac{\phi - 1}{1 + p}\right]$$

$$p = \sqrt{1 + \frac{1}{NC_m}}$$

$$\phi = \frac{\cosh 2Np - 1}{\sinh 2Np}$$

If thermal conductivity is negligible, the above equation for effectiveness reduces to the familiar equation

$$E = 1 - \frac{1}{1 + N}$$

When $C_m \to \infty$, the effectiveness equation becomes

$$\lim_{C_m \to \infty} E = 1 - \frac{1}{\frac{\cosh 2N - 1}{\sinh 2N} + 1}$$

and when $N \rightarrow \infty$, the effectiveness equation is in the limit

$$\lim_{N \rightarrow \infty} E = 1 - \frac{C_m}{2 C_m + 1}$$

If in the above equations, $N \rightarrow \infty$ and $C_m \rightarrow \infty$, $E \rightarrow 1/2$ as expected.

The effectiveness equation discussed above was verified by comparison with results obtained by G. D. Bahnke and C. P. Howard (Reference 2). Bahnke and Howard used a numerical finite-difference method to calculate the effectiveness of a periodic flow (rotary) type heat exchanger when heat conduction in the direction of flow is allowed for. Their case of "infinite rotor speed" is equivalent to a direct transfer type counterflow heat exchanger. The verified effectiveness equation was used in the design of all pure counterflow heat exchangers determined during the parametric design study.

APPENDIX C

EXTERNAL MOUNTING SYSTEM

PROPOSED MOUNTING APPROACH

In the detailed BHXU design, it was assumed that the BHXU and BRU components would be mounted on a common frame. The frame must therefore be compatible with the BHXU-BRU bellows design and provide for a load transmission path for shock and vibration inputs. The frame will in turn be attached to the vehicle with isolators that are intended to limit resonance vibrations within the frame and BHXU-BRU package which could lead to amplifications exceeding the design capability of the BHXU or BRU (including their attachment bracket systems). The frame and BHXU-BRU structure acting as a rigid body on the isolator system will therefore have natural frequencies which will be controlled to known acceleration levels. The inertia loads at isolator resonance should be the maximum loads on the system. AiResearch recommends the following criteria as guidelines for achieving the desired system.

(a) A frame will attach to the BHXU-BRU at 11 mount points which provide for internal thermal expansion and pressure load restraint.

(b) The frame will be attached to the vehicle through four isolators.

(c) The maximum natural frequency of the frame BHXU-BRU structure acting as a rigid body on the isolators will be approximately 25 Hz.

(d) The frame BHXU-BRU structure will have no internal natural frequencies less than approximately 50 Hz.

Three examples of suitable mounting approaches are shown in Figure 76. The final selection of a suitable frame will depend on several factors including the location of the BHXU-BRU package, or packages, within the vehicle, the location of suitable vehicle structure to support the loads and the desired accessibility of the BHXU-BRU for repairs or refurbishment. The integral frame shown in Figure 76a utilizes the least space for the system although removable struts (members) would be required if the frame were to be permanent whereas the BXHU or BRU were removable. The external frame shown in Figure 76b could be used to set the BHXU-BRU away from the vehicle structure or to provide convenient removal from the frame. Basically, there is no difference between the two approaches and a combination of the two is likely in a detailed design solution. The common frame in Figure 76c could be utilized to support a pair of BHXU-BRU packages. The isolator placement would probably be restricted to peripheral locations to permit removal of either BHXU-BRU package. The frame supports may be placed on the four sides rather than as shown to be closer to the central BHXU-BRU mounts which carry the highest loads.

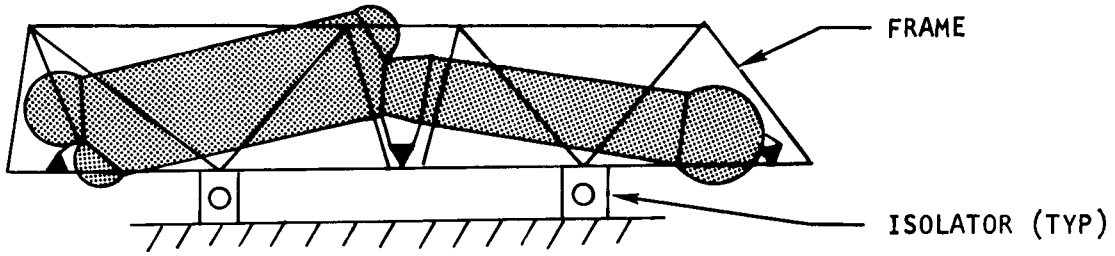

a. Single-BHXU Package, Integral Frame

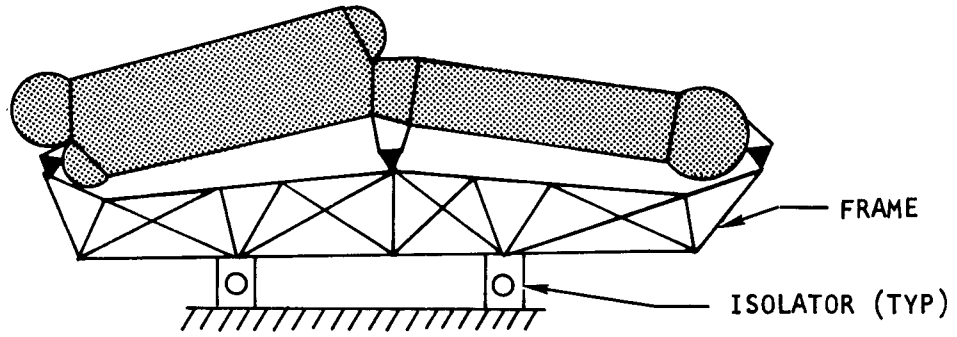

b. Single-BHXU Package, External Frame

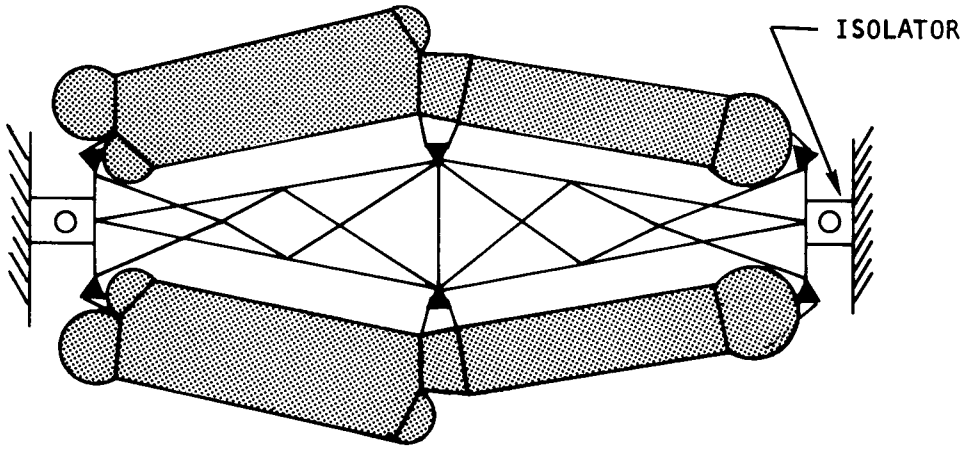

c. Two-BHXU Package, Common External Frame

S-50492

Figure 76. Typical BHXU Package Mounting Systems

STRUCTURAL ANALYSIS

A detailed structural analysis of the component mount system involves an iterative process for any assumed vehicle load pickup points. If optional load points are available on the vehicle structure, the process must be performed for each case to provide a comparison of the relative advantages and disadvantages. The following steps illustrate a typical design procedure.

(a) Select approach and preliminary structure

(b) Estimate load paths and loads

(c) Select preliminary frame and isolator geometry to handle the loads

(d) Perform preliminary sizing of the frame, calculate its contribution to loading

(e) Perform preliminary isolator design, accurately define frequencies and deflections

(f) Detail the frame design

(g) Perform final isolator design

LOAD SPECIFICATION

The inertia load specification outlined above for the BHXU design and will be the same for the combined frame, BHXU and BRU. The inertia load inputs combined with the frame, BHXU and BRU weights and the isolator properties will determine the overall loading of the system and the loads applied to the vehicle support points.

SCHEMATIC OF BHXU-BRU MOUNT SYSTEM LOAD POINTS AND LOADING DIRECTIONS

Figure 77 shows the spatial relationship between the six BHXU mount brackets, the three BRU mount points, and the two duct pickup points for reacting bellows axial pressure load. Force vectors are indicated to show the approximate manner in which the BHXU-BRU loads will be transmitted to the frame.

FRAME FEASIBILITY

A preliminary analysis of a typical frame structure was performed to show that the approach is feasible. It was estimated that a 75-lb frame spanning 50 in. between isolators would support the BHXU-BRU. A total frame and component weight of 750 lb was assumed.

A plane frame was checked to obtain an estimate of member cross-sectional areas. One-half of the estimated package weight, amplified by a 20-g factor, was applied on a 50-in. span with the resulting load picture shown on the following page.

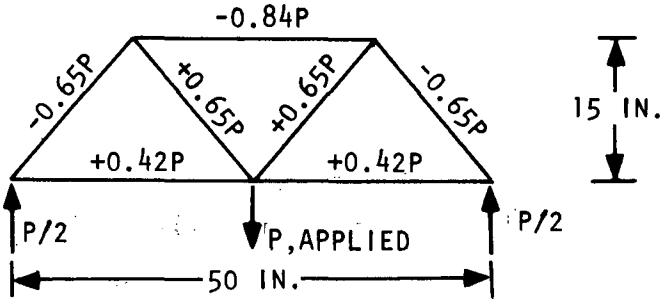

S-50535

For this estimate, the maximum member load is 0.84 P yielding an applied load of of

$$F = 0.84(20)(375) = 6300 \text{ lb}$$

Assuming an allowable stress of 125,000 psi for a typical medium strength structural steel, the required member cross-sectional area is

$$A = \frac{F}{\sigma_{all}} = \frac{6300}{125,000} = 0.05 \text{ in.}^2$$

A 25-in. steel member with this area would have a total weight of about 3.6 lb so that the above 7 member frame would weigh about 25 lb. Two plane frames plus cross members would have a total of 75 lb.

Member buckling was checked to illustrate another design consideration for a supporting frame. The critical buckling load is given by

$$P_c = KEI/L^2$$

For a simply supported 25-in. member, the required I for a 6300-lb load with a 1.5 safety factor is

$$I = \frac{P_{CR} L^2}{KE} = \frac{6300(1.5)(50)^2}{9.87(28)\ 10^6} = 0.087 \text{ in.}^4$$

Therefore the ratio of required section moment of inertia to the required area is

$$I/A = \frac{0.087}{0.051} = 1.7$$

● FIXED POINTS WITH RESPECT TO SUPPORT FRAME

○ PROVISIONS FOR THERMAL MOVEMENT WITH RESPECT TO FRAME

S1 THRU S6, BHXU MOUNTS

SP1 AND SP3, DUCT PRESSURE REACTION MOUNTS

BR1 THRU BR3, BRU MOUNTS

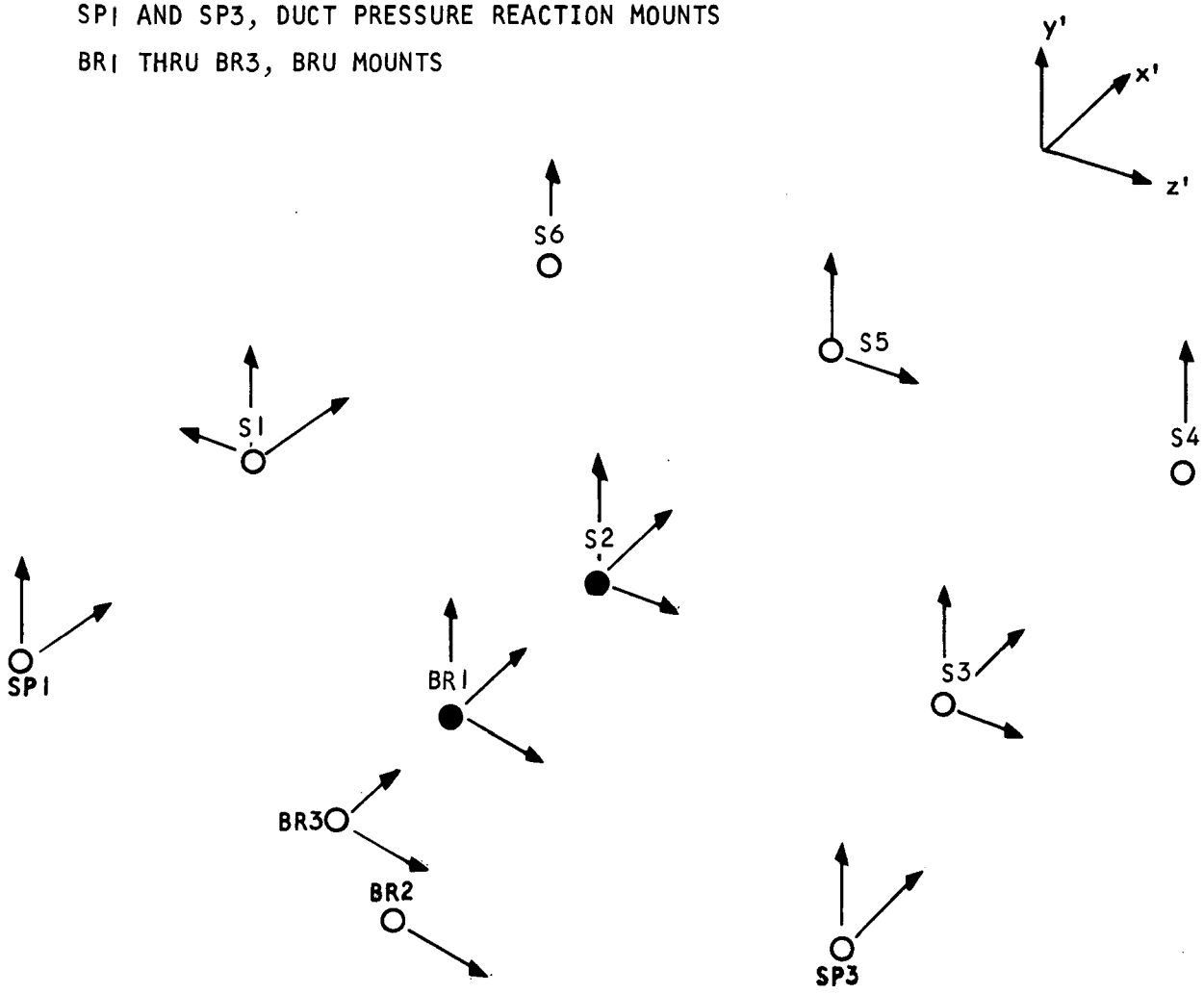

Figure 77. **BHXU-BRU Support Mounts and Load Directions**
(Refer to Figure 46 for Component Arrangement)

S-50493

A rectangle has an I/A ratio of

$$I/A = \frac{bh^3/12}{bh} = \frac{h^2}{12}$$

so that a height of 4.52 in. and a width of 0.012 in. would be approximately adequate, although this strip would not be stable. An I-beam with a flange separation, h, and flange areas, A/2, would have an approximate I/A ratio of

$$I/A = \frac{2\left(\frac{A}{2}\right)\left(\frac{h}{2}\right)^2}{A} = \frac{h^2}{4}$$

Therefore flange separation would be 2.61 in. An I-beam of this height would have flanges of about 1.0 in. width; hence, nominal web and flange thickness would be about 0.011 in. The webs and flanges would be checked for local buckling instability. Generally, this analysis indicates that the frame members will be sized by buckling considerations. Although in a detailed design member lengths can be adjusted to minimize the effect of buckling on frame weight.

The frame members would have natural frequencies above 50 Hz. In addition, one-half the weight of the BHXU-BRU applied to center span would give a rigid body natural frequency of 55 Hz. Taking the latter case, for example, the frame spring rate for a central load assuming simple support and conditions is

$$k = \frac{48EI}{L^3}$$

The moment of inertia for two members with areas of 0.05 sq in. and a 15-in. separation is

$$I = 2(.05)\left(\frac{15}{2}\right)^2 = 5.6 \text{ in.}^4$$

For an elastic modulus of 28×10^6 and a 50-in. span, the spring constant is

$$k = \frac{48(28 \times 10^6)(5.6)}{(50)^3} = 60{,}000 \text{ in.-lb}$$

The natural frequency of a 175-lb weight (about 0.5 lb-sec^2/in. mass) is

$$f = \frac{1}{2\pi}\sqrt{\frac{k}{m}}$$

$$f = \frac{\sqrt{120{,}000}}{2\pi} = 55 \text{ Hz}$$

Frame strength was therefore adequate to ensure that internal frequencies less than 50 Hz will not occur.

ISOLATOR DESIGN CONSIDERATIONS

A standard isolator design would be anticipated for this system. The operating temperatures would probably require use of the metal mesh type rather than rubber or other non-metallic materials. Metal mesh designs to 1200°F are common and this frame may operate at lower temperatures. The damping coefficient and isolator spring rate will be specified to ensure that maximum loads of 20-g lateral and 24-g vertical are achieved. A damping coefficient equal to 10 percent of critical damp will be required for vibratory inputs and the desired shock isolation factor is 0.5.

REFERENCES

1. Hahnemann, H. W., "Approximate Calculation of Thermal Ratios in Heat Exchangers Including Heat Conduction in Direction of Flow," National Gas Turbine Establishment Memo No. M36, also available from the Defense Documentation Center as ATI 74031.

2. Bahnke, G. D., and Howard, C. P., "The Effect of Longitudinal Heat Conduction on Periodic - Flow Heat Exchanger Performance," Paper No. 63-AHGT-16, ASME, 1963.